EXPLORATION OF THE INTERPLAY BETWEEN ALLOSTERIC INTERACTIONS OF PHOSPHOFRUCTOKINASE FROM RAT LIVER

A Dissertation

by

DAVID ALAN HOLLAND III

Submitted to the Office of Graduate and Professional Studies of
Texas A&M University
in partial fulfillment of the requirements for the degree of

DOCTOR OF PHILOSOPHY

Chair of Committee,	Gregory Reinhart
Committee Members,	Ry Young
	Hays Rye
	Coran Watanabe
Head of Department,	Gregory Reinhart

May 2018

Major Subject: Biochemistry

ABSTRACT

The key metabolic enzyme phosphofructokinase (PFK) catalyzes the phosphorylation of fructose-6-phosphate (Fru-6-P) by MgATP in the first committed step of glycolysis. PFK's phosphorylation activity is tightly regulated by allosteric effectors who act by either increasing or decreasing its affinity to substrate Fru-6-P. Liver PFK from rats (RLPFK) is allosterically regulated by several metabolic byproducts including MgATP, citrate and AMP. Despite the importance of precise regulation of this enzyme, the interplay between the different allosteric effectors has not been thoroughly characterized. Presented here are the effects of MgATP on the ability of allosteric activator (AMP) or inhibitor (citrate) to modulate the activity of RLPFK. We see that MgATP dramatically decreases the ability of both AMP and citrate to allosterically regulate RLPFK. RLPFK has additionally been implemented to be subjected to activation through a novel self-association mechanism. This is difficult to prove unequivocally as the kinetic assays used to measure enzyme activity are performed (by necessity) at concentrations thought to be too low for self-association to occur. It has been demonstrated that at a physiological enzyme concentration Fru-6-P promotes self-association. We propose that if Fru-6-P promotes the formation self-associated species, then self-association must increase its affinity for Fru-6-P. Utilizing Fluorescence Correlation Spectroscopy (FCS) we measured the size of RLPFK particles at concentrations that span the gap between those used for kinetic assays

and those representing physiological conditions. Additionally, we varied the concentration of ligand (either MgATP or Fru-6-P). Our data demonstrate that Fru-6-P acts cooperatively with concentration of RLPFK to increase the extent of self-association, whereas no self-association occurs in the presence of MgATP. These FCS data provide exciting insight into the role of activation by self-association and provides the foundation for which future experiments can expound.

DEDICATION

To Kelvin and Alan.

May our children's future be forever greater than our father's past.

ACKNOWLEDGEMENTS

I would like to thank my boss and committee chair, Dr. Reinhart, for all the mentorship, advice and support that he has provided through the years. I would also like to thank my committee members, Dr. Young, Dr. Watanabe and Dr. Rye for their guidance and support throughout the course of this research. I am grateful for the abundance of technical expertise and scientific advice on fluorescence experiments provided by Dr. Lasagna. In addition, I am grateful for the FCS instrumental and theoretical support that I received through countless phone calls to Dr. Liao.

I would like to thank all of the former and current members of the Reinhart lab who provided scientific conversation on a daily basis. Pepe's has earned a permanent place in my heart and burned a permanent hole in my stomach. Thanks to Dr. Amy Whitaker for endless conversation, scientific and otherwise. You have greatly enriched my time here. Thanks also to friends and colleagues, my softball teams BuckyBallers and Wild Things, the BGA and the entire Biochemistry and Biophysics faculty and staff for making my time at Texas A&M University a great experience.

I would like to thank my parents for challenging and encouraging me to be the best that I can be. I would especially like to thank my wife, Michal, for the love and support that she has shown me during this journey. Thank you for putting up with long nights and lonely weekends. Thank you for comforting me when I was

stressed and frustrated, and you only wanted me home. And for sharing in my excitement when I was ecstatic about results that you would otherwise care less about. There really is no way to overstate how important you have been to me completing this thesis, this achievement is as much yours as mine.

NOMENCLATURE

A	Substrate
ACF	Autocorrelation function
ATP	Adenosine triphosphate
ADP	Adenosine diphosphate
AMP	Adenosine monophosphate
APD	Avalanche photodiode
cAMP	Cyclic Adenosine monophosphate
CPS	Counts per second
Da	Daltons
DTT	Dithiothreitol
E	Enzyme
EGFP	Green fluorescence protein
FCS	Fluorescence Correlation Spectroscopy
FITC	Fluorescence Isothiocyanate
FRET	Forester resonance energy transfer
EAM	Ensemble allosteric mode
EDTA	Ethylenediamine tetraacetic acid
FPLC	Fast protein liquid chromatography
Fru-2,6-BP	Fructose-2,6-bisphosphate

Fru-6-P	Fructose-6-phosphate
ΔG_{ay}	Coupling free energy for the binding of substrate and effector
K_{cat}	Turnover number
K_a	Apparent dissociation constant for substrate A
K_{ia}^0	Dissociation constant for A in the absence of effector
K_{ia}^∞	Dissociation constant for A in the presence of effector
K_{iy}^0	Dissociation constant for Y in the absence of substrate
K_{iy}^∞	Dissociation constant for Y in the presence of substrate
K_m	Michaelis constant
IPTG	Isopropyl β-D-1-thiogalactopyranoside
KNF	Sequential model
LB	Lysogeny broth
MgATP	Magnesium Adenosine triphosphate
MOPS	3-(N-Morpholinio)propanesulfonic acid
MWC	Concerted model
NADH	Nicotinamide adenine dinucleotide, reduced form
NBD	Nucleotide binding domain
n_H	Hill number
P_i	Phosphate
PEP	Phospho-(enol)pyruvate
PEG	Polyethylene glycol

PCH	Photon counting histogram
PFK	phosphofructokinase
PMSF	Phenylmethaneslfonylfluoride
PpPFK	Phosphofructokinase from *Pichia pastoris*
PSF	Point Spread Function
Q_{aa}	Coupling constant for the binding of two substrates (K-type)
Q_{ay}	Coupling constant for the binding of the substrate and effector (Y) (K-type)
Q_{ax}	Coupling constant for the binding of the substrate and effector (X) (K-type)
Qxy	Coupling constant for the binding of the effector (X) and effector (Y) (K-type)
Q_{axy}	Coupling constant for the binding of substrate and effectors X and Y (K-type)
RLPFK	Phosphofructokinase from Rat Liver
rRLPFK	Recombinantly expressed phosphofructokinase from Rat Liver
RLPFK-FITC	Rat liver phosphofructokinase labeled with fluorescein isothiocyanate
SDS-PAGE	Sodium sodecyl sulfate polyacrylamide gel electrophoresis
SBD	Substrate Binding Domain

v	Initial velocity
V	Maximum velocity
X	Primary Effector
Y	Secondary Effector

CONTRIBUTIONS AND FUNDING SOURCES

This work was supervised by a dissertation committee consisting of Professor Gregory Reinhart, Professor Ry Young, and Professor Hays Rye of the Department of Biochemistry and Biophysics and Professor Coran Watanabe of the Department of Chemistry. The electron microscopy images presented in Chapter 4 and Chapter 5 were generated by Jeng-Yih Chang in the laboratory of Professor Junjie Zhang from the Department of Biochemistry and Biophysics. All other work for the dissertation was completed independently by the student.

This work was made possible in part by the National Institutes of Health under grant number R01 GM 033216, the National Institutes of Health Chemistry-Biology Interface Predoctoral Training Program under grant number T32 GM008523-13A2, the Welch Foundation under grant A-1543, the Willie May Harris Fellowship from Texas A&M University, and support from Texas A&M AgriLife Research. Its contents are solely the responsibility of the authors and do not necessarily represent the official views of the supporting agencies.

TABLE OF CONTENTS

CHAPTER Page

LIST OF FIGURES

FIGURE Page

FIGURE Page

FIGURE Page

FIGURE Page

FIGURE Page

FIGURE Page

LIST OF TABLES

CHAPTER I

INTRODUCTION

A Brief History of the Theory and Application of Allostery

Nineteenth century investigations into digestion and fermentation led scientists to observe reactions that could not be reproduced in the laboratory. The ability to perform reactions that seemed to defy the laws of nature led many prominent scientists, including the famed Louis Pasteur, to assume that living systems must possess some "vital force" that exempted them from the laws of nature.[1] Indeed, living systems complete reactions in seconds which if attempted in the laboratory would require years if they could occur at all. However, it is not the miracle of a "vital force" that allows these reactions to happen, instead it is the miracle of enzymes. Shortly after James Sumner helped establish the identity of enzymes with his work on crystallized jack bean urease, a rush to find new enzymes and their functions ensued.[2] As the multitudes of enzymes were discovered, the reaction specificity and metabolic complexity afforded by enzymes proved to be remarkable indeed. However, it became apparent that simply understanding the catalytic function of enzymes was not sufficient for understanding their role in biological systems. An organism must be able to precisely control the rate of synthesis or breakdown of material in order to

coordinate its complex system of metabolic processes. Research on the ability of an organism to regulate enzymes has become as critical as research on enzyme activity.

Regulation occurs by either controlling the amount of enzyme present by adjusting rates of synthesis and degradation, or by controlling the enzyme activity. The activity of an enzyme can be regulated by many ways, including covalent modification, protein-protein interactions, changes in pH, substrate availability, or by ligand binding. A variety of methods of covalent modification exist including, but not limited to, phosphorylation, acetylation, carboxylation, glycosylation, ubiquitination, myristoylation, sulfation, ADP-ribosylation and Farnesylation.[3] Post translational modifications, a catalytically driven process, can modify the activity of an enzyme by perturbing the quaternary structure, sterically hindering active site, marking an enzyme for compartmentalization or even for degradation. Non-Covalent interactions with other proteins can activate or deactivate an enzyme as well. Changes in pH can affect an enzymes activity by changing the shape of the enzyme, by protonating/deprotonating key catabolic residues and/or by protonating/deprotonating the substrate. The concentration of substrate available for catalysis determines the catalytic rate according to the enzyme's K_m for substrate. If a non-substrate ligand binds to the activate site, it performs dead end inhibition. The specific case in which the ligand is the catalytic product is known as product inhibition. A ligand can activate or inhibit an enzymes activity by binding to a site away from the active site through a phenomenon known as allostery.

Among the other forms of regulating enzyme activity, allosteric regulation benefits from the intrinsic reversibility of non-covalent interactions, the rapid response time allowed by a fast-diffusing small molecule and the specificity provided by a discrete ligand binding site. Additionally, allosteric effectors are not structurally confined to substrate or product analogs. This allows selection of allosteric effectors that specifically report on physiological conditions of interest to the responsive enzyme. Together, these factors allow allosteric enzymes to rapidly sense the current condition and metabolic needs of a cell, making allosteric regulation particularly well suited for modulating the activity of enzymes that catalyze the committed step of a metabolic pathway. Unsurprisingly, allosteric enzymes are responsible for catalyzing the first step of many metabolic pathways including glycolysis, the Krebs cycle, pyrimidine biosynthesis and glycogenolysis.

The physiological role of allostery has recently received renewed interest and attention. Allostery is involved in transcriptional control[4], motor work[5], signal transduction[6] and metabolic regulation[7]. Unsurprisingly, improper allosteric regulation has been implemented in a number of disease states.[8-10] Previous attention on deregulation of metabolic enzymes during cancer progression has focused on the role of transcription factors which trigger increased expression of metabolic enzymes.[11] Focus on transcriptional anomalies has perhaps distracted from the importance of anomalous allosteric regulation on metabolic reprograming.[12, 13] The critical role allosteric enzymes play in physiological processes, and their intrinsic ability to be regulated make them attractive targets

for drug design.[9] Two benefits are ascribed to targeting allosteric sites with pharmaceutical drugs. Molecules targeting allosteric sites are highly specific to the target enzyme and the allosteric effect of a ligand is saturable, meaning there is a maximum effect that can be achieved. These two benefits combined, mean that drugs that target an allosteric site may result in fewer side effects when compared to drugs targeting the active site.[9] In order to further efforts at rational drug design for allosteric binding sites, a greater understanding of how enzymes are allosterically regulated at the molecular level is needed.

Before discussing allostery in depth, it is important to define a few terms. An allosteric ligand can regulate the activity of an enzyme by altering the maximum velocity (V-type) or by altering the affinity of another ligand (K-type). Since a majority of allosteric enzymes are K-type we will focus our attention on effects involving substrate affinity. An allosteric interaction can be between identical ligands (homotropic) or between different ligands (heterotropic). We reserve the term "cooperativity" to refer to a K-type homotropic allosteric response.

The homotropic allosteric response known as cooperativity is defined by a non-hyperbolic binding curve and is perhaps the most readily recognized manifestation of allostery. Linus Pauling discussed cooperative oxygen binding to hemoglobin[14] 25 years before the word "allostery" was coined by Monod and Jacob.[15, 16] Positive cooperativity occurs when the binding of a ligand facilitates the binding of additional identical ligands resulting in the defining sigmoidal binding curve. Allostery leading to negative cooperativity occurs when the ligand

dissociation constant increases with subsequent binding events, and produces a shallow binding curve. Although less common than positive cooperativity, negative cooperativity does occur.[17, 18] The binding curves of an enzyme subjected to K-type homotropic cooperative substrate binding are not described by the Michaelis-Menten equation. Archibald Hill worked out a formulism which has been adapted for describing the non-hyperbolic binding curves in cooperative enzymes.[19] The resulting "Hill equation" introduces a term known as the Hill number (n_H) to describe the deviation from a hyperbolic binding curve. A Hill number greater than 1 indicates positive cooperativity and a Hill number less than 1 indicates negative cooperativity.

Heterotropic allosteric communication occurs when the binding of a ligand has an effect on the binding of another ligand to a distant binding site. Allosteric views generally fall into three categories. 1. Conceptual views provide the framework from which to describe and explain observed allosteric phenomena. Conceptual views do very little to quantitate an allosteric signal or describe the structural elements necessary to achieve it. 2. The structural view of allostery considers the quaternary, tertiary and secondary perturbations that occur upon a triggered allosteric response. The goal of structural studies is to identify the interactions among residues necessary for signal transfer. 3. The thermodynamic view of allostery provides a way to quantitate an allosteric response without regard for the means or method by which it is achieved. In the following sections we

discuss the most common approaches to describing allostery and their respective conceptual, structural and thermodynamic views.

Classic models of allostery

The first model proposed for explaining the phenomenon of allosteric regulation came from Jacques Monod, Jeffries Wyman Jr., and Jean-Pierre Changeux in 1965 and has since become known as the MWC model.[20] Inspired by observations of two conformational states of hemoglobin (deoxy- and oxy-), the MWC model proposes that allosteric enzymes exist as a finite number of discrete conformations to which particular properties, such as binding properties, are ascribed. In the simplest case, only two states need exist, the high substrate affinity relaxed (R) and the low substrate affinity tensed (T). The MWC model presumes two fundamental premises; 1. There is a pre-existing equilibrium between the two states with differing affinities for substrate and/or allosteric ligand. 2. The symmetry of the structure must be maintained. The binding of a ligand to the respective high affinity form stabilizes that form. By mass action, ligand binding shifts the equilibrium towards the high affinity form.

The requirement of symmetry maintains that an oligomer cannot exist as a mixture of R and T subunits. When a substrate binds to the free enzyme it shifts the equilibrium to the R state in a concerted transition. (Figure 1-1 A). The concerted transition explains the occurrence of positive cooperativity because the binding of substrate to a single site shifts all remaining sites towards the high affinity form.

The magnitude of substrate cooperativity depends on the probability that the protein is not in the R state prior to substrate binding. Inhibitor binding, which facilitates a concerted transition to the T state, increases substrate cooperativity by reducing the number of R sites prior to substrate binding. Activator binding, which favors the R state reduces or eliminates substrate cooperativity. While the MWC model does well to explain cooperativity in the form of positive cooperativity, it is unable to explain negative cooperativity.

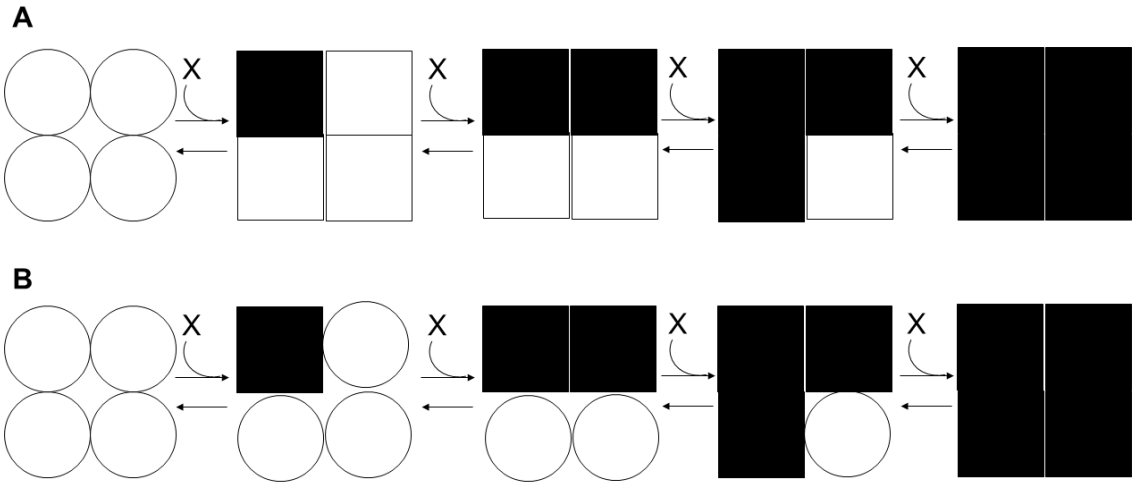

Figure 1-1: Schematic diagram of the two classic allosteric models. A ligand (X) is shown binding to a protein with two conformations, the tensed state (T) shown as a circle and a relaxed state (R) shown as a square. Ligand bound subunits are colored black, unligated (apo) subunits are colored white. A. The MWC model predicts a concerted transition to the relaxed state upon binding of the first ligand. B. The KNF model requires 4 equivalents of ligand for the protein to be converted from the T state to the R state.

A year after the MWC model was published, Kushan, Nemethy and Filmer released their model, now known as the KNF model.[21] As with the MWC model, the KNF model regards a finite number of enzyme conformations possessing particular substrate affinities. However, the KNF model does away with the requirement for symmetry. The fundamental deviation between the MWC model and the KNF model rest upon the assumed relationship between ligand binding and enzyme conformation. (Figure 1-1 B) The KNF model builds on the assumption that ligand binding induces a conformational change.[22] The induced conformation change within one subunit propagates across the subunit interface to increase the substrate affinity in neighboring subunits. The KNF model thereby explains cooperativity by step-wise substrate binding with induced sequential conformational changes that subsequently increases the affinity of the remaining unoccupied binding sites. The term "sequential model" has been bestowed onto the KNF model to distinguish it from the concerted nature of the MWC model. A sequential model allows the existence of hybrid oligomers and can explain negative cooperativity. Enzyme activation in the KNF model occurs progressively with each subsequent conformational change. Accordingly, the enzyme does not achieve full activation until substrate occupies all the binding sites.

Application of the classical models (MWC and KNF) to an allosterically regulated protein rely on conformational changes that can be explained in simple, well defined structural terms. For example, the binding of an allosteric ligand could result in the displacement of a key residue in a distant site, a structural shift in a

folding domain, or a quaternary rotation of subunits. To understand the allosteric response within a protein, one needs only to determine the structure of the activated and inhibited forms and define the differences between them. The conformations of a protein could be investigated by any experimental techniques that provide structural information, such as circular dichroism, fluorescence resonance energy transfer, nuclear magnetic resonance and, most commonly, X-ray crystallography.

According to both classic models of allostery conformational change occurs upon ligand binding. The models differ in whether the ligand selects (MWC) or induces (KNF) the conformational change. The other commonality is a shared reliance on two conformational states, one with a low substrate affinity and the other with a high substrate affinity. It has been claimed that over the past 50 years, the MWC model has generally fared better than the KNF model at explaining observed allosteric phenomena.[16, 23] Arguments for the MWC model typically rely on crystal structures or other static images which arguably impose a selective bias towards the MWC model. Static images are ensemble averages of the structure and are typically obtained in saturating conditions of a ligand. Together, these two factors leave it unlikely that an intermediate conformation would be observed.

The MWC model is more restrictive than the KNF model, as it is unable to explain negative cooperativity and is limited to symmetric oligomers. By the author's own admission, the original MWC model was oversimplified to favor elegance over completeness.[23] However, with slight modifications, arguments have

been made toward the use of the MWC to account for previously unexplained phenomena such as negative cooperativity.[24] For the most part, these modifications involve adding structural conformations to the obligatory two.[25-27] Even with additional conformations, the MWC model does a poor job of explaining the occurrence of allostery in monomers[28], entropy dominated allostery[29], and allostery of asymmetric oligomers. To address these shortcomings, and to create more comprehensive description of allostery, statistical models have arisen that incorporate populations of enzyme conformations.

Energy landscape models

As with the influence of published crystallographic images on the development of MWC model, advances in allosteric theory closely coincide with developments in field of structural biology. In the 1990s it became increasingly apparent that proteins do not exist as rigid structures, but as dynamic ever-changing entities.[30] The flexibility of a protein allows a protein to adopt a population of conformations that interconvert on a variety of timescales. The developing model suggests that the structure of a protein should therefore be described by the population of states that are in equilibrium with each other. The relative quantity of protein occupying a given state at any moment in time is equal to the probability of its occurrence, which is determined by its respective free energy. Consideration of all possible conformations produces the energy landscape, a plot of free energy levels as a function of conformational states. The importance of

the energy landscape was first applied to the dilemma of protein folding. It had long been known that a protein of appreciable length would require a lifetime to fold if left to a random search for the most stable thermodynamic state.[31] The initial proposition was that a folding pathway must exist, but this was inconsistent with experimental data.[32] Instead it has been argued that multiple folding pathways exist in parallel. A better model describes the progressive displacement across an energy landscape of multiple partially folded conformations. [33]

For a given protein, the free energy landscape could range from a single funnel, to a relatively flat plane with multiple hills and valleys, and countless variations in between. The protein structures corresponding to these free energy landscapes range from a rigid protein with a well define structure to an intrinsically disordered protein. The ensemble of states defined by the free energy landscape has been adapted to explain the catalytic function of an enzyme. According to this view of catalysis, each progressive step in catalysis redistributes the population of an ensemble of preexisting states.[34] What appears to be a deliberate reaction pathway is actually a step-wise series of statistical energy minimizations. Any modification to an enzyme alters the free energy landscape, these modifications could include posttranslational modification, amino acid substitutions and ligand binding. Such a modification could redistribute the free energy landscape so that a previously low population conformation becomes the predominantly populated conformation. The new predominant conformation may have altered kinetic properties compared to the native state, resulting in an allosteric response. The

energy landscape describes allosteric regulation using the same mechanistic arguments used to describe catalysis.[35]

The concept that enzyme function could be explained by shifts in a population of conformational states in a dynamic ensemble was not a new idea. Gregorio Weber first to propose such an idea in 1972.[36] Substantiation of this model required technological advancements in NMR and computational methods. Inclusion of protein modifiers such as post translational modification, site specific mutations, and pH potentially extends the field of allostery to all proteins.[37] Application of the energy landscape model to allostery has proven to be incredibly versatile[38]. According to the energy landscape model, an allosteric trigger could perform its respective response through any of three methods, 1. Further stabilization of the predominant native conformation and destabilization of minor conformations resulting in a decrease in heterogeneity. 2. Stabilization of a previously minor native state conformation resulting in an apparent conformational change. 3. Increase in heterogeneity of the free energy landscape without changing the average conformational state. [35] Collectively, these 3 potential functions of an allosteric effect could explain an allosteric response in a monomer or any number of oligomers, it could account for entropy or enthalpy dominated allostery, and even allostery without conformational change[39].

Two different models have emerged from the free energy landscape description of allostery. The population shift model[40] and the ensemble allosteric model (EAM)[41]. Both models describe allostery as a reshaping of the free energy

landscape that describes an ensemble of conformational states. The population shift model diverges from the EAM in its emphasis of the role of ligand interactions on reshaping the free energy landscape. In the population shift model, allostery occurs as a direct result of ligand binding and the interactions formed with the ligand binding site determines the magnitude and direction of the allosteric effect. Applying the population shift model to an allosteric protein system whose energy landscape can be explained in simple terms as an equilibrium between an inactive and active conformation yields a description of allostery nearly indistinguishable from the MWC model.[16]

Tsai and Nussinov formulated a thermodynamic description of an allosteric two state system using population shift model.[40] This model presumes a protein whose free energy landscape contains two separate energy wells for an inactive (R) and active (R*) conformations. (Figure 1-2 A) The population of the active and inactive conformations is defined by the equilibrium constant (L). An allosteric modifier (A) binds to protein with a dissociation constant K_A. The result of the binding of A is a shift the population of R and R* such that the new equilibrium constant is αL. (Figure 1-2 B) In this formulation, α is the allosteric coupling constant. This model was largely developed with G-protein coupled receptors (GPCR) in mind, and thus carries some of the classic terminology for GPCRs. A value of $\propto > 1$ indicates that R increases the population of its active conformation and is therefore an agonist. A value of $\propto < 1$ indicates that R decreases the population of

its active conformation and is therefore an inverse agonist. α is related to the coupling free energy according to equation 1-1.:

$$\Delta\Delta G_{1\rightarrow 2} = -RTln\alpha \qquad 1\text{-}1$$

The coupling free energy is referred to in this formalism as $\Delta\Delta G_{1\rightarrow 2}$ and is equal to the difference between change in free energy of the active state $\left(\Delta G_{1\rightarrow 2}(R^*)\right)$ and the change in free energy of the inactive state $\left(\Delta G_{1\rightarrow 2}(R)\right)$ (Figure 1-2 C). The dependence of fraction of protein in the active state (f_R^*) on the concentration of "A" is given by equation 1-2:

$$f_R^*([A]) = \frac{(L+\propto LK_A[A])}{(1 + L + K_A[A]+\propto LK_A[A])} \qquad 1\text{-}2$$

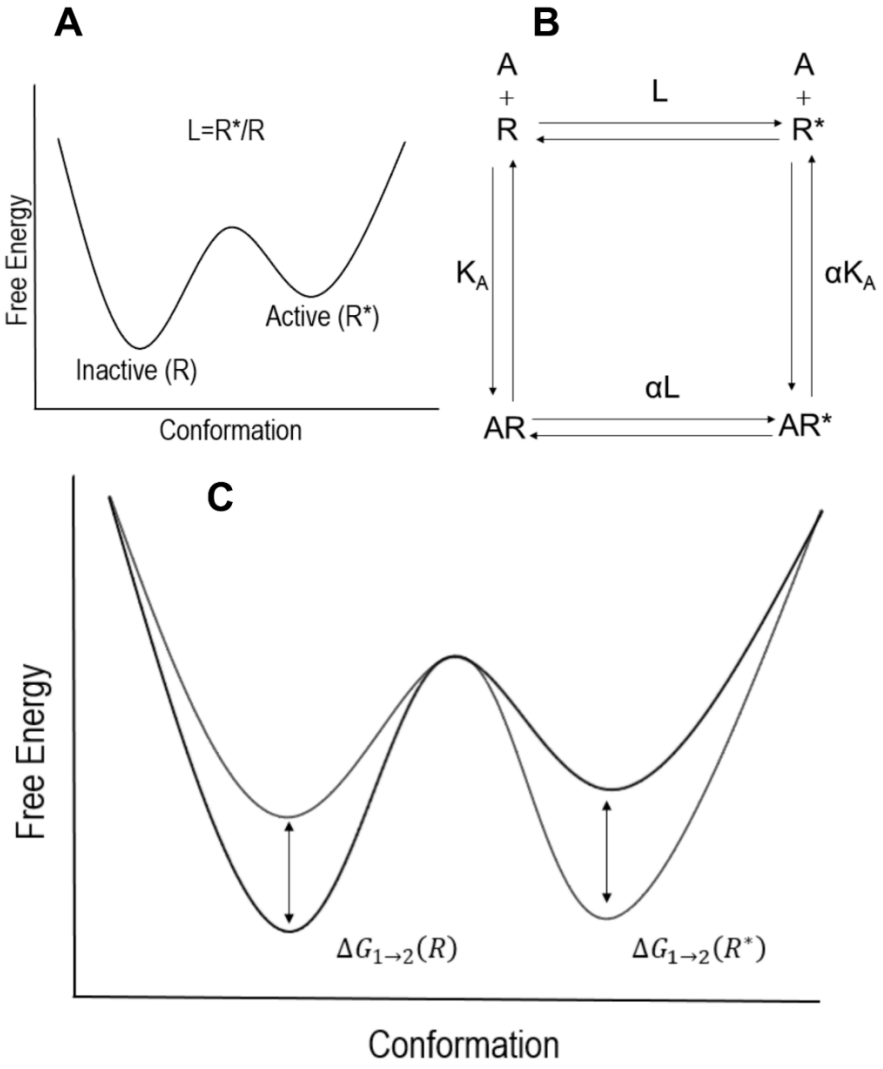

Figure 1-2: Schematic demonstrating thermodynamic interpretation of the population shift model. A. Free energy landscape of a protein with an inactive conformation (R) and an active conformation (R*) whose population is determined by the equilibrium constant L. B. Two-state model for a protein in equilibrium between an inactive and active state. An allosteric modifier (A) binds the inactive state with a dissociation constant of $\boldsymbol{K_A} = [\boldsymbol{AR}]/([\boldsymbol{A}][\boldsymbol{R}])$ and to the active state with a dissociation constant of $\propto \boldsymbol{K_A} = [\boldsymbol{AR^*}]/([\boldsymbol{A}][\boldsymbol{R^*}])$. Due to reciprocity, the equilibrium constant between AR and AR* is $\boldsymbol{\alpha L} = [\boldsymbol{AR^*}]/[\boldsymbol{AR}]$. C. Free energy landscape of Apo enzyme (black) or ligand bound (gray). The ligand induced change in free energy of the inactive state is given by $\Delta \boldsymbol{G_{1\rightarrow 2}}(\boldsymbol{R})$, and the ligand induced change in the free energy of the active state is given by $\Delta \boldsymbol{G_{1\rightarrow 2}}(\boldsymbol{R^*})$. The coupling free energy is calculated by $\Delta\Delta \boldsymbol{G_{1\rightarrow 2}} = \Delta \boldsymbol{G_{1\rightarrow 2}}(\boldsymbol{R^*}) - \Delta \boldsymbol{G_{1\rightarrow 2}}(\boldsymbol{R})$.

The EAM model regards allosteric signals as being robustly encoded in the ensemble of conformations. The EAM reaches this conclusion by treating each functional domain (allosteric or active) as existing within their own sub-ensembles. For an example, an allosteric domain equilibrium ensemble of conformations A, B and C and an active domain equilibrium ensemble of X, Y and Z may exist. If the conformations of A, B and C exist completely independently of X, Y and Z then no allosteric pathway exist. If, the B conformation of the allosteric domain increases the probability of Y conformation of the active domain then a functional linkage exists between the two domains. A ligand which preferentially binds the B conformation of the allosteric domain would stabilize said domain. The allosteric response is elicited by stabilizing the functionally linked conformations. The population shift model provides a more deterministic description of the allosteric signal where-as the EAM provides a more statistical description. An allosteric protein described by the EAM is not constricted to having a single functional linkage between conformations. A modifier reshapes the entire energy landscape and can therefore create complicated networks of interactions. A modifier (covalent, pH, temperature, mutation second allosteric ligand) can reshape the functional linkage between two sites diminishing, augmenting or even reversing the effect of an allosteric ligand.[41] Such a phenomenon is difficult to describe using a population shift model.

The ensemble allosteric model (EAM) calculates the thermodynamics of allostery by considering the free energy of all possible protein conformations. An

allosteric perturbation that results in a net change in the relative free energy of conformations associated with the active state, is assigned a coupling free energy equal to the magnitude and direction of the net change.[42] The thermodynamic formalism for the EAM model is experimentally applied by using a high-resolution structure of the unligated state as a templet to generate a large ensemble of conformational states. The free energy of each conformation is calculated, and the protein is presumed to sample each conformation according to their free energies, i.e. lower energy conformations are sampled more often than high energies. A computer algorithm then introduces single amino acid mutations to each residue and considers the effects of the mutation on the distribution of conformations. The goal is to identify a network of interactions within a protein.

The allosteric coupling energy is determined by the degree of coupling within the network of association. The binding of a ligand to any conformation reduces the free energy of that conformation and thus increase the degree by which it is sampled. Interactions association with that conformation are thereby also stabilized and sampled more frequently. Allostery occurs if these interactions have any functional consequence at another site. According to the EAM model, ligand binding results in the actualization of the allosteric effect but does not contribute to its magnitude. This distinction differs from the population shift model in the treatment of two different allosteric effectors which trigger the same allosteric signal. According to the EAM, the magnitude of allosteric effect is the same for both

ligands. In the population shift model the different ligands can trigger an allosteric signal with different magnitudes.

The morpheein model

The classic paradigm for protein conformation is that a peptide sequence dictates a single structure. While most allosteric enzymes are homo-oligomeric enzymes, it is generally assumed that the oligomeric form is an intrinsic consequence of the structure of the monomer. Intermonomer interactions drive the arrangement of symmetric oligomers made of a discrete number of monomers. It has been observed that some enzymes can form multiple distinct oligomeric forms which have unique enzymatic properties. The term morpheein has been coined to describe such enzymes.[43] Morpheein is a portmanteau of the words morph and protein and describes the quaternary level conformational change that facilitates the allosteric response. Application of the morpheein model to an enzyme requires functionally distinct oligomeric forms of the enzyme exist. Each oligomeric form must be consisted of a finite number of identical subunits (homo-oligomeric). Interconversion between the two oligomeric forms must proceed through a dissociated form of the enzyme. Direct interconversion between the two oligomeric forms cannot occur because each must satisfy their own symmetry.[44] The intermediate form can occupy different conformations that proceed to the unique oligomeric structures. Interconversion between forms must occur in conditions physiologically feasible.[45]

As a hypothetic example imagine a monomeric enzyme with a proto-tetramer and proto-trimer conformation. The mature tetramer may be the active form of the enzyme whereas the mature trimer is the inactive form. In an unperturbed state, the enzyme exists in a dynamic equilibrium of mature tetramer, proto-tetramer monomer, proto-trimer monomer and mature trimer (Figure 1-3). An allosteric ligand that stabilizes one form over the other may activate or inactivate the enzyme by modulating the dynamic equilibrium to favor the respective form. The prototypical example of a morpheein is porphobilinogen synthase.[46] Porphobilinogen synthase catalyzes the biosynthesis of monopyrrole, which is the building block for tetrapyrrolic cofactors including porphyrin and chlorophyll. It exists as an active octamer and as an inactive hexamer and the interconversion between the two requires dissociation to a dimer form that can exchange between a pro-octamer and pro-hexamer dimer.

Defining characteristics of morpheeins include hysteresis in kinetics, protein concentration dependent specific activity, non-Michaelis-Menten kinetics, dependence of kinetics on the order of addition of assay components, pH effects and multiple quaternary structures.[45] These characteristics have been observed in RLPFK.[47-52] As defined by the morpheein model, relevant species must exist with finite number of subunits. This excludes proteins such as prions whose oligomers do not have a size limit.

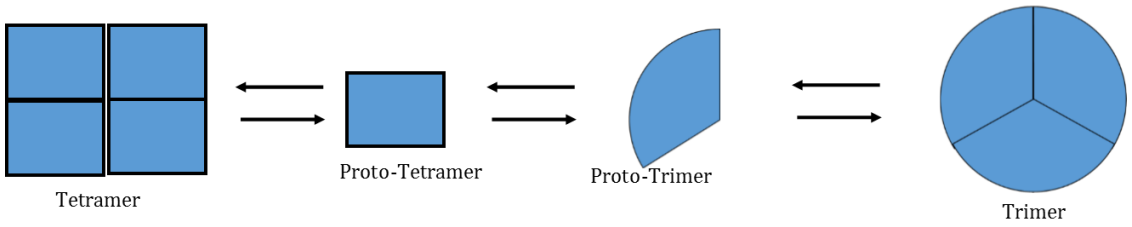

Figure 1-3: Schematic showing the Morpheein model of allostery. Hypothetical protein can occupy two oligomeric states (tetramer and trimer) which possess distinct regulatory properties. Conversion from one oligomeric state to the other requires a conformational change in a transitory monomeric state.

Metabolic enzymes with key regulatory roles have been seen to undergo oligomerization without clear size limits.[53 54] These protein oligomers have been referred to as aggregates[49] filaments[55], and polymers [56]. To avoid implying any structural properties implicitly associated with the terms aggregate and filament, we use the term polymers for this dissertation. The polymers are seen to have altered catalytic properties that either enhance or repress enzymatic function.[49, 55-60]. A recent review by Aughey and Liu highlights recent developments in this field of enzyme regulation as well as discuss some possible physiological mechanism for polymerization.[55] Models to account for the enzymatic regulation by polymerization are, as of yet, non-existent. The previously stated structural models

are insufficient for describing regulation by polymerization. Here we apply thermodynamic linkage analysis to study allosteric regulation by polymerization.

Thermodynamic linkage analysis

The previously described conceptual models relies on structural information to provide a framework by which the function of allosteric response can be explained. Thermodynamic linkage analysis considers the function of an allosteric response first and foremost by using observable parameters to measure the magnitude and direction of allosteric regulation without any a priori assumptions about the role of structural changes. The foundation to the thermodynamic approach is allosteric linkage, a concept that indicates mutual influence between ligands binding to the same protein at different binding sites. Wyman was the first to introduce the concept of allosteric linkage, shortly after his seminal collaboration with Monod and Changeux.[61] Using chemical potentials, Wyman demonstrated that the influence of an effector on substrate affinity equals the influence of substrate on the affinity for effector; a concept known as reciprocity. The magnitude of an allosteric effect was quantified by the allosteric binding potential.

In the 1970s, Weber expanded on and clarified the concept of allosteric linkage.[36, 62] Critically, Weber established that allosteric linkage can be expressed in terms of free energy. The expression of allosteric linkage by thermodynamic parameters enables the establishment of relationships between the magnitude of an allosteric response and the molecular forces that cause it. Reinhart

demonstrated that the concept of coupling free energy can be applied to enzymes and clarified the formulism of Weber by combining the single substrate-single modifier scheme of Frieden[63] and the kinetic notations of Cleland[64]. Using the apparent Michaelis constant, Reinhart demonstrated that the regulation of an allosteric enzyme can be described in terms of free energy provided the rapid equilibrium assumption is valid.[65]

The simplest allosteric mechanism of an enzyme (E) binding a single substrate (A) and a single modifier (X) is shown in Figure 1-4

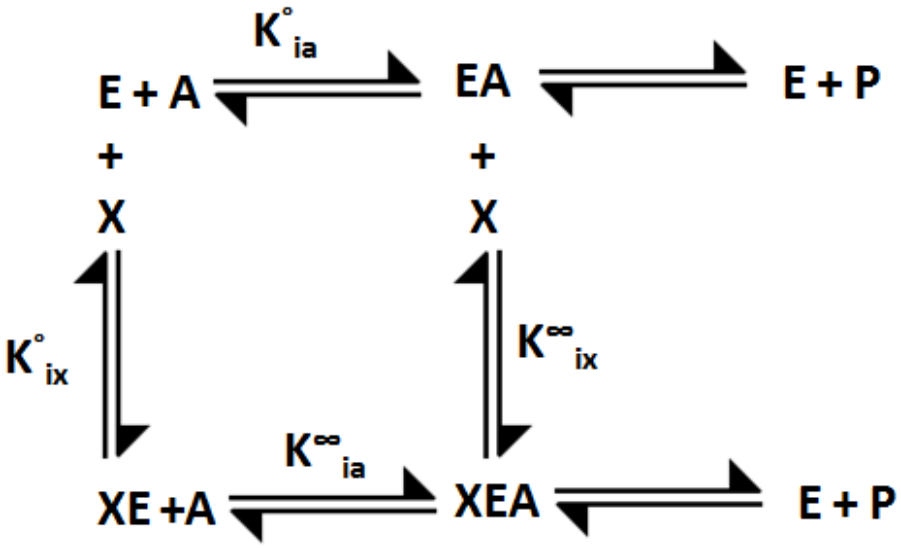

Figure 1-4 Scheme showing simplest mechanism of a single substrate (A) single modifier (X). Enzyme and product are denoted E and P respectively. K values are equilibrium constants as defined in the text.

In Figure 1-4, K_{ia}^{0} and K_{ia}^{∞} are the respective dissociation constants of substrate in the absence and saturating presence of allosteric effector (X). K_{ix}^{0} and K_{ix}^{∞} are the respective dissociation constants of X in the absence and saturating presence of A. The dissociation constants are defined as follows.

$$K_{ia}^{0} = \frac{[E][A]}{[EA]} \qquad 1\text{-}3$$

$$K_{ia}^{\infty} = \frac{[XE][A]}{[XEA]} \qquad 1\text{-}4$$

$$K_{ix}^{0} = \frac{[E][X]}{[XE]} \quad 1\text{-}5$$

$$K_{ix}^{\infty} = \frac{[EA][X]}{[XEA]} \quad 1\text{-}6$$

The relationship between A and X is given by the coupling constant (Q_{ax}) as defined below:

$$Q_{ax} = \frac{K_{ia}^{0}}{K_{ia}^{\infty}} = \frac{K_{ix}^{0}}{K_{ix}^{\infty}} \quad 1\text{-}7$$

$$Q_{ax} = \frac{[E][XEA]}{[EA][XE]} \quad 1\text{-}8$$

The value of Q_{ax} gives the magnitude and direction of the allosteric effect. A value of $Q_{ax} < 1$ indicates that X acts as an inhibitor. A value of $Q_{ax} > 1$ indicates that X acts as an activator. When $Q_{ax} = 1$, X does not elicit an allosteric effect on A. By substituting the definitions of each equilibrium constants (equations 1-3-1-6) into the definition of Q_{ax} (equation 1-7), we get equation 1-8 which shows that Q_{ax} is the thermodynamic disproportionation equilibrium constant for the following reaction:

$$Q_{ax} = [EA] + [XE] \leftrightarrow [E] + [XEA] \quad 1\text{-}9$$

Recognition of Q_{ax} as an equilibrium constant allows for the calculation of the coupling free energy according to:

$$\Delta G_{ax} = -RTlnQ_{ax} \quad 1\text{-}10$$

where R is the gas constant and T is the temperature in Kelvin. Activation has a negative free energy ($\Delta G_{ax} < 0$), inhibition has a positive free energy ($\Delta G_{ax} > 0$)

and no coupling free energy ($\Delta G_{ax} = 0$), indicates no allosteric response. Provided the rapid equilibrium assumption is valid, the following rate equation applies to the mechanism shown in Figure 1-4:

$$\frac{v}{[E]} = \frac{V^0 K_{ix}^0 [A] + V^0 Q_{ax} W_x [A][X]}{K_{ia}^0 K_{ix}^0 + K_{ia}^0 [X] + K_{ix}^0 [A] + Q_{ax}[A][X]} \qquad 1\text{-}11$$

where v is the initial velocity, $[E]$ is the total enzyme concentration, V^0 is the maximum activity in the absence of Y, and W_x is the ratio of V^∞/V^0, where V^∞ is the maximal activity in the saturating presence of effector X. W_x only has a value other than 1 when the allosteric effector X has an influence on the turnover rate.

The coupling constant Q_{ax} can be experimentally determined by measuring the apparent dissociation constant of substrate (A) as a function of effector (X). The effect of X on A is graphically represented for an inhibitor (top) and an activator (bottom) in Figure 1-5. The coupling constant is represented as the ratio of the two plateaus (K_{ia}^0/K_{ia}^∞) regardless of whether X is an inhibitor or an activator. The dependence of the apparent dissociation constant (K_a) on the concentration of allosteric effector can be described by the following equation:

$$K_a = K_{ia}^0 \left[\frac{K_{ix}^0 + [X]}{K_{ix}^0 + Q_{ax}[X]}\right] \qquad 1\text{-}12$$

Equation 1-12 can be derived from equation 1-11 by solving for $[A]$ at the concentration of A at which $v/E = V^0/2$. ($[A] = K_a$).

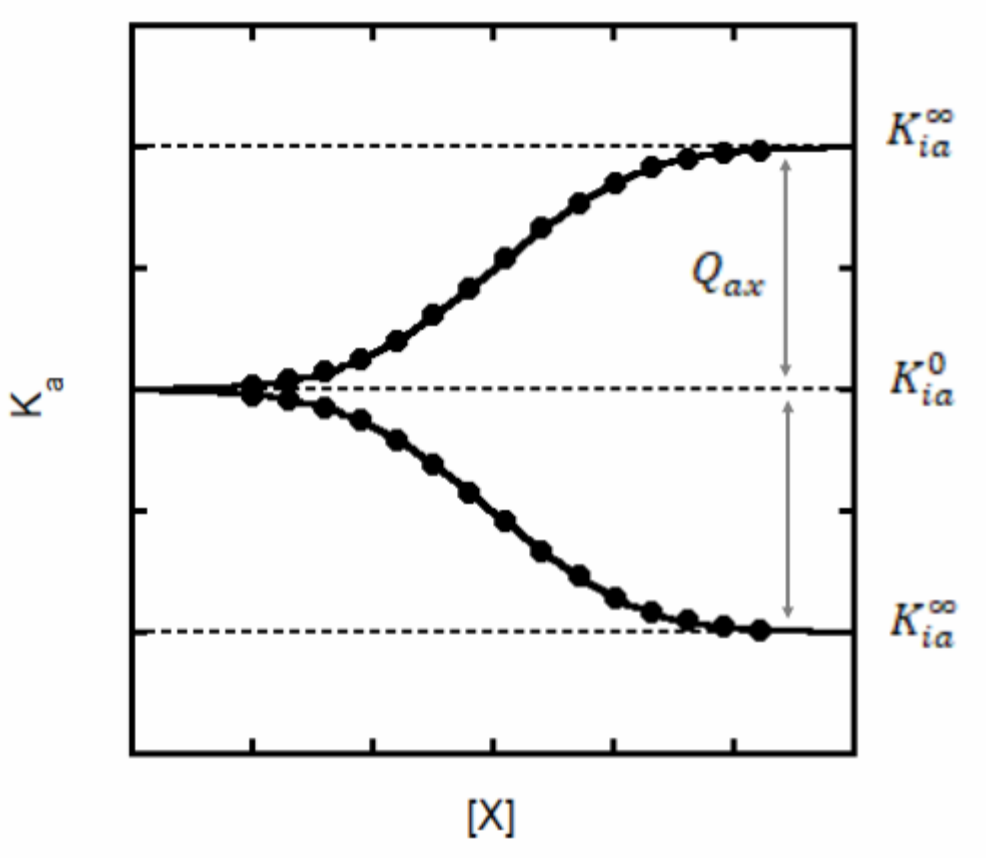

Figure 1-5: Graphic representation of the allosteric coupling ($\boldsymbol{Q_{ax}}$) between substrate (A) and an allosteric effector (X). The allosteric effector is demonstrated as an inhibitor (top), and an activator (bottom)

The rate equation for a homotetrameric enzyme such as phosphofructokinase must include additional parameters for homotropic cooperativity. However, the relationship between K_a and Q_{ax} formulated in equation 1-12 applies even to more complicated regulatory systems. The apparent

dissociation constant is equal to the concentration of substrate at which the catalytic rate is ½ maximum and is described by the Hill equation:

$$\frac{v}{[E]} = \frac{k_{cat}[A]^{n_H}}{K_a^{n_H} + [A]^{n_H}} \quad \text{1-13}$$

where k_{cat} is the turnover number and n_H is the Hill number which depicts the degree of cooperativity in substrate binding. A Hill number greater than 1 ($n_H > 1$) indicates positive cooperativity, a Hill number less than 1 ($n_H < 1$) indicates negative cooperativity. When the value of $n_H = 1$ no cooperativity is observed, and the resulting binding curve behaves according to Michaelis Menten kinetics. The Hill number is related to the coupling constant between associated binding sites. For a dimer, this relationship can be expressed according to the following equation[66]:

$$n_H = \frac{2(Q_{aa})^{1/2}}{1 + (Q_{aa})^{1/2}} \quad \text{1-14}$$

where Q_{aa} is the coupling constant between two substrate binding sites. The mathematically limiting values of n_H (2-0) could only occur in the impossible conditions that the coupling constant was either ∞ and 0 respectively. Reinhart suggested a range of n_H values for dimer of 1.7-0.3 based on a practical maximum of coupling free energies.[66] Abeliovich developed a statistical interpretation of n_H for a system of multiple identical binding sites.[18] This study found the range of possible values to be $1/N \leq n_H \leq N$, where N is the number of binding sites.

An enzyme can have multiple allosteric ligand binding sites. A second ligand (Y) which changes the apparent K_a of the substrate could achieve its effect by a modification to any combination of the parameters K_{ia}^0, K_{ix}^0, Q_{ax}. Each of these three effects can be qualitatively determined by inspecting the effect of Y on a plot of K_a as a function of X.[52] (Figure 1-6.)

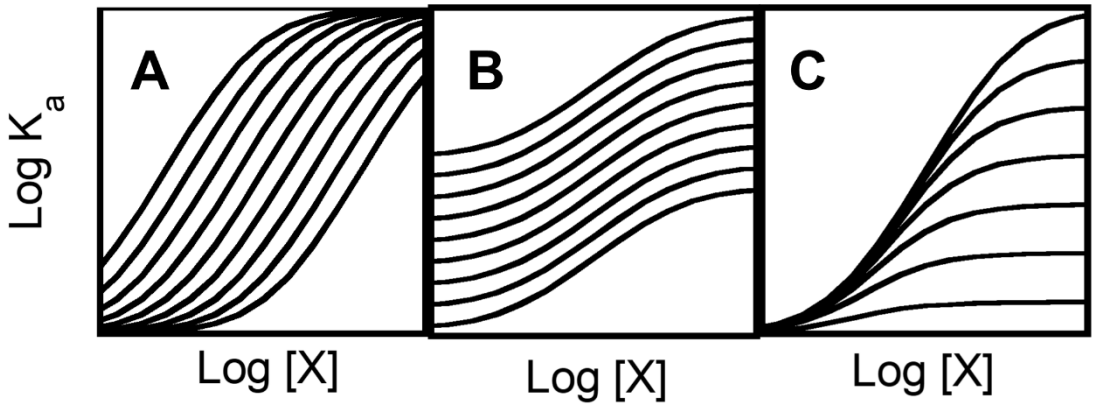

Figure 1-6: Simulated data demonstrating the three mechanisms by which a second allosteric ligand (Y) can appear to modify the apparent $\boldsymbol{K_a}$ for substrate. The solid curves in each are calculated using equation 1-12 which describes the relationship between X and A when X is an inhibitor. Each individual curve is simulated assuming a different concentration of Y. If Y acts on the dissociation constant of X $\left(\boldsymbol{K_{ix}^0}\right)$, the resulting change in the curve is demonstrated in panal A. If Y acts independently of X to modify $\boldsymbol{K_{ia}^0}$, the change in the curve occurs as presented in panel B. If the effect of Y is to modify the value of $\boldsymbol{Q_{ax}}$ then panel C gives the expect change in the curve.

A quantitative description of these effects can be obtained from the rate equation of a system with one substrate and two allosteric effectors in which the rapid equilibrium assumption is valid:[52, 65]

$$\begin{aligned} & v/[E] \\ & = \left(V^0 K_{ix}^0 K_{iy}^0 [A] + V^0 K_{iy}^0 Q_{ax} W_x [A][X] + V^0 K_{ix}^0 Q_{ay} W_y [A][Y] \right. \\ & \left. + V^0 Q_{axy} W_{xy} [A][X][Y]\right) \\ & /\left(K_{ix}^0 K_{iy}^0 [A] + K_a^0 K_{iy}^0 [X] + K_a^0 K_{ix}^0 [Y] + K_{iy}^0 Q_{ax} [A][X] \right. \\ & + K_{ix}^0 Q_{ay} [A][Y] + K_a^0 Q_{xy} [X][Y] + Q_{axy} [A][X][Y] \\ & \left. + K_a^0 K_{ix}^0 K_{iy}^0 \right) \end{aligned} \qquad \text{1-15}$$

where K_{iy}^0 is the dissociation constant of Y in the absence of X or A, Q_{ay} is the coupling constant between A and Y, Q_{xy} is the coupling constant between X and Y, W_y is the effect of Y on the turnover number, W_{xy} is the collective effect of X and Y on the turnover number, and Q_{axy} is the coupling constant between all three ligands. The coupling free energy between all three ligands $\left(\Delta G_{axy}\right)$ is the difference between the free energy of binding of all three ligands and the sum of the binding free energies of each ligand to free enzyme.

The value of apparent Michaelis constant under the influence of both X and Y is given by an expression derived from equation 1-15 in the same manner as equation 1-12 is derived from 1-11:[52]

$$K_a = K_a \left[\frac{K_{ix}^0 [X] + K_{ix}^0 [Y] + Q_{xy} [X][Y] + K_{ix}^0 K_{iy}^0}{K_{iy}^0 Q_{ax} [X] + K_{ix}^0 Q_{ay} [Y] + Q_{axy} [X][Y] + K_{ix}^0 K_{iy}^0}\right] \qquad \text{1-16}$$

The effect of a secondary effector Y on the parameters of a primary effector X can be expressed according to the following relationships:[52]

$$K_a^{0\prime} = K_a^0 \left[\frac{K_{iy}^0 + [Y]}{K_{iy}^0 + Q_{ay}[Y]}\right] \quad 1\text{-}17$$

$$K_{ix}^{0\prime} = K_{ix}^0 \left[\frac{K_{iy}^0 + [Y]}{K_{iy}^0 + Q_{xy}[Y]}\right] \quad 1\text{-}18$$

$$Q'_{ax} = \frac{\left(K_{iy}^0 + [Y]\right)\left(K_{iy}^0 Q_{ax} + Q_{axy}[Y]\right)}{\left(K_{iy}^0 + Q_{ay}[Y]\right)\left(K_{iy}^0 + Q_{xy}[Y]\right)} \quad 1\text{-}19$$

Due to reciprocity, equations 1-17. 1-18 and 1-19 can describe the effect of ligand X on the allosteric parameters of ligand Y by simply switching the occurrences of X and Y in the equations.[65] Substituting equations 1-17, 1-18, and 1-19 into equation 1-16 yields the following equation:

$$K_a = K_{ia}^{o\prime}\left(\frac{K_{ix}^{o\prime} + [X]}{K_{ix}^{o\prime} + Q'_{ax}[X]}\right) \quad 1\text{-}20$$

Equation 1-20 is functionally indistinguishable from equation 1-12 and describes the relationship between the apparent dissociation constant of substrate and primary allosteric effector at any non-variable concentration of secondary allosteric effector.

Thermodynamic linkage analysis differs from the previously described models of allostery in two regards. The first point of divergence is in the direction of the structure function relationship. Most models of allostery strive to determine the structural elements of an allosteric signal and then ascribe them to a functional response. Thermodynamic linkage analysis determines the functional response first, which can then be imposed as functional restraints when interpreting structural elements. The second point of divergence is in number of protein states

necessary to describe the allosteric signal. Although not necessary to the model's foundation, every model presented above utilizes a two-state description of allostery; an active and inactive state. Thermodynamic linkage analysis requires four protein states; Apo, effector bound, substrate bound and ternary.

The two differences between thermodynamic linkage and other allosteric models do not make them mutually exclusive. A two-state model can be obtained in a handful of limiting conditions in which the structure of each of the two ligand bound states are indistinguishable from Apo and/or ternary complex. However, reliance on a two-state model detracts from the critical elements necessary to define an allosteric signal. Additionally, any structure first approach becomes far too complicated to rationalize in systems of increasing complexity. For an example, consider the application of structural models to the allosteric regulation of eukaryotic phosphofructokinase (PFK). PFK has at least 5 ligand binding sites[67] plus it polymerizes.[49] Thus, absent of a two-state assumption, structural models require consideration of at least 16 different structures and an additional model to account for the role of polymerization.

Brief History of Phosphofructokinase

Glycolysis is important in nearly all organisms[68]. The first committed step of glycolysis is the MgATP dependent phosphorylation of Fru-6-P to Fru-1,6-BP catalyzed by phosphofructokinase (PFK; EC 2.7.1.11). As the gatekeeper of

glycolytic flux, PFK is heavily regulated, in part by small molecule allosteric effectors. The importance of regulating glycolytic flux extends well beyond energy regulation and includes carbon distribution, redox balance, cell cycle regulation, tumor formation and the adaption of cells to oxidative stress.[69, 70] PFK can be found in nearly all organisms. While the relatively simple allosteric regulation of prokaryotic PFK can be summarized by two effectors[71], regulation of eukaryotic PFK is considerably more complex and diverse.[72] The specific demands of various eukaryotic organisms required extensive differentiation of PFK, resulting in a several PFK homologs. While the catalytic activity of various PFK homologs remains highly conserved, the regulatory properties greatly vary to serve their individual purposes. Three different PFK homologs; muscle, platelet and liver PFK; are produced by mammalian organisms. The regulatory properties of each of these homologs are tuned for the specific needs of their respective tissues. It is the aim of this introduction to explore the considerable complexities of mammalian PFK, and particularly liver PFK.

The reaction catalyzed by phosphofructokinase was first discovered in red blood cells by Dische[73], and later in muscle by Ostern et. al[74]. Mammalian PFK was first purified from rabbit muscle by Ling et. al.[75] and has subsequently been the subject of extensive study; for reviews see [72, 76]. The physical and kinetic properties of mammalian PFK, as well as its mechanisms of regulation, are considerably complex. A long list of ligands has been identified as allosteric effectors of mammalian PFK; principle among these are the metabolites MgATP, Fru-1,6-BP,

Fru-2,6-BP, Citrate, AMP, cAMP, P_i, as well as $(NH_4)_2SO_4$ and pH. Perhaps the most important of these is inhibition by the substrate MgATP. MgATP is a substrate, and hence obligatory for PFK catalytic activity. MgATP is also the end-product of glycolysis and thus, allosteric inhibition by MgATP represents classic feedback inhibition. A feedback rationale can be applied to many of the other metabolites as well. Conditions indicating an energy rich environment, such as high citrate, inhibit the enzyme whereas conditions indicating energy poor conditions, such as AMP and P_i activate PFK. Another important allosteric effector of PFK is Fru-2,6-BP. Unlike other allosteric effectors of PFK, Fru-2,6-BP does not represent a downstream metabolite but instead is produced by an enzyme whose activity is under hormonal control.[77]

Attempts to ascertain the kinetic mechanism are complicated by the allosteric regulation of mammalian PFK by free Mg^{2+}, ATP and Fru-1,6-BP, especially when performed at low pH. The effects of Mg^{2+} can be ignored by including a saturating amount of Mg^{2+} and kinetic assays can be performed at a pH above 8.0 to, in the case of rabbit muscle PFK, mitigate the allosteric inhibition by MgATP. Initially it was thought that PFK operated by a Ping Pong mechanism[78] due to the nearly parallel double reciprocal plots of initial velocity kinetics. However, later initial velocity kinetics measurements found non-parallel double reciprocal plots, [79, 80] thus ruling out a ping pong mechanism and indicating that the reaction is sequential. Product inhibition experiments distinguish between random or ordered addition of substrates. If the mechanism was random, product Fru-1,6-BP would be

competitive with Fru-6-P but noncompetitive with MgATP whereas the product ADP would be competitive with ATP but noncompetitive with Fru-6-P[81]. Bar-Tana and Cleland provided the evidence to support a random mechanism in rabbit muscle PFK[82, 83]

Taylor and Bew reported in 1970 that PFK obtained from rat liver tissue was chromatographically distinct on DEAE-cellulose from PFK obtained from rat muscle.[84] This supported a growing hypothesis that multiple isozymes of PFK might exist, and could account for the differing regulation of glycolysis in various tissues.[85, 86] By 1983 it was accepted that at least 3 separate PFK isozymes exist in mammalian tissues[87]. PFK-M and PFK-L are found primarily in the muscle and liver tissue of rats, respectively[88, 89]. A third isozyme, designated as PFK-C in rabbits [90] and PFK-F [91] or PFK-P[92] in humans, was found in various tissues in combination with PFK-M and PFK-L. The existence of 3 isozymes was ultimately confirmed when three different PFK genes were identified on separate chromosomes.[93-95] The kinetic and regulatory properties of the three isoforms are qualitatively very similar, although they differ in subtleties. For example, PFK-M is less sensitive to ATP inhibition than PFK-L or PFK-P[96] and PFK-P is nearly completely insensitive to activation by AMP[97]. An extensive review on the different isoforms and their properties has been written by Dunaway[87].

While muscle tissue exclusively expresses the muscle PFK isoform, liver tissue has 2 cell types. Dunaway et al. suggest that two isozymes of PFK are expressed in liver tissues.[98] The major isozyme, PFK-L_2, is thought to be made

entirely of liver PFK subunits (PFK-L), whereas the minor isozyme, PFK-L_1, is suggested to be a hybrid of 3 PFK-L monomers and 1 PFK-M monomer. Using a combination of immunological and chromatographic techniques, Dunaway et. al. demonstrated that, with the exception of muscle tissue, a combination of PFK isozymes are expressed in all tissues leading to a complex mixture of PFK isoforms.[99, 100] This was demonstrated in humans and in rats but is thought to extend to most mammalian organisms[72]. It has been shown that hybrid species can be formed with kinetic properties intermediate to that of the parent species.[101]

The most widely studied source of eukaryotic PFK has historically been rabbit muscle, which exclusively expresses the aptly named muscle form of the enzyme.[51] PFK from rat livers and isolated hepatocytes has also been extensively studied.[47, 49-52, 69, 96, 98, 102-108] Studies directed towards a direct comparison between rabbit muscle and rat liver PFK reveal that they share qualitative similarities in terms of activity and allosteric regulation.[96] However, liver PFK is more sensitive to pH and MgATP inhibition, and demonstrates diminished activation by AMP and inhibition by citrate. Liver PFK also forms higher order oligomers more readily than muscle PFK. PFK has been isolated and studied from various other tissues including heart, brain, spleen, testes, and kidneys, and found to have kinetic and allosteric properties different than that reported for either muscle or liver. However, these tissues, and others, do not represent any pure form of PFK, but instead a complicated mixture of PFK-M, PFK-L and the third form which will be referred to as platelet PFK (PFK-P). Despite lending its name to PFK-P platelet

isolations do not express exclusively platelet PFK.[99, 100] In fact, no natural tissue expresses PFK-P much beyond a 50% mixture. Efforts were made to isolate PFK-P out of native tissues to study its properties separated from its co-expressed isozymes, but the process has been made much easier through recombinant expression.[109, 110] PFK-P is more similar to PFK-L than PFK-M in terms of its activity and allosteric regulation. When compared to PFK-M, both PFK-P and PFK-L have a lower affinity for Fru-6-P, a higher affinity for catalytic MgATP binding, and an increased sensitivity for inhibition from MgATP and pH.[67, 111] PFK-P and PFK-L differ in that PFK-P is not activated by Fru-1,6-BP and is subjected to inhibition by phosphoenolpyruvate.[111]

Regulation of RLPFK by covalent modification

Eukaryotic enzymes are often post translationally modified to regulate their activity, cellular location or to mediate interaction with other proteins. Proteins expressed recombinantly in *E. coli* are not subjected to post translational modification; and therefore, properties that are dependent on a modification will be improperly represented in *in vitro* studies performed with recombinant protein. PFK has been observed to undergo phosphorylation, glycosylation and acetylation and it is important to understand how these modifications alter the properties of mammalian PFK. The reported effects of posttranslational modifications are disused in the following paragraph. To briefly summarize, phosphorylation is not thought to have any direct effect on the kinetics or ligand binding properties of

RLPFK, and glycosylation and acetylation are seen to inhibit mammalian PFK activity in some fashion.

The effect of phosphorylation on RLPFK was debated over the course of a decade and is still considered uncertain. Brand and Söling were the first to demonstrate phosphorylation of PFK isolated from rat livers[112, 113]. They presented data that suggested RLPFK was activated through phosphorylation by a cyclic 3',5' – AMP (cAMP) independent phosphorylase.[112] Nearly every aspect of this paper was subsequently disproven. Six years later it was understood that the enzyme activation and phosphorylation were two separate events; and that the phosphorylating enzyme actually was cAMP dependent[114]. The activation Brand and Söling observed in their 1976 paper was not due to phosphorylation, but MgATP facilitated re-association of inactive protomers to restore the obligatory active tetramer. This paper has been cited as providing definitive evidence of regulation by phosphorylation by papers published as recently as 2014.[115, 116] However the question of regulation by phosphorylation continued well beyond the initial Brand and Söling paper.

Other labs published observations of RLPFK phosphorylation enhanced by administration of glucagon in vivo[117], in perfused livers [118] and isolated hepatocytes[119]. In each case, introduction of glucagon resulted in phosphorylation of RLPFK with simultaneous increase in cAMP concentration as well as inhibition of RLPFK in the form of decreased Fru-6-P affinity. Glucagon was known to cause a decrease in glycolysis and increase in gluconeogenesis.[120] It was appealing to

conclude that phosphorylation triggered inhibition of PFK could contribute to glucagon's regulatory effect. However, the differential Fru-6-P affinity only existed in crude isolations and disappeared upon further purification[119]. This observation combined with the observations that direct cAMP induced phosphorylation does not inhibit RLPFK suggested that the apparent inhibition of RLPFK was not induced by phosphorylation but some other mechanism of glucagon. It would soon be understood that the glucagon triggered inhibition of RLPFK was caused by depletion of the activator, fructose 2,6-bisphosphate[121, 122].

Before the identification of the elusive "activator factor" as Fru-2,6-BP[123], Furuya and Uyeda isolated a high and a low phosphate containing form of RLPFK and observed a greater affinity for "activating factor" in the high-phosphate form.[124] It was postulated that the decreased MgATP sensitivity previously observed in phosphorylated PFK was due to activating factor (Fru-2,6-BP) preferentially binding to the high phosphate form of PFK.[124-126] However, Pilkis et al published a contrasting study by cycling through dephosphorylated and phosphorylated states of RLPFK *in vitro* and monitoring effects to activity and allosteric regulation.[122] This *in vitro* study demonstrated that purified RLPFK is a substrate for phosphorylation by cAMP dependent protein kinase, but phosphorylation had no effect on the kinetics or ligand binding properties of RLPFK.[122] It was demonstrated, however, that RLPFK could be made more sensitive to activation by Fru-2,6-bisphosphate after limited proteolysis. The proteolysis removed the carboxyl terminal phosphorylation site, lending to the proposal that the low phosphate form studied

by Furuya and Uyeda was a proteolytically cleaved form of RLPFK.[122] The cautionary tale here is that simple enzymatic assays may not be sufficient to verify functionality when the properties of allosteric regulation are the topic of interest.

Some insight into a physiological role of phosphorylation of liver PFK could be gained by looking at the role that phosphorylation plays in the homologs of RLPFK. Both liver and muscle isoforms of PFK are phosphorylated on a conserved serine, 6 residues from the C-terminus.[127] For years, researchers of mammalian skeletal muscle PFK experienced many of the same frustrations of uncertainty. It was observed that covalent phosphorylation of PFK occurs in the skeletal muscle of mice and rabbit.[128-131] However, phosphorylation by cAMP-dependent protein kinase was not seen to cause a significant change in the properties of muscle PFK save for a minor increase in sensitivity to ATP inhibition.[125, 132] A physiological role for phosphorylation was suggested when it was observed that phosphorylation promotes association of rabbit muscle PFK with F-actin.[133] F-actin acts as an effector of phosphorylated muscle PFK[134], but not de-phosphorylated muscle PFK[133]. According to these data, phosphorylation can act as an activator of muscle PFK by redirecting its cellular location to the cytoskeleton where it is subsequently activated. Despite phosphorylation occurring on the same serine residue in both muscle and liver tissues, it is unlikely that liver would experience the same process of activation as muscle PFK. In muscle PFK, conditions that promote phosphorylation of PFK (i.e. insulin) also promote an increase in glycolysis, giving cause to PFK activation. However, conditions that promote phosphorylation in liver

instead inhibit glycolysis and stimulate gluconeogenesis. Indeed, it has been shown that conditions that activate PFK in muscle, as well as effects muscle PFKs cytosolic localization can inhibit liver PFK while having no effect on the cytosolic distribution.[135] Perhaps the phosphorylation site on RLPFK is merely an evolutionary artifact not fully lost after the tissue specific differentiation of glycolytic needs.

In addition to phosphorylation, muscle PFK has been observed to be reversibly inactivated by acylation on the residues Cys-114, Cys-170, Cys-351, and Cys-577. This has not been demonstrated in liver PFK.[136] Glycosylation of PFK has been observed in human lung cancer cells.[137] Although this glycosylation event has not been directly demonstrated in liver PFK, the glycosylation site, Ser529, is a highly conserved residue important for regulation of PFK1 by fructose-2,6-bisphosphate. The resulting modification down regulates PFK by inhibiting the binding of Fru-2,6-BP.[137]

In summary, post translational modification may play a role in regulating PFK. However, it is not obligatory for regulation by small molecule allosteric effectors. In-vitro studies performed on recombinantly expressed rat liver PFK should adequately represent the allosteric regulation the enzyme experiences in the cell.

Structure and evolutionary history of eukaryotic PFK

Eukaryotic PFK is thought to have evolved from prokaryotic PFK through gene duplication and tandem fusion followed by differentiation[138] (Figure 1-7). The yeast PFK was subjected to a second duplication event[139], resulting in an octamer. Crystal structures have been obtained from a dimeric form of rabbit muscle PFK [140] and human muscle PFK[141], and the tetrameric human platelet PFK[109, 142]. These structures illustrate an oblate ellipsoid with the dimensions of approximately 14X10nm. (Figure 1-8) Within the structure, 2 of the 4 catalytic sites are marked by the substrate Fru-1,6-P and product ADP on the polar ends of the tetramer. The FBP allosteric site (F') is at the tetramer interface. Putative allosteric sites for citrate (E'), ADP (N2) and ATP (N1/E) are marked. (Figure 1-8)

Each protomer of eukaryotic PFK can be characterized by two roughly symmetric halves; here named the N-terminus and C-terminus halves. Each protomer half begins with a nucleotide binding domain (NBD) followed by a substrate binding domain (SBD). The sequence of the N-terminal half of eukaryotic PFK is highly conserved both among eukaryotic isozymes and their prokaryotic precursors. The C-terminal half shares significantly less sequence homology and has undergone considerable evolutionary migration away from its duplicated template.

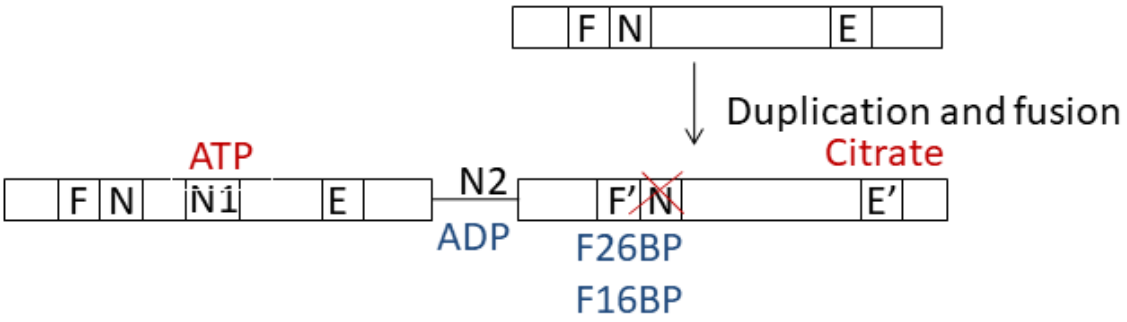

Figure 1-7: Evolutionary history of mammalian PFK. Gene duplication of and tandem fusion of prokaryotic ancestral gene resulted in a two-domain mammalian PFK. Sugar and nucleotide binding sites are represented as F and N respectively. Allosteric ligand binding sites are labeled E. Prime sites are duplicate sites that have undergone evolutionary drift. Novel nucleotide sites (N1 and N2) evolved independently from ancestral sites after duplication.

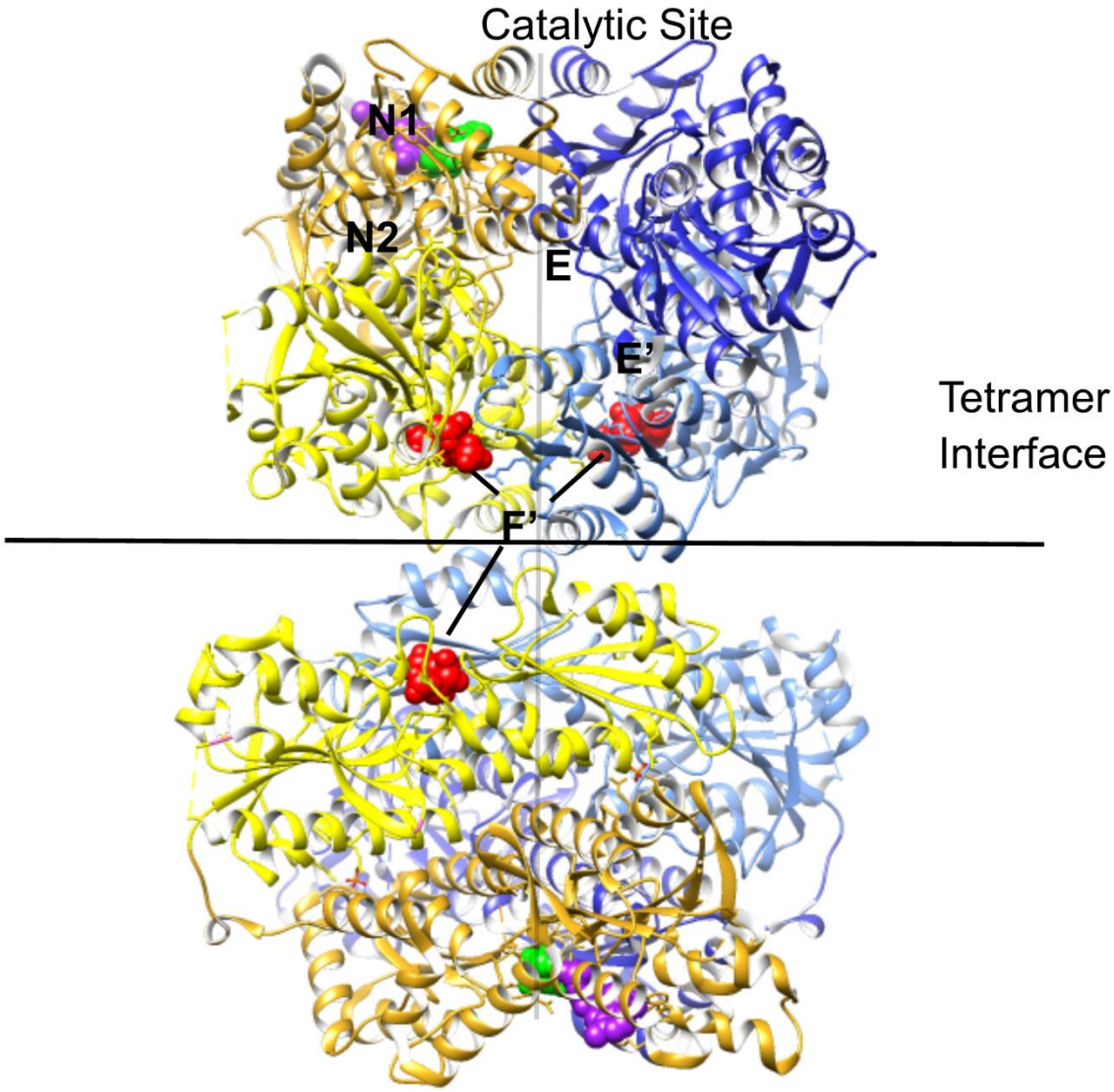

Figure 1-8: Crystal structure of human platelet PFK (PDB 4XZ2). Four chains are represented, two in yellow and two in blue. N-terminal halves are represented by a darker color than the C-terminal halves. Two of the four catalytic sites are represented by reaction substrate Fru-6-P and reaction product ADP (shown as green and purple spheres respectively). Activator Fru-1,6-BP (red spheres) is shown bound to the F' site. Putative binding sites for citrate (E'), ADP (N2) and ATP (E/N1) are indicated.

The catalytic activity is composed by the N-terminal halves of two monomers. The two monomers align in an anti-parallel conformation, with the NBD of one N-terminal half interacting with the SBD of the other N-terminal half. The dimer resembles the prokaryotic tetramer with important catalytic residues conserved among eukaryotic and prokaryotic homologs. The catalytic site rests in the dimer interface.

The C-terminal half of the protomer is responsible for regulation of enzymatic activity. The C-terminal ancestral catalytic site no longer binds nucleotide to any measurable amount and the sugar binding residues have been adapted to bind activating sugars Fru-1,6-BP and Fru-2,6-BP. Fru-2,6-BP is bound to the crystal structure of *Saccharomyces cerevisiae* PFK[140] and Fru-1,6-BP is bound to the crystal structure of HpPFK.[142] Both sugars bind to the same site but do so in opposite conformations. The residues predicted to interact with the activators agree with mutational studies performed with rabbit muscle PFK.[143, 144] The occupation of Fru-1,6-BP and Fru-2,6-BP at the same site is consistent with the observation that unlike AMP which acts synergistically with Fru-2,6-BP[123, 145], Fru-1,6-BP can act antagonistically to the activation by Fru-2,6-BP[146]. Although the F-2,6-BP binding site is at the tetramer interface, it is constructed only of residues interacting at the dimer interface.

Duplication of the ancestral prokaryotic allosteric effector binding site resulted in two putative ligand binding sites designated as E in the N-terminal half and E' in the C-terminal half (Figure 1-7). In prokaryotic PFK, ADP and PEP bind at

the tetramer interface. However, in eukaryotic PFK the two halves within a subunit fold over onto each other so that the E and E' sites are constructed by a single subunit. (Figure 1-8) The sites are highly divergent from the prokaryotic sites that once bound ADP and PEP, but several key polar residues still line the site. The citrate binding site is thought to be an adaptation of the ancestral allosteric site retained on the C-terminal half of the eukaryotic monomer, designated as E' in (Figure 1-7). Site directed mutagenesis to E' residues in rabbit muscle PFK abolished inhibition by citrate.[144] No structures of PFK with citrate bound exist. Instead, phosphate is seen coordinated with polar residues lining E' in both structures of human platelet PFK and rabbit muscle PFK.[140, 142, 147]

The location of the ATP allosteric site remains more controversial than the citrate allosteric site. The ancestral E site is an obvious suspect as an ATP binding site. Site directed mutagenesis to residues within the E site diminished ATP inhibition.[144] However, crystal structures of rabbit muscle PFK[140] and *Pichia pastoris* PFK (PpPFK)[148] contain electron density attributed to ATP bound at a novel nucleotide binding site, N1, located 11Å away from the E site. Site directed mutagenesis to residues interacting with ATP at N1 also resulted in a RMPFK with greatly reduced sensitivity to MgATP.[149] It is possible that multiple MgATP binding sites exist as Reinhart found duel allosteric functions of MgATP.[108] No ATP was seen bound to either the N1 or the E site of the hpPFK structures despite inclusion of 10mM MgATP.[109, 142] Phosphate, a known activator of eukaryotic PFK, is bound to the E site of hpPFK.[150] It was suggested that phosphate binding and MgATP binding

are mutually exclusive[109]. More studies, structural and otherwise, will be necessary to unambiguously assign the site of allosteric regulation by MgATP.

A second novel nucleotide binding site, N2, was found containing ADP in the middle of the RMPFK subunit.[140] It is assumed that this is the ADP/AMP activation site. In the crystal structure, the ADP diphosphate moiety is coordinated by Ser^{377} and Lys^{678}. Mutating these residues to an alanine decreased sensitivity to ADP activation, without perturbing activation by AMP.[149] Asn341, which is seen interacting with the ribose of ADP was mutated to alanine resulting in enzyme activation by both ADP and AMP, giving credence to the location of N2 as the site of allosteric activation by AMP and ADP.

Study of RLPFK polymerization

The ability of mammalian PFK to oligomerize to species larger than the obligatory tetramer has been known since the first isolation of PFK from rabbit muscle [75] Polymerization has been seen in all three mammalian isoforms, but the greatest propensity for self-association is ascribed to PFK from liver sources. [96, 151] Polymerization can be problematic for many biochemical assays, efforts were even made to circumvent polymerization in order to crystalize PFK.[142] However, polymerization has also been exploited to great success in efforts of purification by gel filtration.[51, 102] It would seem as though biology also exploits polymerization, as it has been proposed that self-association of RLPFK activates the enzyme by increasing its affinity for substrate Fru-6-P.[49, 50, 104, 152] Unfortunately, the extent of

this activating effect has yet to be demonstrated and consequently its physiological relevance is uncertain. Concentration dependent activation of RLPFK provides an appealing explanation for the notable difference in catalytic activity between activity measured in liver perfusion assays[153, 154] and activity predicted based on *in-vitro* kinetic assays[51].

The degree at which an enzyme is self-associated strongly depends on the concentration. Fluorescence polarization studies performed on RLPFK at concentrations of physiological relevance, and gel filtration experiments of liver homogenate, both suggest that at the relatively high concentrations of the cell, RLPFK primarily exist in the polymerized form. [49]. PFK from both liver and muscle have been demonstrated to exist almost entirely in the tetramer form at the sub-nanomolar concentrations necessary for *in-vitro* kinetic assays,.[50, 155] Sub-nanomolar concentrations are necessary for the commonly used coupled kinetic assays of RLPFK in order to avoid NADH depletion as well as product induced activation. In addition to concentration dependences, the extent of RLPFK polymerization strongly depends on the solution conditions. Activating conditions stabilize the polymer form and inhibiting conditions promote the tetramer form.[49, 50, 104, 107] Specifically, Fru-6-P stabilizes the polymer and MgATP stabilizes the tetramer.[49, 50] A Weber linkage argument presented by Reinhart and Lardy[36, 98] suggest that the shift in tetramer-polymer equilibrium induced by Fru-6-P indicates that the polymer has a greater affinity for Fru-6-P.[49]

To relate the catalytic and regulatory properties of RLPFK measured in *in-vitro* assays[49, 105] to properties of RLPFK in cellular conditions[153, 154] it is important to understand the role of concentration dependent polymerization on substrate affinity. Some efforts have been made to measure the catalytic properties of RLPFK in the polymerized state. These include increasing the concentration of RLPFK in kinetic assays[49] and inducing polymerization with polyethylene glycol (PEG) without increasing the concentration of RLPFK.[107] Other than these two exceptions, assays have been performed under conditions in which the tetramer is the predominant species. The implication is that all the known regulatory properties of RLPFK are relative to an already inhibited form. A thorough description of the regulatory pathways of RLPFK must include the interplay between ligand concentration and oligomerization state of the enzyme.

A method is needed that can rapidly and accurately measure the size of RLPFK oligomer at a wide range of RLPFK concentrations to further the understanding RLPFK self-association and its role in regulation. Fluorescence polarization[50], analytical ultracentrifugation[156], size exclusion chromatography[157], dynamic light scattering[158] and electron microscopy[159] have all been used to characterize the oligomer size. These techniques work best at high enzyme concentrations, and therefore cannot span the range of sub-nanomolar to micromolar concentrations. Fluorescence correlation spectroscopy (FCS) can be used to determine the oligomeric size of RLPFK. The advantages of FCS include; (i) the ability to resolve particle sizes over a broad range of potential sizes, (ii)

capability of assaying enzyme concentrations ranging from sub nanomolar to micromolar and (iii) is time and cost effective enough to justify repetitive measurements following minute, systematic changes in assay conditions. Using FCS, one can address questions such as whether RLPFK is a tetramer at concentrations used for kinetic assays, the presence of discrete or mixed species in the polymerized form, rate of tetramer dissociation from polymerized form, and critical ligand concentration necessary to stabilize polymerized species.

Fluorescence Correlation Spectroscopy

Fluorescent correlation spectroscopy (FCS) is a method that can measure kinetic properties that result in a change in a fluorescent signal. The information by which FCS measures kinetic properties is the fluctuations around an average fluorescent signal. FCS can be used to measure photophysical effects, chemical kinetics and diffusion.

The intensity of a signal fluctuations is inversely proportional to the number of particles. A large number of particles will mask signal fluctuations in the average fluorescence signal. Therefore, autocorrelation of fluorescent fluctuations requires either very low concentrations of emitting fluorophores, or very small observation volumes. The theory of FCS was worked out by Elson and Magde in 1972,[160, 161] however, the technical challenges of measuring very small volumes and/or very low concentrations were too great at the time. It would be several decades before

the technology could catch up so that the theory could widely be put into practice. Advances in light sources, detector sensitivity and microscope optics were necessary to reach the low occupation numbers at which FCS performs best.[162]

A greater sensitivity in detectors was one necessary advancement as it allowed for the ability to detect particles in the single molecule range. Of equal importance is the ability to excite fluorophores in a tightly confined space. This ability was afforded by stable, high quality coherent light sources as well as high numerical aperture objectives. These advancements allow for the focusing of a light beam to near diffraction limited volumes. Objectives can only confine the radial axis of the light beam, it does not confine the axial pathway. The axial length could be confined by restricting the sample volume, such as between glass slides or in capillary tubes, but most often this is done by confocal techniques. A confocal microscope uses a pinhole to eliminate any out of focus light and thereby restricts the axial length of the observation volume. Two-photon excitation naturally confines the observation volume due to the quadradic dependence of 2-photon excitation on the light intensity.[163]

FCS measures the diffusion of fluorophores moving through a small, open observation volume, in which, they fluoresce. (Figure 1-9 A) The diffusion of fluorophores into and out of the observation volume is measured as temporal fluctuations in a fluorescent signal. (Figure 1-9 B) The autocorrelation function is a statistical analysis used to extract information from the fluctuations:[164]

$$g(\tau) = \frac{\langle \delta F(t) \delta F(t+\tau) \rangle}{\langle F \rangle^2} \quad \text{1-21}$$

where F is the fluorescence signal, $\delta F(t)$ is the fluctuation in the fluorescent signal at time t $(F(t) - \langle F \rangle)$, and $\delta F(t+\tau)$ is the fluctuation in the fluorescent signal at time $t + \tau$. The angular brackets denote a time average over the fluorescence signal. The value of $g(\tau)$ defines how long an average fluctuation persist after a period of time (τ) has passed. The autocorrelation function measures how long fluctuations persist, and an autocorrelation curve describes the temporal decay of fluorescence fluctuations. (Figure 1-9 C).

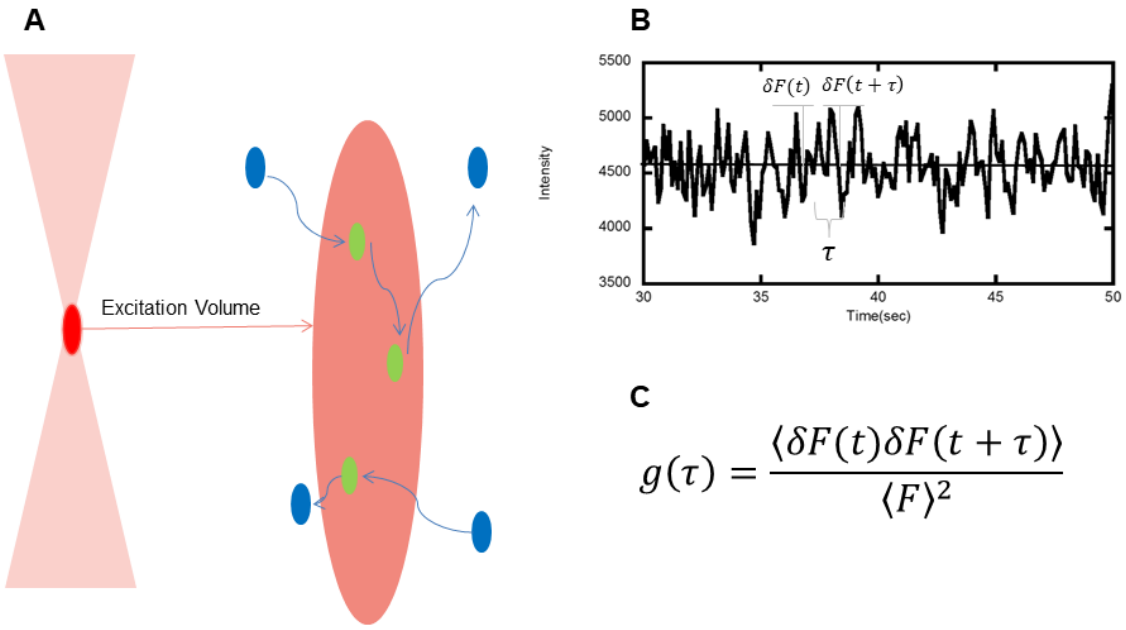

Figure 1-9: Schematic of fluorescence fluctuation measurements. 1.Laser light source is focused by a high numerical aperture objective to a fine point. Light red double cone is full path way of the light source. Dark cone is region in which the laser is focused enough to achieve a photon density high enough for 2-photon excitation to occur. B. Time dependent fluorescence signal. Signal fluctuates around an average signal. Fluctuations at an arbitrary time $\boldsymbol{t}$ are correlated with fluctuations at a time $\boldsymbol{t} + \boldsymbol{\tau}$. C. Autocorrelation function, see text.

Two pieces of information are apparent from the autocorrelation curve (Figure 1-10). The first is from the value of $g(0)$ which is inversely proportional to the number of particles in the observation volume according to:

$$g(0) = \frac{\gamma}{N} \qquad 1\text{-}22$$

where N is the number of particles and the factor γ has a value of 0.5, 0.35 and 0.076 for a two-dimensional Gaussian point spread function (PSF), three-dimensional Gaussian PSF and Gaussian Lorentzian PSF respectively (see below). The second piece of information is the persistence time (τ_p) defined as the value of τ at which $g(\tau) = g(0)/2$. In a system in which temporal fluctuations are exclusively due to diffusion, the persistence time can also be called the characteristic diffusion time (τ_D), as it defines the time at which a particle can diffuse through an observation volume. The observed value of $g(0)$ and τ_D depend on both the properties of the sample and the instrumental setup and thus are not comparable from one system to another. To extract kinetic properties from an autocorrelation curve, a model must be used to interpret the data.

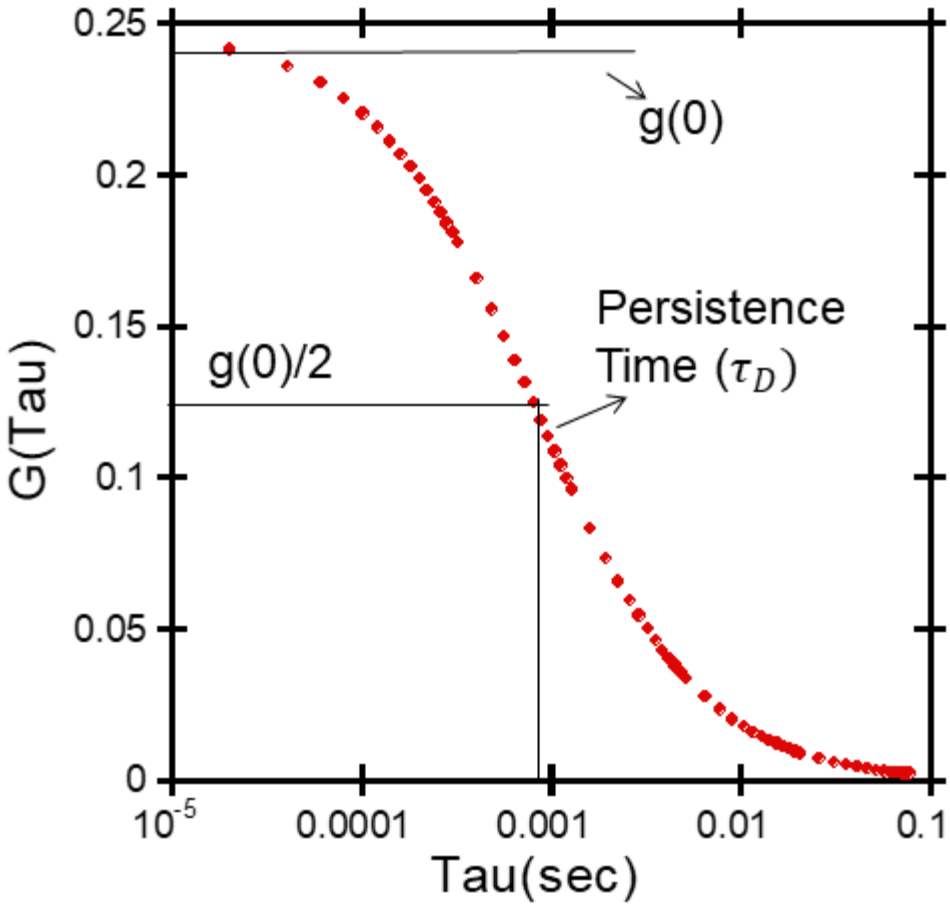

Figure 1-10: Example of an autocorrelation curve. $\boldsymbol{g(\tau)}$ values are calculated from fluorescence fluctuation data by equation 1-21. The value of $\boldsymbol{g(0)}$ is the value of $\boldsymbol{g(\tau)}$ when $\boldsymbol{\tau = 0}$ and is inversely proportional to the number of particles. Persistence time ($\boldsymbol{\tau_D}$) is the value of $\boldsymbol{\tau}$ at which $\boldsymbol{g(\tau)}$= $\boldsymbol{g(0)/2}$

Temporal fluorescence fluctuations occur as a function of the spatial and temporal properties of excitation light and particle concentration, as well as the physical properties of the fluorophores.[164] These three factors are accounted for according to the following function:[163]

$$F(t) = \alpha \int I^2(\vec{r}, t) C(\vec{r}, t)\, dV \qquad 1\text{-}23$$

where α is a value that accounts for the physical properties of the fluorophore (cross-section absorptivity, quantum efficiency and experimental collection efficiency), $I^2(\vec{r})$ is the light excitation profile, $C(\vec{r}, t)$ is the fluorophore density at position $\vec{r}$ and time t, $\vec{r} = (x, y, z)$, dV is the volume element and the integral is over all space. The relevant excitation profile is the square of the spatial intensity profile $\big(I(\vec{r}, t)\big)$ because of the quadradic dependence of 2-photon excitation on intensity.[163] The spatial intensity profile is dependent on the wavelength and coherent properties of the excitation light as well as the optical properties of the microscope.

Assuming a stable light source, the temporal fluorescence fluctuations are due only to temporal fluctuations in particle concentrations. The fluctuation of the concentration at position $\vec{r}$ and time t from the average value of $\langle C \rangle$ is

$$\delta C(\vec{r}, t) = C(\vec{r}, t) - \langle C \rangle \qquad 1\text{-}24$$

From equation 1-23, it follows that the average fluorescence and the fluorescence fluctuation at time t are[164]

$$\langle F \rangle = \alpha \langle C \rangle \int I^2(\vec{r}) dV \quad 1\text{-}25$$

$$\delta F(t) = \alpha \int \delta\, C(\vec{r}, t) I^2(\vec{r}) dV \quad 1\text{-}26$$

Using equations 1-25and 1-26 in equation 1-21 gives the fluorescence fluctuation autocorrelation function as:

$$g(\tau) = \frac{\iint I^2(\vec{r})\, I^2(\overrightarrow{r^*}) f(\vec{r}, \overrightarrow{r^*}, \tau) dV dV}{\left[\langle C \rangle \int I^2(\overrightarrow{r^*})\, dV\right]^2} \quad 1\text{-}27$$

where

$$f(\vec{r}, \overrightarrow{r^*}, \tau) = \langle \delta C(\vec{r}, t) \delta C(\overrightarrow{r^*}, t + \tau) \rangle \quad 1\text{-}28$$

is the correlation between a concentration fluctuation at position r and a concentration fluctuation at position r^* after a period of time τ. The sample is presumed to be stationary and so equation 1-28 depends upon τ but not absolute time t.

$$f(\vec{r}, \overrightarrow{r^*}, \tau) = \langle \delta C(\vec{r}, 0) \delta C(\overrightarrow{r^*}, \tau) \rangle \quad 1\text{-}29$$

Equation 1-29 attributes temporal fluctuations in the fluorescence signal precisely to fluctuations in fluorophore concentrations in a defined excitation profile. To interpret an experimental measurement in terms of particle diffusion, $\delta C(\overrightarrow{r^*}, \tau)$ must be expressed in these terms. Changes in particle concentration due to a particle undergoing diffusion can be expressed in terms of the diffusion coefficient (D) according to:[160]

$$\frac{d\delta C(\vec{r}, t)}{dt} = D \nabla^2 C(\vec{r}, t) \quad 1\text{-}30$$

A solution for equation 1-30 can be verified via Fourier transform:

$$\delta C(\vec{r},t) = \frac{\langle C \rangle}{\sqrt{4\pi D\tau}} exp\left(\frac{r^2}{4Dt}\right) \quad 1\text{-}31$$

This expression provides the relationship between temporal concentration fluctuations and the diffusion of a particle. However, it does not give any correlation information. Recognizing that the solution is stationary, as argued in equation 1-29, we get:

$$f\left(\vec{r},\overrightarrow{r^*},\tau\right) = \frac{\langle C \rangle}{\left(\sqrt{4\pi D\tau}\right)^3} exp\left(\frac{(r-r^*)^2}{4Dt}\right) \quad 1\text{-}32$$

Equation 1-32 is the probability of finding a diffusing particle at position r^* at time $t+\tau$ provided it was at position r at time t. This concludes half the equation necessary to explain an autocorrelation curve in terms of a diffusing particle. Equation 1-32 explains the temporal behavior of a particle diffusing through an observation volume, now we must define the volume in terms of the spatial intensity profile of excitation light. The spatial intensity profile is dependent on the light source, optics and wavelength of excitation. Below we list two common intensity profile models used for a well-focused light source

3D gaussian model with

$$I(\vec{r}) = I(x,y,z) = I_0 exp\left(-\frac{2(x^2+y^2)}{w_o^2} - \frac{2z^2}{z_0^2}\right) \quad 1\text{-}33$$

where w_0 is the beam waist and z_0 length in the direction of the excitation beam

3D Gaussian-Lorentzian model

$$I(\vec{r}) = I(x,y,z) = I_0 \frac{2I_0 w_0^2}{\pi w^2(z)} exp\left(\frac{-2(x^2+y^2)}{w^2(z)}\right) \quad 1\text{-}34$$

where

$$w^2(z) = w_0^2\left(1+\left(\frac{z}{z_R}\right)^2\right) \text{ and } z_R = \frac{\pi w_0^2}{\lambda} \quad 1\text{-}35$$

Substituting equation 1-32 and 1-33 into 1-27 gives

$$G(\tau) = \frac{2\sqrt{2}}{\pi\sqrt{\pi} w_0^2 z_0 \langle C\rangle}\left(1+\frac{8D\tau}{w_0^2}\right)^{-1}\left(1+\frac{8D\tau}{z_0^2}\right)^{-\frac{1}{2}} \quad 1\text{-}36$$

Substituting equation 1-32 and 1-34 into 1-27 gives

$$G(\tau) \quad 1\text{-}37$$

$$= \frac{2w_0}{\lambda\pi N\sqrt{4\pi D t}} \int_0^\infty \frac{b exp\left(-\frac{z_R^2 b^2}{4D\tau}\right)}{\left(\frac{16D\tau}{w_0^2}\right)+2+b^2} \frac{1}{\sqrt{1+b^2(b^2+2)}} \cos\left(\frac{z_R^2\sqrt{1+b^2}}{2D\tau}\right) db$$

Equations 1-36 and 1-37 interpret the autocorrelation curve to provide information on the particle concentration and the diffusion coefficient of particles. Both parameters are valuable in studying processes of oligomerization. The diffusion coefficient is inversely proportional to the radius according to the Stokes Einstein equation[165]

$$D = \frac{kT}{6\pi\eta R} \quad 1\text{-}38$$

where T is the temperature, measured to be 294K, η is the solution viscosity (taken as pure water) and k is the Boltzmann's constant. An observed change in diffusion coefficient as a result of experimental conditions can be interpreted as a change in

the oligomeric state of a sample protein. A change in oligomerization state would also result in a change in particle concentration.

The goal of this study is to apply thermodynamic linkage analysis to elucidate the interdependence of the multiple allosteric ligands and polymerization on regulation of phosphofructokinase from rat liver (RLPFK). We establish a recombinant system of expressing large quantities of fully active RLPFK and characterize the interdependence of MgATP inhibition and either citrate inhibition or MgATP activation. Additionally, we use Fluorescence Correlation Spectroscopy to characterize the ligand dependent oligomerization state of RLPFK. Although we were not able to obtain the suitable description of RLPFK polymerization necessary to apply thermodynamic linkage analysis, the efforts made in this study lay the foundation for future efforts.

CHAPTER II

EXPRESSION, PURIFICATION AND CHARACTERIZATION OF RECOMBINANT RAT LIVER PHOSPHOFRUCTOKINASE

Introduction

Phosphofructokinase (PFK; EC 2.7.1.11) catalyzes the MgATP dependent phosphorylation of Fru-6-P to Fru-1,6-BP and ADP. PFK is a prime target for regulation due to its role in catalyzing the first committed step of glycolysis. As such, PFK is highly allosterically regulated by small molecule effectors. For a review of PFK see the following references[72, 76]. Mammalian PFK is a homotetramer made of four identical subunits of 86kDa each. With the exception of muscle tissue, a combination of PFK isozymes are expressed in all tissues leading to a complex mixture of PFK isoforms.[99, 100] In liver tissues, expression of both the muscle and liver forms of PFK results in a complicated mixture of species who have distinct properties[87] including hybrid species whose kinetic and regulatory properties are dependent on the subunit composition[101]. Recombinant expression ensures a purely homogenous species of PFK by exclusively expressing only one isozyme.

Efforts at recombinant expression have resulted in isolated rabbit muscle PFK [166], human muscle PFK [167], mouse platelet PFK [168] and human platelet PFK [109]. The sources of these forms of PFK are primarily glycolytic tissues. The

carbohydrate metabolism of tissues capable of performing gluconeogenesis, such as liver and kidney, is more complex and PFK isolated from these tissues is seen to have altered properties. The allosteric properties of PFK from rat liver (RLPFK) has been extensively studied using PFK purified from rat liver homogenate. [47, 49-52, 104-108] We report here the recombinant expression of codon-optimized PFK from rat liver (rRLPFK) and the evaluation of its kinetic and allosteric properties as they compare to PFK isolated from liver tissue (RLPFK). We denote recombinant RLPFK as rRLPFK in this chapter to distinguish between recombinant RLPFK and RLPFK from fresh liver tissue.

Kinetic measurements of PFK is complicated by its strong inhibition by the substrate MgATP. The affinity for the substrate Fru-6-P, for example, is highly dependent on MgATP concentration and pH[51]. We have chosen assay conditions representative of the conditions likely to be experienced in the cell; pH=7.0, 3mM MgATP, 100mM KCl. Good expression of rRLPFK has been observed with high specific activity and allosteric properties qualitatively consistent with previous publications [51]. However, these preparations exhibit a lower Fru-6-P binding affinity, and the magnitude of the allosteric responses to various effectors are different than previously reported. The maximum velocity is more greatly affected by citrate, AMP, phosphate and pH whereas the response of Fru-6-P binding to allosteric effectors is reduced.

Material and Methods

Reagents and enzymes were from the following sources: NADH, and TRIS, Research Products International, triosephosphate isomerase and glycerol-3-phosphate dehydrogenase (ammonium sulfate suspensions), Roche; Isopropyl β-D-1-thiogalactopyranoside (IPTG), and dithiothreitol (DTT), Fisher; ATP, Fru-6-P, EDTA, phenylmethanesulfonylfluoride (PMSF), $MgCl_2$, KCl, $(NH_4)_2SO_4$, Aldolase (ammonium sulfate suspension), Sigma-Aldrich; chromatography resins, Mono-Q HR 10/10, Sepharose 2B, Pharmacia, Macro Prep HiQ, Bio-Rad. Deionized, distilled water was used throughout. Enzymes purchased as ammonium sulfate suspensions were dialyzed extensively against 50mM MOPS-KOH, 100mM KCL, 2mM $MgCl_2$ and 100μM EDTA.

Bacterial strains and vectors

E. coli strain JM-109 (Promega) was grown in LB medium or on LB agar with 100μg/mL ampicillin added for strains bearing the plasmid pUC-19 or 15μg/mL tetracycline for strains bearing plasmid pALTER-EX1 (Promega). rRLPFK was expressed in the *E. coli* strain RL257 [169], which is a K-12 derivative strain missing the endogenous pfkA and pfkB genes. The RL257 strain used for this publication was made to be phage resistant and is thus designated RL257 ton A-.[170] Protein expression from the pALTER-EX1/RLPFK plasmid occurs via the tac promoter.

RL257 containing protein expression plasmid pALTER-EX1/RLPFK was grown on LB medium or on LB agar with 15μg/mL tetracycline.

Recombinant DNA techniques

Standard molecular biology techniques were performed as described in Current Protocols in Molecular Biology. [171] Oligonucleotides were synthesized and purchased from Integrated DNA technologies (Coralville IA) and dissolved in water to a final concentration of 1μg/μL. PCR amplification was performed using FastStart Taq DNA polymerase kit (Roche) as per kit directions. Ligation was performed using Instant Sticky-end Ligase Master Mix (NewEngland Biolabs), as per kit directions. Restriction enzymes were purchased from NewEngland Biolabs. Digested vector was separated from cleavage fragment by 2% agarose gel electrophoreses. Plasmid DNA, PCR products, and size-fractionated DNA fragments were purified with the appropriate Qiagen isolation kits. DNA sequencing services were purchased by Eton Bioscience. N-terminal sequencing was performed by the Protein Chemistry Laboratory at Texas A&M University.

Codon optimization and cloning of the pfk gene

The complete coding sequence for the phosphofructokinase open reading frame (NCBI accession number XM-001079376) from *Rattus norvegicus* (Rat) liver was codon optimized in silico using proprietary gene optimization software by Biomatik Corp. The subsequent gene sequence (Supplemental Materials Fig. S1)

was synthesized by Biomatik and provided as an insert within pUC19. The *rlPfk* gene was PCR amplified out of pUC19 using forward primer (5'-ACGTCAGGATCCATGGCGACCGTTGATCTGG -3') and the reverse primer (5'-CGACAAAGGCTTCTAATGAATTCGCTGGCCG-3'). The forward primer contains the BamH1 site on the 5' end of *rlPfk* and the reverse primer contains double redundant internal stop codons and the EcoR1 site on the 3' end. The PCR amplified product and empty pALTER-EX1 vector were digested independently for 1 hour. The *rlPfk* gene was ligated into the multiple cloning site of pALTER-EX1 and transformed into freshly competent JM109 cells. The plasmid construct was confirmed by agarose gel electrophoresis, DNA sequencing and N-terminal peptide sequencing were performed by Edman degradation. The resulting plasmid (Figure 2-1) was named GDR999.

Expression and purification

RL257 was transformed with the recombinant plasmid and plated on LB agar supplemented with 15μg/mL tetracycline and a single colony was selected and used to inoculate a 10mL culture of LB-tetracycline. The LB culture was incubated with shaking at 37^0C overnight for 8 hours. 9mL of the overnight culture was used to inoculate 9L of LB-tetracycline media. Inoculated media was grown at 30^0C to an OD of 0.6 before being induced by 1mM IPTG. Cells were grown for 40 hours before harvesting at 3500xg for 30min.

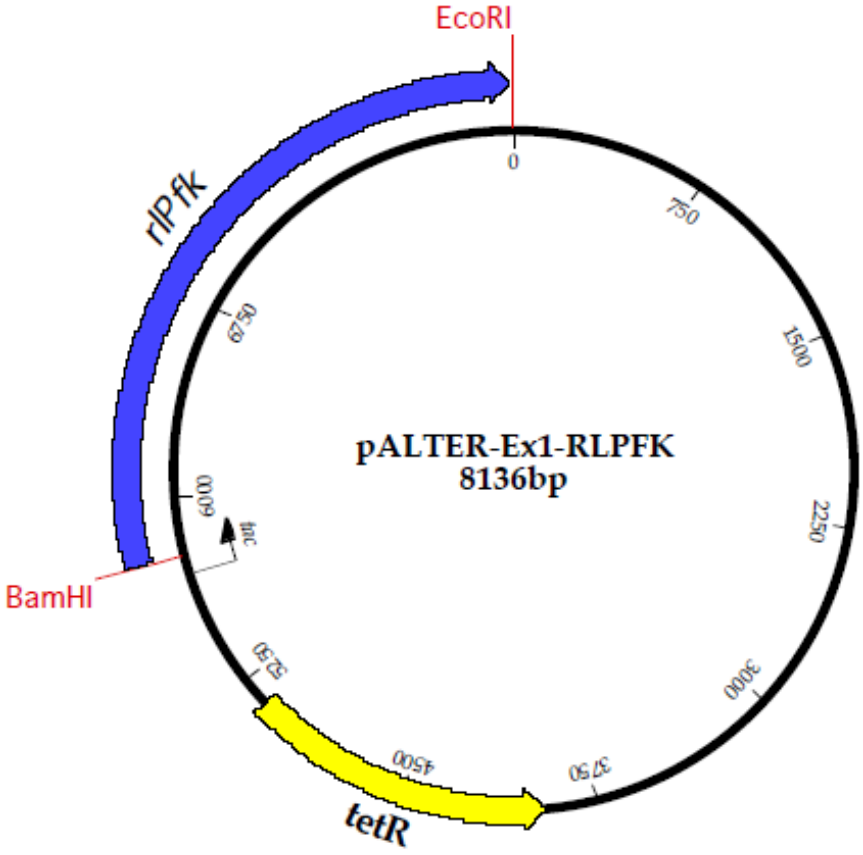

Figure 2-1: Plasmid map of pALTER-EX1 containing *rlpfk.*

The cell pellet (~25g wet weight) was re-suspended into 100mL purification buffer (50mM Tris, 0.1mM EDTA, 5mM DTT, 1mM ATP, 0.1mM PMSF, pH=8.0). Cell suspension was ruptured by discontinuous sonication using a Fisher 550 sonic dismembrator at 70% amplitude with 15s on and 45s off for a total sonication time of 12min. Insoluble material was removed by 45min centrifugation at 14,000xg.

Clarified supernatant was rapidly heated to 58^0C in a boiling water bath. Temperature was maintained at 58 ± 1^0C for 3min and then rapidly cooled to 10^0C in a salt-ice bath. Precipitated protein was again removed by 45min centrifugation at 14,000xg.

Ammonium sulfate was slowly stirred into clarified supernatant to a final concentration of 18g per 100mL. The mixture was incubated at 4^0C in the presence of $(NH_4)_2SO_4$ for 90min before being centrifuged for 20min at 7,000xg. The supernatant solution was discarded, and the pellet was re-suspended into a minimal volume of anion exchange buffer (20mM Tris, 3mM $MgCl_2$, 20mM $(NH_4)_2SO_4$, 0.1mM EDTA, 5mM DTT, 1mM Fru-6-P pH=8.0). Re-suspended protein solution was dialyzed extensively against anion exchange buffer.

The solution was centrifuged at 7000xg for 20min to clarify before being diluted to a concentration of 0.25mg/mL and loaded onto a pre-equilibrated HiQ column with the dimensions 0.8X15cm. Protein was eluted from the column using a 0-1M KCl gradient. All fractions containing activity were pooled and precipitated by $(NH_4)_2SO_4$ (60% saturation). Precipitated protein was pelleted by centrifuging at 10,000xg for 30min followed by re-suspension into a minimum volume of anion

exchange buffer and dialyzed against four iterations of 100mL anion exchange buffer.

Dialyzed pooled fractions were centrifuged at 7000xg for 20min to clarify before being diluted to 50mL with anion exchange buffer and loaded onto a Pharmacia/GE healthcare Mono-Q HR 10/10 anion exchange column that had been pre-equilibrated with anion exchange buffer. Protein was eluted by a 0-1M KCl gradient. Fractions containing activity were pooled and precipitated by 60% $(NH_4)_2SO_4$. Pellet was re-suspended into 4mL of gel filtration buffer (20mM Phosphate (P_i), 3mM $MgCl_2$, 0.1mM EDTA, 5mM DTT, 1mM Fru-6-P, pH=7.6) and clarified by centrifugation.

The solution was loaded onto a Sepharose 2B gel filtration column with the dimensions of 1.7X38cm. Protein elution was tracked by activity and A280, typically, the majority of rRLPFK comes out in the void volume. Additional activity is seen to elute in an extended tail which was not pooled. Protein was concentrated using PEG to a concentration of 2mg/mL and dialyzed against storage buffer (20mM Phosphate, 3mM, $MgCl_2$, 0.1mM EDTA, 5mM DTT, 1mM Fru-6-P, 20% glycerol pH=7.6. Purity was assessed as a single band on a 12% SDS-PAGE gel. Protein concentration determined by BCA.

Kinetic assays

The PFK catalyzed conversion of Fru-6-P to Fru-1,6-BP was coupled to the oxidation of NADH, which resulted in a decrease in absorbance at 340nm. The rate

of the decrease in A340 was monitored using a Beckman Series 600 spectrophotometer. All assays were performed at 25^0C and initiated by the addition of 6µL PFK to a final volume of 600µL buffer. Dilution of PFK into cuvette contributes the addition of 0.2mM P_i, 0.2% glycerol, 10µM Fru-6-P, and 30µM $MgSO_4$ to all assays. PFK activity is presented as units per milligram where 1 unit is equal to the production of 1 µmol of Fru-1,6-BP per min. An intermediate dilution of rRLPFK into storage buffer is made prior to assay initiation. The intermediate dilution of rRLPFK was incubated at room temperature for 30min before initiation of assays.

Optimal enzyme activity assays were performed in the following buffer; 50mM Tris-HCL, 100mM KCl, 20mM $(NH_4)_2SO_4$, 2mM DTT, 3mM $MgCl_2$, 1mM ATP, 1mM Fru-6-P, 0.2mM NADH, 100µM EDTA, pH 8.0, 250µg/ml of aldolase, 50µg/ml of glycerol-3-phosphate dehydrogenase, 5µg/ml of triosephosphate isomerase. Assays performed during purification were measured in the presence and absence of Fru-6-P to subtract any rate contributed by background NADH oxidation.

Allosteric kinetic properties of rRLPFK were investigated in the following buffer; 50mM MOPS-KOH, 100mM KCL, 100µM EDTA, 2mM DTT, 0.2mM NADH, pH=7.0 250µg/ml of aldolase, 50µg/ml of glycerol-3-phosphate dehydrogenase, 5µg/ml of triosephosphate isomerase. Most assays were performed at a fixed concentration of 3mM ATP with a total $MgCl_2$ concentration of 5mM. The term "standard conditions" refer to assay conditions at which the concentration of MgATP is 3mM and pH=7.0. Standard conditions are taken to reflect physiological

concentrations to a close approximation.[51] In experiments where ATP concentration was varied, total $MgCl_2$ was always kept in 2mM excess of the ATP. Stock solutions of Fru-6-P, ATP and AMP were assayed enzymatically and kept frozen between experiments. Assays were terminated either after 15min or when the substrate concentration had decreased by 20μM, whichever occurred first.

Data measured with varying concentrations of Fru-6-P were fit using the nonlinear least-squares fitting analysis of Kaleidagraph software (Synergy). The initial velocity data were plotted against concentration of Fru-6-P and fit to the following equation:

$$v^0 = \frac{V[A]^{n_H}}{K_a^{n_H} + [A]^{n_H}} \tag{2-1}$$

where v° is the initial velocity, [A] is the concentration of the substrate Fru-6-P, V is the maximal velocity, n_H is the Hill coefficient, and K_a is the concentration of substrate that gives one-half the maximal velocity. For a reaction in rapid equilibrium, K_a is equivalent to the dissociation constant for the substrate from the binary enzyme–substrate complex.

The K_a values obtained from the initial velocity experiments were plotted against effector concentrations and fit to the following equation:

$$K_a = K_{ia}^o \left(\frac{K_{iy}^o + [Y]}{K_{iy}^o + Q_{ay}[Y]} \right) \tag{2-2}$$

where K_{ia}^o is the dissociation constant of Fru-6-P in the absence of allosteric effector, Y is allosteric effector, K_{iy}^o is the dissociation constant of allosteric effector

in the absence of Fru-6-P and Q_{ay} is the coupling constant between Fru-6-P and allosteric effector [65, 172].

The coupling constant,Q_{ay}, describes the effect of an allosteric effector on the dissociation constant of the substrate as show in equation 2-3:

$$Q_{ay} = \frac{K_{ia}^{o}}{K_{ia}^{\infty}} = \frac{K_{iy}^{o}}{K_{iy}^{\infty}} \tag{2-3}$$

where K_{ia}^{∞} is the dissociation constant of substrate in the saturating presence of allosteric effector and K_{iy}^{∞} is the dissociation constant of allosteric effector in the saturating presence of substrate.

The coupling free energy of an allosteric response ΔG_{ay} is calculated from the coupling constant by equation 2-4:

$$\Delta G_{ay} = -RTln(Q_{ay}) \tag{2-4}$$

where R is the gas constant (R=1.99calK^{-1}mol^{-1}), and T is the absolute temperature in K.

Results

Expression and purification of Pfk

Codon optimization and subsequent synthesis, provided by Biomatik, allowed for optimal expression of rRLPFK in E. coli. Codon changes amount to 21%

of the 2343 nucleotide native sequence, corresponding to 492 codon triplets (see Supplemental Material Fig. S1 for the optimized gene sequence).

The purification procedure was largely adapted from the procedure published for purifying PFK directly from rat liver homogenate [51]. The purification procedure resulted in pure protein, as assessed by a single band on an SDS gel (Figure 2-2). Molecular weight was estimated to be approximately 82,000 kDa, consistent with the value published by Reinhart and Lardy [51] and Brand and Soling [102]. Data from a typical purification are shown in Table 2-1. The purification procedure resulted in a 47% yield with 60-fold purification compared to cell free extract. The final specific activity was between 100 and 120units/mg, around 20% higher than the value reported by Reinhart and Lardy (85units/mg)[51]. This difference could reflect a higher level of purity as Reinhart and Lardy noted a slight containment.

Purification proved to be reproducible and the final product appears as a single band on an SDS-PAGE gel (Figure 2-2). The rRLPFK was stable throughout the purification; however, care was taken to avoid prolonged storage at low concentration (e.g. following chromatography) as decreased stability is seen at lower concentrations. Significant loss of activity is seen if the temperature exceeds 60^0C during the heat step, and it is critical that Fru-6-P or MgATP remain in the buffer at all times. rRLPFK has a propensity to precipitate if the concentration exceeds 4mg/ml. The enzyme retains full activity as a suspension and regains solubility upon dilution. Loss of rRLPFK has been seen to occur during anion

exchange. The extent of loss correlates with the amount of rRLPFK activity in the column load. It is thought that the loss is due to precipitation triggered by over concentration during column purification. Best results were obtained when column load was restricted to 3000 units to avoid significant loss.

Figure 2-2: SDS-Polyacrylamide gel electrophoresis demonstrating purity of rat liver PFK purified as described in text. The gel contains 5ug of rRLPFK stained with Coomassie blue.

Table 2-1: Summary of Rat liver PFK Purification

	Vol (mL)	act (units/mL)	Protein (mg/mL)	Sp act.	Total Units	Yield (%)	Purifin (x-fold)
Sup.	100	39	24	1.6	3900	100	1
Heat	86	36	10	3.6	3120	80	2
$(NH_4)_2SO_4$	11	280	10	30	3080	79	19
HiQ	140	21	0.5	44	2950	76	28
Mono-Q	34	66	1.2	53	2240	57	33
Seph. 2B	8	220	2.2	100	1820	47	63

Complex hysteretic behavior is observed in assays of rRLPFK (Figure 2-3). Assays are seen to accelerate or decelerate depending on the conditions of the assay as well as the order of addition of components. In the presence of non-saturating Fru-6-P concentrations, assays initiated by the addition of either PFK or ATP display a burst pattern, characterized by an initially high rate of reaction that gradually slows down (Figure 2-3A). Alternatively, initiation by Fru-6-P did not display a burst rate but appeared linear. After a time of approximately 12 minutes the rates obtained in all conditions became mostly linear (Figure 2-3B). Hysteretic behavior was reported for RLPFK from liver tissue.[51]

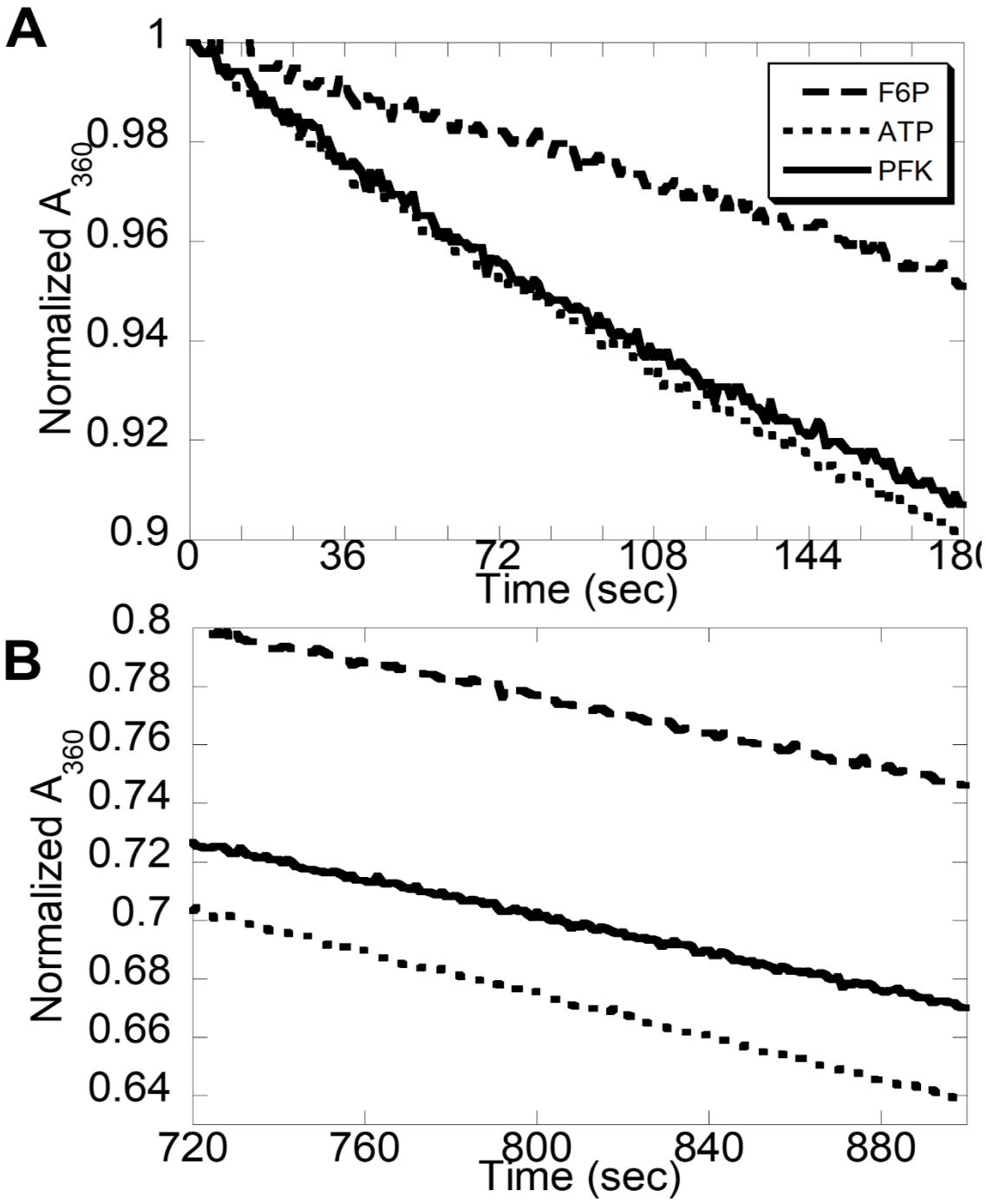

Figure 2-3: Typical rate velocities of rat liver PFK observed in the first 3min (A) and 8min after initiation (B). Assay were performed at pH = 7.0 with [MgATP] = 3mM [Fru-6-P] = 15mM. Assays were initiated with addition of either ATP (dotted), Fru-6-P (dashed) or PFK (solid). All other conditions were identical

To assess whether the kinetic properties of rRLPFK were consistent with RLPFK purified from rat livers, we determined the effect of several allosteric modifiers on the steady-state activity of rRLPFK as a function of Fru-6-P concentration. The effect of inhibitor MgATP is demonstrated in Figure 2-4. At a pH of 7.0 the K_a increased from 5.0±0.2mM in the presence of 0.2mM MgATP to 24.0±0.9mM in the presence of 5mM MgATP Table 2-2. Very little if any effect on k_{cat} was observed. The K_a values reported for RLPFK from native source changed from just over 1mM at 0.2mM MgATP to just under 10mM at 5mM MgATP [51]. The apparent K_a values were higher at all concentrations of MgATP with recombinant rRLPFK than values reported for PFK from native source[51]. Possible explanations for this are discussed below. Additionally, a 5-fold change in K_a compared to the published 10-fold change would suggest that rRLPFK is less sensitive to MgATP inhibition. To further explore this possibility, we measured the coupling free energy of MgATP and Fru-6-P. Figure 2-5 shows the effect of MgATP concentration on K_a of Fru-6-P. The values of the dissociation of MgATP in the absence of Fru-6-P (K_{iy}^{o}) and the coupling free energy between Fru-6-P and MgATP ΔG_{ay} are both very similar to reported values [52] (Figure 2-5 insert).

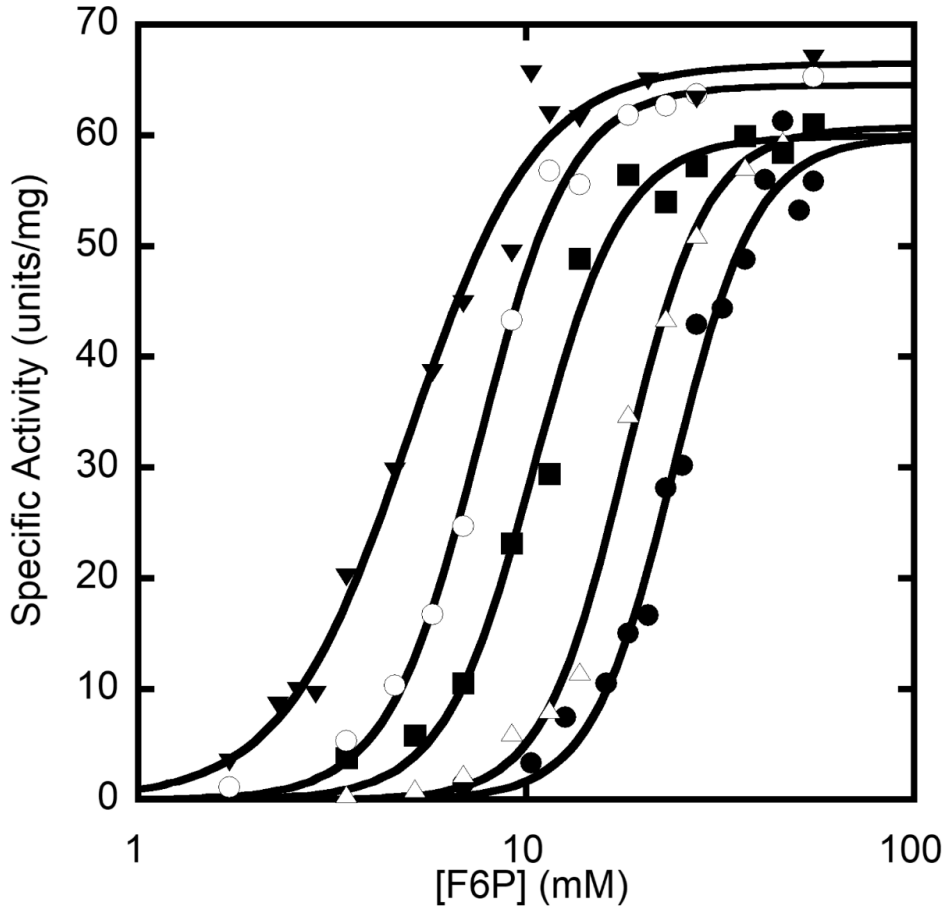

Figure 2-4: Effect of MgATP on the kinetic properties of rRLPFK at pH =7.0. [MgATP]: 0.2mM (closed triangles) 0.5mM (open circles) 1mM (closed squares) 3mM (open triangles) 5mM (closed circles)

Table 2-2: Dependence of kinetic parameters on the concentration of MgATP at pH=7.0 and 25^{0}C

[MgATP] (mM)	k_{cat} (sec^{-1})	Fru-6-P K_a (mM)	Hill number
0.2	95±3	5.0±0.2	2.6±0.2
0.5	93±1	7.6±0.2	3.7±0.3
1	86±3	10.5±0.4	3.8±0.5
3	87±1	18.0±0.5	4.1±0.3
5	86±4	24.0±0.9	4.1±0.6

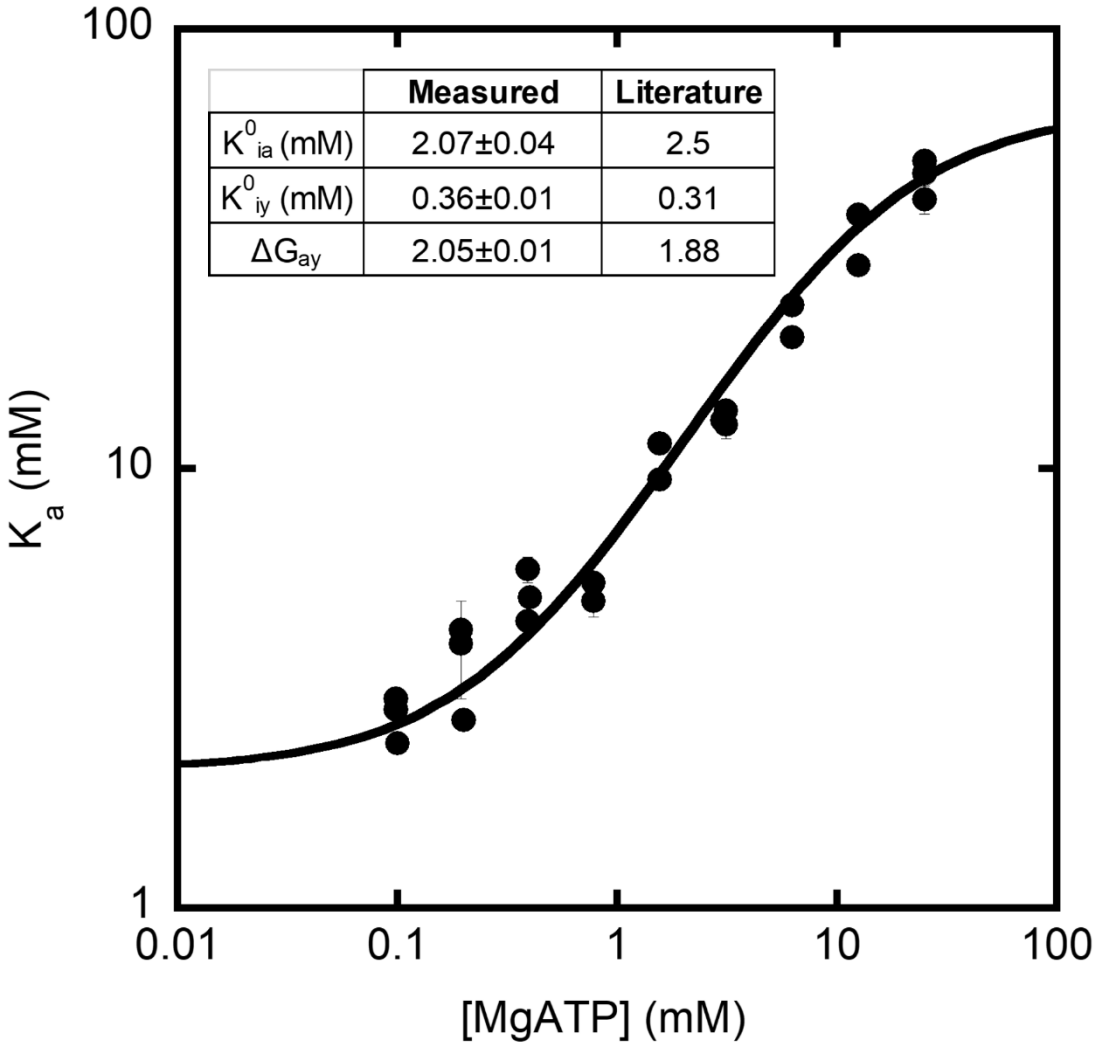

Figure 2-5: Dependence of K_a on concentration of MgATP. Data represents combined data points from 3 repetitions performed with 3 separate enzyme preps. Data are fit to equation 2-2. Insert list parameters obtained from fit. Literature values are obtained by extrapolating data points from figure published in reference[52]. Error bars represent error of K_a values obtained from fitting to equation 2-1

The effect of pH on the value of Fru-6-P K_a and k_{cat} is presented in Figure 2-6. The high dissociation constant of Fru-6-P at low pH made it difficult to reach saturating substrate concentrations. At a pH of 6.7 the Fru-6-P binding plot does not demonstrate a clear upper plateau resulting in an appreciable amount of uncertainty in both the value of k_{cat} and K_a. However, it is clear that rRLPFK showed an increased Fru-6-P affinity and increased k_{cat} at higher pH when the concentration of MgATP is kept constant at 3mM. This trend is consistent with PFK purified from rat liver. [51] Fru-6-P affinity increased almost 30-fold and k_{cat} increased nearly 2-fold as pH was increased from 6.7 to 8 (Table 2-3). Studies on PFK isolated from rat livers reported a 15-fold increase in Fru-6-P affinity and a 40% increase in k_{cat} [51]. The apparent K_a values of Fru-6-P binding were higher in our recombinant protein than literature values at each pH. The 30-fold change in K_a and the 2-fold change in k_{cat} from pH=6.7 to pH=8.0 is twice that of published data [51]. The rRLPFK reported in this paper is more sensitive to pH.

In standard assay conditions (3mM MgATP, pH=7.0), the addition of 10mM citrate increased the apparent K_a by almost 50% while decreasing the k_{cat} by about 40% (Figure 2-7; Table 2-4). Reinhart and Lardy reported a greater change in K_a (2-fold compared to 50%) and a similar change in k_{cat} (30% compared to 40%).[51]

Addition of 10mM phosphate to assay solutions at pH=7.0 with 3mM MgATP decreased K_a of Fru-6-P nearly 5-fold and increased the k_{cat} by 10%. (Figure 2-8, Table 2-5) Phosphate is not seen to induce a significant change of k_{cat} in data reported by Reinhart and Lardy [51]. However, a 7-fold decrease in K_a was reported

for enzyme purified from rat liver, significantly greater than what we observe with rRLPFK [51].

5mM AMP decreases the K_a by 3-fold and increase the k_{cat} by 10% (Figure 2-9, Table 2-6). Enzyme from native source experienced a 4-fold activation by 5mM AMP; however, no increase in k_{cat} was observed.[51]

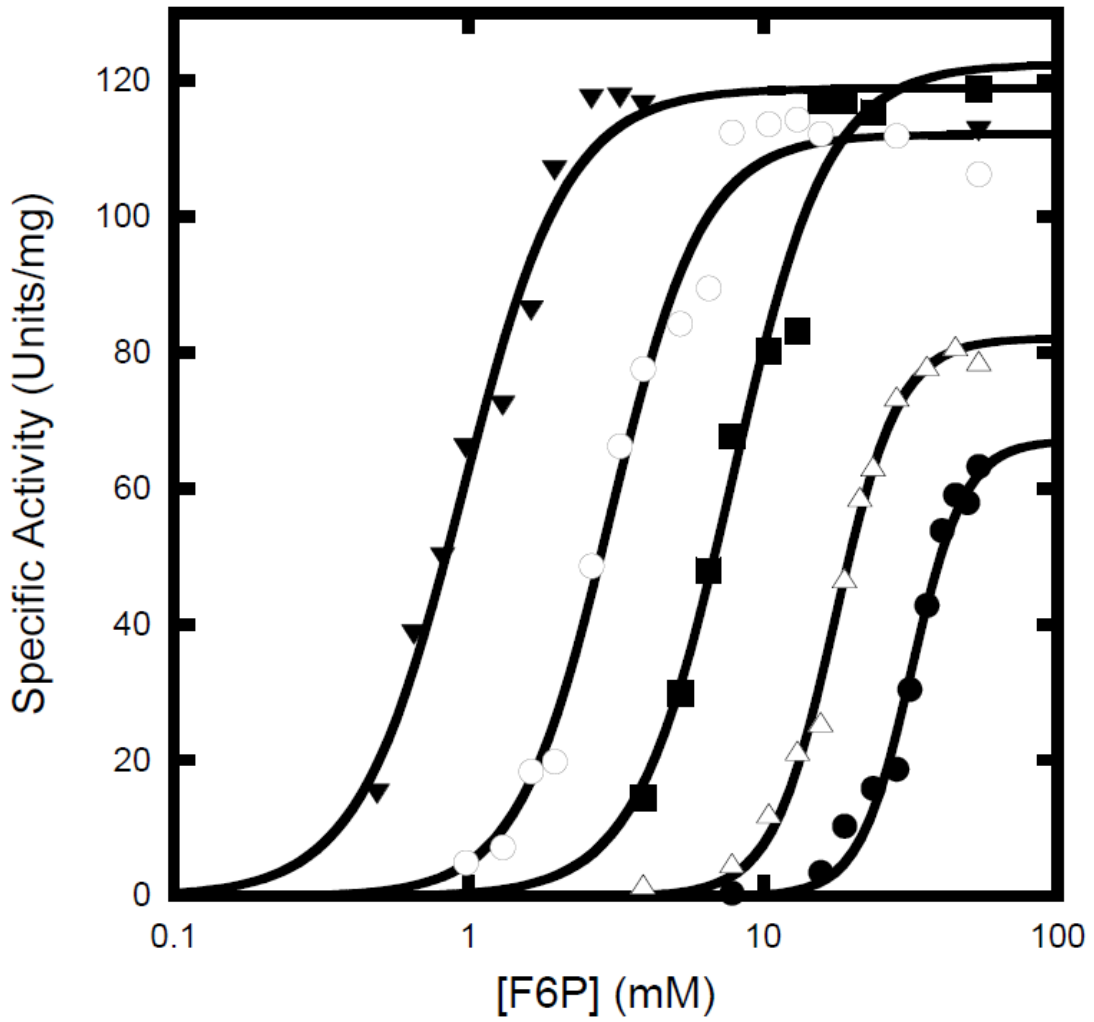

Figure 2-6: Effect of pH on the kinetic properties of rRLPFK in the presence of 3mM MgATP. pH: 6.7 (closed circles), 7 (open triangles), 7.3 (closed squares), 7.6 (open circles) and 8 (closed triangles).

Table 2-3: Dependence of kinetic parameters on pH with 3mM MgATP at 25^0

pH	k_{cat} (sec^{-1})	Fru-6-P K_a (mM)	Hill Number
6.7	96±4	32±1	4.8±0.6
7	117±3	17.6±0.4	4.1±0.4
7.3	170±10	7.8±0.6	2.7±0.4
7.6	160±4	3.0±0.1	2.8±0.3
8	170±6	0.95±0.05	2.5±0.3

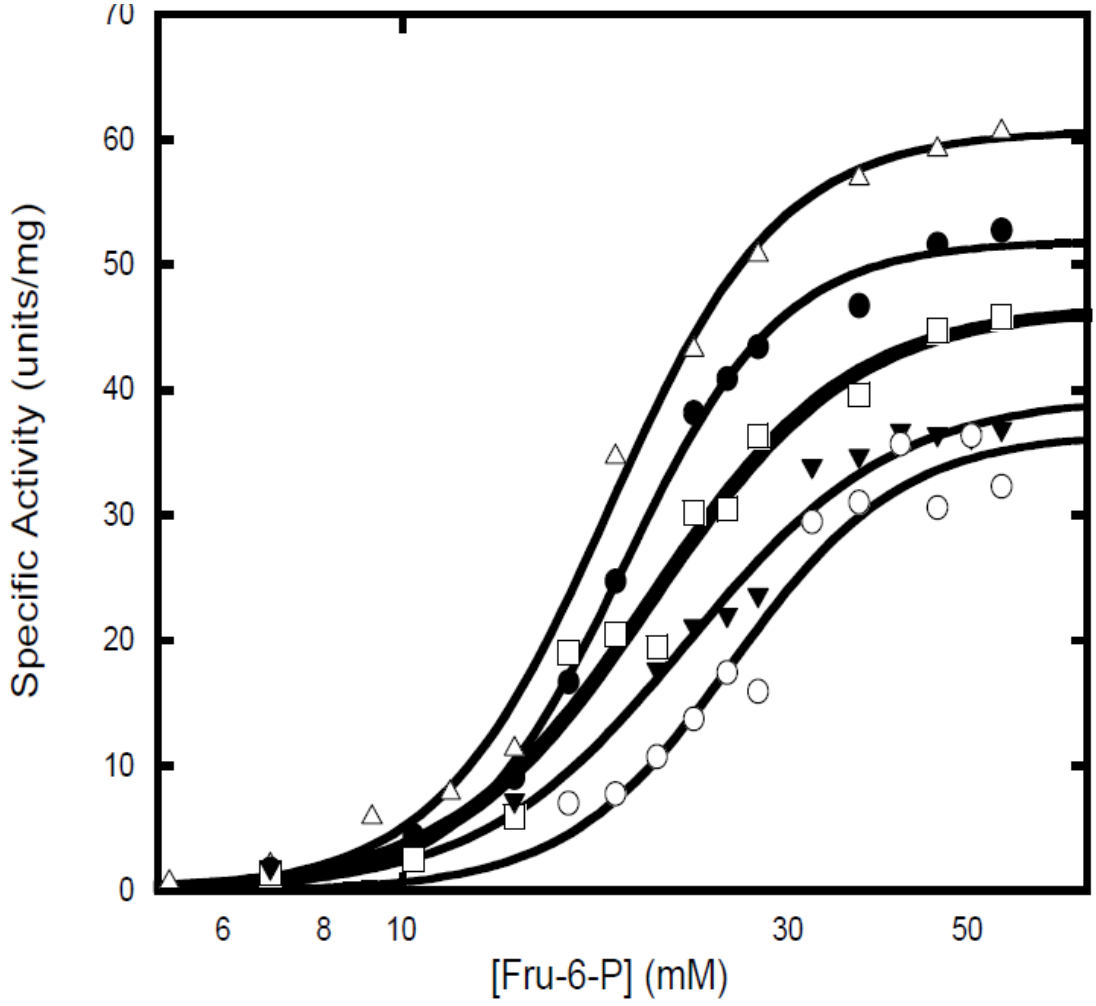

Figure 2-7: Effect of citrate on the kinetic properties of rRLPFK in the presence of 3mM MgATP and at pH =7.0. [citrate]: 0mM (open triangles), 0.2mM (closed circles), 1mM (open squares), 5mM (closed triangles), 10mM (open circles).

Table 2-4: Dependence of kinetic parameters on citrate concentration with 3mM MgATP at pH=7.0 and 25^{0}C

[Citrate] (mM)	k_{cat} (sec^{-1})	Fru-6-P K_a (mM)	Hill number
0	87±1	18±0.5	4.1±0.3
0.2	75±1	18.8±0.3	4.5±0.3
1	67±4	20±1	3.5±0.6
5	57±3	22.5±0.9	3.4±0.5
10	53±4	26±2	4.1±0.9

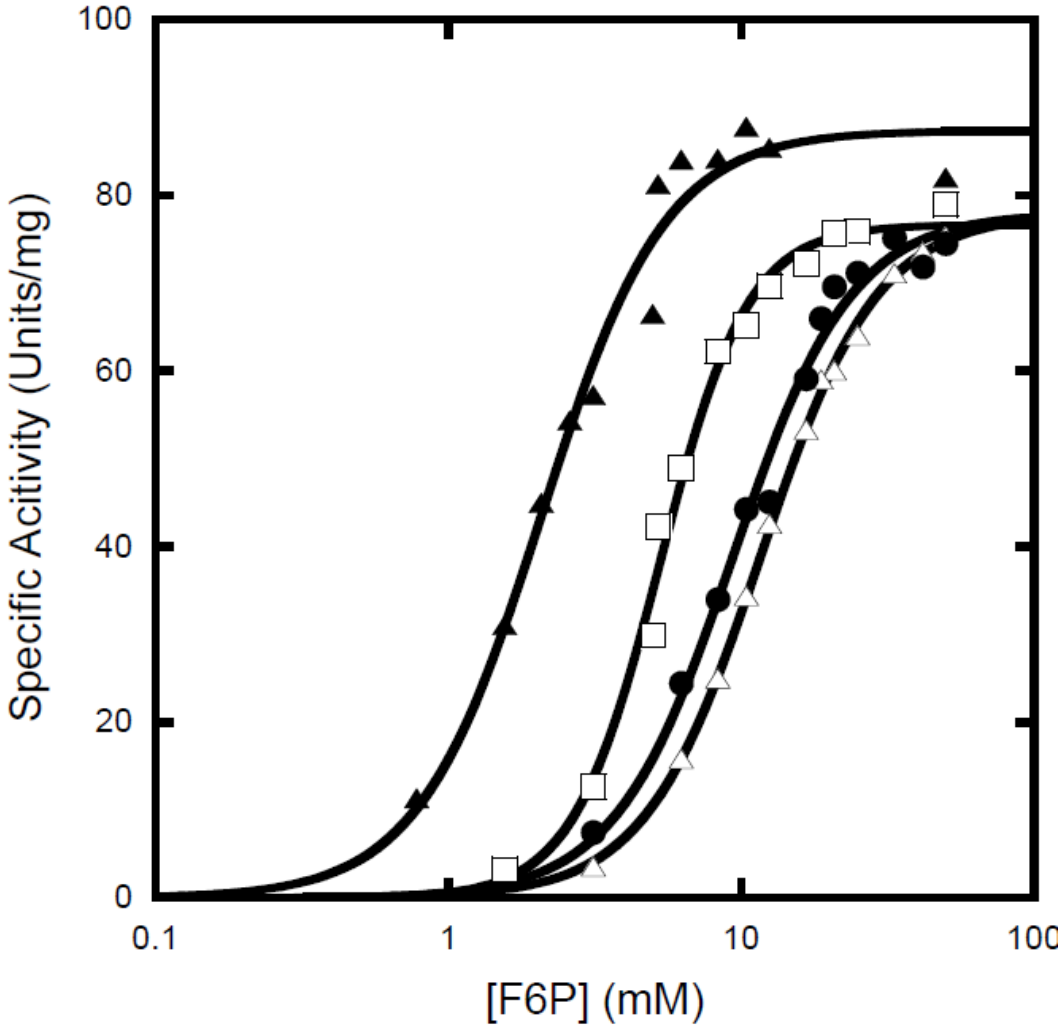

Figure 2-8: Effect of Pi on the kinetic properties of rRLPFK in the presence of 3mM MgATP and at pH =7.0. [Pi]: 0mM (open triangles), 0.1mM (closed circles), 1mM (open squares), 10mM (closed triangles).

Table 2-5: Dependence of kinetic parameters on phosphate concentration with 3mM MgATP at pH=7.0 and 25^{0}C

[Phosphate] (mM)	k_{cat} (sec^{-1})	Fru-6-P K_a (mM)	Hill number
0	111±1	11.6±0.2	2.2±0.1
0.1	111±3	9±0.5	2.1±0.2
1	110±3	5.2±0.2	2.9±0.3
10	125±4	2.1±0.1	2.1±0.3

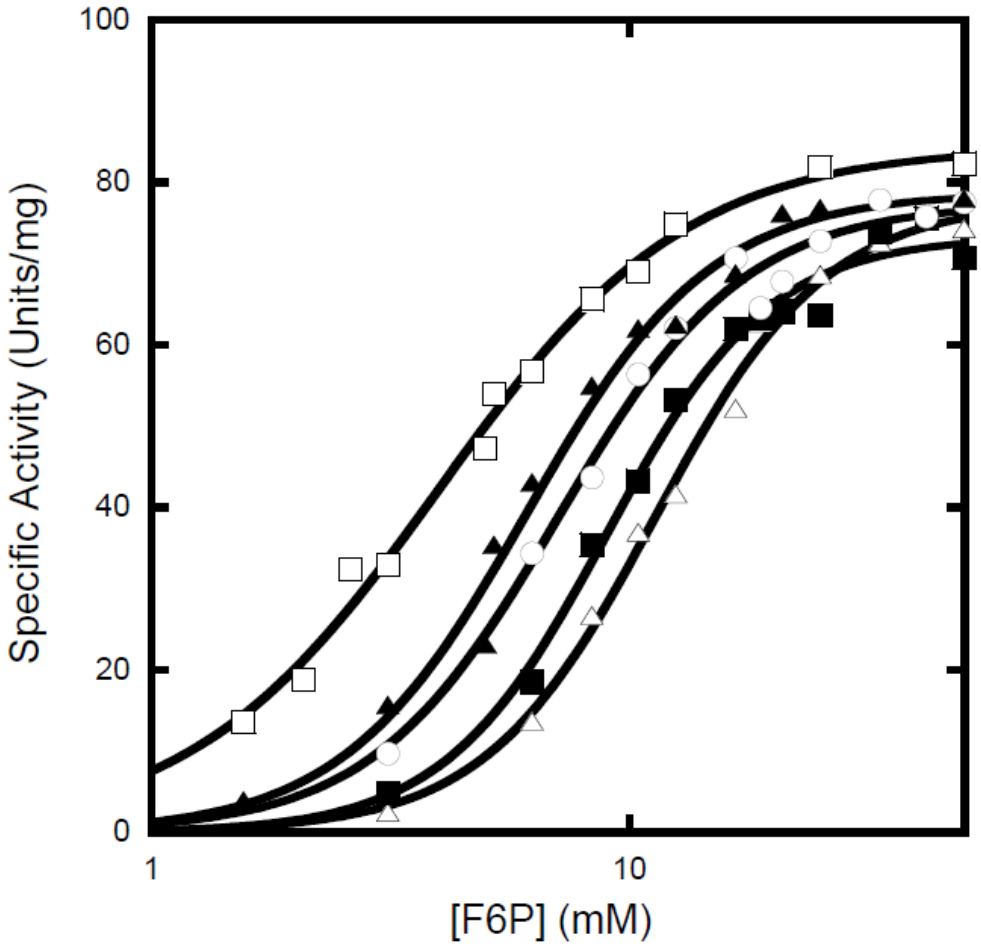

Figure 2-9: Effect of AMP on the kinetic properties of rRLPFK in the presence of 3mM MgATP and at pH=7.0. [AMP]: 0mM (open triangles), 0.05mM (closed squares), 0.1mM AMP (open circles), 0.2mM (closed triangles) or 2.5mM AMP (open squares).

Table 2-6: Dependence of kinetic parameters on AMP concentration with 3mM MgATP at pH=7.0 and 25^{0}C

[AMP] (mM)	k_{cat} (sec^{-1})	Fru-6-P K_a (mM)	Hill number
0	110±3	11.3±0.5	2.4±0.2
0.05	104±3	8.9±0.3	2.6±0.3
0.1	110±3	7.1±0.3	2.2±0.2
0.2	113±4	6.1±0.3	2.3±0.3
2.5	120±3	4.0±0.2	1.7±0.1

Discussion

We report here expression and purification of recombinant RLPFK (rRLPFK) from *E. coli* with a specific activity of 100-120units/mg and the subsequent characterization of the kinetic properties.

Consistent with RLPFK purified from fresh liver tissues [51], the kinetic measurements were complicated by curvature of assays (Figure 2-3 A&B). Reinhart and Lardy pointed out that the dependence on the order of addition of the metabolites indicates that the initial rates reflect the conditions of the enzyme prior to the assay.[51] One example of pre-assay conditions that was implicated in contributing to the rate curvature is oligomeric state of RLPFK.[49] RLPFK is capable of forming oligomeric species larger than a tetramer with differing affinities to Fru-6-P [49]. Fru-6-P stabilizes the larger oligomeric form while MgATP promotes dissociation to the tetrameric form [50]. In assays initiated by addition of RLPFK or ATP, RLPFK is initially in the presence of Fru-6-P and thus populates the large oligomeric species.[49] The introduction to MgATP steadily dissociates the enzyme to smaller species with lower affinity for Fru-6-P, resulting in an increasingly depressed rate. Conservation of the rate curvature in rRLPFK purified out of *E. coli* is an important observation to ensure rRLPFK is behaving similar to RLPFK purified from fresh livers.

Contrary to many enzymatic reactions, the initial rate should not be taken as the steady state rate of the enzyme; instead the rate after the transient rate should

be taken. For the purpose of this publication the 'true' rate was taken to be the linear rate obtained after any burst. Care was taken to ensure that the rate obtained was no longer changing over time. A low enzyme concentration was utilized to prevent significant depletion of substrate over the course of the assay. A high concentration of aldolase was used to ensure a negligible buildup of product Fru-1,6-BP.

Experiments in which the concentration of MgATP and pH were held constant were performed in the presence of 3mM MgATP and at pH equal to 7.0. These conditions (denoted standard conditions) were chosen to maintain physiological conditions and because previous characterizations of RLPFK were performed in these conditions [51]. The value of K_a measured for Fru-6-P binding to rRLPFK in standard conditions varied within a single prep between 14-22mM with the typical value at 18mM (Table 2-7).

Inspection of an overlay of multiple replicates suggest that variability of K_a indicates the uncertainty in the value obtained by fitting to equation 2-1 (Figure 2-10). The difficulty in fitting the data arises from the uncertainty of V_{max} calculated from curves whose upper plateau is only established by a narrow range of substrate concentrations (Figure 2-10). The fitted V_{max} ranged from 58-71 units/mg (k_{cat}=83-102s^{-1}) and, typically speaking, data fitted with a larger k_{cat} was also fitted with a larger Fru-6-P K_a (Table 2-7). To calculate k_{cat} and Fru-6-P K_a in a way that accounts for the variability in measurements, 6 replicates were fitted as a single data set (Figure 2-11). The six replicates together resulted in a k_{cat} of 90±3 s^{-1}, a

Fru-6-P K_a of 17.7±0.5mM and a Hill number of 3.8±0.3 (Table 2-7). These values were used as the reference point to interpret perturbations by effectors. For simplicity, graphs showing a shift in kinetic parameters used data obtained from replicate 4.

The variability in the value of K_a for Fru-6-P was far greater between multiple preparations than within a single preparation. Replicate measurements of Fru-6-P K_a across 7 preparations of rRLPFK yielded values ranging from 9mM to 18mM (Figure 2-12, Table 2-8). A 2-fold difference in Fru-6-P affinity from one preparation to the other cannot be dismissed, however the source of this variation is unknown. The inconsistency between preparations seemed to be primarily reserved to the dissociation constant of Fru-6-P. For example, rRLPFK with the highest Fru-6-P affinity yielded nearly identical values for MgATP dissociation constant (K_{iy}^{o}) and coupling free energy between MgATP and Fru-6-P (ΔG_{ay}) when compared to values obtained from the cumulative fitting of three "low affinity" preparations (Figure 2-13, Table 2-9).

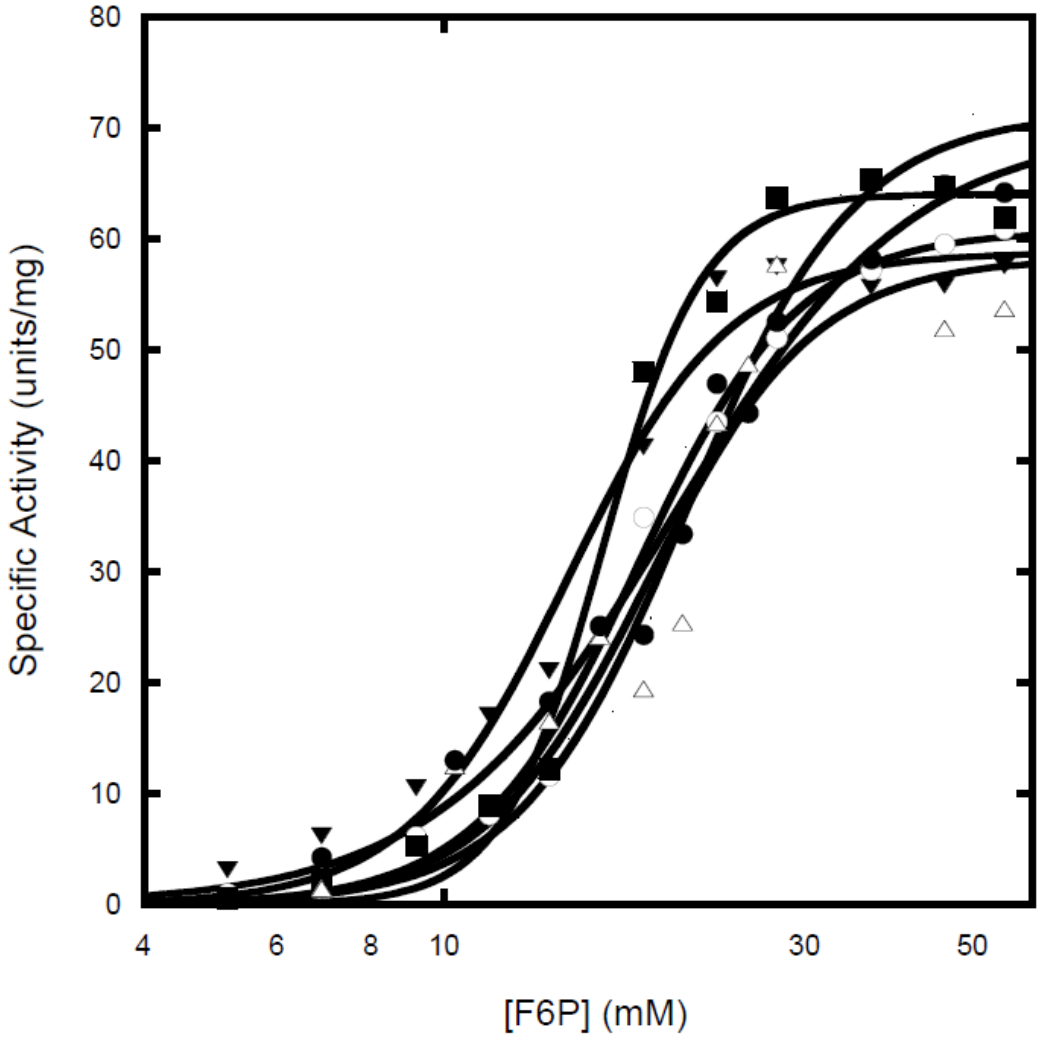

Figure 2-10: Variability in the measurements of Fru-6-P affinity of rRLPFK. Measurements were taken in the presence of 3mM MgATP at a pH of 7.0. Six repetitions are individually fit to equation 2-1, fitted parameters are listed in Table 2-7. Each of the six repetitions were performed with a single preparation of rRLPFK.

Table 2-7: Variability in the measurements of Fru-6-P affinity of rRLPFK with 3mM MgATP, pH=7.0 and 25^{0}C

Repetition #	k_{cat} (sec^{-1})	Fru-6-P K_a (mM)	Hill number
1	85±3	14.5±0.6	4.1±0.6
2	87±1	17.9±0.5	4.1±0.3
3	92±3	16.1±0.4	6.6±0.8
4	83±7	18±1	4±1
5	100±7	20±1	2.7±0.4
6	102±6	20.9±0.9	3.9±0.5
Single Fit	90±3	17.7±0.5	3.8±0.3

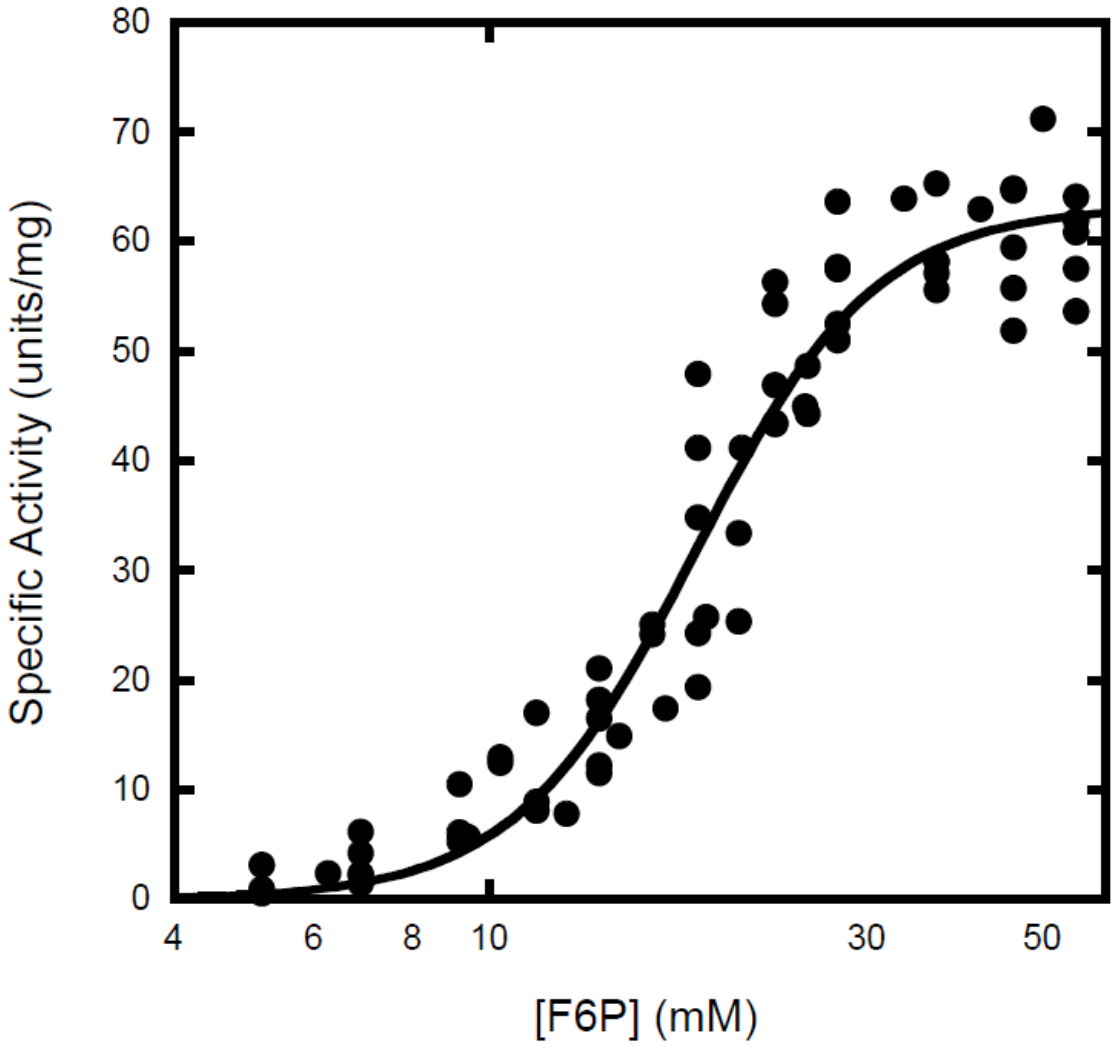

Figure 2-11: Fru-6-P affinity of rRLPFK measured in the presence of 3mM MgATP at a pH of 7.0. Data obtained by six replications are presented as a single data set. Fitted parameters obtained through a cumulative fit of data to equation 2-1. Fitted parameters listed in Table 2-7.

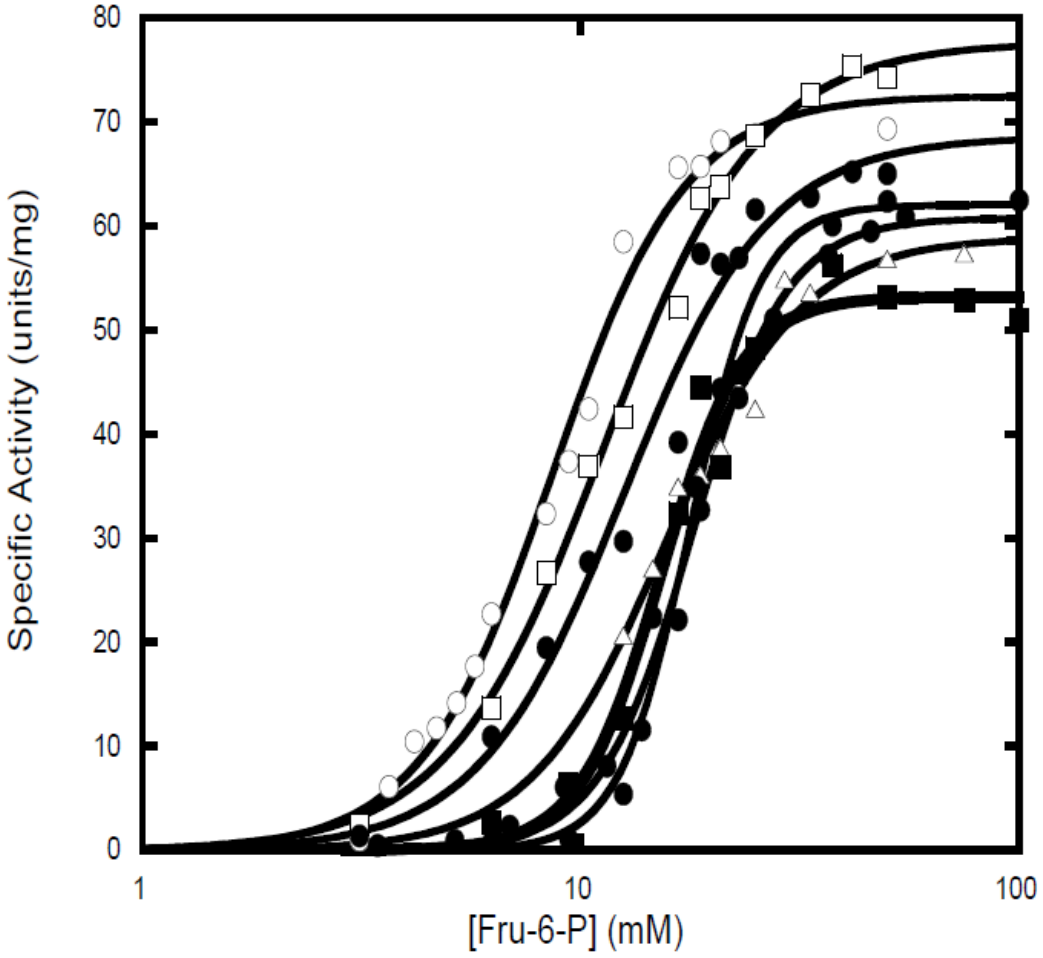

Figure 2-12: Variability in measured Fru-6-P affinity in rRLPFK across multiple preparations. Fitted parameters are listed in Table 2-8.

Table 2-8: Variability in the measurements of Fru-6-P affinity of rRLPFK across multiple preparations of rRLPFK

Prep #	k_{cat} (sec^{-1})	Fru-6-P K_a (mM)	Hill Number
1	89±4	17.8±0.6	5.4±0.8
2	85±3	15.6±0.6	2.8±0.3
3	76±3	15.2±0.6	4.7±0.7
4	103±3	8.7±0.3	2.9±0.2
5	87±1	18.0±0.5	4±0.3
6	110±3	11.3±0.4	2.4±0.2
7	99±6	12.5±0.8	2.6±0.4

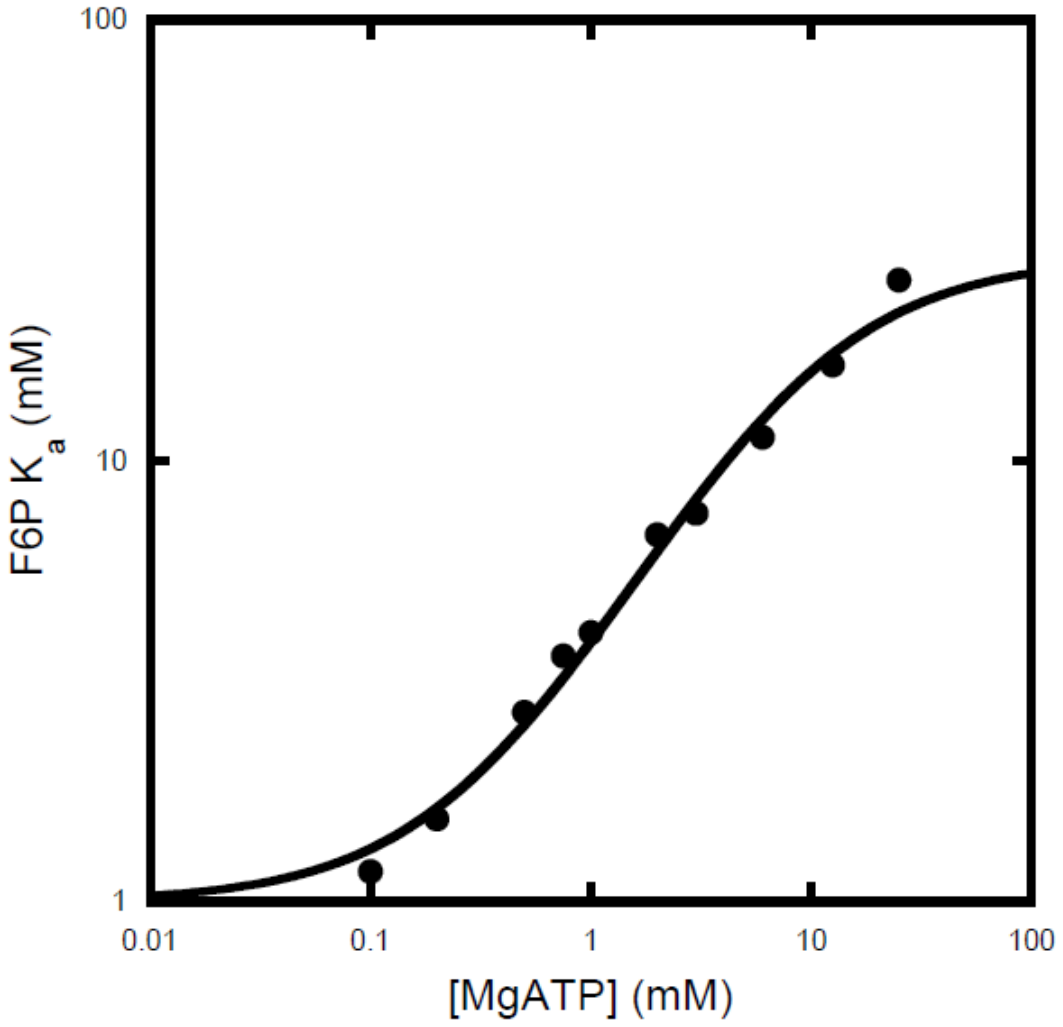

Figure 2-13: Dependence of Fru-6-P K_a values on the concentration of MgATP for preparation #4 (see text). Fitted parameters obtained by fitting data to equation 2-2 and listed in Table 2-9. Error bars represent error in value of Fru-6-P K_a obtained from equation 2-1.

Table 2-9: Fitted kinetic parameters measured for preparation 4 compared to fit of compiled data

	Compiled Fit	Preperation #4
K^0_{ia} (mM)	2.07±0.04	1.00±0.03
K^0_{ix} (mM)	0.36±0.01	0.30±0.01
ΔG_{ay} (kcal/mol)	2.05±0.01	1.989±0.002

The Fru-6-P dissociation constant observed in this publication is about two or three times lower than what was reported by Reinhart and Lardy [51]. However, the response of Fru-6-P K_a to the allosteric effector MgATP was very consistent with that reported by Reinhart and Lardy [51, 52]. Both the dissociation constant of MgATP in the absence of Fru-6-P (K_{iy}^{o}) and the maximum allosteric effect (ΔG_{ay}) were comparable to published values, but the value of Fru-6-P K_a was two times larger in nearly all conditions tested (Figure 2-13). Extrapolation to the axis of plots published in a later paper by Reinhart[52] suggest a dissociation constant of Fru-6-P in the absence of MgATP (K_{ia}^{o}) of 1.88mM. This value is very near to the value of 2mM measured in this publication (Figure 2-13). The qualitative response of rRLPFK to pH, citrate, AMP and phosphate were comparable to published data [51, 52] but the magnitudes of responses vary.

The effect of citrate on the dissociation constant of Fru-6-P was analyzed in 4 separate preparations of Fru-6-P. In three of the preparations, citrate increased the value of Fru-6-P K_a by 45-55% with approximately 10-15% of the increase occurring between 5 and 10mM citrate. Each were also subject to a 20-40% decrease in k_{cat} upon addition of citrate. Reinhart and Lardy reported a 2-fold increase in the value Fru-6-P K_a with only 5mM citrate and a 30% depression of k_{cat}. [51] In terms of Fru-6-P binding affinity, the rRLPFK we have purified is either less sensitive to citrate inhibition than the RLPFK reported on by Reinhart and Lardy, or is already in an inhibited form that is partially resistant to further inhibition by citrate. The effect of citrate was measured in a fourth preparation of rRLPFK

(mentioned above), which demonstrated a 2-fold increase in Fru-6-P K_a from 8.6mM to 16.7mM (Figure 2-14, Table 2-10). The fourth preparation of rRLPFK responded to citrate in a manner closer to the response described by Reinhart and Lardy [51].

At citrate concentrations above 10mM, the Fru-6-P K_a value began decrease reversing the inhibitory effect of citrate (data not shown). The decrease in the value of K_a for Fru-6-P seen at high concentrations of citrate is not thought to be relevant to the allosteric regulation of rRLPFK as the concentration of citrate at which it occurs is well above those physiologically relevant. The true maximum inhibitory potential of citrate may be masked by the sudden shift from increasing values of K_a for Fru-6-P to decreasing.

Activation by AMP has been observed in four separate preparations of rRLPFK (Figure 2-15). In each preparation AMP decreased the value of Fru-6-P K_a by 3 to 4-fold and increased the k_{cat} by 10-20%. The variation in value of Fru-6-P K_a at a given concentration of AMP is representative of the degree of variation in K_a seen between preparations (Figure 2-12). The magnitude of activation is comparable between each preparation and thus demonstrates that rRLPFK is consistently allosterically activated by AMP. Reinhart and Lardy reported a 4-fold activation of RLPFK by 5mM AMP [51], consistent with what is observed in this publication. However, Reinhart and Lardy did not report an increase in k_{cat}, as is observed in Figure 2-9 of this paper. The increase in k_{cat} reported in this paper is quite small and is most likely irrelevant to its regulatory mechanism.

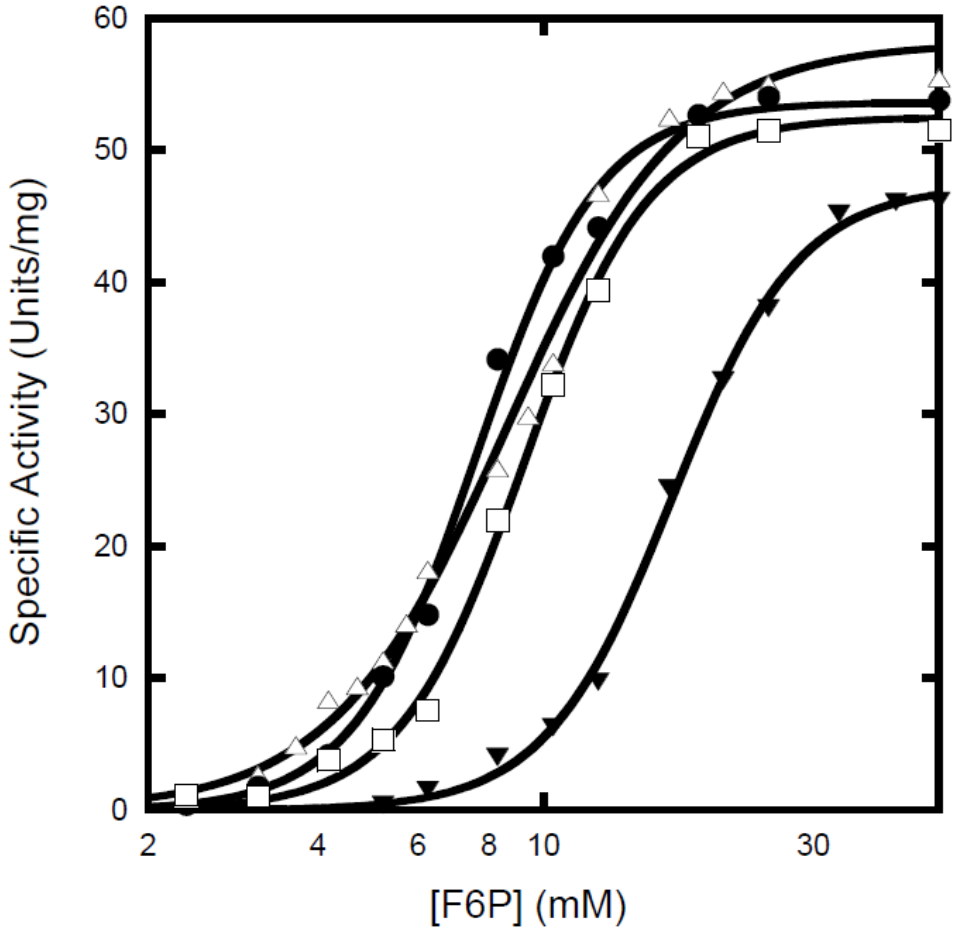

Figure 2-14: Effect of citrate on the kinetic properties of rRLPFK at standard conditions as measured with the "fourth preparation" of rRLPFK. [Citrate]: 0mM (open triangles), 0.1mM (closed circles), 1.5mM (open squares) or 12.5mM (closed triangles). Parameters obtained from fitting data to equation 2-1 is listed in Table 2-10.

Table 2-10: Fitted kinetic parameters measured for preparation 4 at several concentrations of citrate 3mM MgATP, pH=7.0 and 25^{0}C

[Citrate] (mM)	k_{cat} (sec^{-1})	Fru-6-P K_a (mM)	Hill number
0	83	8.6±0.3	2.8±0.2
0.1	76±1	7.6±0.2	4.0±0.3
1.5	75±1	9.2±0.2	3.9±0.2
12.5	68±1	16.9±0.3	3.9±0.2

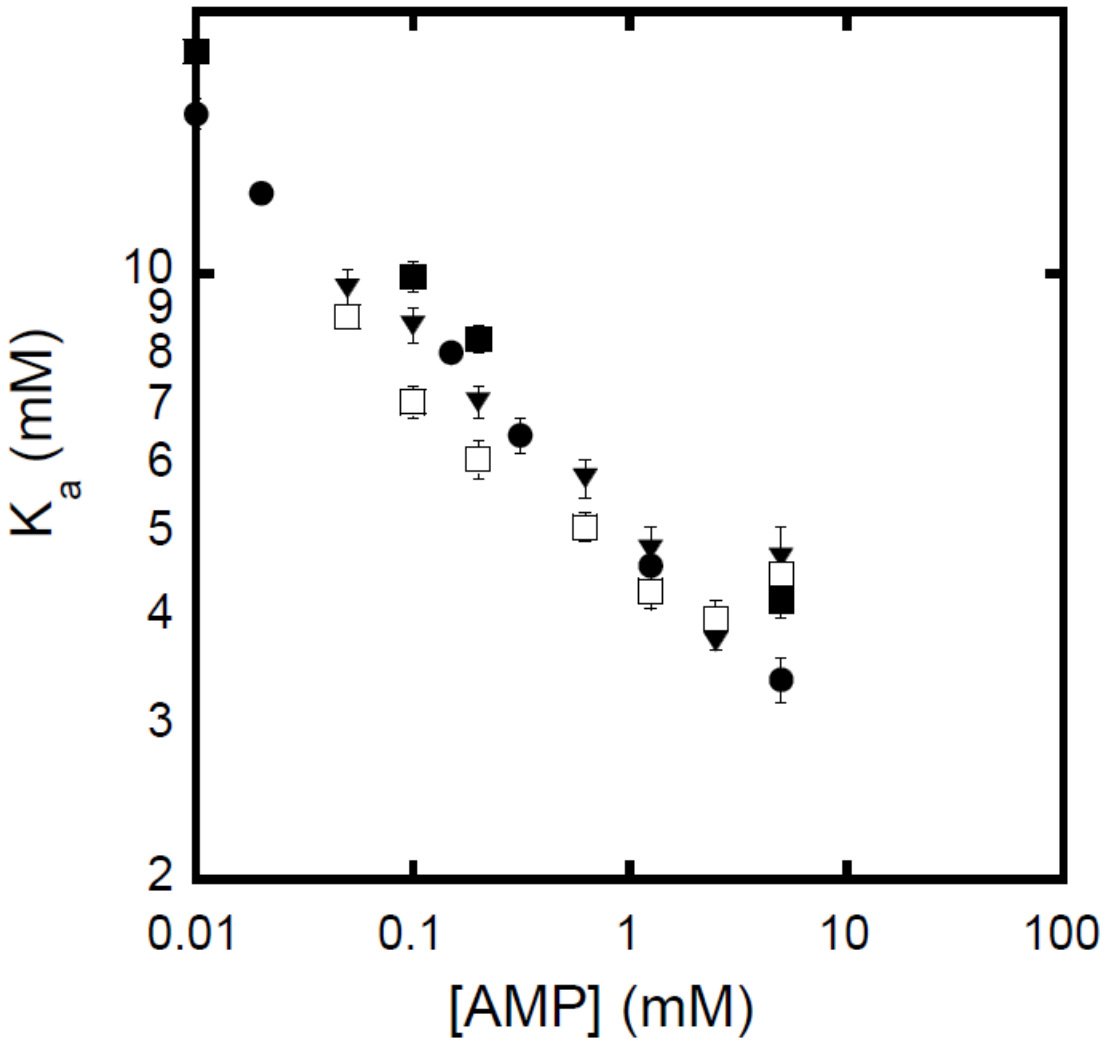

Figure 2-15: Dependence of Fru-6-P affinity on AMP concentrations in four preparations of rRLPFK. Data presented in figure 9 of this paper is represented as closed squares, data from addition preparations is represented as closed circles, closed triangles and open squares. Error bars represent fitted error.

The sensitivity of rRLPFK to pH has been examined in four separate preparations (Figure 2-16). In each, the value of Fru-6-P K_a increased by 20 to 30-fold as the pH increased from 6.7 to 8.0. The rRLPFK studied in this publication is twice as sensitive to pH as the enzyme purified by Reinhart and Lardy [51], both in terms of Fru-6-P binding affinity and k_{cat}. Phosphate is seen to consistently decrease the Fru-6-P dissociation constant of rRLPFK by 4-5-fold and increase the k_{cat} by 10-25%. The slight increase in k_{cat} was not noted by Reinhart and Lardy [51] and does not significantly contribute to the enzymes activation.

The response of rRLPFK to MgATP measured in this publication is consistent with published data [51], but the magnitude of the response to other effectors differs. The response of Fru-6-P binding to P_i, citrate, AMP, and MgATP is muted, whereas the response of Fru-6-P binding to pH is more dramatic. By far the most striking difference between the rRLPFK studied here and that published by Reinhart and Lardy is the 2-3-fold decrease in Fru-6-P binding affinity measured in all conditions. It is worth considering possible reasons that RLPFK purified out of a recombinant *E. coli* system may behave differently than RLPFK purified from fresh liver tissue.

Activation of RLPFK by post translational modifications in liver tissue could account for the different properties seen in rRLPFK. However, no posttranslational modification has been demonstrated to increase Fru-6-P binding affinity. Brand and Söling demonstrated that RLPFK can be phosphorylated [112], however, this

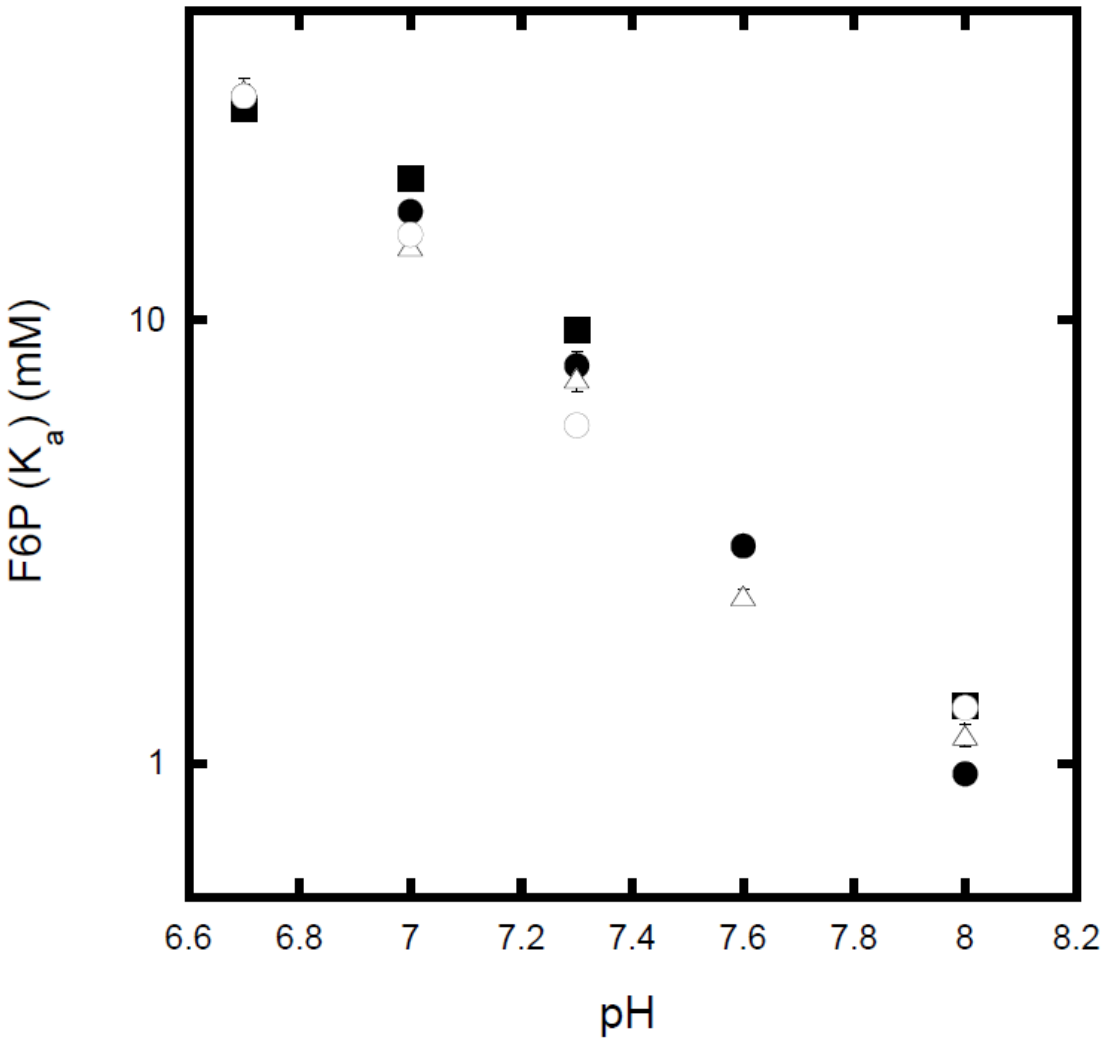

Figure 2-16: Effect of pH on the kinetic properties of rRLPFK in the presence of 3mM MgATP measured in four separate preparations of rRLPFK.

phosphorylation event is not believed to have any impact on the binding affinity of Fru-6-P [122]. Muscle PFK has been observed to be reversibly inactivated by acylation on the residues Cys-114, Cys-170, Cys-351, and Cys-577.[136] This has not been demonstrated in liver PFK. Glycosylation of PFK has been observed in human lung cancer cells.[137] Glycosylation occurred at Ser529, a highly conserved residue important for regulation of PFK by fructose-2,6-bisphosphate. The resulting modification down regulates PFK by inhibiting the binding of Fru-2,6-BP. No post translational modifications have been demonstrated to increase the Fru-6-P binding affinity and thus cannot explain the higher affinity for Fru-6-P observed in RLPFK purified from rat livers.

Another possible explanation could be a heterogeneous mixture of PFK isoforms in enzyme purified from liver tissue. Using immunological, electrophoretic and chromatographic techniques, Dunaway et al. suggest that two isozymes of PFK are expressed in liver tissues.[98] The major isozyme, PFK-L_2, is thought to be made entirely of liver PFK subunits (PFK-L), whereas the minor isozyme, PFK-L_1, is suggested to be a hybrid of 3 PFK-L monomers and 1 muscle PFK (PFK-M) monomer. Recombinant expression of the promoter denoted as PFK-L by Dunaway et al. assures that the RLPFK studied contains only "PFK-L_2" isoform. A minor component of PFK-L_1 may explain the minor differences between the data published here and that published using PFK purified from rat tissue. The data presented here is insufficient to support or reject that hypothesis.

It is interesting to note that a single preparation of rRLPFK yielded a Fru-6-P affinity closer to that reported by Reinhart and Lardy (Figure 2-12, Table 2-8). Additionally, the minor differences in behavior upon citrate inactivation were less apparent in this preparation. The differences between the value of Fru-6-P affinity reported here and that reported by Reinhart and Lardy[51] may have less to do with differences between recombinant and native RLPFK and more to do with the variation between one enzyme preparation and another. Ignoring the comparison to RLPFK from fresh liver tissue, the variation between recombinant RLPFK preparations shown in Figure 2-12 suggest that the affinity of rRLPFK for Fru-6-P is sensitive to subtle deviations in preparation procedures.

Conclusions

Recombinant expression of RLPFK in *E. coli* has proved to be an effective and efficient method of producing substantial quantities of fully active RLPFK. The kinetic and physical properties of rRLPFK is consistent of that described for enzyme purified out of rat liver homogenate. rRLPFK is sensitive to activation by phosphate, AMP and pH and is inhibited by MgATP, and citrate. The response of rRLPFK affinity for Fru-6-P upon binding of P_i, citrate, AMP, and MgATP reported here is slightly less than that reported by Reinhart and Lardy[51]. The response of rRLPFK Fru-6-P binding affinity to changes in pH is more dramatic. The most interesting difference between the rRLPFK studied here and that published by Reinhart and Lardy is the 2-3-fold decrease in Fru-6-P binding affinity measured in

all conditions. The cause of subtle differences between rRLPFK and RLPFK reported on by Reinhart and Lardy[51] is uncertain. However, given that the general response to allosteric effectors is conserved when RLPFK is expressed in a recombinant system, we propose that rRLPFK purified from *E. coli* is a suitable source for studying the biophysical and biochemical properties of RLPFK.

CHAPTER III

EFFECT OF MGATP ON THE ALLOSTERIC REGULATION OF RAT LIVER PHOSPHOFRUCTOKINASE BY MGAMP AND CITRATE

Introduction

Phosphofructokinase (PFK, EC 2.7.1.11) catalysis the phosphorylation of Fructose-6-phosphate (Fru-6-P) by MgATP to form fructose-1,6-bisphosphate (Fru-1-6-BP) and ADP. As the first committed step of glycolysis, PFK plays a key regulatory role in maintaining the energy demands of the cell. Mammalian organisms possess three PFK genes (L, M and P)[93-95] which have evolved from prokaryotic PFK via gene duplication and tandem fusion followed by functional diversification of the catalytic and effector sites.[138] Depending on the relative gene expression levels, specific isozymes are present in different tissues with distinct allosteric and catalytic properties.[100] Adult skeletal muscle expresses exclusively MPFK, liver expresses predominantly LPFK and the brain expresses large quantities of PPFK. Common to all isozymes are four distinct allosteric binding sites removed from the catalytic site for Fru-6-P and MgATP. These include activator sites for fructose-2,6-bisphospate (Fru-2,6-BP) and AMP or ADP, and inhibitor sites for MgATP and citrate.[67, 109, 140, 142]. The ancestral N-terminal active site maintained catalytic function whereas the C-terminal active site specified to form the site for

Fru-2,6-BP.[143] Additionally, the ancestral C-terminal allosteric site became the citrate binding site.[143] Interestingly, it seems that the novel allosteric sites for nucleotides AMP and MgATP did not evolve from any preexisting sites.[140, 142, 173]

Hormonal and nutritional signals regulate the expression and allosteric control of liver PFK (LPFK), acutely tuning glycolytic flux to the energy demands of both the individual cell and whole organism.[51, 72, 98, 174-176] Compared to other isozymes, PFK from liver is more strongly inhibited by MgATP resulting in relatively low levels of constituent glycolytic activity.[111] Unlike muscle tissue, which undergoes anaerobic respiration, the concentration of MgATP in liver tissues remains consistently high. Consequently, *in vivo* liver PFK activity does not fluctuate as greatly[111] Conditions in which it does are generally ominous indicators of deleterious circumstances. For example, increased PFK inhibition resulting from hormonal induced depletion of Fru-2,6-BP occurs in conditions of starvation[177] or diabetes[178], as metabolism is redirected towards increased gluconeogenesis. And liver PFK activation occurs in conditions of hypoxia as a consequence of decreased concentrations of inhibitor MgATP and increased concentrations of activator AMP.[179]

Cancer cells demonstrate increased glycolysis and decreased oxidative phosphorylation, a phenomenon known as the Warburg effect.[180-182] The Warburg effect is triggered in part by hypoxia, resulting from insufficient vascularity to the tumor.[183] Under conditions of hypoxia the ratio of cellular AMP/ATP[13] increases significantly resulting in allosteric activation of phosphofructokinase (PFK)[49].

Allosteric activation of RLPFK has been demonstrated to increase glycolysis and glucose uptake in liver cancer cells even without increased expression of glycolytic enzymes.[13] Additionally, down regulation of citrate synthase reduces the concentration of citrate further alleviating PFK inhibition.[184] The metabolic aberrations observed in the Warburg affect may also be relevant to stem cells.[185] Understanding the interdependence of ATP and citrate inhibition and AMP activation of liver phosphofructokinase is critical for understand the hypoxia triggered increase in glycolysis.

Allosteric studies of liver PFK are often performed by measuring the reaction rate as a function of ligand concentration at a set concentration of substrate. The resulting measurements are only meaningful within the precisely defined condition in which they were performed. In order to understand the nature of allosteric regulation of PFK within a cell undergoing metabolic flux, a system whose components are constantly variable, it is critical to determine the thermodynamic allosteric parameters which are responsible for manifesting the allosteric response.[65] Allosteric effectors of liver PFK primarily effect the activity by shifting the value K_m of Fru-6-P (K-type effects).[51] For a system with multiple allosteric binding site, such as is the case of RLPFK, it is critical to not only understand the relationship between the individual allosteric effectors and the substrate, but also the nature of interaction of the various allosteric ligands with each other. Previous reports have determined the interdependence between MgATP and H^+(which can be viewed as an allosteric inhibitor)[52] and between

MgATP and Fru-2,6-BP[106, 108]. To round out the quintet of allosteric effectors, we have measured the interdependence between MgATP and citrate and between MgATP and AMP. We report here the thermodynamic parameters defining allosteric regulation by citrate and AMP at physiological pH as well as the dependence of these parameters on the concentration of inhibitor MgATP.

Materials and Methods

Recombinant rat liver PFK (RLPFK) was expressed from p-ALTER EX2 plasmid within E. coli strain RL257[169]. Growth, expression and purification procedures were performed as describe previously. (chapter 2) All materials used for enzymatic assays were analytical grade and purchased from either Fisher Scientific, Sigma-Aldrich, Research Products International or VWR. Distilled, deionized Mili-Q water was used throughout. Dithiothreitol (DTT) was purchased from Fisher. ATP, AMP, citric acid, fructose-6-phosphate (Fru-6-P), EDTA, $MgCl_2$, MOPS-KOH, KCl, $(NH_4)_2SO_4$ and aldolase (ammonium sulfate suspension) were purchased from Sigma-Aldrich. Ammonium sulfate suspensions of triosephosphate isomerase and glycerol-3-phosphate dehydrogenase were purchased from Roche. Enzymes purchased as ammonium sulfate suspensions were dialyzed extensively against 50mM MOPS-KOH, 100mM KCL, 2mM $MgCl_2$ and 100μM EDTA.

All assays were performed at 25^0C and initiated by the addition of 6μL PFK to a final volume of 600μL buffer. Dilution of PFK into the cuvette contributes the

addition of 0.2mM P_i, 0.2% glycerol, 10μM Fru-6-P, and 30μM $MgSO_4$ to all assays. Allosteric kinetic properties of PFK were investigated in the following buffer; 50mM MOPS-KOH, 100mM KCL, 100μM EDTA, 2mM DTT, 0.2mM NADH, pH=7.0, 250μg/ml of aldolase, 50μg/ml of glycerol-3-phosphate dehydrogenase, 5μg/ml of triosephosphate isomerase. The term "standard conditions" refer to assay conditions at which the concentration of MgATP is 3mM and is taken to reflect physiological concentrations to a close approximation.[51] Most assays were performed at a fixed concentration of 3mM ATP with a total $MgCl_2$ concentration of 5mM. In experiments where the ATP concentration was varied, total $MgCl_2$ was always kept in 2mM excess of the ATP. Stock solutions of Fru-6-P, ATP and AMP were assayed enzymatically and kept frozen between experiments. Assays were terminated when the substrate concentration had decreased by 20μM to ensure negligible depletion of MgATP and buildup of the activating reaction product, fructose-1,6-bisphosphate (Fru-1,6-P).

The rate of catalyzed substrate depletion was monitored using a Beckman Series 600 spectrophotometer. Data measured with varying concentrations of Fru-6-P were fit using the nonlinear least-squares fitting analysis of Kaleidagraph software (Synergy). The initial velocity data were plotted against concentration of Fru-6-P and fit to the following equation:

$$v^0 = \frac{V[A]^{n_H}}{K_a^{n_H} + [A]^{n_H}} \qquad 3\text{-}1$$

Where v° is the initial velocity, [A] is the concentration of the substrate Fru-6-P, V is the maximal velocity, n_H is the Hill coefficient, and K_a is the concentration of substrate that gives one-half the maximal velocity. For a reaction in rapid equilibrium, K_a is equivalent to the dissociation constant for the substrate from the binary enzyme–substrate complex.[65] The K_a values obtained from the initial velocity experiments were plotted against effector concentrations and fit to the following equation:

$$K_a = K_{ia}^o \left(\frac{K_{ix}^o + [X]}{K_{ix}^o + Q_{ax}[X]} \right) \qquad 3\text{-}2$$

where K_{ia}^o is the dissociation constant of Fru-6-P in the absence of allosteric effector, X is allosteric effector, K_{ix}^o is the dissociation constant of allosteric effector in the absence of Fru-6-P and Q_{ax} is the coupling constant between Fru-6-P and allosteric effector.[65, 172]

Equation 3-2 describes the effect of a single allosteric ligand on the value of K_a for fru-6-P binding. For an enzyme whose kinetics is regulated by the binding of two independent allosteric ligands, the apparent dissociation constant is defined by the following equation:[52, 65]

$$K_a = K_a^0 \left[\frac{K_{iy}^0[X] + K_{ix}^0[Y] + Q_{xy}[X][Y] + K_{ix}^0 K_{iy}^0}{K_{iy}^0 Q_{ax}[X] + K_{ix}^0 Q_{ay}[Y] + Q_{axy}[X][Y] + K_{ix}^0 K_{iy}^0} \right] \qquad 3\text{-}3$$

where K_a is the concentration of substrate A (Fru-6-P) producing half-maximal velocity, X and Y are the primary and secondary allosteric effectors respectively, K_{ia}^0 is the value of K_a when $[X] = [Y] = 0$, K_{iy}^0 is the dissociation constant of Y when

$[X] = [A] = 0$, K_{ix}^0 is the dissociation constant of X when $[Y] = [A] = 0$, Q_{xy} is the coupling constant between the allosteric effectors X and Y, Q_{ax} is the coupling constant between substrate A and allosteric effector X, Q_{ay} is the coupling constant between substrate A and allosteric effector Y, Q_{axy} is the coupling constant between all three ligands ($A, X\ and\ Y$). Each of the four coupling constants describes the effect of the binding of one ligand on the binding of the other ligands.[65] Each can be expressed in free energy terms according to the relationship:

$$\Delta G = -RTlnQ \qquad 3\text{-}4$$

where R is the gas constant and T is the absolute temperature and ΔG is the coupling free energy.[65] For an illustrative example, consider the coupling constant Q_{ax}. A value of $Q_{ax} = 1$ indicates that A and X bind independently, a value of $Q_{ax} < 1$ indicates that the binding of X is antagonistic to the binding of A and a value of $Q_{ax} > 1$ indicates that the binding of X encourages the binding of A. In this chapter A indicates substrate fru-6-P, X indicates the primary allosteric effector (either citrate of AMP) and Y indicates the secondary allosteric effector MgATP.

The effect of a secondary effector Y on the parameters of a primary effector X can be expressed according to the following relationships:[52]

$$K_a^{0\prime} = K_{ia}^0 \left[\frac{K_{iy}^0 + [Y]}{K_{iy}^0 + Q_{ay}[Y]}\right] \qquad 3\text{-}5$$

$$K_{ix}^{0\prime} = K_{ix}^0 \left[\frac{K_{iy}^0 + [Y]}{K_{iy}^0 + Q_{xy}[Y]}\right] \qquad 3\text{-}6$$

$$Q'_{ax} = \frac{\left(K^0_{iy} + [Y]\right)\left(K^0_{iy}Q_{ax} + Q_{axy}[Y]\right)}{\left(K^0_{iy} + Q_{ay}[Y]\right)\left(K^0_{iy} + Q_{xy}[Y]\right)} \qquad 3\text{-}7$$

Due to reciprocity, equations 3-5. 3-6 and 3-7 can describe the effect of ligand X on the allosteric parameters of ligand Y by simply switching the occurrences of X and Y in the equations.[65] Substituting equations 3-5, 3-6, and 3-7 into equation 3-3 yields the following equation:

$$K_a = K^{o\prime}_{ia}\left(\frac{K^{o\prime}_{ix} + [X]}{K^{o\prime}_{ix} + Q'_{ax}[X]}\right) \qquad 3\text{-}8$$

Equation 3-8 is functionally indistinguishable from equation 3-2 and describes the relationship between the apparent dissociation constants of substrate and primary allosteric effector at any non-variable concentration of secondary allosteric effector.

Results

Activation by AMP

We measured the apparent dissociation constant of RLPFK for Fru-6-P (K_a) in standard conditions at 12 concentrations of AMP (Figure 3-1). The addition of AMP is seen to decrease the K_a up to 5mM AMP and then slightly increase the K_a at 10mM and 20mM AMP. Fitting the AMP dependent K_a data to equation 3-8 (where X=AMP) yields a dissociation constant of Fru-6-P in the absence of AMP ($K^{0\prime}_{ia}$) of 13.2±0.2mM, a dissociation constant of AMP in the absence of Fru-6-P ($K^{0\prime}_{ix}$) of

0.75±0.06mM and a coupling constant between Fru-6-P and AMP (Q'_{ax}) of 4.7±0.1 (Figure 3-1-insert).

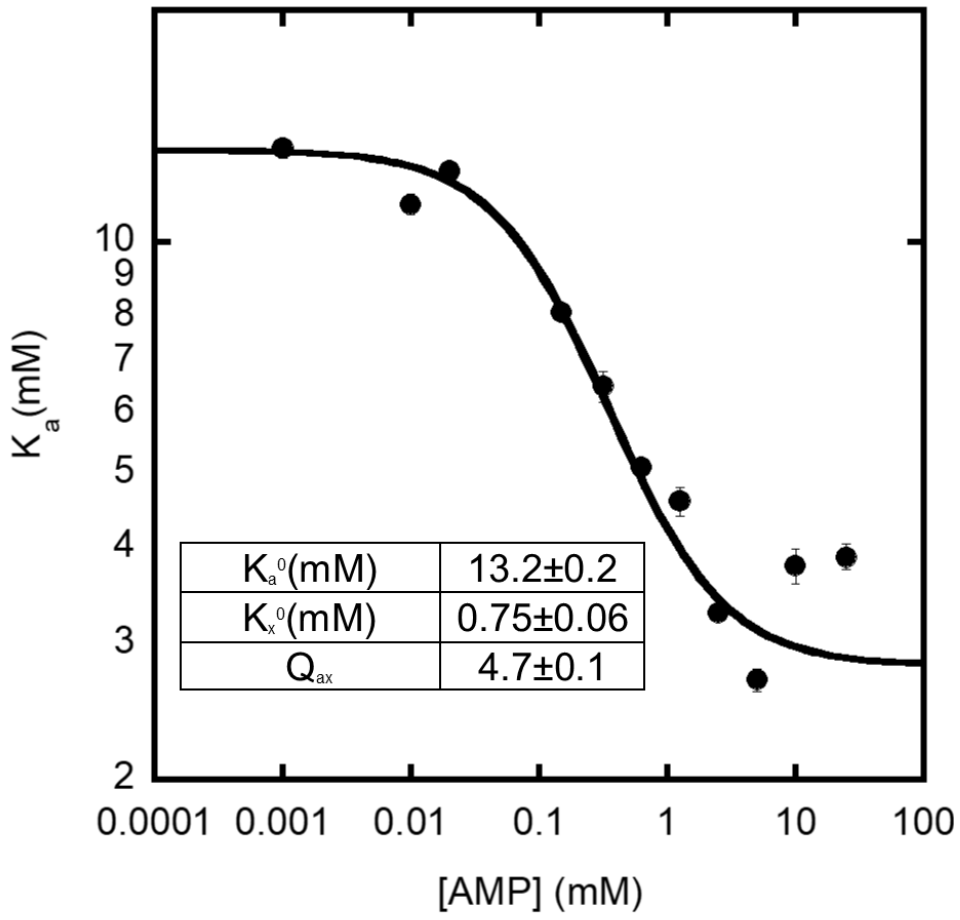

Figure 3-1: Influence of AMP on the apparent Michaelis constant for Fru-6-P in the presence of 3mM MgATP and pH=7.0. Data is fit to equation 3-2 and the parameters obtained from the fit are listed in the insert. Error bars represent standard error of fit.

The AMP dependent K_a data presented in Figure 3-1 were obtained in the presence of 3mM MgATP and therefor represents AMP activation of an inhibited RLPFK. To approximate the effect of AMP on RLPFK in the absence of MgATP as well as to determine the effect of MgATP on AMP activation, we measured the apparent dissociation constant of Fru-6-P with 98 different combinations of MgATP and AMP concentrations. (Figure 3-2) The concentration of MgATP ranged from 0.1mM to 25mM, and the concentration of AMP ranged from 0-50mM. The curves in Figure 3-2 represent the best fit of data obtained at each MgATP concentration to equation 3-2 (where X=AMP), and provides a good description of the data. As the concentration of MgATP increases the curves shift up, and the distance between the top and bottom plateau decrease, indicating that MgATP effects at least 2 of the kinetic parameters describing AMP activation ($K_{ia}^{0}\ and\ Q_{ax}$).[52] The dependence of $K_{ia}^{0\prime}$, $Q_{ax}^{\prime}$ and $K_{ix}^{0\prime}$ on the concentration of MgATP is demonstrated in Figure 3-3. In agreement with visual inspection of Figure 3-2, Figure 3-3 shows that as MgATP concentration is increased, the value of K_a^0 increases and the value of Q_{ax} decreases. The dependence of K_{ix}^{0} on MgATP concentration is not clear from inspection of the data presented in Figure 3-3. Interpretation of the dependence of K_{ix}^{0} on MgATP concentration that is suggested by the fit is discussed below.

A model of allosteric activation in which both ligands bind to the enzyme simultaneously predicts that an activator will decrease the apparent K_a for substrate until a plateau is reached at which point additional activator no longer has an effect on the apparent K_a.[65] We see a steady decrease in the apparent K_a

with increasing AMP, however we see that in at least 4 experiments, high concentrations of AMP increases the K_a slightly. (Figure 3-2; 25mM, 3mM, 0.4mM and 0.2mM MgATP) The slight inhibition only occurs above 10mM AMP (in the presence of MgATP), a concentration well above that which is physiologically relevant.[13] We suggest that this activation is a result of some secondary effect of AMP (possible AMP binding to the MgATP allosteric site) and is not related to its mechanism of allosteric activation. Any concentration of AMP high enough to elicit an increase in the Fru-6-P K_a was excluded from fitting to equation 3-2 or 3-3.

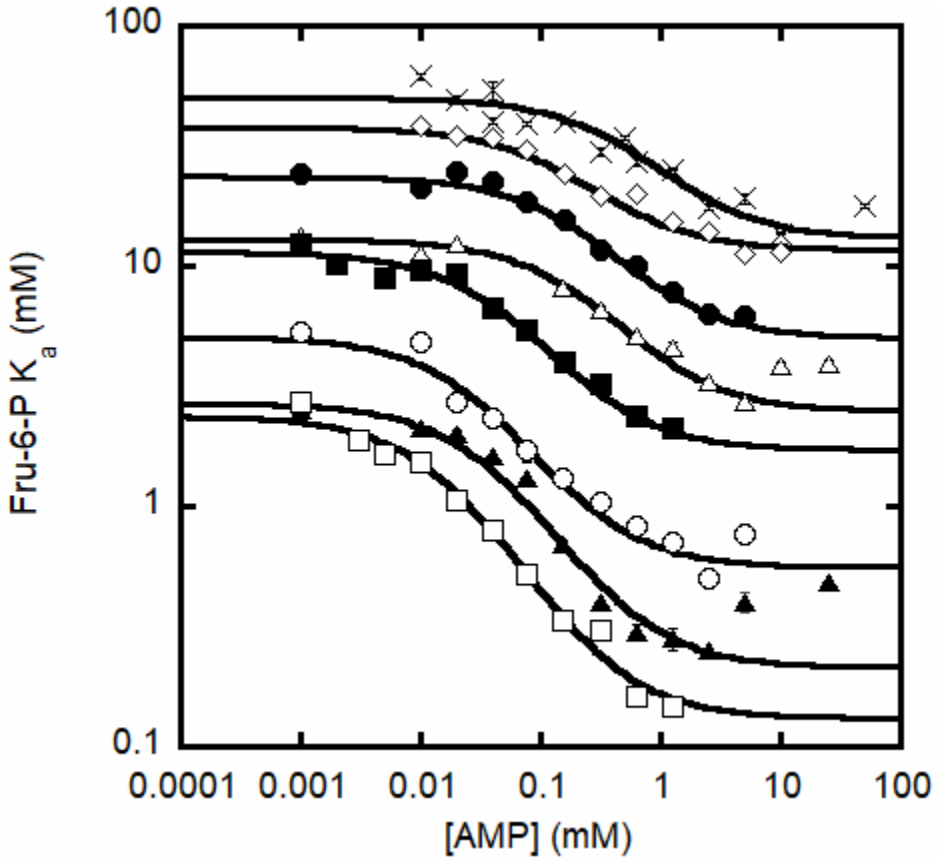

Figure 3-2: Influence of AMP on the apparent Michaelis constant for Fru-6-P at various concentrations of MgATP. Concentration of MgATP is 0.1mM (open squares), 0.2mM (closed triangles), 0.4mM (open circles), 1.5mM (closed squares), 3mM (open triangle), 6.25mM (closed circles), 12.5mM (open diamond), and 25mM (X). Curves are fit individually to equation 3-2, error bars represent standard error of fit.

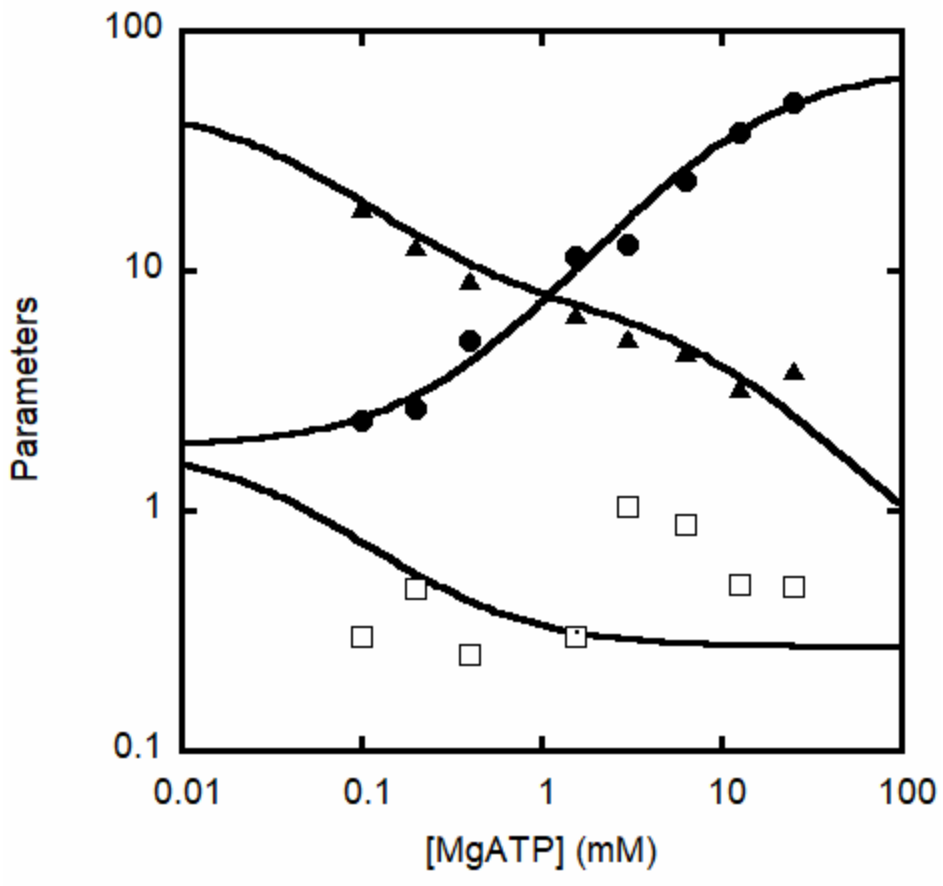

Figure 3-3: Influence of MgATP on the parameters describing allosteric activation by AMP. Values of $\boldsymbol{K_{ia}^{0\prime}}$ (closed circles), $\boldsymbol{K_{ix}^{0\prime}}$ (open squares) and $\boldsymbol{Q_{ax}'}$ (closed triangles) were determined by fitting data in Figure 3-2 to equation 3-2. Error bars represent standard error of fit. Curves represent predicted values of these parameters based on an overall fit to equation 3-3. Curves were generated from equations 3-5, 3-6 and 3-7 using the parameters listed in Table 3-1.

To determine the parameters describing allosteric regulation of RLPFK under the influence of both AMP and MgATP, the K_a data presented in Figure 3-2 was fit to equation 3-3. The initial estimates were made by visual inspection of Figure 3-3 as follows; K_{ia}^{0}=2mM ($K_{ia}^{0\prime}$ when [MgATP]=0.1mM); K_{iy}^{0}=0.3mM ([MgATP] of the transition of K_{ia}), Q_{ay}=0.03 (ratio of $K_{ia}^{0\prime}$ at low [MgATP] and $K_{ia}^{0\prime}$ at high [MgATP]); K_{ix}^{0}=0.4mM ($K_{ix}^{0\prime}$ when [MgATP]=0.1mM); Q_{ax}=20 ($Q_{ax}^{\prime}$ when [MgATP]=0.1mM); Q_{xy}=0.5 (ratio of $K_{ix}^{0\prime}$ at low [MgATP] and $K_{ix}^{0\prime}$ at high [MgATP]); Q_{axy}=0.05 ($Q_{ay} * Q_{axy} *$($Q_{ax}^{\prime}$ at high [MgATP]) [52, 65] Interestingly, these values failed to converge to a reasonable fit. Simulated plots of $K_{ia}^{0\prime}, K_{ix}^{0\prime}$ and $Q_{ax}^{\prime}$ vs [MgATP] reveal that if $Q_{xy} \leq 1$ no combination of the remaining parameters could reproduce the systematic decrease in $Q_{ax}^{\prime}$ seen as a function of [MgATP]. One can conceptualize this phenomenon by recognizing that AMP decreases the K_a of Fru-6-P both directly and, if antagonistic to MgATP, indirectly by palliating the inhibition by MgATP. The magnitude of the latter would be greatest at intermediate concentrations of MgATP, at which slight changes in the apparent dissociation constant of MgATP would result in significant changes in degree of bound MgATP. Alternatively, in the case of a cooperative interaction between AMP and MgATP, AMP self-sabotages its efforts at activation by simultaneously promoting inhibition by MgATP. Simulation of $K_{ia}^{0\prime}, K_{ix}^{0\prime}$ and $Q_{ax}^{\prime}$ data using a value of $Q_{xy} = 4$ and $Q_{axy} = 0.3$ generated a good approximation of Figure 3-3. By using these values as initial estimates, in addition to the previously listed values, non-linear regression analysis

converged yielding the values and standard error for these parameters listed in Table 3-1. The behavior of $K_{ia}^{0\prime}, K_{ix}^{0\prime}$ *and* $Q_{ax}^{\prime}$ as a function of MgATP that is predicted by the parameters in Table 3-1 is shown by the solid lines in Figure 3-3.

Table 3-1: Parameters resulting from fitting apparent Michaelis constant data obtained at various concentrations of MgATP and AMP or citrate to equation 3-3

	Ligand	
	AMP	Citrate
K_{ia}^{0} (mM)	1.85±0.03	0.96±0.05
K_{ix}^{0} (mM)	1.9±0.1	2.4±0.3
K_{iy}^{0} (mM)	0.29±0.01	0.30±0.02
Q_{ax}	50±3	0.18±0.01
ΔG_{ax} (k_{cal}/mol)	-2.32±0.06	1.02±0.06
Q_{ay}	0.026±0.001	0.028±0.001
ΔG_{ay} (k_{cal}/mol)	2.16±0.04	2.12±0.04
Q_{xy}	7.0±0.6	0.58±0.07
ΔG_{xy} (k_{cal}/mol)	-1.15±0.09	0.3±0.1
Q_{axy}	0.07±0.01	0.009±0.002
ΔG_{axy} (k_{cal}/mol)	1.6±0.1	2.8±0.2

A=Fru-6-P, X=AMP or Citrate, and Y = Fru-2,6-BP. Coupling free energies were calculated according to equation 3-4 with T=25^{0}C

The influence of MgATP on the value of K_a at several concentrations of AMP is displayed in Figure 3-4. The data presented in Figure 3-4 could be well described by equations 3-3 using the parameters in Table 3-1. However, non-linear regression analysis using equation 3-2 does not converge to meaningful values when the data is plotted in the form of K_a as a function of MgATP concentration (save for those measured in the presence of very low concentrations of AMP). The reason the experimental data could not be fit by equation 3-2 is due to a failure to define the top and bottom plateaus of the sigmoidal binding curve. This is partially due to a value of Q_{xy} that is greater than 1, which means that increasing concentrations of AMP decreases the value of $K_{iy}^{0\prime}$ (Figure 3-4 B). When the value of $K_{iy}^{0\prime}$approaches 0.1mM (the lowest concentration of MgATP used) it becomes very difficult to approximate the lower plateau. Fitting is further complicated by a value of Q_{axy} that predicts increasing MgATP inhibition as AMP is increased (Figure 3-4 B). For an illustrative example, consider MgATP inhibition in the presence of saturating AMP. In the presence of saturating AMP, the predicted value of $K_{iy}^{0\prime}$ is 0.04mM, $Q_{ay}^{\prime}$ is 0.0002 $\left(\frac{Q_{axy}}{Q_{ax}*Q_{xy}}\right)$, $K_{ia}^{0\prime}$ is 0.037mM $\left(\frac{K_{ia}^{0}}{Q_{ax}}\right)$ therefore, the $K_{ia}^{\infty\prime}$ (the value of K_a in the saturating presence of MgATP) is a staggering 185mM $\left(\frac{K_{ia}^{0\prime}}{Q_{ay}^{\prime}}\right)$.[65] Clearly, neither the value of $K_{ia}^{0\prime}$ or $K_{ia}^{\infty\prime}$ are experimentally determinable in the presence of saturating AMP.

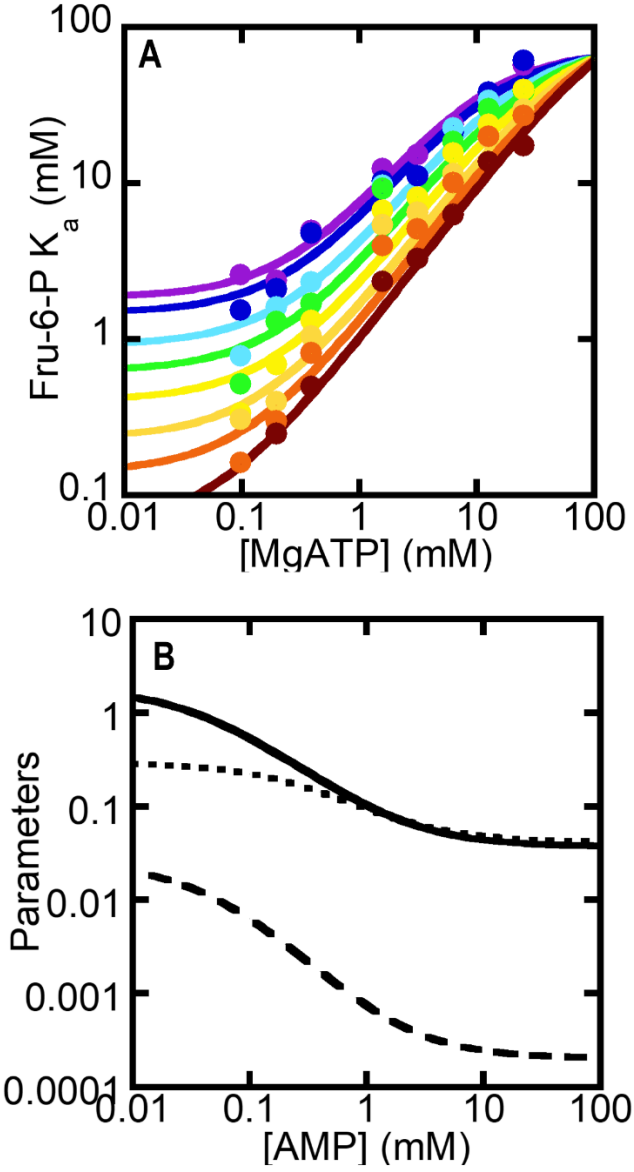

Figure 3-4: Influence of AMP on the parameters describing allosteric inhibition by MgATP. A. Influence of MgATP on the apparent Michaelis constant for Fru-6-P at various concentrations of AMP. Some data is not displayed for the sake of clarity. Concentration of AMP is 0mM (purple), 0.01mM (blue), 0.04mM (light blue), 0.8mM (green), 0.15mM (yellow), 0.3mM (yellow-orange), 0.625mM (orange) and 2.5mM (Red). Error bars represent standard error of fit. Solid curves represent predicted values of K_a generated using equation 3-3 and the parameters in Table 3-1. B. Simulated values of $\boldsymbol{K_{ia}^{0\prime}}$ (solid line), $\boldsymbol{K_{iy}^{0\prime}}$ (dotted line) and $\boldsymbol{Q_{ay}^{\prime}}$ (dashed line) generated using the parameters in Table 3-1 with equations 3-5, 3-6 and 3-7.

Inhibition by citrate

At any given concentration of MgATP, increasing the concentration of citrate raised the value of K_a until the concentration of citrate exceeded 25mM, at which point additional increases in citrate concentration reduced the value of K_a. In the presence of 6mM MgATP, 200mM citrate produces a value of K_a that is even lower than that measured in the absence of citrate. (Figure 3-5) Citrate induced activation of RLPFK was seen at all concentrations of MgATP when the concentration of citrate exceeded 25mM. (data not shown) Concentrations of citrate above 25mM were excluded from further analysis because the activation seen above 25mM citrate is unlikely to be relevant to the allosteric regulation of RLPFK in physiological conditions.

The apparent dissociation constant of Fru-6-P (K_a) was measured for 109 combinations of MgATP and citrate concentrations. (Figure 3-6) At each concentration of MgATP, the dependence of the apparent K_a of Fru-6-P on the concentration of citrate was equation 3-8. The resulting parameters were plotted as a function of MgATP. (Figure 3-7) The value of $K_{ia}^{0\prime}$ increases with increasing MgATP concentrations (Figure 3-7 circles). An observation expected given the role of MgATP as an allosteric inhibitor of RLPFK. The value of $Q_{ax}^{\prime}$ increased as a function of MgATP concentration, indicating that MgATP impairs the ability of citrate to inhibit RLPFK (Figure 3-7 open squares). A small increase (amid a lot of noise) in the value of $K_{ix}^{0\prime}$ (where x=citrate) was seen as a function of MgATP concentration, indicating MgATP impaired binding of citrate.

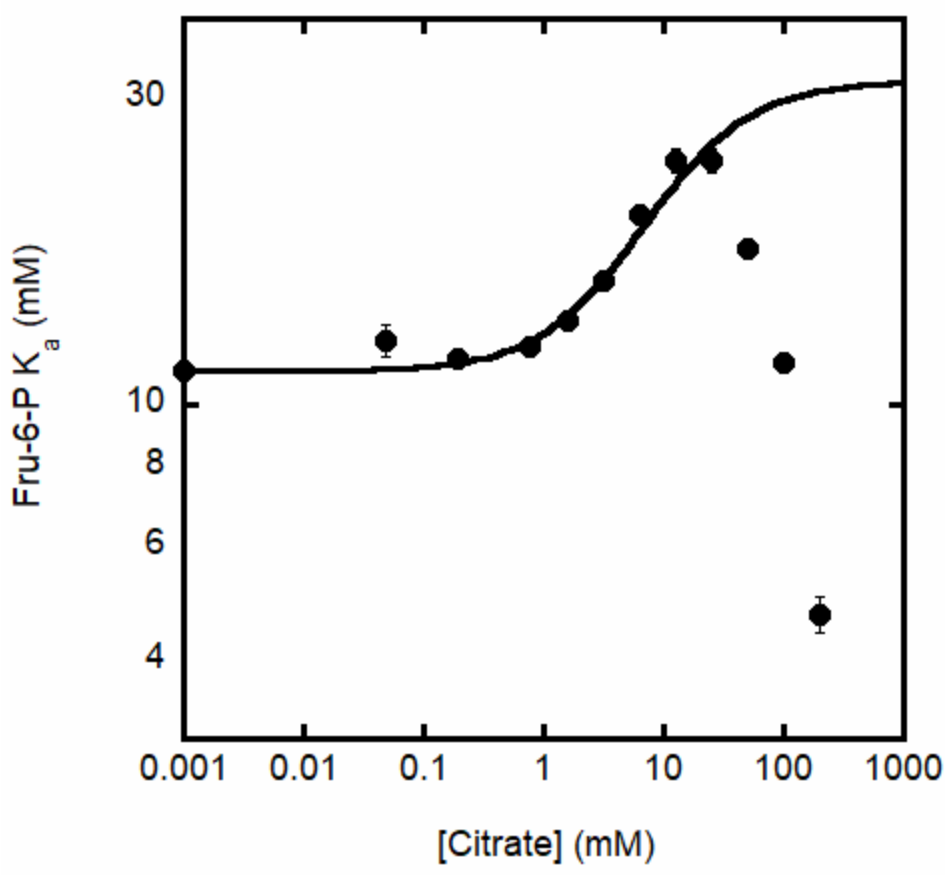

Figure 3-5: Influence of citrate on the apparent Michaelis constant for Fru-6-P in the presence of 6mM MgATP and pH=7.0. Data is fit to equation 3-2 and the parameters obtained from the fit are listed in the insert. error bars represent standard error of fit. Values of $\boldsymbol{K_a}$ measured at citrate concentrations greater than 20mM were excluded from the fit to equation 3-2.

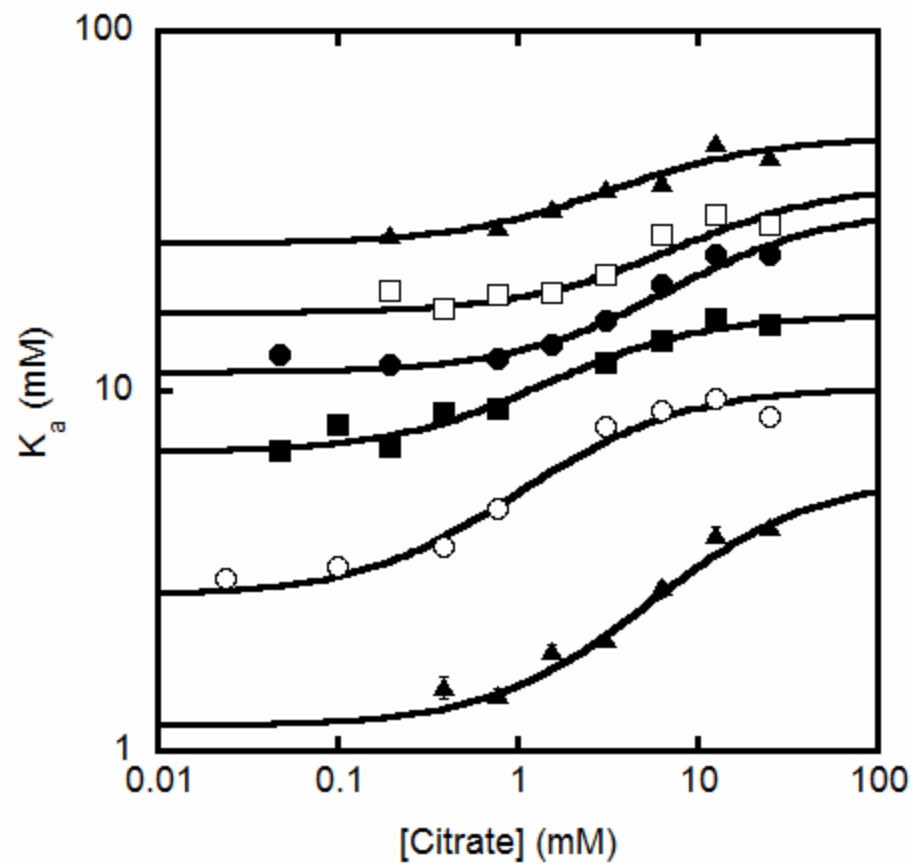

Figure 3-6: Influence of citrate on the apparent Michaelis constant for Fru-6-P at various concentrations of MgATP. Only partial data is displayed for clarity. Concentrations of MgATP displayed is 0.1mM (closed triangles), 0.5mM open circles, 2mM (closed squares), 6mM (closed circles), 12.5mM (open squares), and 25mM (closed triangles). Curves are fit individually to equation 3-2 and error bars represent standard error of fit.

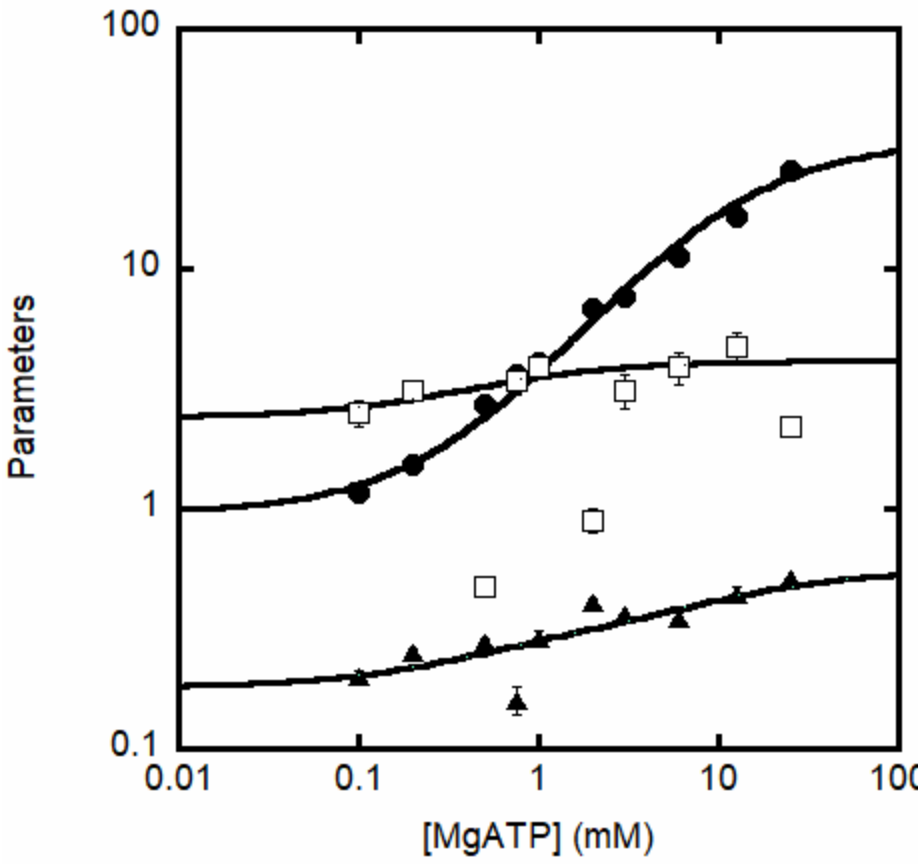

Figure 3-7: Influence of MgATP on the parameters describing allosteric inhibition by citrate. Values of $\boldsymbol{K_{ia}^{0\prime}}$ (closed circles), $\boldsymbol{K_{ix}^{0\prime}}$ (open squares) and $\boldsymbol{Q_{ax}^{\prime}}$ (closed triangles) were determined by fitting the data in Figure 3-5 to equation 3-2. Error bars represent standard error of fit. Curves represent predicted values of these parameters based on an overall fit to equation 3-3. Curves were generated from equations 3-5, 3-6 and 3-7 using the parameters listed in Table 3-1.

To determine the parameters describing allosteric regulation of RLPFK under the influence of both citrate and MgATP, the K_a data was collectively fit to equation 3-3. The following initial estimates were made by visual inspection of Figure 3-7 as described above; K_{ia}^0=1mM; K_{iy}^0=0.3mM; Q_{ay}=0.03; K_{ix}^0=2.5mM; Q_{ax}=0.2; Q_{xy}=0.5; Q_{axy}=0.0067. Using these values as initial estimates, the fit converged to give the parameter values listed in Table 3-1. The parameter values in Table 3-1 were used along with equations 3-5, 3-6 and 3-7 to simulated expected values of $K_{ia}^{0\prime}$, $K_{ix}^{0\prime}$ and $Q_{ax}^{\prime}$ as a function of MgATP (Figure 3-7 solid lines). Figure 3-7 demonstrates that the parameters listed in Table 3-1 do a good job of describing the experimental data. The values of K_{iy}^0 and Q_{ay} determined from these data are in very close agreement with those determined from AMP-MgATP data (Table 3-1). The value of K_a^0 differs by a factor of 2 between the different experiments (Table 3-1) because of the anomalously activated preparation of RLPFK used for the citrate data.

Discussion

It has been reported that AMP relieves MgATP and citrate inhibition,[76] acts synergistically with Fru-2,6-BP activation[186], but is competitive with cAMP activation of liver PFK.[67] Citrate has been reported to synergistically inhibit liver PFK with MgATP.[111] The term synergistic is used in these instances to indicate that the addition of two modifiers produces an effect greater than that observed for any one at saturation.[51] The primary conclusion from an observations of "synergism", as presented in previous publications, is that the allosteric effects of the ligands are not mutually exclusive, indicating distinct allosteric binding sites.[51] For example, Fru-2,6-BP binds to a different site than AMP and is therefore seen as "synergistic" whereas cAMP binds to the same site as AMP and therefore lacks "synergy".[67]

According to linkage theory[187], the binding of a second allosteric ligand (Y) in addition to the first (X) could affect the affinity of the enzyme for substrate (A) through some combination of an effect on the dissociation constant of X in the absence of A ($K_{ix}^{0\prime}$), the coupling free energy between X and A ($\Delta G_{ax}^{\prime}$), or the dissociation constant of A in the absence of X ($K_{ia}^{0\prime}$)[52] Any combination of those effects (positive or negative) would lead to the appearance of "synergism" between the two allosteric ligands, provided the directional effects on (K_a) are the same. The appearance of "synergism" could be observed even in the case in which two allosteric ligands exert their effect completely independently (X and Y only affect K_{ia}^{0}).

The term synergism could also be defined as a combined effect of multiple modifiers that is greater than the sum of the effects of the individual modifiers. We distinguish between the two definitions of synergism by referring to the later term as "true synergism". Absent of quantitative measurements of the coupling parameters, it is impossible to determine if "true synergism" exist between two ligands. True synergism only occurs in the cases in which Y positively affects the affinity for X (decreases the value of $K_{ix}^{0\prime}$) or increases the absolute value of $\Delta G_{ax}^{\prime}$ while simultaneously affecting the value of $K_{ia}^{0\prime}$ in the same direction as X. It is therefore necessary to measure the thermodynamic parameters describing the allosteric response to determine the relationship between two allosteric effectors. The distinction between the qualitative assessment of "synergy" and the quantitative determination of "true synergy" is perfectly illustrated in the case of citrate and MgATP. Citrate inhibits liver PFK in the presence of inhibitory concentrations of MgATP (Figure 3-5) and therefore could be passed as "synergistic" with MgATP as reported previously. However, we report here that MgATP increases the value of K_{ix}^{0} and decreases the value of Q_{ax} (Figure 3-7), a behavior not consistent with "true synergy".

While the discussion of the term synergistic is semantic, it speaks to the danger of viewing allostery through an oversimplified structural model. The classic models of allostery, such as the concerted MWC model[20] and the sequential KNF model[21], rely on the assumption that an allosteric enzyme exists in two possible conformations, relaxed (R) or tense (T), which have different affinities for

substrate. Even expanded models such as the population shift model[188], which considers an ensemble of conformational states, invokes a high affinity structure and a low affinity structure in order to explain allostery in terms of an allosteric two state model.[40] In such a model, an allosteric response manifest from an inhibitor or an activator stabilizing the inactive, or active form respectively. Therefor one would imagine that the binding of one inhibitor would promote the binding of another inhibitor to a separate binding site, as they would both bind to the same structural form. Conversely, the binding of an activator should be antagonistic to the binding of an inhibitor given that they stabilize different conformations of the enzyme. This assumption was found to be generally true for RLPFK in the presence of Fru-2,6-BP and MgATP, i.e. the binding of activator Fru-2,6-BP was antagonistic to the binding of inhibitor MgATP.[106] However, it has also been stated that AMP activates PFK by reducing the inhibition of MgATP without performing the necessary experiments to verify such a claim.[76, 189] We report evidence that an inhibitor (citrate) is antagonistic to the binding of MgATP, and an activator (AMP) promotes the binding of the inhibitor MgATP.

The absolute value of AMP-MgATP coupling is greater (ΔG_{xy}=-1.15k_{cal}/mol) than citrate-MgATP coupling (ΔG_{xy}=0.3k_{cal}/mol). However, the slight antagonism between MgATP and citrate binding is demonstrated reasonably well by the experimentally determined values of citrate $K_{ix}^{0\prime}$ as a function of MgATP concentration (Figure 3-7 open squares) whereas the MgATP facilitated increase in AMP binding is not empirically demonstrated by $K_{ix}^{0\prime}$ data (Figure 3-3 open

squares). The apparent failure of empirical evidence to corroborate modeled data is dampened upon recognition that although a plot of $K_{ix}^{0\prime}$ vs $[Y]$ provides the clearest indication of coupling between X and Y, it is not the only data in Figure 3-3 that depends on the value of ΔG_{xy}. The value of ΔG also influences the nature of the dependence of Q'_{ax} on $[Y]$. The values we present in Table 3-1 provide a good description of the value of Q'_{ax} as a function of MgATP, further, the general trend observed could only be explained by a value of Q_{xy} that ranged from 4-12 (data not shown). Two reasons are responsible for a poor empirical description of the dependence of AMP $K_{ix}^{0\prime}$ as a function of MgATP concentration; 1. error and uncertainty in the experimental determination of $K_{ix}^{0\prime}$ 2. difficulty performing experiments at the concentration of MgATP in which the coupling is most pronounced. The second of these reasons is a result of a 0.1mM lower limit of MgATP concentration imposed by the catalytic K_m of MgATP). Inspection of Figure 3-3 reveals that much of the MgATP induced perturbation of AMP $K_{ix}^{0\prime}$ takes place at concentrations of MgATP lower than 0.1mM.

An additional surprising detail is that the parameters listed in Table 3-1 predicts that at a high enough concentration of MgATP, Q_{ax} decreases to a value less than 1. The proposition that AMP can be converted into an inhibitor by MgATP is an extraordinary claim indeed. Fitting the collective K_a data while confining Q_{axy} to a value greater than 0.2 results in a reasonable description of the data without implying a complete inversion of AMP coupling at high concentrations of MgATP.

Ultimately, we decided on the fit presented in Table 3-1 because it required the fewest number of assumptions and provided a slightly better fit ($\chi^2 =$ $7000\ vs\ 8000$). Conformation or rejection of MgATP induced AMP inhibition could not be performed because at the concentration of MgATP in which inversion is expected to occur, the, K_a of Fru-6-P becomes so high as to make substrate saturation impossible. Such a measurement may be obtainable at high pH where the affinity for Fru-6-P is much higher.[51, 52] Unfortunately, changing the pH may also fundamentally change the allosteric behavior of MgATP and AMP.[108]

Determination of the dissociation constant of AMP in the absence of MgATP would be extremely valuable as it would provide a measurement of the true value of K_{ix}^0. ITP has been demonstrated to work as a catalytic substrate for rabbit muscle PFK but is unable to inhibit rabbit muscle PFK.[190] Measuring the effect of AMP on Fru-6-P K_a in the presence of ITP instead of MgATP could be an easy and efficient way to measurement of the true value of K_{ix}^0. If possible, such an experiment could be performed at several concentrations of AMP to measure the coupling between AMP and Fru-6-P in the complete absence of MgATP, thus giving the true value of Q_{ax}. Determining the value of K_{ix}^0 and Q_{ax}, as well as establishing the behavior of AMP coupling at concentrations of MgATP beyond 25mM would inform the proper variable constraints when fitting the K_a data to equation 3-3, and would therefore greatly enhance the interpretability of the resulting fit.

Surprising effects on K_a were seen at very high concentrations of both citrate and AMP. Specifically, we see an AMP induced increase in K_a, and a citrate

induced decrease. In some mammalian PFK homologs, ADP has been demonstrated to activate PFK at low (μM) concentrations and inhibit at higher (mM) concentrations.[173, 191] Presumably, this dualistic function is due to a high affinity for an activation site and a low affinity for the MgATP inhibition site.[140, 142, 148] It is reasonable to expect that AMP could bind to the MgATP inhibition site as well. Anecdotal observations suggested that the magnitude of AMP inhibition decreased with increasing concentrations of MgATP, lending credence to a MgATP inhibition site binding hypothesis (data not shown). It seems less likely that citrate binding to MgATP allosteric site could be responsible for the profound reversal of inhibition seen at high citrate concentrations. Regardless of the reason for the observed effects, we chose to exclude these data from analysis. However, it is important to remember that whatever is causing the observed effects does not manifest in the first data point in which it is undeniable. The secondary effect is likely affecting the apparent K_a values at concentrations of the allosteric ligand nearing saturation. Consequentially, the measured absolute value of ΔG_{ax} is likely less than the "true" value. Additionally, the value of $K_{ix}^{0\prime}$ is determined with less certainty because of the uncertainty in determining the plateaus.

Even when allowing the maximum amount of uncertainty, the data presented here does not support antagonistic binding between activator AMP and MgATP, nor synergistic binding between citrate and MgATP as would be expected from a 2-state model. Assuming a reasonable degree of confidence in the values reported here, we have identified a previously uncharacterized functional linkage

between MgATP and AMP. Bruser et. al reported a functional linkage between the ADP and MgATP allosteric sites in human muscle RLPFK.[173] They found that mutations that affected one allosteric ligand also affected the other. However, they found that the mutations were additive to a net outcome. For example, mutations that abolished activation by AMP concomitantly increased inhibition by MgATP resulting in an additive net reduction of catalytic activity. It would be very interesting to perform the experiments reported here on liver and muscle PFK with and without the mutations describe by Bruser et. al. Colombo et. al. reported citrate binding measurements with rabbit muscle PFK that indicated that MgATP was necessary for citrate inhibition.[190] This suggest a linkage between the two sites but is inconsistent with what we observed here. Again, performance of the experiments described in this chapter with muscle and liver PFK could clarify this apparent inconsistency.

Just about any structural model could be modified to accommodate the observations presented here by simple adding additional structural conformations. For example, the population shift model[188] could be used to explain the relationship between AMP and MgATP by visualizing an energy landscape in which at least 4 energy wells exist. However, it is not apparent from the population shift model that such an energy landscape would occur, and using this model to derive an equilibrium equation capable of quantifying it would be complicated.[40] The ensemble allosteric model (EAM) is a structural model of considerable flexibility and has been used to explain a hypothetical example in which the binding of an

allosteric ligand could turn an allosteric activator into an inhibitor.[41] What the EAM gains in flexibility it loses in applicability. Calculations of thermodynamic coupling parameters by the EAM are done *in silico.* The EAM does not provide a practical way to calculate the thermodynamic coupling parameters experimentally. The power of linkage analysis is that it allows for experimental determination of both the quantity and direction of an allosteric interaction without any preconceived notion of what the nature of the relationship may be.

Allosteric regulation of RLPFK by metabolites ensures that PFK activity responds acutely to the metabolic requirements of the cell. A rapid depletion of MgATP to AMP would indicate that it was imperative for RLPFK to ramp up its activity.[13] It is therefore a bit surprising that RLPFK would self-sabotage its activation via AMP facilitated increases in the affinity for the depleting MgATP. Perhaps avoiding unnecessary PFK activation is more critical than a synergistic response to increasing AMP/ATP ratios. For healthy liver tissue, which does not undergo anaerobic respiration, the best indicator of the metabolic needs is ATP. An increase in AMP amid a steady 3mM concentration of MgATP may be extraneous. The increase AMP concentration would buffer its own activation by simultaneously promoting inhibition from MgATP. In this manner, RLPFK is protected from superfluous activation when an increase in metabolism is not actually needed. Additionally, although a depletion of MgATP increases the K_{ix} of AMP, it also increases its activation potential (e.g. $Q_{ax} = 4.7 \pm 0.1$ at 3mM MgATP and 50±3 in the complete absence of MgATP). If an increase in metabolism is needed, the

conversion of MgATP to AMP ensures there will be plenty of AMP to induce activation, despite the diminished affinity, and the ramped-up activation potential of AMP ensures RLPFK will respond appropriately. Admittedly, the magnitude of the coupling between MgATP and citrate or AMP is relatively small. The coupling constant between AMP and MgATP (7.0±0.6) and citrate and MgATP (0.58±0.07) indicates a 7-fold and 2-fold modulation in binding. By contrast, MgATP exerts a 40-fold decrease in Fru-6-P binding.

The relationship between MgATP and citrate/AMP presented here is hardly a comprehensive description of the network of allosteric regulation guiding the activity of RLPFK. For the sake of simplification, we have completely ignored the effect of allosteric ligands on k_{cat} and the degree of Fru-6-P cooperativity.[65] This simplification is justified because the effect of citrate, AMP and MgATP are primarily on the value of K_m of Fru-6-P binding.[51] More importantly, we are missing information on the coupling between the dominant activator Fru-2,6-BP and effectors AMP and citrate. Cells under hypoxia or under influence by the Warburg effect see a decrease in MgATP and citrate, and an increase in AMP and Fru-2,6-BP. While the role of citrate on RLPFK activity can perhaps be ignored in these conditions, it is critical to understand how the trifecta of allosteric regulators (AMP, Fru-2,6-BP and MgATP) coordinate their respective influences to manipulate the affinity of RLPFK for Fru-6-P. Understanding the effect of glycosylation on these parameters is also important for understanding the roll of mammalian PFK in regulating metabolism in cancer cells.[137] It has been demonstrate that PFK is

glycosylated in cancer cells to inactivate glycolysis and redirect metabolism to the pentose phosphate pathway, giving a selective growth advantage to cancer cells.[137] Such a process is contrary to the allosteric activation from changes in concentration of MgATP, AMP and citrate. It is important to determine whether allosteric activation can lessen or prevent inhibition by glycosylation, or if glycosylation overrides allosteric responses.

Reinhart and Lardy found that RLPFK activation by Fru-2,6-BP alone was insufficient to overcome the allosteric inhibition of RLPFK by MgATP at physiological conditions, leading to the hypothesis that additional activating factors are still unaccounted for. Had AMP been seen to have a strongly antagonistic relationship with MgATP it may have made significant advances in closing the gap between experimentally measured rates and those expected to occur in liver tissue. The prevailing concentration of AMP in healthy liver tissue is 0.25mM.[13] The value of AMP $K_{ix}^{0\prime}$ is expected to be 0.3mM in the presence of 3mM MgATP (Table 3-1). Therefore, 0.25mM AMP is at the crux of activating potential. Should Fru-2,6-BP be observed to have a strongly synergistic relationship with AMP, the roll of AMP at physiological conditions may again be worth considering. The final variable that needs to be considered is the observed potential of polymerization to activate RLPFK.[49, 50, 104, 107] In the following chapters, we explore the polymerization properties of RLPFK and the influence of MgATP and Fru-6-P on the polymerization properties.

CHAPTER IV

USE OF FLUORESCENCE CORRELATION SPECTROSCOPY TO INVESTIGATE THE SELF ASSOCIATION OF RAT LIVER PHOSPHOFRUCTOKINASE

Introduction

Phosphofructokinase catalyzes the MgATP dependent phosphorylation of fructose-6-phosphate (Fru-6-P) to fructose-1,6-bisphosphate. As the first committed step of glycolysis, phosphofructokinase is highly regulated.[76, 177, 192] The smallest active form of PFK is a homotetramer, consisting of 4 identical 86kDa subunits. The ability of eukaryotic PFK to self-associate forming oligomers larger than a tetramer has been known since the first isolation of rabbit muscle PFK.[75] Among the 3 mammalian PFK isoforms, PFK from liver sources possesses the greatest propensity to self-associate.[96, 151] While, presumably, this property of mammalian PFK has caused countless frustration for experimenters, it can be exploited in efforts of purification by gel filtration to great success.[51, 102] Self-association has been proposed to activate PFK from rat livers (RLPFK) by increasing the affinity for substrate Fru-6-P.[49, 50, 104, 152] Concentration dependent activation of RLPFK provides an intriguing explanation for the striking contrast in

catalytic activity at physiological conditions between that measured in liver perfusion assays[153, 154] and that predicted by *in-vitro* kinetic assays[51].

In the cellular environment, RLPFK exist as a highly associated polymer, as evident by fluorescence polarization studies performed with RLPFK at near physiological concentrations, as well as gel filtration experiments of liver homogenate.[49] Kinetic assays of RLPFK must be performed at sub nanomolar concentrations in order to avoid NADH depletion as well as product induced activation. At the sub-nanomolar concentrations necessary for *in-vitro* kinetic assays, PFK from both liver and muscle have been demonstrated to exist almost entirely in the tetramer form.[50, 155] The oligomeric form of RLPFK stabilized at intermediate concentrations strongly depend on the solution conditions, with activating conditions promoting a polymer form and inhibiting conditions promoting the tetramer form.[49, 50, 104, 107] Most notably, Fru-6-P stabilizes the polymer form and MgATP induces formation of the tetramer. [49, 50] The argument presented by Reinhart and Lardy utilizes a Weber linkage argument[36, 98] to propose that the shift in tetramer-polymer equilibrium induced by Fru-6-P indicates that the polymer has a greater affinity for Fru-6-P.[49]

A polymerization induced increase in substrate affinity could explain why RLPFK is catalytically active in cellular conditions[153, 154] despite evidence from *In-Vitro* kinetic measurements suggesting a negligible rate of catalysis at physiologically relevant concentrations of Fru-6-P.[49, 105] A RLPFK concentration induced increase in Fru-6-P affinity has been demonstrated in kinetic assays.[49] And

efforts to measure the kinetic properties of the self-associated state without increasing the concentration RLPFK have been made by measuring rates in the presence of polyethylene glycol (PEG).[107] However, the vast majority of assays have been performed in conditions in which the tetramer is the predominant species. The implication is that all the known regulatory properties of RLPFK are relative to an already inhibited form. A thorough description of the regulatory pathways of RLPFK must include the interplay between ligand concentration and oligomerization state of the enzyme.

To further the understanding of RLPFK self-association and its role in regulation, a method is needed that can rapidly and accurately measure the size of RLPFK oligomer at a wide range of RLPFK concentrations. Methods capable of characterizing oligomer size include fluorescence polarization[50], analytical ultracentrifugation[156], size exclusion chromatography[157], dynamic light scattering[158] and electron microscopy[159]. Each of these have their own limitations and none can span the range of sub-nanomolar to micromolar concentrations. We utilize two photon fluorescence correlation spectroscopy (FCS) to determine the oligomeric size of RLPFK. The advantages of FCS include; (i) the ability to resolve particle sizes over a broad range of potential sizes, (ii) capability of assaying enzyme concentrations ranging from sub nanomolar to micromolar and (iii) is time and cost effective enough to justify reparative measurements following minute, systematic changes in assay conditions. Using FCS, one can address questions such as whether RLPFK is a tetramer at concentrations used for kinetic assays, the presence of

discrete or mixed species in the polymerized form, rate of tetramer dissociation from polymerized form, and critical ligand concentration necessary to stabilize polymerized species.

Here we present the use of two photon FCS to investigate the oligomeric state of physiologically relevant concentrations of RLPFK in the presence of either MgATP or Fru-6-P. Model fitting is constrained by structural information gained by electron microscopy.

Materials and Methods

Materials

All materials used for buffers in protein purification, enzymatic assays and fluorescence experiments were analytical grade and purchased from either Fisher Scientific, Sigma-Aldrich, Research Products International or VWR. Distilled, deionized Mili-Q water was used throughout. Ammonium sulfate suspensions of triosephosphate isomerase and glycerol-3-phosphate dehydrogenase were purchased from Roche. Aldolase was purchased as an ammonium sulfate suspension from Sigma-Aldrich. MonoQ and Sepharose 2B resin used for protein purification was purchased from Pharmacia. MonoQ resin was purchased as a prepacked column (HR 10/10) for use on an FPLC. Macro Prep HiQ resin for protein purification was purchased from Bio-Rad. Enzymes purchased as ammonium sulfate suspensions were dialyzed extensively against 50mM MOPS-

KOH, 100mM KCL, 2mM $MgCl_2$ and 100μM EDTA. Goldseal® cover glass of No.1 thickness was purchased Ted Pella Inc. Sigmacote® siliconizing reagent was purchased from Sigma-Aldrich. Bovine serum albumin (98%) was purchased by Sigma-Aldrich. Fluorescein Isothiocyanate was purchased from Fisher Scientific. Sephadex G25 resin for protein desalting was purchased from Sigma. N, N-Dimethylformamide (99.8%) was purchased from Acros Organics.

Protein expression and purification of RLPFK

PFK-A and PFK-B deficient RL257 was transformed with the recombinant plasmid and plated on LB agar supplemented with 15μg/mL tetracycline and a single colony was selected and used to inoculate a 10mL culture of LB-tetracycline. The LB culture was incubated with shaking at 37^0C overnight for 8 hours. 9mL of the overnight culture was used to inoculate 9L of LB-tetracycline media. Inoculated media was grown at 30^0C to an OD of 0.6 before being induced by 1mM IPTG. Cells were grown for 40 hours before harvesting at 3500xg for 30min.

The cell pellet (~25g wet weight) was re-suspended into 100mL purification buffer (50mM Tris, 0.1mM EDTA, 5mM DTT, 1mM ATP, 0.1mM PMSF, pH=8.0). Cell suspension was ruptured by discontinuous sonication using a Fisher 550 sonic dismembrator at 70% amplitude with 15s on and 45s off for a total sonication time of 12min. Insoluble material was removed by 45min centrifugation at 14,000xg.

Clarified supernatant was rapidly heated to 58^0C in a boiling water bath. Temperature was maintained at 58 ± 1^0C for 3min and then rapidly cooled to 10^0C

in a salt-ice bath. Precipitated protein was again removed by 45min centrifugation at 14,000xg.

Ammonium sulfate was slowly stirred into clarified supernatant to a final concentration of 18g per 100mL. The mixture was incubated at 4^0C in the presence of $(NH_4)_2SO_4$ for 90min before being centrifuged for 20min at 7,000xg. The supernatant solution was discarded, and the pellet was re-suspended into a minimal volume of anion exchange buffer (20mM Tris, 3mM $MgCl_2$, 20mM $(NH_4)_2SO_4$, 0.1mM EDTA, 5mM DTT, 1mM Fru-6-P pH=8.0). Re-suspended protein solution was dialyzed extensively against anion exchange buffer.

The solution was centrifuged at 7000xg for 20min to clarify before being diluted to a concentration of 0.25mg/mL and loaded onto a 30mL HiQ column that had been pre-equilibrated with anion exchange buffer. Protein was eluted from the column using a 0-1M KCl gradient. All fractions containing activity were pooled and precipitated by $(NH_4)_2SO_4$ (60% saturation). Precipitated protein was pelleted by centrifuging at 10,000xg for 30min followed by re-suspension into a minimum volume of anion exchange buffer and dialyzed against four iterations of 100mL anion exchange buffer.

Dialyzed pooled fractions were centrifuged at 7000xg for 20min to clarify before being diluted to 50mL and loaded onto an 8mL MonoQ column equilibrated with anion exchange buffer. Protein was eluted by a 0-1M KCl gradient. Fractions containing activity were pooled and precipitated by 60% $(NH_4)_2SO_4$. Pellet was re-

suspended into 4mL of gel filtration buffer (20mM Phosphate (P_i), 3mM $MgCl_2$, 0.1mM EDTA, 5mM DTT, 1mM Fru-6-P, pH=7.6) and clarified by centrifugation.

The solution was loaded onto a Sepharose 2B gel filtration column with the dimensions of 1.7X38cm. Protein elution was tracked by activity and A280, typically, the majority of RLPFK comes out in the void volume with an extended tail. The tail was not collected. Protein was concentrated to a concentration of 2mg/mL by dehydration through a dialysis membrane. PEG provided the dehydrant. Concentrated protein was then dialyzed against storage buffer (20mM Phosphate, 3mM $MgCl_2$, 0.1mM EDTA, 5mM DTT, 1mM Fru-6-P, 20% glycerol pH=7.6). Purity was assessed as a single band on a 12% SDS-PAGE gel. Protein concentration determined by BCA.

Kinetic assays

The PFK catalyzed conversion of Fru-6-P to Fru-1,6-BP was coupled to the oxidation of NADH, which resulted in a decrease in absorbance at 340nm. The rate of the decrease in A340 was monitored using a Beckman Series 600 spectrophotometer. All assays were performed at 25^0C and initiated by the addition of 6µL PFK to a final volume of 600µL buffer. Dilution of PFK into cuvette contributes the addition of 0.2mM P_i, 0.2% glycerol, 10µM Fru-6-P, and 30µM $MgSO_4$ to all assays. PFK activity is presented as units per milligram where 1 unit is equal to the production of 1 µmol of Fru-1,6-BP per min.

Optimal enzyme activity assays were performed in the following buffer; 50mM Tris-HCL, 100mM KCl, 20mM $(NH_4)_2SO_4$, 2mM DTT, 3mM $MgCl_2$, 1mM ATP, 1mM Fru-6-P, 0.2mM NADH, 100μM EDTA, pH 8.0, 250μg/mL of aldolase, 50μg/mL of glycerol-3-phosphate dehydrogenase, 5μg/mL of triosephosphate isomerase.

Labeling

Before labeling, the protein was concentrated to 4mg/mL and the pH of the protein solution was adjusted to pH 9.2 by a dialysis against storage buffer (pH 9.2). A stock solution of FITC was prepared by dissolving 1mg of FITC in 200μL N,N-Dimethylformamide. Protein labeling reaction was initiated by dropwise addition of a minimal volume of FITC stock solution with constant stirring. The target FITC concentration was a 50-molar excess relative to protein concentration. Protein-FITC solution was incubated at room temperature with constant stirring for one hour. The reaction was stopped by dialysis against storage buffer supplemented with 100mM Tris-HCL (pH 9.2). The labeled PFK solution was then dialyzed for ~1 week against five 100mL changes of storage buffer supplemented with 100mM Tris-HCL (pH 9.2) and three additional 100mL changes storage buffer (pH 7.6). After dialysis, the enzyme solution was passed through a desalting column equilibrated with storage buffer (pH 7.6) to remove any residual free dye. Efficiency of free dye removal was assessed by anisotropy measurements (maximum of 0.31) and stoichiometry was determined assuming a fluorescein extinction coefficient of $7X10^4$.[193] Efforts were made to minimize light exposure throughout labeling

procedure. Specific activity was determined after labeling and the final enzyme concentration was adjusted to 2mg/ml. Labeled enzyme was stored at 4°C.

Fluorescence anisotropy

Steady-State Fluorescence anisotropy measurements were performed with an ISS Koala spectrofluorometer. Excitation wavelength was 495nm with 0.5mm slit width. Emission fluorescence was collected through a Schott OG-520 cut-on filter. Intensity was attenuated as needed using neutral density filters in the excitation path.

Fluorescence anisotropy is conceptually equivalent to fluorescence polarization and the two values can be interchanged by a simple mathematical transformation.[194] As a matter of personal preference, data presented in this dissertation is expressed in the form of fluorescence anisotropy. To preserve the historical context of the two terms, data originally published in terms of fluorescence polarization will be referred to as such.

Fluorescence correlation spectroscopy

Fluorescence Correlation spectroscopy was performed using ISS ALBA FCS instrument including a Nikon Eclipse TE300 inverted microscope with a Nikon 60X 1.2NA water immersion objective lens. The two-photon excitation source was provided by Tsunami Ti/Sapphire (Spectra Physics) pulsed-laser with <100fs pulse-length mode locked at 80MHz and tuned to 900nm. The Tsunami laser was

optically pumped using a 10W Spectra Physics Millennia-Pro 532nM Nd:YVO_4 operating at 7.6W. The average output of the Tsunami laser was 0.86W before attenuation to 10% using a 90% transmittance, 10% reflectance broadband dielectric beam splitter (Newport). The excitation beam was passed through a HB-4XAR.16 beam expander (Newport) to overfill the back aperture of the objective lens. At the sample, excitation power was measured to be approximately 16mW. A Chromo Technologies E700SP-2P dichroic mirror was used to separate the path of the emission light from the excitation light and emission light was collected by an avalanche photodiode (APD) detector. Samples were measured as 20μL drops on No.1 thickness cover glass (Goldseal) that had been siliconized according to the instruction provided by Sigmacote®. Data were collected at 50 kHz for 2min. Samples containing labeled RLPFK were analyzed in the presence of 0.1mg/mL BSA. Data were analyzed using ISS VistaVision software and were plotted using Kaleidagraph. Excitation volume was calibrated daily using fluorescein and a diffusion coefficient of 436μm^2/sec.

FCS data analysis

All FCS data analysis was performed using VistaVision Software by ISS. In FCS, the temporal behavior of fluctuations in the fluorescence signal are analyzed according to the autocorrelation function, $g(\tau)$. [160, 164]

$$g(\tau) = \frac{\langle \delta I(t) \delta I(t+\tau) \rangle}{\langle I(t) \rangle^2} \quad (4\text{-}1)$$

Here, angle brackets denote an average over the time of data accumulation, $I(t)$ is the fluorescence intensity at a specific time t, and τ is the delay time after time t. $\delta I(t)$ represents the fluctuation from the mean $\delta I(t) = I(t) - \langle I(t) \rangle$. [160, 164] In the simplest case of a single species of fluorescent particles diffusing through a quasi-cylindrical volume, the autocorrelation function can be expressed in terms of the particles diffusion coefficient (D) with the following equation:[164]

$$g(\tau) = \frac{2\sqrt{2}}{\pi\sqrt{\pi}w_0^2 z_0 \langle C \rangle}\left(1 + \frac{8D\tau}{w_0^2}\right)^{-1}\left(1 + \frac{8D\tau}{z_0^2}\right)^{-\frac{1}{2}} \quad (4\text{-}2)$$

where w_0 and Z_0 are the radial and axial semiaxes of the three-dimensional Gaussian volume and C is the concentration of fluorescent particles. The previous equation assumes that the point spread function can be described by a three-dimensional Gaussian. In our experience, the point spread function is best described by a Gaussian-Lorentzian form. Gaussian-Lorentzian point spread function is commonly found to be the most appropriate for 2-photon FCS.[163, 195, 196] The autocorrelation function derived from this model is an integral function and cannot be written in closed form.[163] The autocorrelation function of a mixture of species is expressed a linear sum of the autocorrelation function describing each individual species. The waist of the excitation beam (w_0) was calibrated daily using fluorescein ($D=436\mu m^2 s^{-1}$)[197] and is usually found to be within the range of $0.335\mu m^2 s^{-1}$ and $0.351\mu m^2 s^{-1}$.

Anomalous intensity spikes caused by insoluble protein aggregates or dust particles were curated from the raw data using the multi-segment analysis feature

of ISS VistaVision version 4.1.038. With the multi-segment analysis feature autocorrelation curves are generated for segments of user defined intervals (we used 1 sec intervals). Any segment whose autocorrelation curve yielded a value of $g(0)$and characteristic diffusion time that was significantly different than the average was discarded. Here we consider a significant difference to be a value for $g(0)$ and persistence time that is 3-fold greater than the average. Using modeling to obtain an actual value for $g(0)$ and characteristic diffusion time is computationally unfeasible, however visual inspection of the autocorrelation curves is generally sufficient. In instances where the significance of a difference is uncertain, we tended to keep the data.

Electron microscopy

4µl of 0.1µg/mL RLPFK containing either 3mM MgATP or 5mM fru-6-P were applied to glow discharged carbon-coated grids and stained with uranyl acetate (2% w/v). The grids were examined in a JEOL 1200 electron microscope operated at 100kV and images were recorded by a SIA-15C at x48906 magnification (2.45 Å/pixel). Three-dimensional model of tetrameric RLPFK was constructed from 2936 PFK particles selected from micrographs imaged in the presence of MgATP. The image processing software EMAN2 was used to build and refine model.

Results

The propensity of RLPFK to form oligomers larger than a tetramer has been demonstrated [49-51, 102, 104] but the possibility remained that this enzyme, when purified by recombinant methods, would lose this feature. To address conservation of aggregation properties, we have used a combination of electron microscopy images and fluorescence correlation spectroscopy (FCS) to investigate RLPFK assembly in conditions believed to either stabilize large oligomers or promote dissociation to tetramers.

Electron microscopy

We obtained electron microscopy images of our recombinantly purified RLPFK in conditions that have been demonstrated to stabilize large oligomers of native enzyme [50](Figure 4-1). The conditions chosen for this experiment (MOPS buffer pH 7.0, 10μg/mL RLPFK, 5mM Fru-6-P) were chosen to emulate the conditions used by Reinhart and Lardy to study RLPFK self-association using fluorescence polarization.[50] The resulting electron microscopy image (Figure 4-1) shows a clear presence of oligomers much larger than a tetramer, some reaching a size of over 30 tetramers. Figure 4-1 provides some implications into the assembly method of these oligomers. They do not form amorphous spheres or crystalline aggregates but instead assemble end on end like beads on a string. The amount of

variation in shape between oligomers suggest that the strings are loose and flexible, not rigid fibrils. One is given an impression of a "spaghetti" like assembly with a great degree of freedom to kink and bend, even fold back onto itself so that both ends overlap. Polymers display a great degree of heterogeneity, both in terms of the shape of the assembly, and the number of tetramers in an assembly. Numbers of tetramers per assembly range from isolated tetramers to 20 or 30 tetramers, with intermediate sizes equally populated. A high level of heterogeneity was also seen for pig liver PFK.[103]

Juxtaposing the long chains of RLPFK seen in Figure 4-1, the electron microscopy image presented in Figure 4-2 portrays RLPFK as a nearly homogeneous population of tetramers. The image presented in Figure 4-2 was generated using nearly identical conditions as those in Figure 4-1 (10μg/mL RLPFK MOPS buffer pH=7.0), the sole exception being the presence of 3mM MgATP instead of Fru-6-P. Again, these conditions were inspired by Reinhart and Lardy.[50] The contrast between the assembly sizes of species in Figure 4-1and Figure 4-2 is striking and highlights the powerful impact that ligand condition has on the self-assembly process. In the presence of MgATP the RLPFK tetramer is uniform enough to obtain a low resolution topographic map of the tetramer (Figure 4-3).

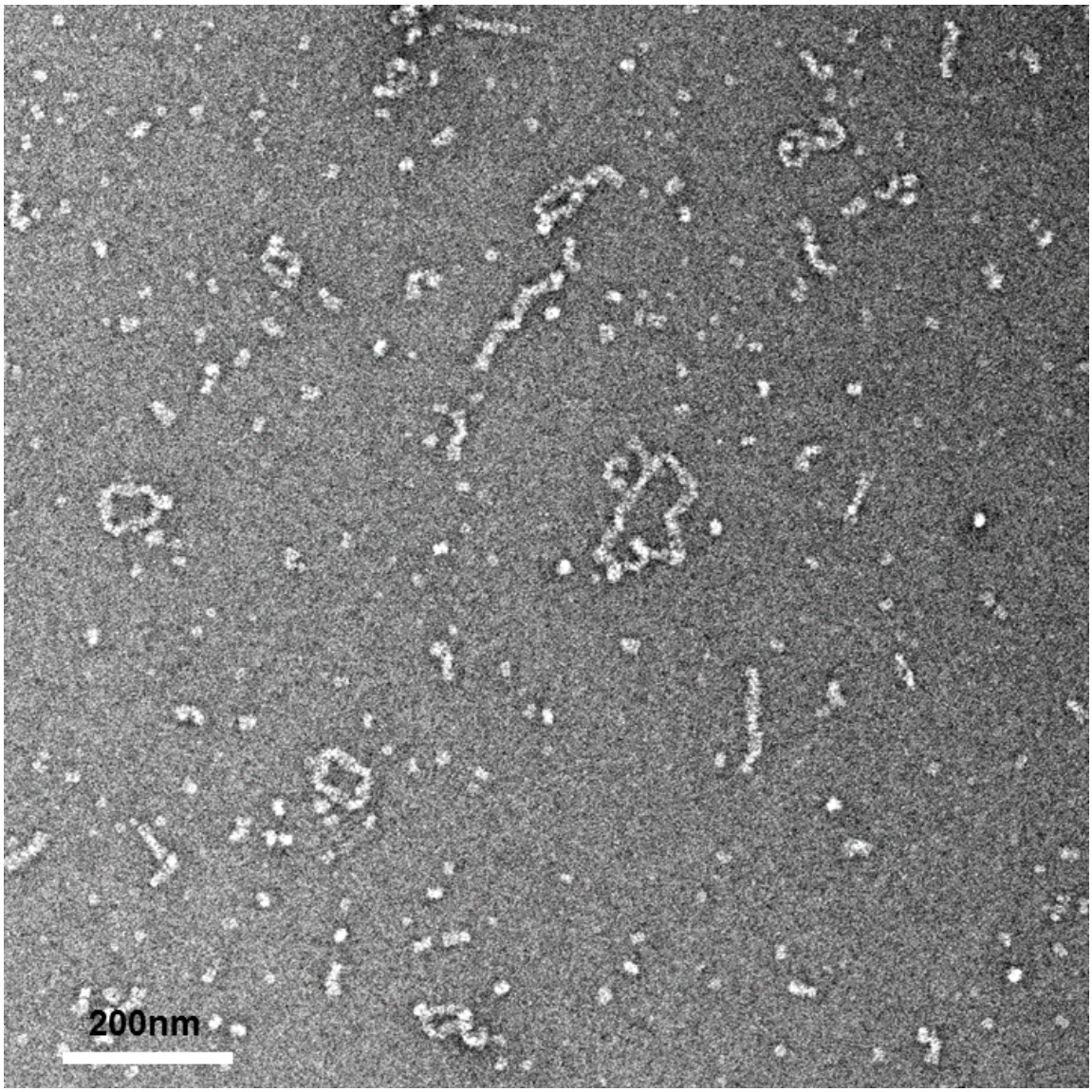

Figure 4-1: Representative image of negative stained electron microscopy image of RLPFK in the presence of 5mM Fru-6-P. Protein was diluted 200-fold from a stock concentration of 20μM and 4μl was applied to grids. PFK was negative stained with uranyl acetate. Scale bar included for size reference.

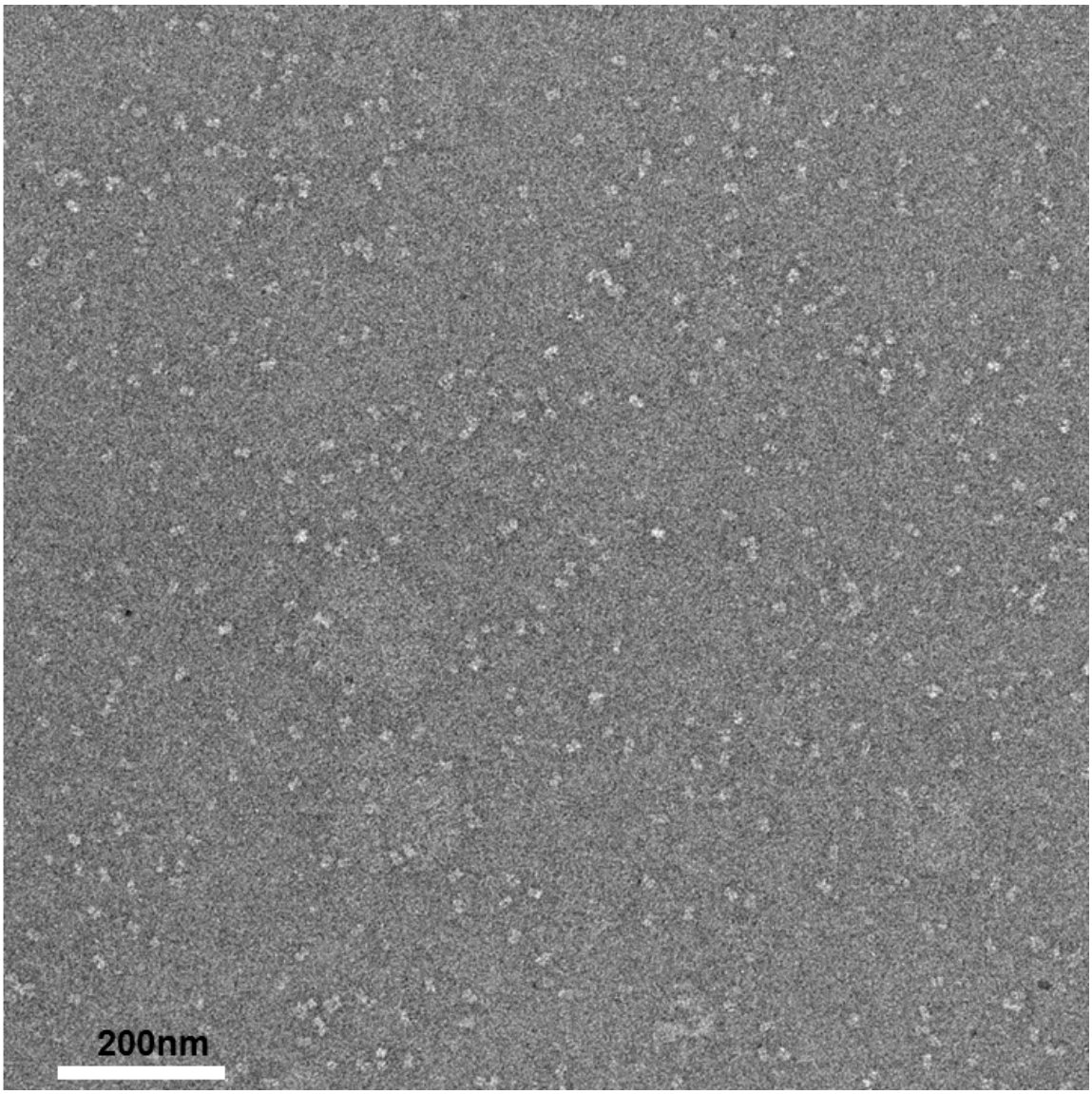

Figure 4-2: Representative image of negative stained Electron Microscopy image of RLPFK in the presence of 3mM MgATP. Protein was diluted 200-fold from a stock concentration of 20μM and 4μl was applied to grids. PFK was negative stained with uranyl acetate. Scale bar included for size reference.

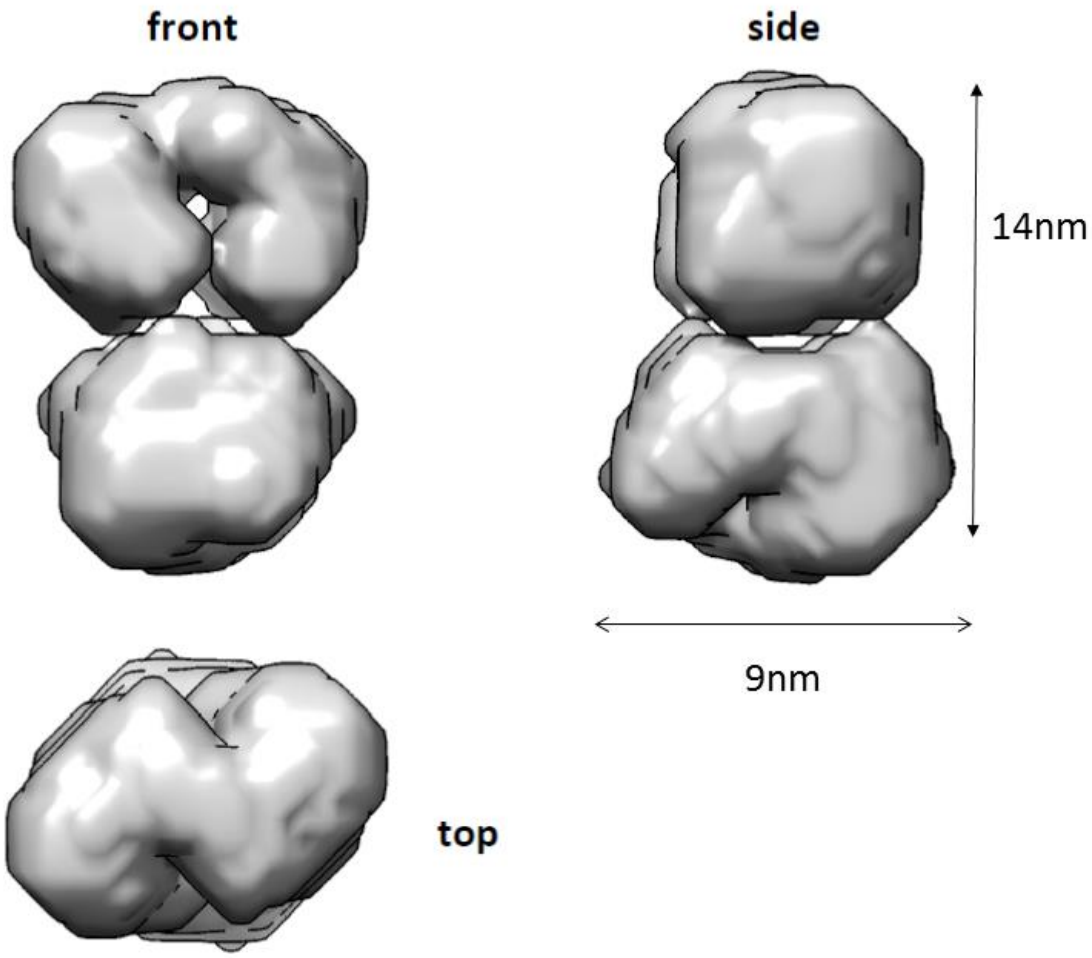

Figure 4-3: Low resolution topographic map of tetramer obtained from ensemble electron microscopy images.

Labeling RLPFK with fluorescein

While electron microscopy provides a direct look at the physical state of protein oligomers, it is not rapid or flexible enough to probe the oligomerization state of RLPFK in the myriad of conditions possible. For a more rapid approximation of oligomeric size, we utilize fluorescence correlation spectroscopy. We attached fluorescein to RLPFK using the reactive group isothiocyanate. A typical reaction yielded a sample with 1 dye for every 2 tetramers with no reduction in the specific activity. The optimal specific activity of RLPFK was maintained when the extent of fluorescein incorporation was between 0.2-2 dyes per tetramer however a 20% loss of activity was seen in a single labeling preparation that obtained 4 dyes per tetramer. RLPFK conjugated to fluorescence was found to have the same affinity to Fru-6-P and the same response to inhibition by MgATP (data not shown). Kinetic measurements support the assertion that labeling of RLPFK with FITC does not affect the properties of the enzyme.

The extent of label incorporation was assessed by independently calculating protein concentration and fluorescein concentration by BSA and maximum absorbance at 495nm respectively. Slight turbidity of the labeled RLPFK solution resulted in an elevated baseline even after buffer subtraction (Figure 4-4). The baseline was subtracted from the peak at 495nm to calculate the adjusted fluorescein concentration. The labeling ratio was disappointingly low. FITC labeling efficiency decreases dramatically as protein concentration decreases[198], however

increasing the concentration of RLPFK was not experimentally feasible. We observed a propensity for RLPFK to precipitate out of solution at concentrations greater than 4mg/ml. The suspended RLPFK particles remain active and regain solubility upon dilution. A single attempt was made to label a suspension of RLPFK at a concentration of 6mg/ml. A labeling ratio of 6mg/mL is slightly lower than achieved with lower enzyme concentrations, suggesting precipitation prevents access to the conjugation sites.

Other reactive moieties tested include maleimide, sulphodichlorophenol ester, and succinimidyl ester. Attempts to label RLPFK with Alexa 488 maleimide were met with complete loss of enzyme activity even when sub stoichiometric amounts of dye were used (data not shown). The maleimide reactive group primarily targets sulfhydryl groups[199], so it would seem that at least one accessible cysteine is necessary for catalytic function. RLPFK labeled with maleimide retained only 10% enzyme activity when the labeling ratio was approximately 1 dye per tetramer. A highly reactive cysteine has been well demonstrated in muscle PFK[200-202] and *E. coli* PFK[203]. Targeting amine groups for labeling is preferable to cysteine groups. In addition to FITC, we attempted to label RLPFK with the amine targeting dyes Alexa488 sulphodichlorophenol ester[204] and Alexa488 succinimidyl ester[205]. Neither of these dyes labeled with a greater efficiency than FITC.

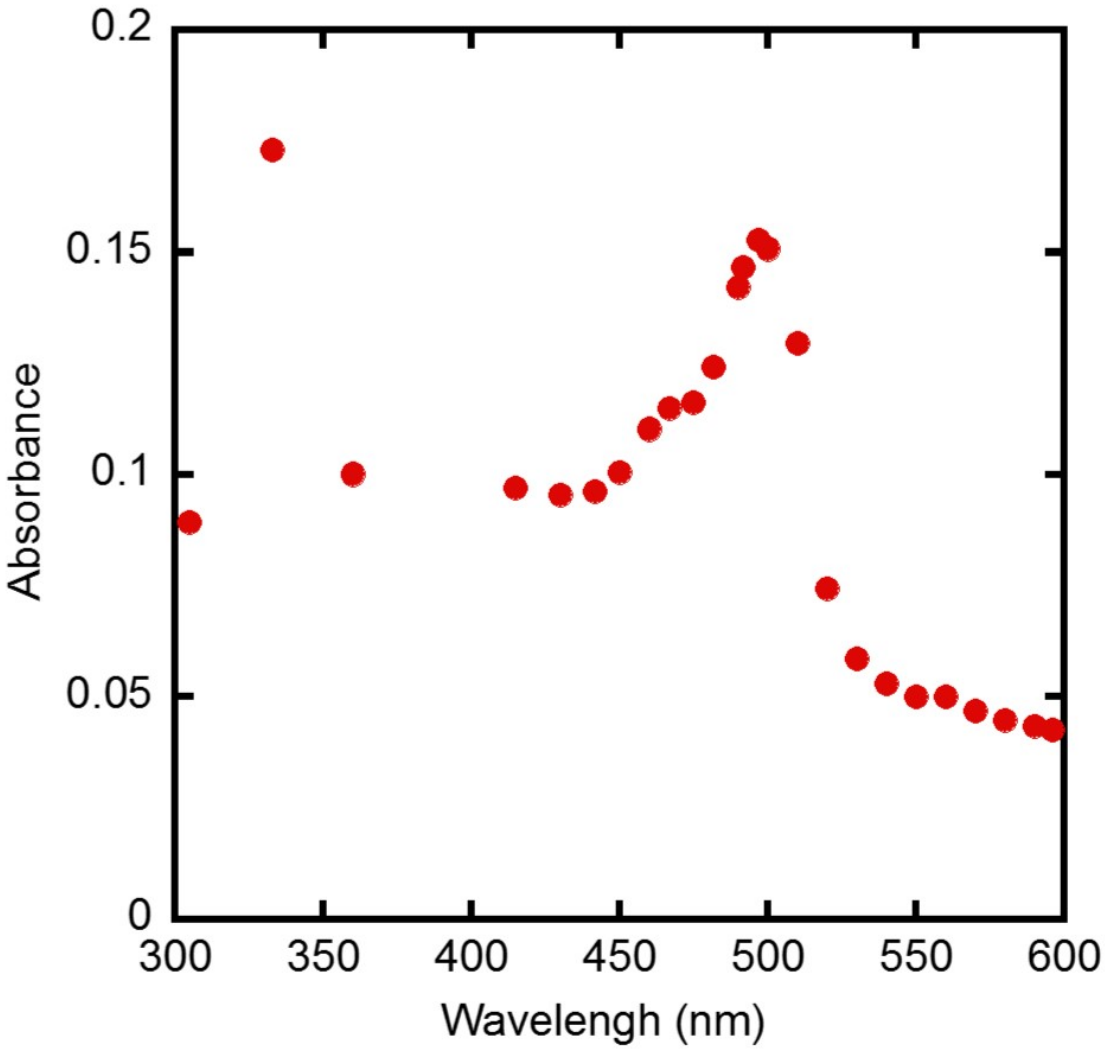

Figure 4-4: Representative absorbance spectrum of RLPFK labeled with fluorescein.

RLPFK retained non-covalently attached FITC with a high affinity. Likely this is due to hydrophobic interactions with the dye[198]. Removal of this "sticky" dye required extensive dialysis. The majority of unreactive FITC could be removed by only three changes of 100mL buffer but a slow process of leaching occurred over a long period of time. The progress of this leaching could be monitored by observing fluorescence in the dialysate. A final desalting column removed trace amounts of unconjugated fluorescein after dialysis[198]. Fluorescence anisotropy was used to ensure that all remaining dye is conjugated to RLPFK. The rotational relaxation time of the tetramer form of RLPFK (821ns)[50] is significantly greater than the lifetime of fluorescein (4ns) so one would expect the measured anisotropy of RLPFK fluorescein conjugate to be very near the limit anisotropy of 0.373±0.002[206]. The measured anisotropy of a RLPFK fluorescein conjugate was typically around 0.308±0.003 when the labeling ratio was 1 dye per two tetramers. Surprisingly the anisotropy was consistently lower in conditions that stabilized self-associated species than in conditions that promoted dissociation. For example, in one instance a preparation of RLPFK-FITC gave an anisotropy value of 0.271±0.002 when measured at a concentration of 12μM in storage buffer with Fru-6-P. When diluted to 0.012μM into buffer with 3mM MgATP the value of anisotropy increased to 0.313±0.002. We propose energy transfer is responsible for depressing the anisotropy value.[207] One could reason that energy transfer will be most prominent when fluorescein molecules are held within close proximity of each other, such as during self-association of RLPFK.

FCS experimental details

We observed a loss of RLPFK to the cover glass during FCS measurements. Loss of RLPFK manifested itself in FCS experiments by a decrease in detected fluorescence (CPS) and an increase in in the $g(0)$ value of the autocorrelation curve[162] but it can be most directly observed by a loss in activity. Figure 4-5 shows the loss of RLPFK activity over 10min after a 20μL drop was placed on a glass slide. Even after siliconizing the cover glass, a significant loss of protein was seen to occur after 10min, the extent of which is dependent on the concentration of RLPFK (Figure 4-6). The inclusion of BSA prevents the loss of protein, as evident by a full retention of activity after 10min (Figure 4-6). The activity after 10min is actually greater than the initially measured activity (Figure 4-6), most likely due to evaporation facilitated concentration of RLPFK. Subsequent FCS experiments were only performed for two minutes after placement of protein on the cover glass to prevent effects of evaporation.

A common method utilized to circumvent the problem of protein adhesion is the use of "chambered" cover glass such as the ones provided by Nunc™ Lab-Tek™[208]. Chambered cover glass has small surface to volume ratios so the amount of protein loss to the surface is negligible compared to the total protein in solution. Indeed, activity measurements of a 1nM RLPFK solution in these cambers suggest negligible loss of protein (data not shown). However, observations during FCS experiments suggested that protein adhesion was still occurring. Namely, these

observations were a decrease in the detected fluorescence and an increase in $g(0)$[162]. It's difficult to rationalize the contradictory results of the FCS and activity measurements, but the possibility of a problem[209] was enough to discourage us from using the chambered cover glass.

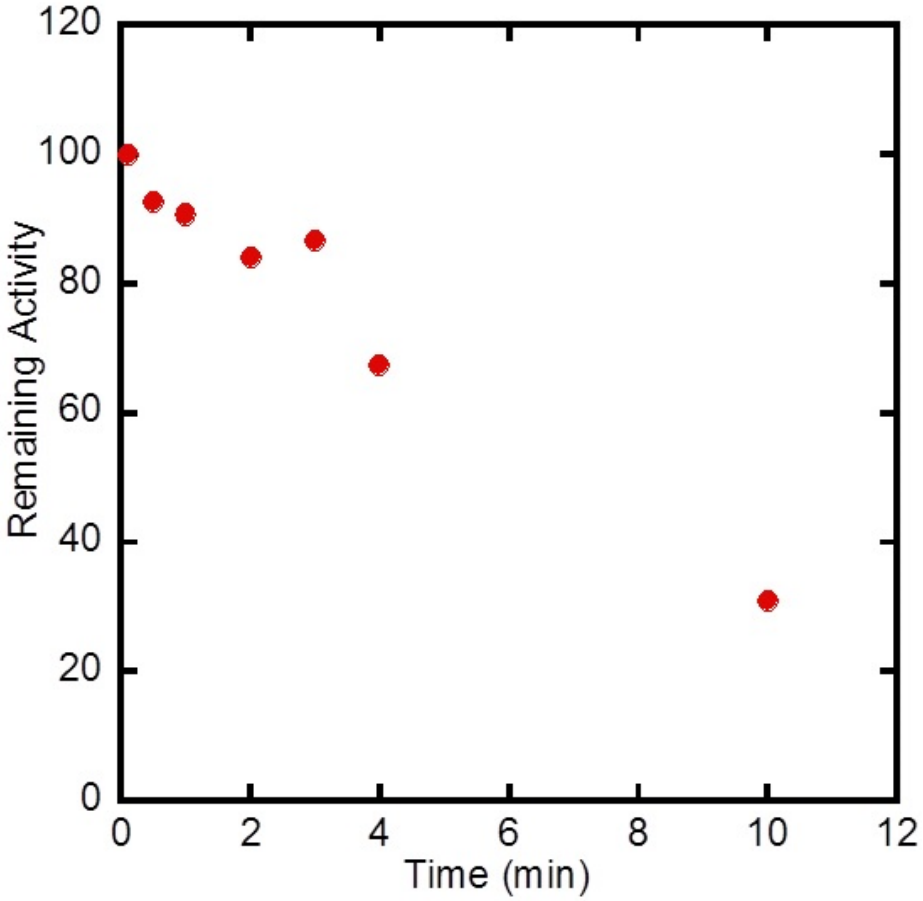

Figure 4-5: Loss of RLPFK activity due to protein adhesion to glass surface. Protein solution was placed on the surface of #1 thickness borosilicate cover glass in the form of a 40µl drop. 6µl was removed at the recorded time intervals and activity were measured as describe in materials and methods. Activities are reported normalized to the activity of RLPFK before being placed on the cover glass.

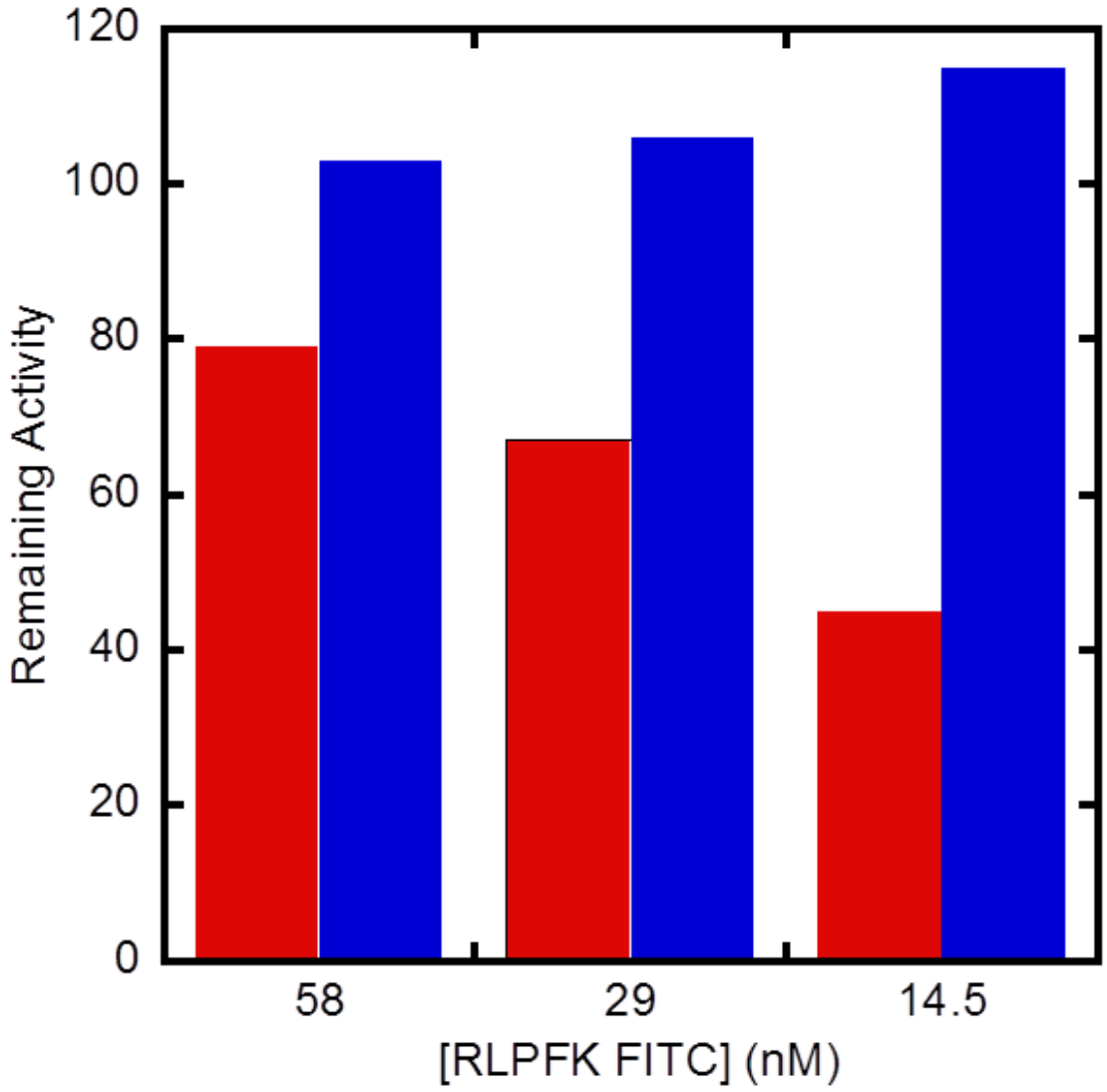

Figure 4-6: Protection against RLPFK loss by BSA. 20µl of protein solution (with or without 0.1mg/mL BSA) was placed on the surface of a #1 thickness borosilicate cover glass that had been treated with Sigmacote® as described in material methods. Activity was measured after 20 minutes and reported as a percentage of the initial activity. The same cover glass was used for samples with and without BSA.

Ligand dependent oligomeric states of RLPFK

To demonstrate the ability of FCS to detect the oligomerization state of RLPFK, we replicated the conditions used to generate the electron microscopy images (Figure 4-1 and Figure 4-2) in FCS experiments. Figure 4-7 shows representative autocorrelation curves obtained from FCS experiments performed on 116nM RLPFK in the presence of either 3mM MgATP or 3mM Fru-6-P. Prior to all measurements RLPFK was stored at a concentration of 23μM in storage buffer. To avoid reporting on a transient state occupied during a period of equilibrium shift, the measurements presented in Figure 4-7 were taken 4 hours after dilution. Four hours is assumed to be sufficient to achieve a state of pseudo equilibrium, we present the justification for this assumption below.

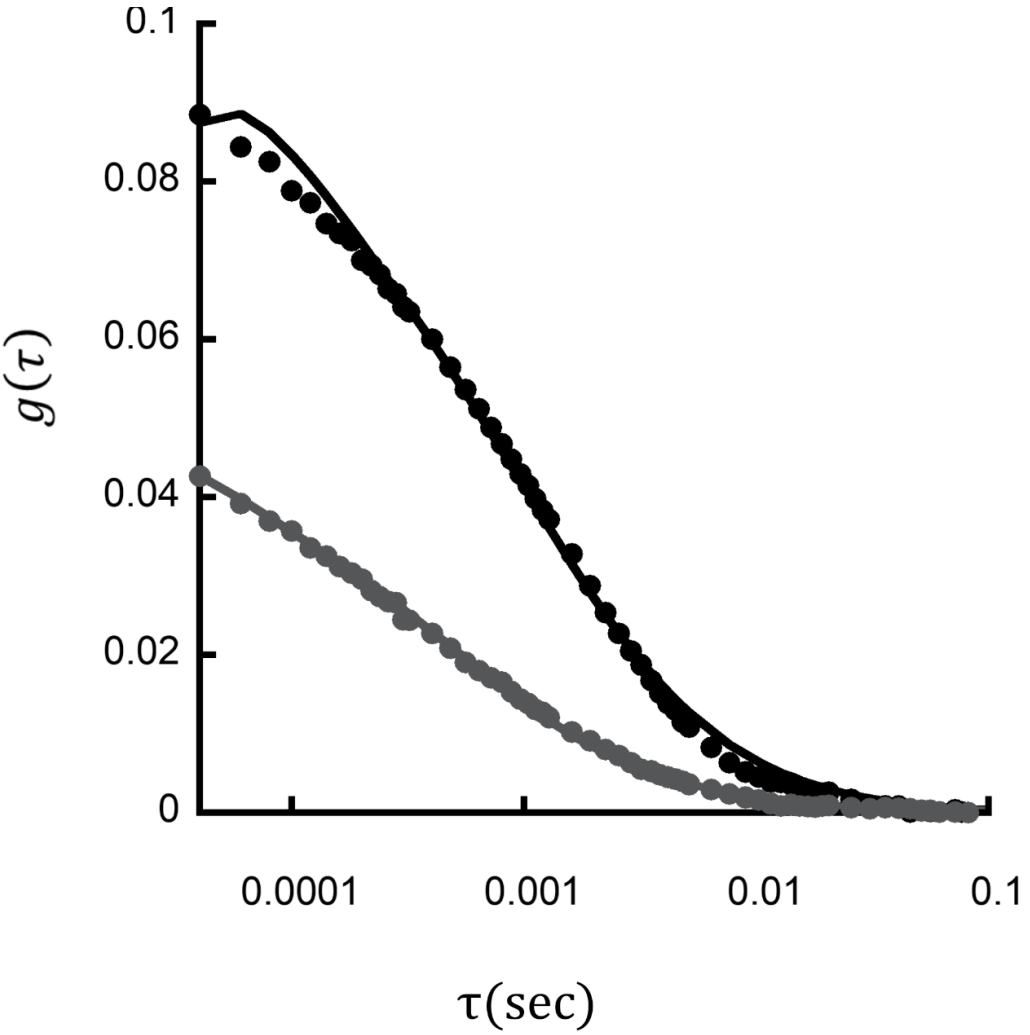

Figure 4-7: Autocorrelation curves of 116nM RLPFK 4 hours after dilution into buffer with either 3mM MgATP (grey) or 3mM Fru-6-P (black). Curves are fit with a single diffuser model. Fitted parameters and χ^2 values are listed in Table 4-1.

Table 4-1: Fitted parameters to autocorrelation functions

	D (μm2/sec)	Concentration	χ^2
MgATP	31	26	2
Fru-6-P	18	13	14

Visual inspection of the autocorrelation curves provides a qualitative sense that RLPFK is more dissociated in the presence of MgATP than in the presence of Fru-6-P. The visually apparent reduction of $g(0)$ suggests a greater number of particles[162] in the presence of MgATP than in the presence of Fru-6-P. The decreased persistence time suggests a RLPFK is a faster diffusing particle[162] in the presence of MgATP than in the presence of Fru-6-P.

For a quantitative interpretation, the autocorrelation curves were fit using a single diffuser model to get the apparent diffusion coefficient (D) in terms of microns per second and the concentration of particles. The fitted parameters are listed in Table 4-1. The fitted g(0) values were calculated to be a concentration of 26 and 13nM in the presence of 3mM MgATP and 3mM Fru-6-P respectively. 26nM is consistent with the number of particles expected if the sole species present was a tetramer and represents a 2-fold increase in the number of particles relative the equivalent concentration of RLPFK in the presence of Fru-6-P. The diffusion coefficient of RLPFK in the presence of MgATP is approximately 1.7 times faster than the diffusion coefficient in the presence of Fru-6-P. Given the cubed root dependence of diffusion coefficient on particle size[210], a 1.7-fold increase in diffusion coefficient suggest an approximately 5-fold increase in particle size.

Moment analysis can be used to quantify the number and brightness of a population of fluorophores.[211] Moment analysis cannot distinguish between multiple species but will instead give single value representative of the average.[211] For 116nM RLPFK in the presence of Fru-6-P we calculated a number of 9.0±0.4

and a brightness of 0.106±0.005cpsm. Using an equivalent concentration of RLPFK in the presence of MgATP we calculated a number of 16.2±0.3 and a brightness of 0.052±0.001cpsm. A 2-fold increase in the number of particles and a 50% decrease in the brightness of the particles is consistent with the change in particle size measured by FCS.

It is assumed that after 4 hours the enzyme is in a state of pseudo-equilibrium with the oligomerization state no longer changing. To verify this, we measured FCS data at several time points after dilution of RLPFK into buffer with Fru-6-P. Figure 4-8 show the diffusion coefficient and concentration measured by fitting the autocorrelation curves. Aside from a small change between minute 2 and minute 30, very little change occurs over the course of 4 hours. We can therefore conclude that the oligomeric state of RLPFK is unchanging over the course of the experiment. We next applied moment analysis to the time course data to report the data in terms of number and brightness. Figure 4-9 shows that the number and brightness of particles does not change significantly over time. Next, we diluted RLPFK to the same concentration but this time in buffer containing MgATP. Figure 4-10 demonstrates an initial increase in concentration and diffusion coefficient that stabilizes after approximately an hour. Moment analysis was performed on this data as well (Figure 4-11) and demonstrates the same trend as Figure 4-10.

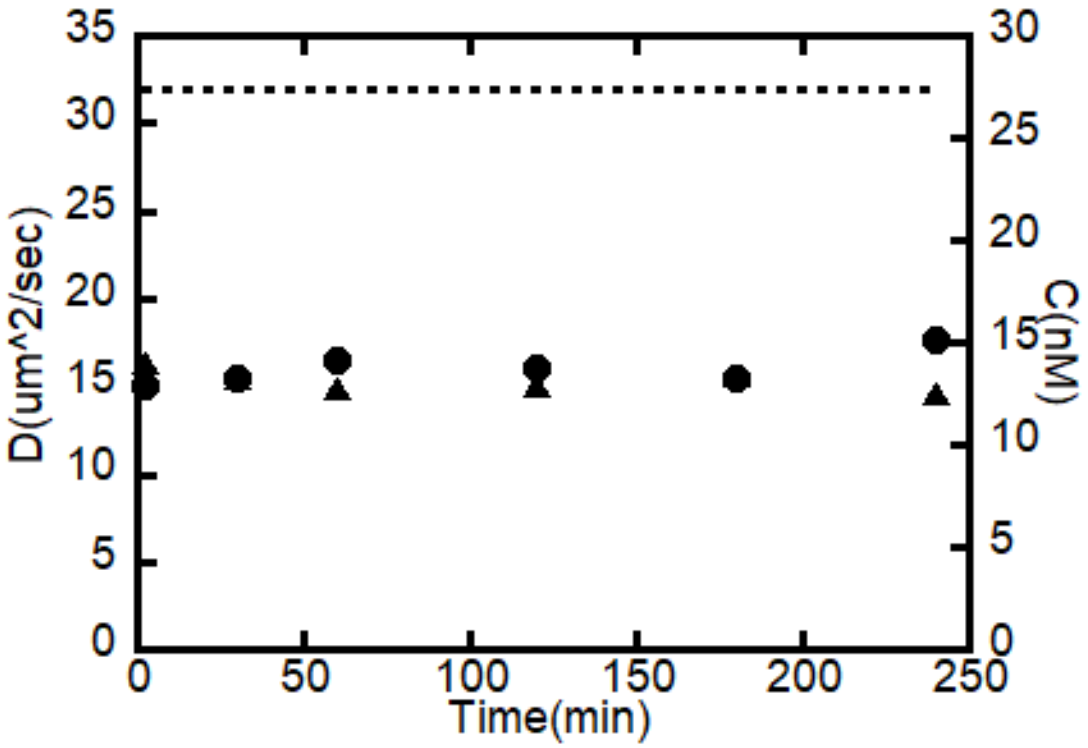

Figure 4-8: Time dependent FCS measurements of RLPFK in the presence of Fru-6-P. 116nM RLPFK was diluted into buffer with 3mM Fru-6-P. FCS data was collected at several time points over a course of 4 hours. Values of diffusion coefficient (circles) and concentration (triangles) were calculated from autocorrelation curves by fitting data to a single diffuser model.

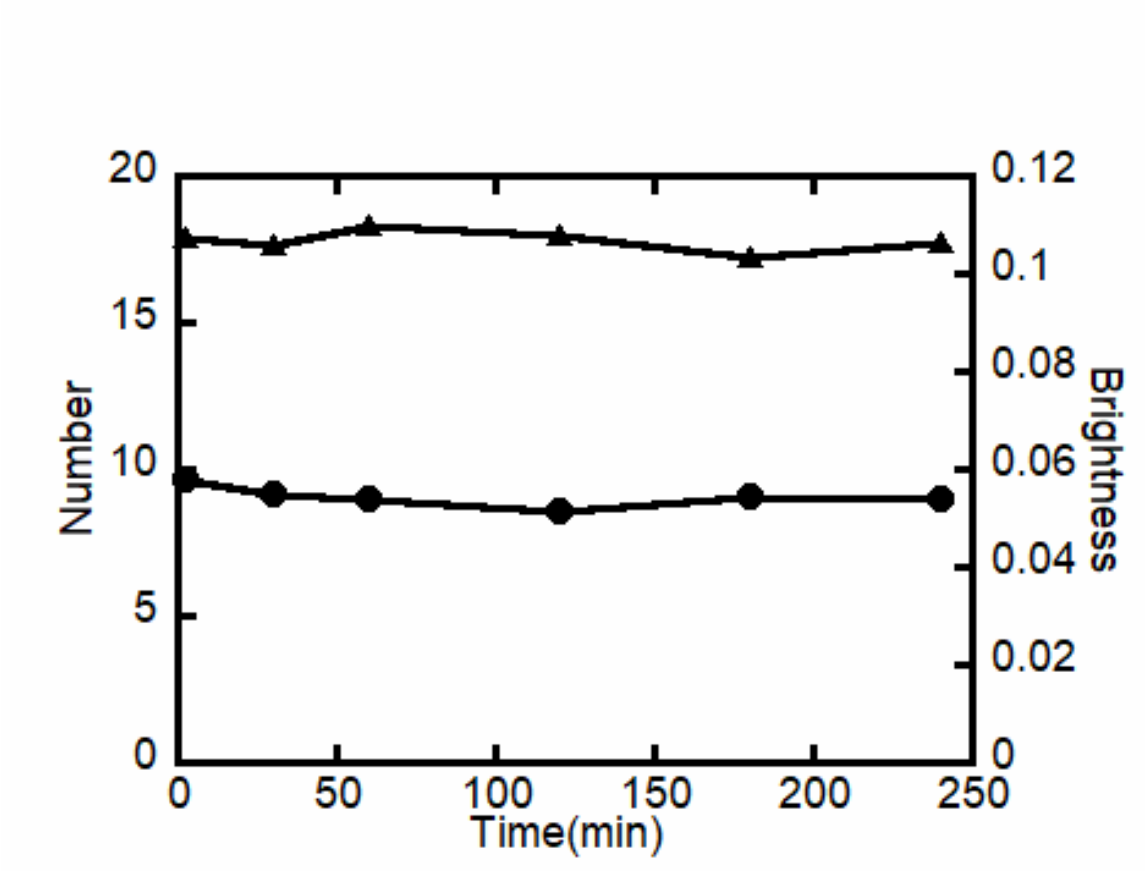

Figure 4-9: Time dependent number and brightness analysis performed on RLPFK in the presence of Fru-6-P. 116nM RLPFK was diluted into buffer with 3mM Fru-6-P. FCS data was collected at several time points over a course of 4 hours. Values of number (circles) and brightness (triangles) were calculated from raw data as described above.

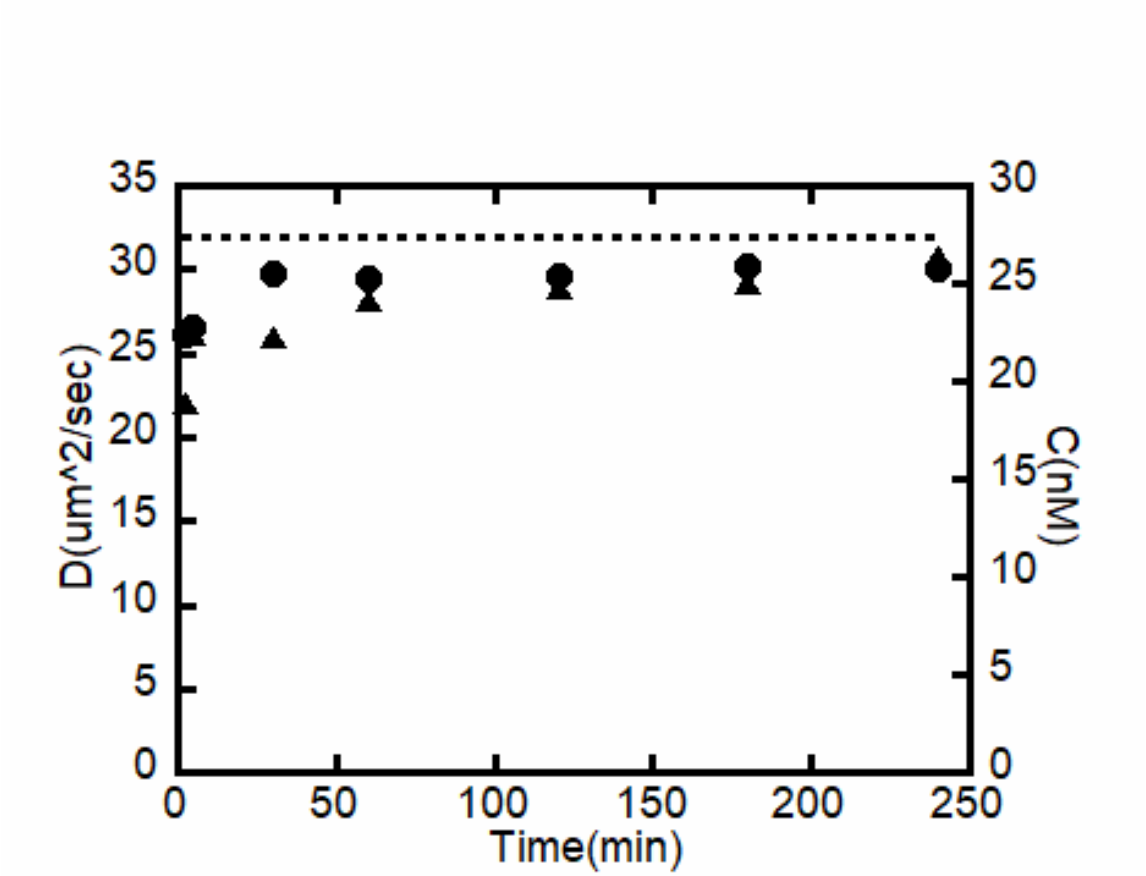

Figure 4-10: Time dependent FCS measurements of RLPFK in the presence of MgATP. 116nM RLPFK was diluted into buffer with 3mM MgATP. FCS data was collected at several time points over a course of 4 hours. Values of diffusion coefficient (circles) and concentration (triangles) were calculated from autocorrelation curves by fitting data to a single diffuser model.

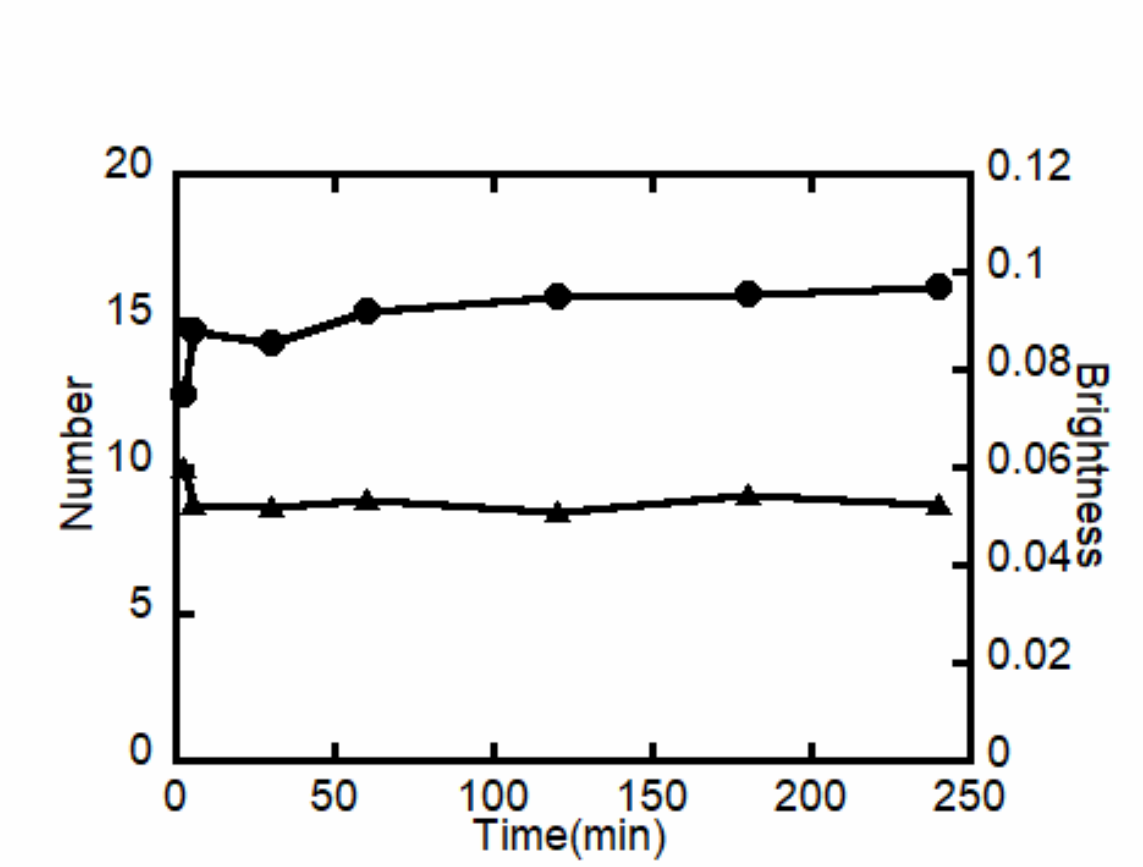

Figure 4-11: Time dependent number and brightness analysis of RLPFK in the presence of MgATP. 116nM RLPFK was diluted into buffer with 3mM MgATP. FCS data was collected at several time points over a course of 4 hours. Values of number (circles) and brightness (triangles) were calculated from raw data as described above.

Before dilution into buffer with MgATP, the RLPFK is stored at high concentration in the presence of Fru-6-P, conditions that stabilize large oligomeric forms of the enzyme. The process monitored by the time course of autocorrelation curves is that of dissociation from large species into tetramers. We attempted to measure a rate of dissociation by fitting data to a single exponential (equation 4-3).

$$g(t) = g_0 e^{-k*t} + g^{\infty} \qquad (4\text{-}4)$$

where g is the $g(0)$ of an autocorrelation curve measured at time (t) after dilution, g_0 is the initial $g(0)$ value before any dissociation has taken place, k is the rate constant of dissociation and g^{∞} is the $g(0)$ sustained after all dissociation has taken place and the species is in a state of pseudo equilibrium. The value of $g(0)$ of each autocorrelation curve was approximated by averaging the first 3 values of $g(\tau)$. The value of $g(0)$ is inversely proportional to concentration but is not calculated using any fitting model. The value of $g(0)$used at time 0 is the $g(0)$ value measured for RLPFK diluted into the presence of Fru-6-P. The assumption is that shortly after dilution into buffer with Fru-6-P RLPFK remains in an oligomerization state reflective of its state before any dissociation has occurred.

We measured a decay constant of 0.48±0.05min^{-1} (Figure 4-12). The equation does not fit the data very well because of a lack of data before 2min, the time in which most of the decay occurs. We can conclude from the decay constant that dissociation occurs very rapidly. A better characterization of the rate of dissociation requires more measurements taken immediately after dilution. A second, slower phase of dissociation seems to occur. The second phase could

possibly be dissociation of the tetramer to species smaller than a tetramer (monomers or dimers).

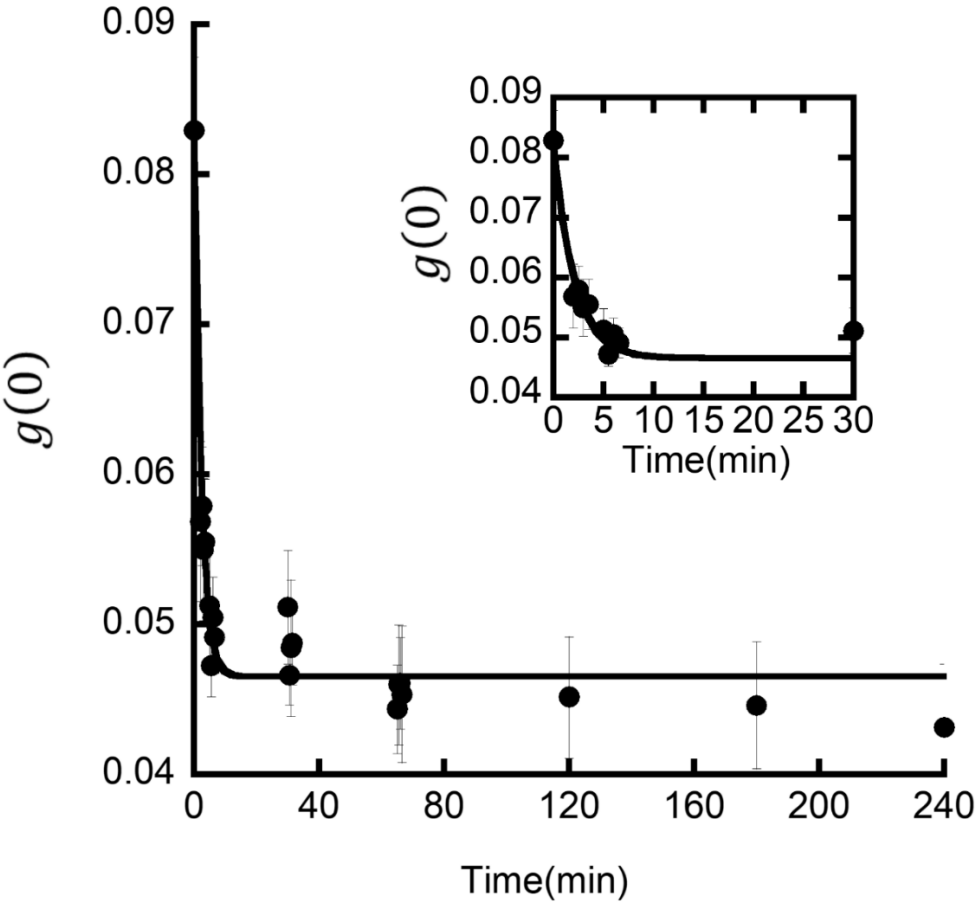

Figure 4-12: Dissociation of RLPFK upon dilution to 116nM in the presence of 3mM MgATP. The value of $\boldsymbol{g}(\mathbf{0})$ used for the zero-time point is the value of $\boldsymbol{g}(\mathbf{0})$ of 116nM RLPFK 2 minutes diluted in the presence of Fru-6-P and is assumed to reflect conditions before any dissociation has occurred. Data is fit to a single exponential decay with a non-zero asymptote.

Discussion

According to the stokes-Einstein equation the diffusion coefficient (D) is inversely proportional to its radius (R) according to the following relationship[165]

$$D = \frac{kT}{6\pi\eta R} \quad (4\text{-}3)$$

where T is the temperature, measured to be 294K, η is the solution viscosity (taken as pure water) and k is the Boltzmann's constant. Reinhart and Lardy[50] determined a Stokes' radius of 67Å according to their fluorescence polarization data. By use of equation 4-4, the diffusion coefficient of a molecule with a Stokes' radius of 67Å is 32$\mu m^2 s^{-1}$. A predicted diffusion coefficient of 32$\mu m^2 s^{-1}$ is in close agreement with the diffusion coefficient measured for 116nM RLPFK 4 hours after dilution into buffer with 3mM MgATP (31 $\mu m^2 s^{-1}$; Table 4-1) supporting the assertion that in these conditions RLPFK exist as a tetramer.

If the only species present is the tetramer (smallest active oligomer) then the concentration of particles is expected to be ¼ the concentration of monomers, or 29nM in the case of Figure 4-7. Any concentration less than 29nM would suggest association of tetramers, and a concentration greater than 29nM would suggest dissociation of tetramers into dimers or monomers. The concentration of particles calculated for 116nM RLPFK 4 hours after dilution into buffer with 3mM MgATP is 26nM (Table 4-1) slightly less but not inconsistent with a tetrameric species.

Calculating the diffusion coefficient and the particle concentration requires knowledge of the excitation volume (see materials and methods). The excitation volume can be approximated by calibration using a fluorophore whose diffusion coefficient is known. However, this method of calibration is known to be inaccurate. One should be cautioned against over interpretation of the absolute values of diffusion coefficient and concentration. The relative values obtained in differing conditions can be compared to each other when the experimental set up has been kept consistent.

The important task of assessing the goodness of fit can be accomplished by calculating the value of χ^2 and by inspecting for shape in the residuals. Confidence in a value is achieved by not only ensuring that the presented value correctly describes the data but that the data cannot also be describe by alternative values. We reported that, at equilibrium conditions, 116nM RLPFK in the presence of MgATP is best described by a diffusion coefficient of 31$\mu m^2 s^{-1}$, a value consistent with a tetramer (Table 4-1). In interpreting the significance of this value, it is important to realize that, as assessed by X^2, the data can be well described by a wide range of diffusion coefficients. Figure 4-13 demonstrates the effect of fitting a single autocorrelation curve to diffusion coefficients ranging from 28-34$\mu m^2 s^{-1}$. The data presented demonstrates that despite differing from each other by 20%, all 4 diffusion coefficients fit with a χ^2 less than 3.

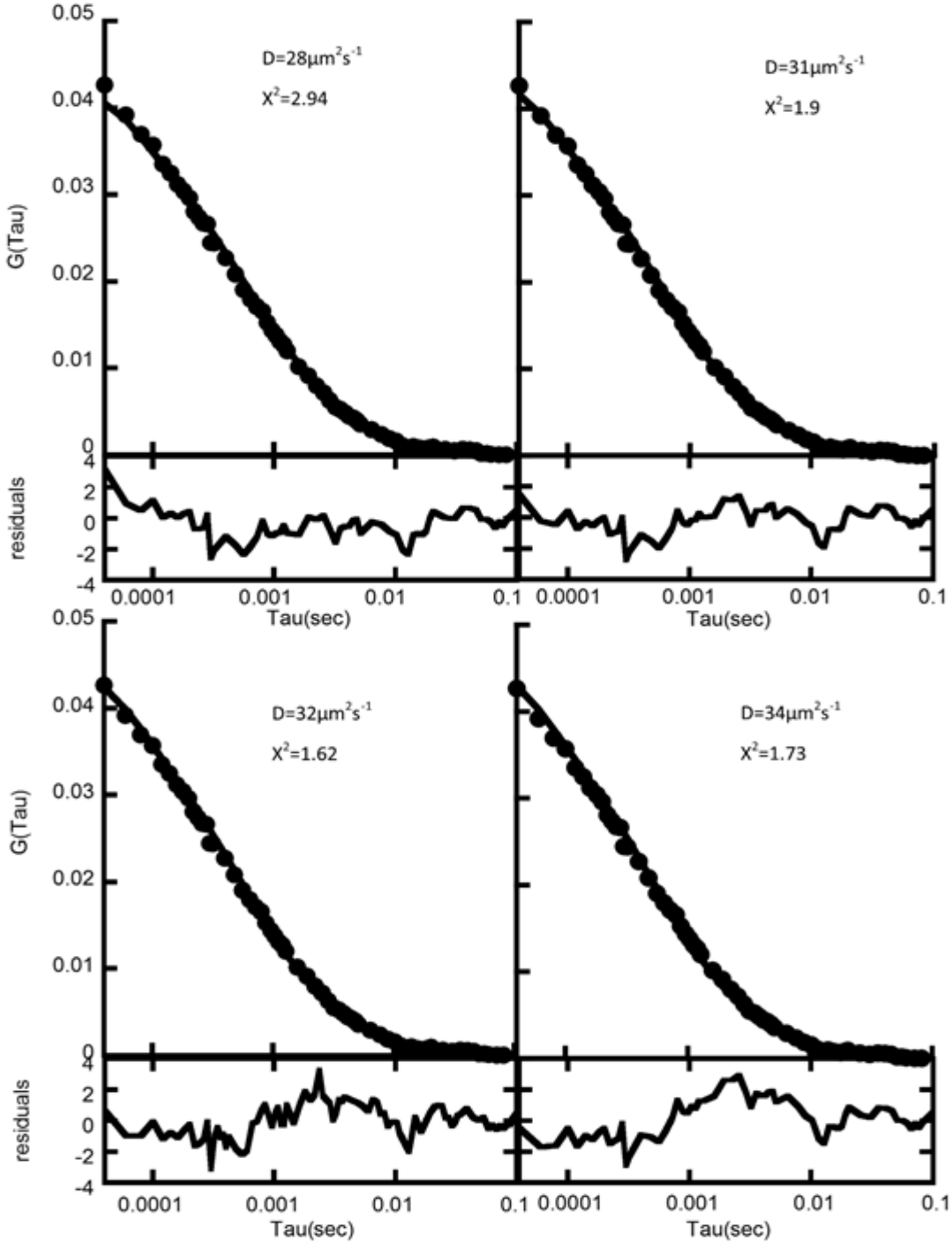

Figure 4-13: Autocorrelation curve of 116nM RLPFK 4 hours after dilution into buffer with 3mM MgATP fit with a single diffuser model. Autocorrelation curves are fit with a diffusion coefficient ranging from 28-34$\mu m^2 s^{-1}$. The x^2 is reported for each and the residuals are plotted below the respective fit.

The value for diffusion coefficient that gives the lowest χ^2 is 32$\mu m^2 s^{-1}$ (Figure 4-13), however the residuals suggest that while 32 $\mu m^2 s^{-1}$ may minimize the cumulative error, it introduces more error in some regions than others. In a good fit, residual values will be scattered around 0 indicating that the error is due to randomness in the data and not a systematic failure to describe the data.[210] When fit to a diffusion coefficient of 32$\mu m^2 s^{-1}$ the residuals display a slight bump from tau=0.001-0.01seconds (Figure 4-13). The "bump" from tau=0.001-0.01seconds becomes more pronounced if the diffusion coefficient is increased to 34$\mu m^2 s^{-1}$ but disappears when decreased to 31$\mu m^2 s^{-1}$. We use the lack of shape in the residuals as the justification for a value of 31$\mu m^2 s^{-1}$.

In addition to the goodness of fit of a value, the goodness of an entire model should also be considered. The data discussed so far came from a fit to a single diffuser model. The data obtained from 116nM RLPFK in the presence of either Fru-6-P or MgATP could be fit to a two-diffuser model with several possible values of diffusion coefficients (data not shown). Two component fits do not provide any noticeable improvement over a single component fit in most instances. The interpretability of a fit must be tempered by EM and activity data. Below we briefly discuss the application of a two-diffuser model to data obtained from RLPFK in the presence of MgATP.

A significant presence of species larger than a tetramer would be apparent in electron microscopy images. The electron microscopy images of RLPFK in the presence of MgATP (Figure 4-2) suggest only a tiny presence of species larger than

a tetramer. Given the negligible presence of species larger than a tetramer, we focus our attention on fits that account for species smaller than a tetramer. Dissociation to species smaller than a tetramer fundamentally results in a loss in activity. A 30% loss of activity was observed when measured concurrently to FCS measurements (Figure 4-14), consistent with tetramer dissociation. A similar loss of activity was reported by Reinhart and Lardy and was seen to correspond to a decrease in polarization indicative of dissociation beyond the tetramer.[50] If the loss of activity directly correlates to the fraction of dissociated RLPFK then 30% of the detected enzyme should be a dimer. The predicted diffusion coefficient of the dimer is 49$\mu m^2 s^{-1}$ based on the Stokes' radius of 44-Å given for a dimer.[212] We described our autocorrelation data assuming a mixture of two species in which 70% of the measured fluorescence comes from tetramers and 30% comes from dimers (Figure 4-15). The data is fit using either a two-diffuser model with discrete diffusion coefficients or a single diffuser model whose diffusion coefficient is the linear sum of the two diffusion coefficients weighted by their fractional contribution. The quality of fits presented in Figure 4-15 are generally poorer than those presented in Figure 4-13. More on the heterogeneity of RLPFK in the presence of MgATP is discussed in the following chapter. For the sake of this chapter, it is suffice to say that in the presence of MgATP, 116nM RLPFK is either a tetramer or a mixture of dimers, tetramers and dimer of tetramers whose average diffusion coefficient is indistinguishable from the diffusion coefficient of the tetramer.

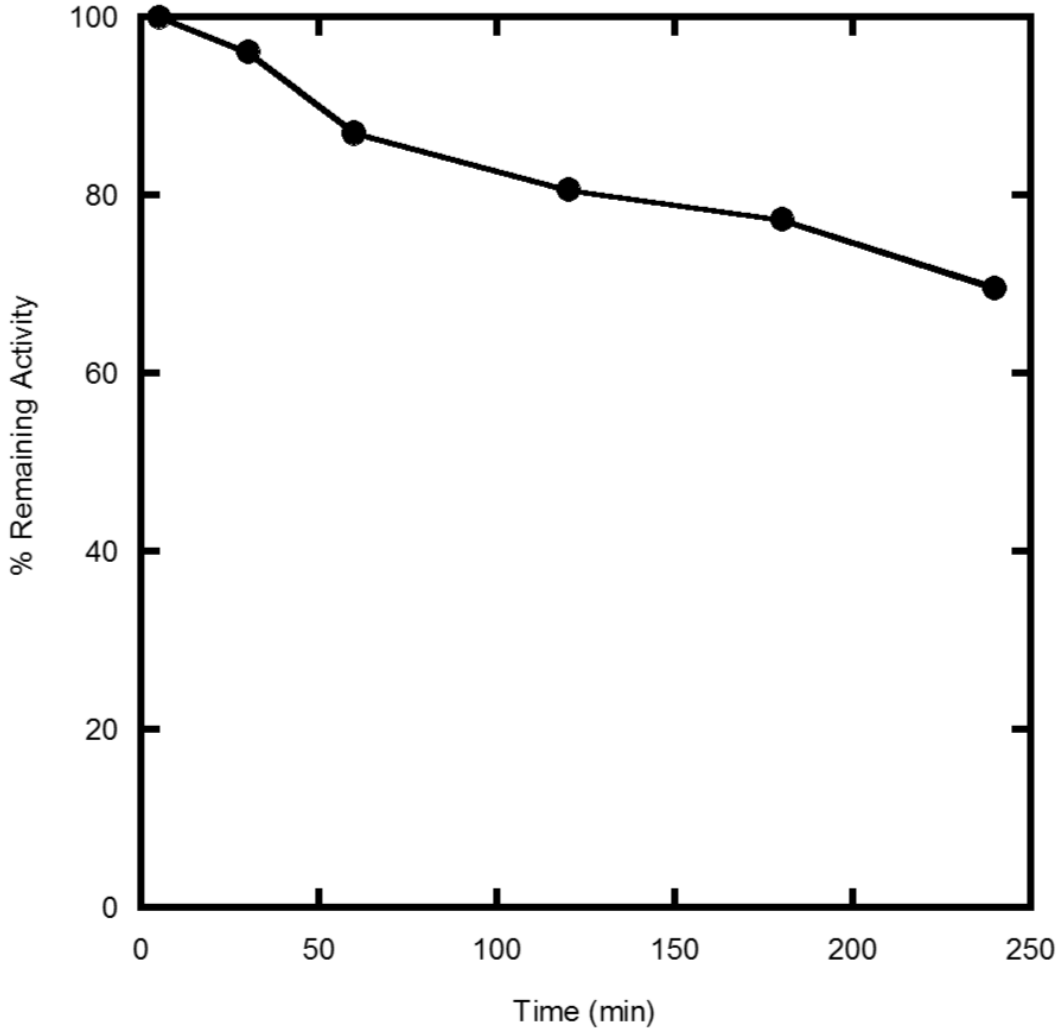

Figure 4-14: Activity plot of 116nM RLPFK 4 hours after dilution into buffer with 3mM MgATP.

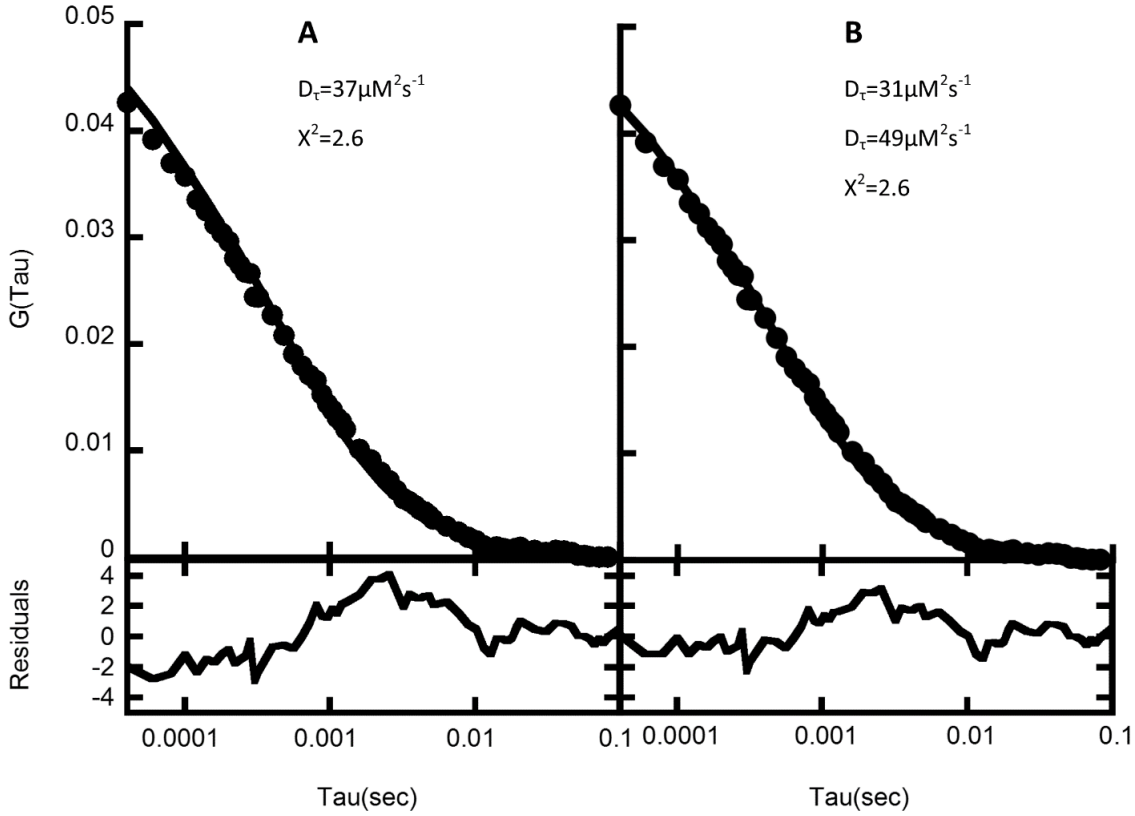

Figure 4-15: Autocorrelation curve of 116nM RLPFK 4 hours after dilution into buffer with 3mM MgATP fit with a two-diffuser model. The same data presented in Figure 4-7 and fit in Figure 4-13 is now fit assuming a mixture of two species. The data are fit using either a two-diffuser model with discrete diffusion coefficients or a single diffuser model whose diffusion coefficient is the linear sum of the diffusion coefficients of each species. The x^2 is reported for each and the residuals are plotted below the respective fit.

While a single diffuser model provides a good fit for 116nM RLPFK in the presence of MgATP, the same cannot be said about 116nM RLPFK in the presence of Fru-6-P. As seen in Figure 4-16a, a single diffuser model does a poor job of describing the data as assed by χ^2 value and by a clear shape in the residuals. An alternative model is necessary to correctly describe this autocorrelation curve. The first approach is to fit with two components; we present two such fits in Figure 4-16b and Figure 4-16c.

It is obvious from the EM images presented in Figure 4-1 that multiple species exist in the presence of Fru-6-P. Heterogeneity does not intrinsically mean that a two-diffuser model is more appropriate than a single diffuser. Meseth et. al. established that in the FCS decay of two-component solutions, the two species must have a diffusion coefficient that differs by 1.6 to be resolvable from each other.[213] Figure 4-1 shows that a substantial population of tetramers exist along with polymers as large as 20-30 tetramers. The requirement of diffusion coefficients that differ by 1.6 is satisfied, therefore in Figure 4-16b we analyze RLPFK in the presence of Fru-6-P with a two-diffuser model that assumes a mixture of tetramers and larger oligomers. By this assumption we find that 32% of the fluorescence signal comes from tetramers ($D=31\mu m^2s^{-1}$) and that the average diffusion coefficient of the larger species is $14\mu m^2s^{-1}$ (Figure 4-16b inset). The fit presented in Figure 4-16b has a larger χ^2 and provides only a small improvement in fit as assessed by the residuals.

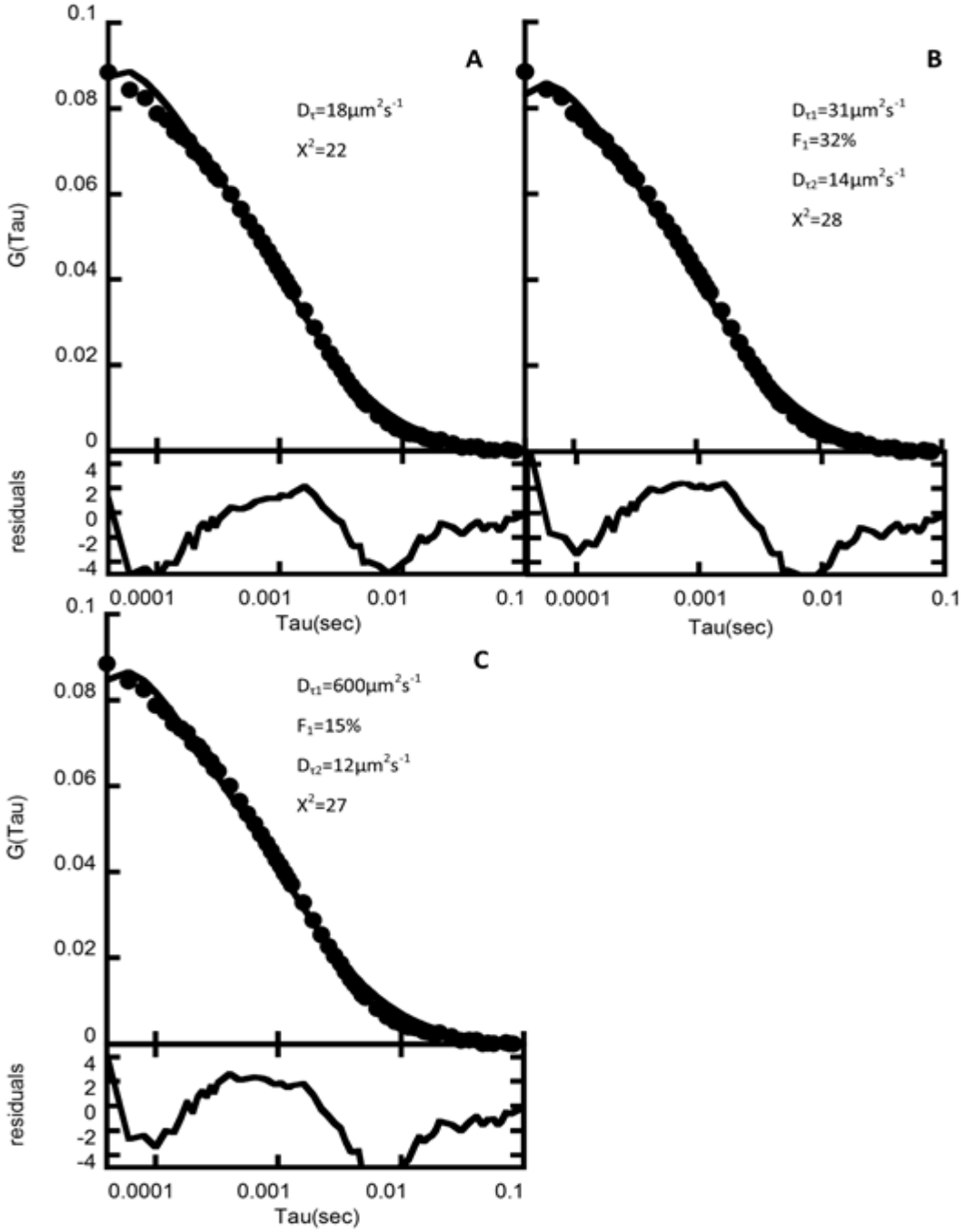

Figure 4-16: Autocorrelation curve of 116nM RLPFK 4 hours after dilution into buffer with 3mM Fru-6-P. The same data is fit with a single diffuser model (A) or with a two-diffuser model (B&C) to compare quality of fits. The diffusion coefficients providing the optimal fits are included in insert as well as the x^2. Residuals are plotted below the respective fit and the implication of each fit is discussed in the text.

Despite the clear relevance of a fit that accounts for the presence of both tetramers and polymers, it does not improve our description of the autocorrelation curve. A possible explanation of the failure of the 2-component fit can be found in Figure 4-1. Previously we emphasized the presence of very large polymers made of 20-30 tetramers, but intermediate sized particles are also present. The apparent diffusion coefficient will be a weighted average of diffusion coefficients from particles whose size ranges from 1-30 tetramers. Additionally, the shape of RLPFK oligomers seen in Figure 4-1 raises the possibility that each species displays two independent diffusion times. RLPFK is seen to self-associate into non-rigid strings of various shapes. The heterogeneity of the oligomer shapes suggest that they are capable of bending and flexing. If a RLPFK oligomer particle was diffusing along the edge of the excitation volume, the bending or "wiggling" of the particle may bring part of the particle into and out of the excitation volume. If the rate of flexing is significantly faster than the rate of diffusion, then it will contribute a unique diffusion time. The autocorrelation curve obtained from RLPFK in the presence of Fru-6-P is not likely the result of a few discrete diffusion coefficients, but from a multitude of diffusion coefficients with incremental values. Absent of more adequate model, we described the autocorrelation curves using a single diffusion coefficient model whose value is a weighted average of all contributing components.

The g values at very short τ values contribute most of the error in the previously described fits of autocorrelation curves obtained from RLPFK in the

presence of Fru-6-P. At short τ values the fitted curves attempt to plateau while data continues going up. The discrepancy between the fit and the data at short τ values prompted us to fit the autocorrelation curve with a two-diffuser model in which one of the diffusion coefficient much faster than the tetramer. A hypothetical fast diffuser could be due to small molecule fluorescent contaminants carried over by Fru-6-P and BSA. We describe the small molecule contaminants with a fast diffuser ($D=600\mu M^2s^{-1}$) that contributes 15% of the fluorescence signal and incorporate all diffusion coefficients related to RLPFK into one diffuser optimally fit to 11.5 μM^2s^{-1} (Figure 4-16c). A fast diffuser did not provide an improvement over the single diffuser model.

Despite coming short of an explicit description of the species present in the presence of Fru-6-P, FCS demonstrates with certainty that RLPFK is more associated in the presence of Fru-6-P than in the presence of MgATP.

Conclusions

The experiments presented in this chapter consider only the differing effect of saturating Fru-6-P and MgATP on a single concentration of RLPFK. Subsequent chapters explore a range of RLPFK and ligand concentrations as well as investigate the relevance of time after dilution. While the nature of the experiments presented in this chapter is simple, many fundamental questions can be answered. For one RLPFK can self-associate free of post translational modifications as verified by the electron microscopy data presented in Figure 4-1. Additionally, the covalent

attachment of a fluorescent dye, necessary to FCS experiments, does not induce dissociation of the RLPFK polymers; evident by Figure 4-7. Although, the discrepancy in the extent of self-assembly between the EM images and the FCS data is of interest. The heterogeneity of the large oligomers complicates efforts to describe the autocorrelation curve with a satisfactory fit. However, this observation in itself answers the import question of whether RLPFK associates to a discrete species. The EM images obtained of RLPFK in the presence of Fru-6-P (Figure 4-1) complemented by the difficulty in fitting autocorrelation curves (Figure 4-16) strongly suggest that RLPFK does not form a discrete species when highly oligomerized. These data set the ground work for future work in which we more thoroughly explore the relationship between oligomerization state, enzyme concentration and ligand condition.

CHAPTER V

USE OF FLUORESCENCE CORRELATION SPECTROSCOPY TO INVESTIGATE THE OLIGOMERIC STATE OF RLPFK IN THE PRESENCE OF MGATP

Introduction

The function of a protein is inextricable from its quaternary structure and thus, any efforts towards functional characterization must include a thorough description of the conditional dependence of the oligomeric composition.[44, 214] The vast majority of proteins form complexes with identical (homooligomers) or non-identical (heterooligomer) proteins.[215] Oligomerization imparts a selective advantage for an organism by making the protein function more resilient to spurious errors, and by affording a greater potential for regulation.[214] It has been long appreciated that homooligomerization provides a convenient mechanism by which an enzyme could be allosterically regulated. For a time, symmetric homooligomerization was presumed to be a necessary feature of all allosterically regulated proteins.[23] Subsequent experiments have observed allosteric regulation occurring in monomers, heterooligomers and asymmetric oligomers.[40] Recently there has been an acute appreciation that a change in the oligomeric composition in itself allosterically regulates enzymatic activity.[45]

Perturbation of a protein's quaternary structure can occur as a result of external factors such as pH, protein concentration, covalent modification, temperature and ligand binding.[44, 214] Ligand binding facilitates a change in the oligomeric composition of rat liver phosphofructokinase (RLPFK)[49], the enzyme responsible for catalyzing the MgATP dependent phosphorylation of fructose-6-phosphate (Fru-6-P) to form fructose-1,6-bisphosphate and ADP. [76, 177, 192] The phosphorylation of Fru-6-P completes the first committed step of glycolysis and thus presents a prime target for regulation. A cornucopia of allosteric ligands subject RLPFK to extensive allosteric control. Most of the allosteric ligands regulating RLPFK are metabolic bi-products, and thus place RLPFK under fine control of the energy needs of the system. [76, 177, 192] The primary inhibitor of RLPFK is the substrate, MgATP.

Phosphofructokinase is a highly conserved enzyme found in all kingdoms of life.[72] PFK in all forms self-associate, with the smallest active form being a tetramer of four identical 86kDa subunits.[216] Mammalian PFK is seen to self-associate to higher order oligomers much larger than a tetramer.[75] The liver isoform of mammalian PFK has a particularly high propensity to self-associate into higher order oligomers, or polymers.[50, 51, 96, 103, 104, 107] Observations reported by Reinhart and Lardy suggest that the highly associated form of RLPFK is the physiologically relevant form.[49]

The general paradigm observed for RLPFK is that allosteric activators stabilize highly associated polymers while allosteric inhibitors promote

dissociation to the tetrameric form.[49] Reducing the multitude of RLPFK regulators to the two most important, ligand dependent modulation of RLPFK polymerization can be described as Fru-6-P stabilization of polymers and MgATP stabilization of tetramers.[50, 103] A ligand stabilized enzyme conformer has a greater affinity for the stabilizing ligand. Therefore, the polymer form of RLPFK likely possess a greater affinity for substrate Fru-6-P than the tetrameric form. Modulation of the oligomeric state of RLPFK by MgATP may provide a method of allosteric regulation on top of the inhibition seen in kinetic assays.

The proposition that the oligomeric composition of (RLPFK) modulates the catalytic function[49] implies a need to understand the dependence of oligomeric composition on the concentration of MgATP and Fru-6-P in solution. In the previous chapter we presented evidence that RLPFK forms a stable tetramer in the presence of MgATP. We demonstrated this at a single enzyme concentration and at a single MgATP concentration. The degree of RLPFK polymerization depends on both the concentration of ligand and the concentration of RLPFK. A description of the complex dependence of the oligomeric composition of RLPFK on enzyme and ligand concentration requires measurements at several ligand and enzyme concentrations. Additionally, we measure the rate of change following perturbation from a highly associated oligomeric conformation. We report here time dependent fluorescence correlation spectroscopy (FCS) measurements of either 116nM, 58nM or 15nM RLPFK in the presence of various concentrations of MgATP. The data suggest that the tetramer is the predominant form when the concentration of

MgATP is greater than 0.4mM but dissociates to dimer or monomer forms at MgATP concentrations lower than 0.4mM.

Materials and Methods

Fluorescence correlation spectroscopy

FCS experiments and data analysis were performed as previously described. In short, fluorescence signal is collected from RLPFK fluorescein isothiocyanate (RLPFK-FITC) excited by a Tsunami Ti/Sapphire (Spectra Physics) pulsed-laser tuned to 900nm. Random spikes of high fluorescence intensity are curated from raw data as described previously. Temporal autocorrelation of fluorescence signal is analyzed by equation 5-1[160]

$$g(\tau) = \frac{\langle \delta I(t) \delta I(t+\tau) \rangle}{\langle I(t) \rangle^2} \tag{5-1}$$

The excitation volume is described by a point spread function (PSF) of Gaussian shape in the x and y direction and Lorentzian in the axial direction. The dimensions of the Gaussian-Lorentzian excitation volume were calibrated daily using a solution of fluorescein in MOPS buffer pH=7.0. Autocorrelation curves were fit to a two-diffuser model with a fixed "slow diffuser" and a variable "protein diffuser". The value of the diffusion coefficient (D) of the "slow diffuser" was fixed at 0.5$\mu m^2 s^{-1}$. The fractional contribution of the "slow diffuser" varied from measurement to measurement. For a given measurement, the fractional

contribution of the slow diffuser was determined by optimal fitting, as assessed by the shape in the residuals at long τ values. The value of D for the "protein diffuser" was determined by optimal fit as assessed by a minimization of χ^2 and lack of shape in the residuals across all values of τ. Most experiments demonstrated negligible contribution from the slow diffuser (0.1% fractional intensity) and no measurement demonstrated a contribution greater than 5%. We presume the slow diffuser is due to some form of contaminant and is not interesting to the process investigated. The "protein diffuser" incorporates the weighted average rate of diffusion of species relevant to the oligomeric conformation of RLPFK. The "protein diffuser" is treated as a single diffuser even in cases when multiple species with unique rates of diffusion is most probable.

Tracking dissociation

The autocorrelation curves contain two pieces of information which provide insight into a process of dissociation/association; the number of particles and the characteristic diffusion time[217]. The number of particles is inversely proportional to the value of g at $\tau = 0$ $\left(g(0)\right)$ according to the relationship

$$\mathrm{g}(0) = \frac{\gamma}{\mathrm{N}} \tag{5-2}$$

where the value of γ depends on the shape of the point spread function (PSF). Calculating an absolute concentration or characteristic diffusion time requires precise knowledge of the effective volume of excitation as well as model fitting. A

change in particle concentration can be monitored without model fitting by simply tracking the value of g at shortest τ value ($\tau = 20\mu s$). Dissociation of protein polymers will result in an increase in the number of particles manifesting itself as a decrease in the apparent $g(0)$ over time.

Stability

Kinetic activity measurements were taken concurrently with FCS measurements to assess the stability of RLPFK tetramers. The PFK catalyzed conversion of Fru-6-P to Fru-1,6-BP was coupled to the oxidation of NADH, which resulted in a decrease in the absorbance at 340nm. The rate of decrease in A_{340} was monitored using a Beckman Series 600 spectrophotometer. Assay conditions were chosen to promote maximum activity (pH=8.0, 50mM Tris-HCL, 100mM KCl, 20mM $(NH_4)_2SO_4$, 2mM DTT, 3mM $MgCl_2$, 1mM ATP, 1mM Fru-6-P). RLPFK was diluted into the cuvette so that the concentration during assays was 0.1µg/ml. Activity is reported as a percentage of the maximum activity measured independently of these experiments.

Oligomeric conformation

The Stokes-Einstein equation (equation 5-3) relates the diffusion coefficient (D) as a function of a particle's stokes radius

$$D = \frac{kT}{6\pi\eta r} \tag{5-3}$$

where k is the Boltzmann constant, T is the temperature in Kelvin and η is viscosity of solution (taken to be pure water) In the previous chapter we presented a diffusion coefficient for the tetramer of 31.1$\mu m^2 sec^{-1}$, corresponding to a Stokes radius of 70.9Å. We normalize the apparent size of experimental species to the size of the tetramer by dividing the diffusion coefficient of tetramer by the measured diffusion coefficient. This normalized diffusion coefficient $\left(\frac{D_{tet}}{D_{app}}\right)$ has a value greater than 1 when RLPFK is associated into species larger than a tetramer and smaller than 1 when species are dissociated to monomers or dimers.

A hypothetical $\frac{D_{tet}}{D_{app}}$ of 0.64 is calculated for a dimer using the stokes radius of 44Å reported by Pavelich and Hammes[212] and substantiated by Reinhart and Lardy[50]. A hypothetic $\frac{D_{tet}}{D_{app}}$ is proposed for a dimer of tetramers by invoking the cubed root dependence of the diffusion coefficient of a spherical particle on its molecular weight shown in equation 5-4.

$$\frac{\mathrm{MW_a}}{\mathrm{MW_b}} = \left(\frac{\mathrm{D_a}}{\mathrm{D_b}}\right)^3 \qquad (5\text{-}4)$$

This likely overestimates the correct diffusion coefficient of a polymer as a consequence of the erroneous assumption that the polymer will be of spherical shape. However, the approximation should be close enough for the interest of this chapter.

Interpreting ligand dependent dissociation

Simulated data was generated by calculating the normalized diffusion coefficient $\left(\frac{D_{tet}}{D_{app}}\right)$ as a function of MgATP using equation 5-5

$$\mathrm{D} = \frac{\Delta \mathrm{D[A]}}{\mathrm{K_d} + \mathrm{[A]}} + \mathrm{D_o} \tag{5-5}$$

where D is the normalized diffusion coefficient $\left(\frac{D_{tet}}{D_{app}}\right)$, D_o is the normalized diffusion coefficient when [A] is 0, and ΔD is equal to the limiting value of $D - D_0$ when [A] is saturating. The simulated data assumes D_0 of 0.45; justification for this value is presented below. Additionally, simulated data assumes no species larger than a tetramer form as a function of MgATP so ΔD is 0.55. Data is simulated using a K_d value for MgATP binding of either 0.04mM or 0.36mM. Justification for these values is presented below.

Results

In the absence of any ligand, RLPFK rapidly dissociates into an inactive mixture of monomers and dimers[50]. RLPFK loses 90% percent of activity in 60 minutes after dilution to 58nM in buffer without stabilizing ligands (Figure 5-1). Figure 5-2 reports the dissociation of RLPFK in the absence of ligand in the form of FCS measurements taken at 2min, 30min and 60min after dilution to a concentration of 58nM. An autocorrelation curve typical of a tetramer (black)

provides a reference curve. The insert lists the fitted parameters of each curve. Shortly after dilution, 58nM RLPFK has dissociated to a species smaller than a tetramer (diffusion of 44.6$\mu m^2 s^{-1}$ compared to 32 $\mu m^2 s^{-1}$). Dissociation continues over the course of an hour until the diffusion coefficient has increased to 71 $\mu m^2 s^{-1}$. According to equation 5-1, the stokes radius of the final species is 31Å, significantly smaller than the 44Å proposed for the dimer[50, 212] and even smaller than the 37Å stokes radius proposed for monomeric PFK from rabbit muscle[155]. FCS measurements suggest that deprived of stabilizing ligand, RLPFK primarily exist as a monomer.

While FCS experiments argue strongly for the monomeric form as the primary species in the absence of ligand, a potentially important piece of information is lost because of analysis. We remove rare spikes in fluorescence signal from the raw data because they interfere with the stochastic nature of the temporal correlation function. We argue that these spikes are primarily due to contaminant particles not relevant to the process of interest. Justification for their removal relies, in part, on subjective observations that their occurrence is not correlated to the controlled variables (time, enzyme concentration, or ligand). However, in experiments of RLPFK diluted in the absence of any ligand, we noticed a time dependent increase in intensity of these rare events (data not shown). The rarity of these events (about 1 per 2 minutes) make them difficult to characterize by statistical analysis. We propose that these spikes

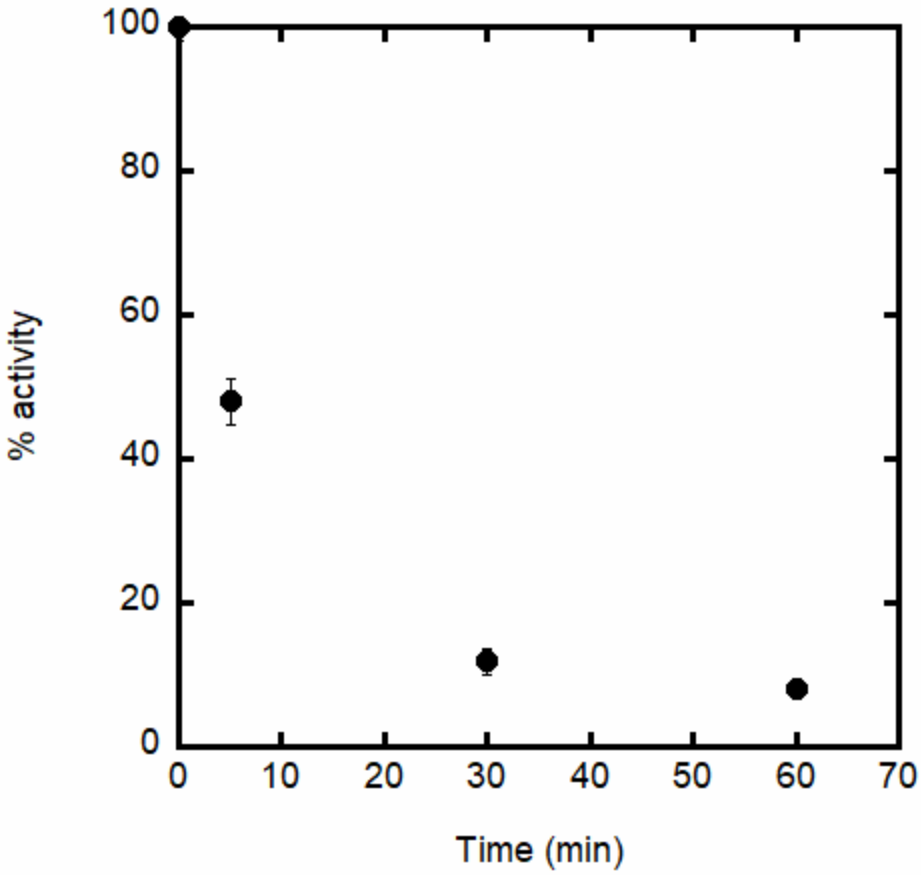

Figure 5-1: Stability plot of 58nM RLPFK diluted into buffer containing no ligand. Activity at time 0 is the specific activity independently measured prior to the experiment and provides the standard for normalization. Error bars reflect the standard deviation from 6 replicate measurements.

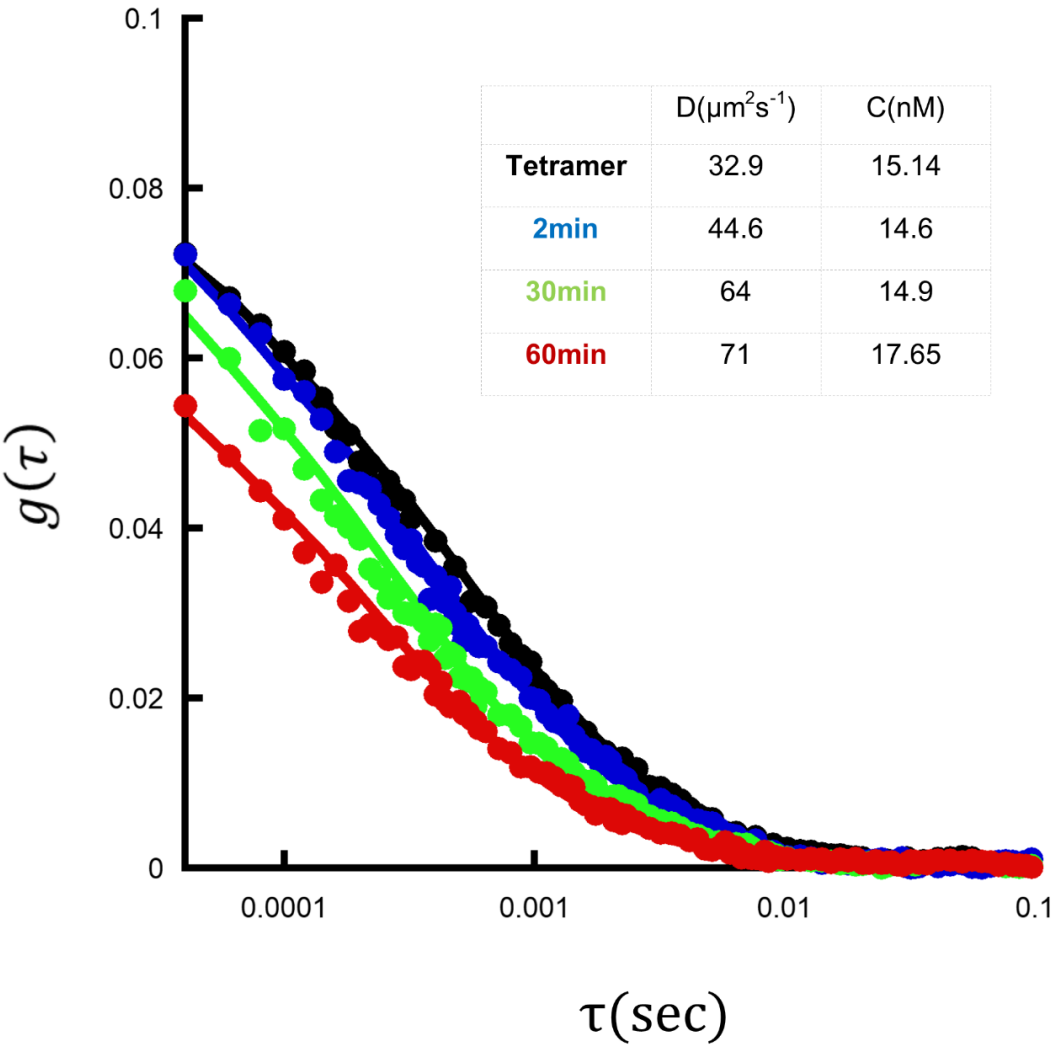

Figure 5-2: Autocorrelation curves of 58nM RLPFK 2min (blue), 30min (green) and 60min (red) after dilution into buffer with no ligand. Autocorrelation curve of 58nM RLPFK 240min after dilution in the presence of 3.2mM MgATP (black) represents a curve typical of the tetramer. Insert lists the diffusion coefficient and concentration obtained from fitting data a two-diffuser model (see text).

are due to aggregate species formed as a consequence of tetramer dissociation, maintaining the long-held observation that the monomeric form of PFK is unstable in solution without denaturing solvents[212]. Therefore, we can expand the process suggested by FCS to say that in the absence of stabilizing ligands RLPFK rapidly dissociates to monomers which subsequently aggregate. The aggregation process undergone by monomers likely involves irreversible denaturation and results in a form other than the string like polymers stabilized by Fru-6-P.

The importance of a secondary aggregation pathway lies in the complexity it introduces into efforts to study the self-association process of RLPFK. Naturally, one would want to describe a process of association according to its smallest species (i.e. monomer). Unfortunately, the monomer does not easily reform tetramer[49, 50], is not stable[212] and seemingly aggregates. Because of the complexities of working with a monomer, and in recognition that the tetramer is the smallest active form, we use the tetramer as the standard unit in our discussion of polymerization. In this chapter, we characterize the tetramer form of RLPFK and how its formation and stabilization depend on enzyme and ligand concentration.

To measure the interrelationship between protein concentration, MgATP concentration and the oligomeric conformation of the enzyme, we performed FCS on three concentrations of RLPFK in six different concentrations of MgATP. While in the previous chapter we established that oligomeric conformation of RLPFK was stable at a concentration of 116nM RLPFK and in the presence of 3.2mM MgATP, it was not certain that this would be true for all conditions of interest. For this reason,

we took measurements at periodic time intervals over a course of 4 hours. We tracked dissociation by plotting the change in $g(0)$ as a function of time after dilution to an enzyme concentration of 116nM, 58nM or 15nM. In addition to varying concentration of RLPFK we varied the concentration of MgATP. Concentrations of MgATP less than 0.8mM were not used with 15nM RLPFK. A $g(0)$ value for 116nM RLPFK immediately after dilution is estimated by measuring the $g(0)$ of RLPFK 2 minutes after dilution to 116nM in buffer with saturating Fru-6-P. It is assumed that Fru-6-P stabilizes the pre-dilution oligomeric state and thus represents the state of the enzyme immediately prior to dilution. For other concentrations of RLPFK, the values of $g(0)$ immediately after dilution are extrapolated from that measured for 116nM. The value we are plotting for $g(0)$ is not a fitted value, but is the first $g(\tau)$ value of the autocorrelation curve (g at τ=20μsec).

Diluted to a concentration of 116nM from a stock concentration of 20μM, RLPFK polymers rapidly dissociate to a $g(0)$ value about half of the initial value before transitioning into a slower phase of dissociation (Figure 5-3). A relatively high $g(0)$ value is only seen shortly after dilution and in the presence of high concentrations of MgATP. The rate and magnitude of the secondary transition increases with decreasing MgATP concentrations.

The smallest active form of the enzyme is a tetramer, so kinetic activity can act as an indicator for dissociation beyond a tetramer. Activity measurements taken concurrently to the FCS measurements on 116nM RLPFK are plotted in Figure 5-4.

The enzyme is most stable in the presence of high concentrations of MgATP, but a significant loss of activity is seen at all concentrations of MgATP.

We fit the autocorrelation curves to a two-diffuser model consisting of a "slow diffuser" whose diffusion coefficient is fixed at 0.5μm^{2}s^{-1} and a "protein diffuser" with a variable diffusion coefficient. The "protein diffuser" represents the average rate of diffusion for RLPFK in the given experimental condition. The apparent diffusion coefficient (D_{app}) was then normalized to the theoretical diffusion coefficient of tetramer (D_{tet}) by dividing 32μm^{2}s^{-1} by D_{app}. The theoretical diffusion coefficient of the tetramer was calculated by the Stokes-Einstein equation using the Stokes radius of 67Å.[50] Normalized diffusion coefficients $\left(\frac{D_{tet}}{D_{app}}\right)$ of 116nM RLPFK are plotted as function of MgATP at several time points after dilution (Figure 5-5). For reference, the insert in Figure 5-5 indicate the theoretical diffusion coefficient for a dimer, tetramer and for 2 tetramers.

At 2 minutes, 116nM RLPFK has a normalized diffusion coefficient greater than 1 for all concentrations of MgATP. By 30minutes after dilution, the normalized diffusion coefficient is approximately equal to 1 at all concentrations of MgATP, but increases slightly with increasing concentrations of MgATP. The normalized diffusion coefficient is relatively stable after 30 minutes except for 0.1 and 0.4mM MgATP which demonstrate a progressive decrease in $\frac{D_{tet}}{D_{app}}$ and reach values much less than 1.

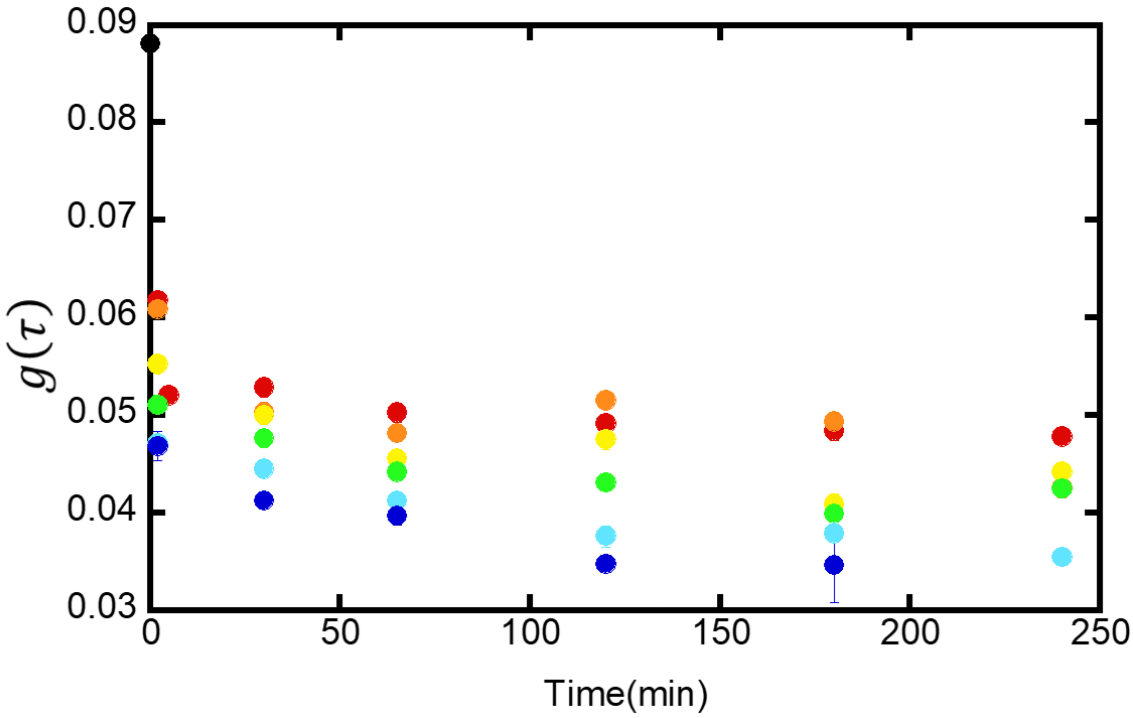

Figure 5-3: Dissociation of 116nM RLPFK as measured by the decrease in the first g(τ) value of the autocorrelation curve. Dissociation is measured for 4 hours after dilution to a concentration of 116nM in the presence of 3.2mM MgATP (red), 1.6mM MgATP (orange), 0.8mM MgATP (yellow), 0.4mM MgATP (green), 0.2mM MgATP (light blue), 0.1mM MgATP (dark blue). The initial G(tau) value listed for time 0 (black) is the value measured for RLPFK in the presence of saturating Fru-6-P and is thought to approximate the state of the enzyme immediately prior to dilution.

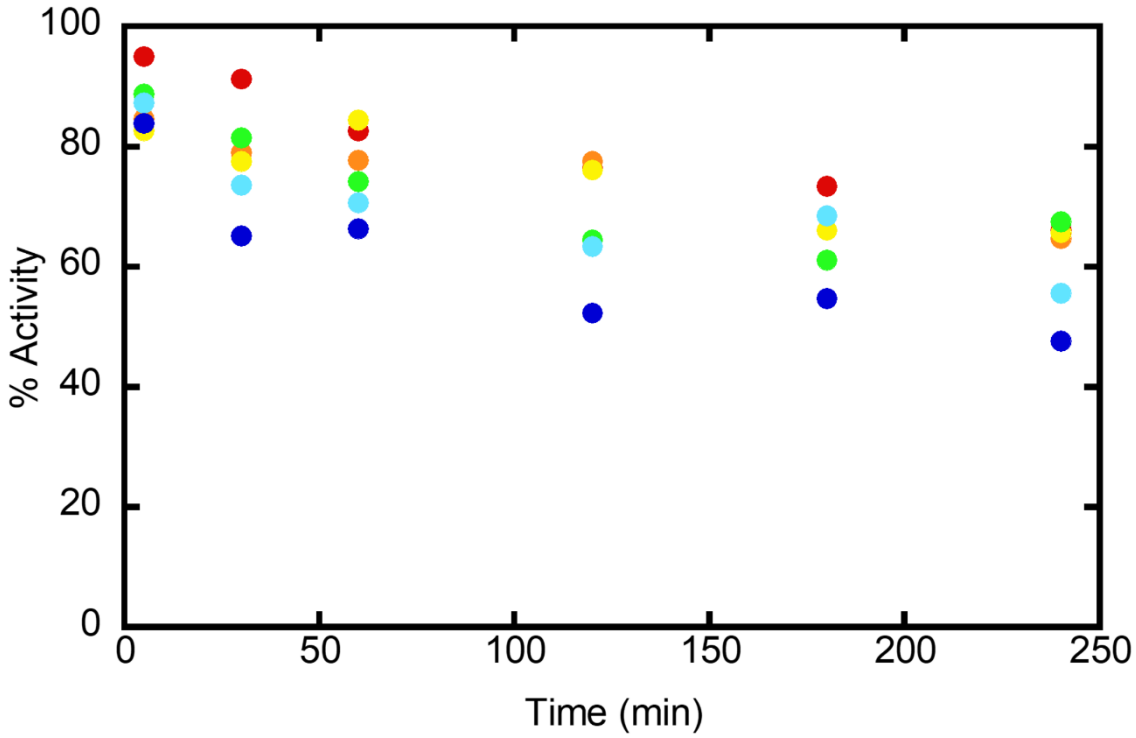

Figure 5-4: Stability of RLPFK after dilution to a concentration of 116nM in the presence of 3.2mM MgATP (red), 1.6mM MgATP (orange), 0.8mM MgATP (yellow), 0.4mM MgATP (green), 0.2mM MgATP (light blue), 0.1mM MgATP (dark blue). Enzymatic activity is measured as described in the material and methods and is normalized to the maximal activity.

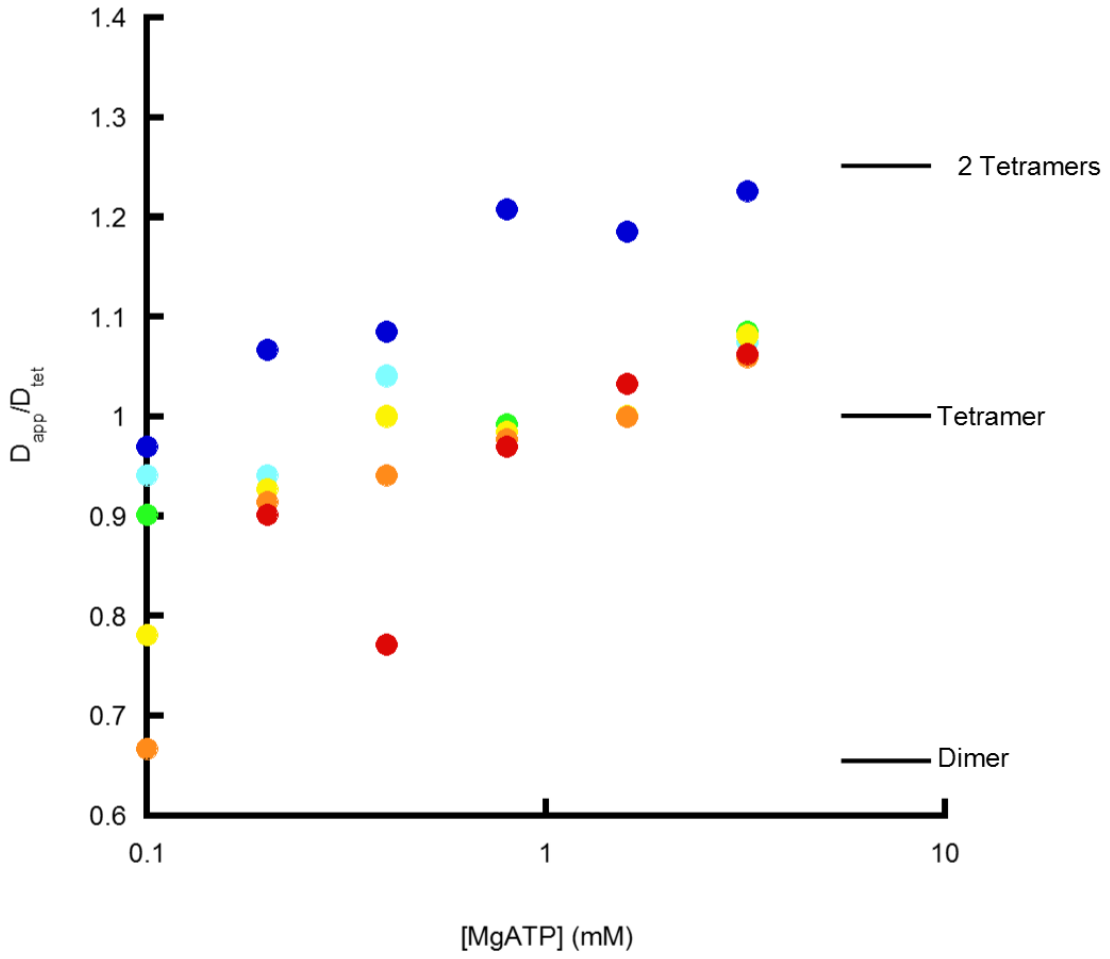

Figure 5-5: Effect of MgATP concentration on the apparent oligomeric size of 116nM RLPFK. Apparent oligomeric size is approximated by the diffusion coefficients measured by fitting autocorrelation curves as described in text. Insert lists the theoretical diffusion coefficients for the stated oligomeric size. The dependence of oligomeric size on MgATP was measured at the following time points after dilution: 2min (dark blue), 30 min (light blue), 60min (green), 120min (yellow), 180min (orange), and 240min (red).

Next, we look at 58nM RLPFK. Figure 5-6 shows the dissociation of rate of 58nM RLPFK tracked by g(τ) at τ=20μsec. No evidence of an intermediate g value is seen at any time and the slow decrease in $g(0)$ does not appear to occur. An even greater decrease in activity is seen with 58nM RLPFK (Figure 5-7) than with 116nm (Figure 5-4). The rate and magnitude of activity lost is dependent on the concentration of MgATP with a 60% loss of activity occurring 4 hours after dilution with 0.1mM MgATP. The dependence of $\frac{D_{tet}}{D_{app}}$ on the concentration of MgATP when the concentration of RLPFK is 58nM is presented in Figure 5-8. As with 116nM RLPFK (Figure 5-5) the tetramer is stabile over the course of 4 hours if the concentration of MgATP is 0.8mM or greater, and dissociation occurs at MgATP concentrations below 0.8mM. Unique to Figure 5-8 is the absence of any evidence of species larger than a tetramer and a more dramatic demonstration of dissociation as MgATP concentrations are decreased below 0.8mM.

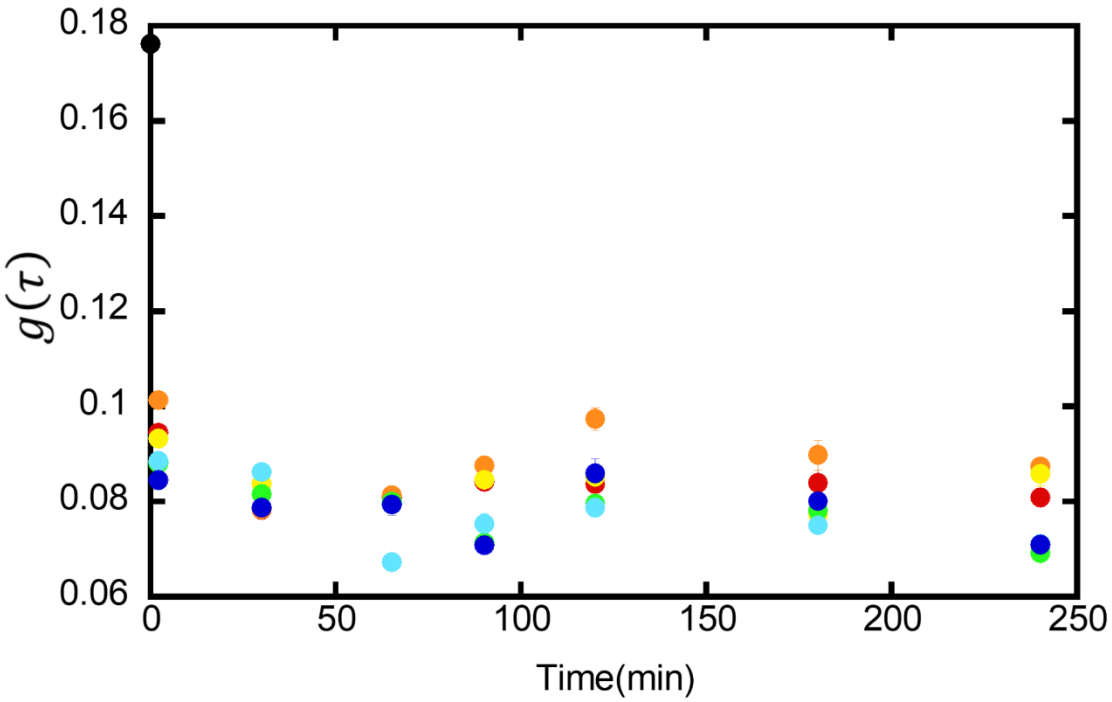

Figure 5-6: Dissociation of 58nM RLPFK as measured by decrease in the first G(tau) value of the autocorrelation curve. Dissociation is measured for 4 hours after dilution to a concentration of 58nM in the presence of 3.2mM MgATP (red), 1.6mM MgATP (orange), 0.8mM MgATP (yellow), 0.4mM MgATP (green), 0.2mM MgATP (light blue), 0.1mM MgATP (dark blue). The initial G(tau) value listed for time 0 is a theoretical value thought to approximate the state of the enzyme immediately prior to dilution.

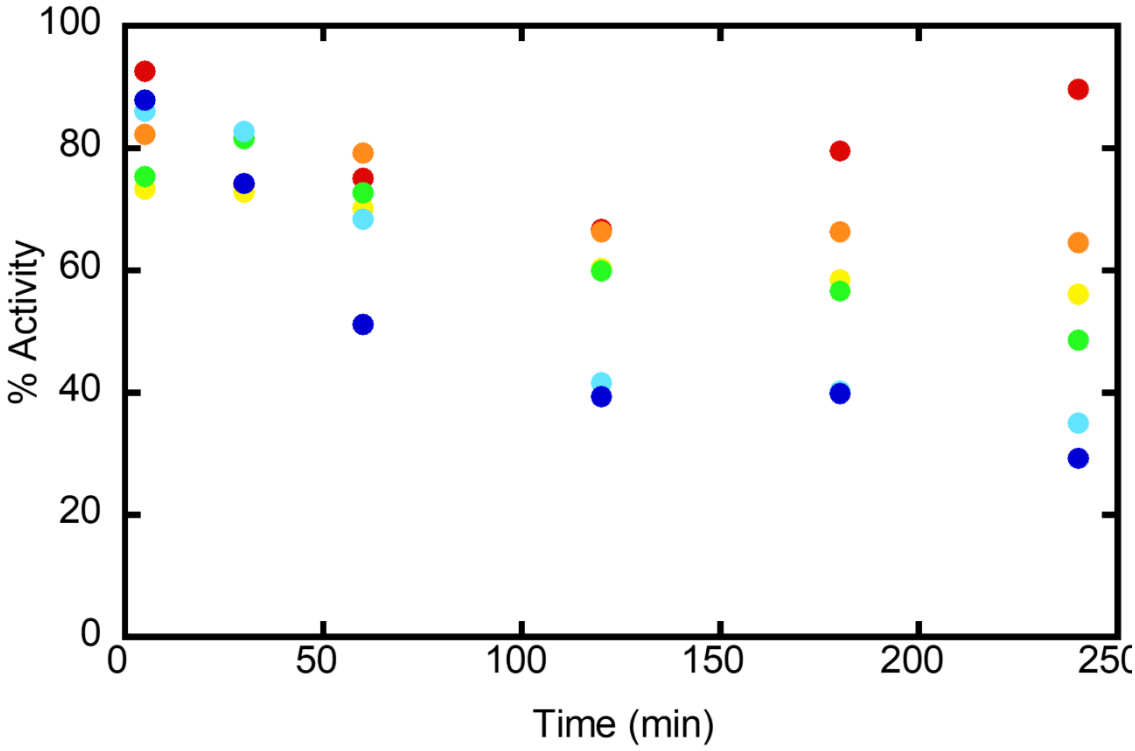

Figure 5-7: Stability of RLPFK after dilution to a concentration of 58nM in the presence of 3.2mM MgATP (red), 1.6mM MgATP (orange), 0.8mM MgATP (yellow), 0.4mM MgATP (green), 0.2mM MgATP (light blue), 0.1mM MgATP (dark blue). Enzymatic activity is measured as described in material and methods and is normalized to the maximal activity.

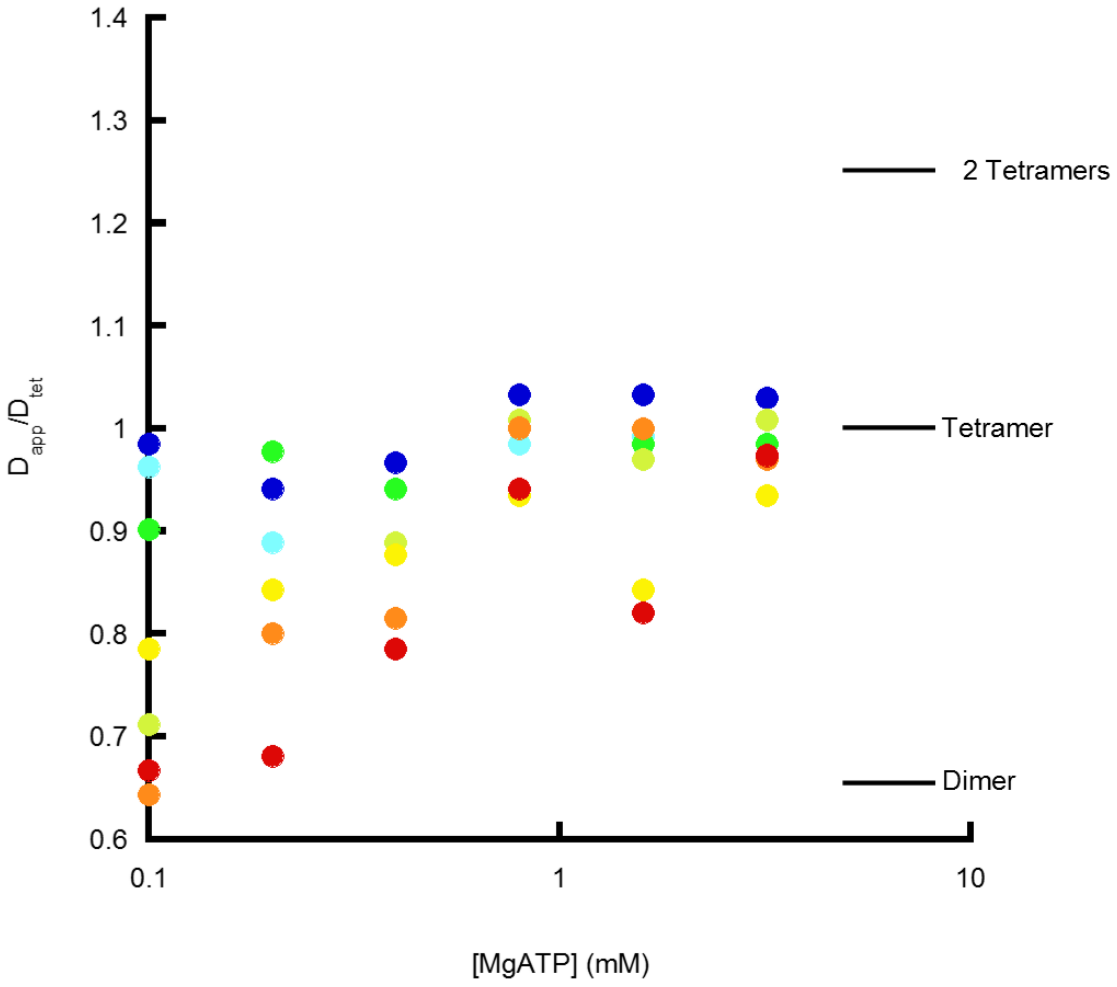

Figure 5-8: Effect of MgATP concentration on the apparent oligomeric size of 58nM RLPFK. Apparent oligomeric size is approximated by the diffusion coefficients measured by fitting autocorrelation curves as described in text. Insert lists the theoretical diffusion coefficients for the stated oligomeric size. The dependence of oligomeric size on MgATP was measured at the following time points after dilution: 2min (dark blue), 30 min (light blue), 60min (green), 90min (chartreuse), 120min (yellow), 180min (orange), and 240min (red).

The effect of MgATP on the oligomeric state of 15nM RLPFK was only analyzed at MgATP concentrations of 3.2mM, 1.6mM and 0.8mM. The general trend of 15nM RLPFK is very similar to 116nM RLPFK. An intermediate $g(0)$ value is seen shortly after dilution before plateauing (Figure 5-9); loss of enzymatic activity limited to 25% (Figure 5-10) and diffusion coefficients consistent with an average particle size larger than a tetramer shortly after dilution (Figure 5-11). The primary difference is that after 4 hours, 15nM RLPFK has a diffusion coefficient consistent with species smaller than a tetramer at all concentrations of MgATP (Figure 5-11). MgATP concentrations lower than 0.8mM were not attempted for this experiment because previous experiments resulted in a 75% loss of activity when using 0.4mM MgATP or less.

Taken together these data suggest that upon dilution RLPFK polymers dissociate to tetramers who are relatively stable but dissociate further to an extent inversely proportional to both enzyme and MgATP concentration. The MgATP could stabilize the tetramer by binding to the allosteric site and/or the active site. Our FCS experiments do not provide any direct structural information useful for accessing a binding site, but we could utilize the different dissociation constants characteristic of the individual binding sites. In Figure 5-12 we plot the normalized diffusion coefficient $\frac{D_{tet}}{D_{app}}$ as a function of MgATP concentration to obtain pseudo dissociation plot and compare it to simulated dissociation plots assuming the stabilizing effect coming from either the allosteric site or the active site. Previously

we reported the extrapolated dissociation constant of MgATP at the allosteric site to be 0.36mM (chapter 2) and have measured the K_m of MgATP at the catalytic site to be approximately 0.04mM (data not shown). We simulated data representing a ligand with a dissociation constant of 0.04mM (red) or 0.36mM (blue). The $\frac{D_{tet}}{D_{app}}$ ranged from a value of 1, representing a tetramer, to 0.45 representing a monomer. The value of 0.45 was obtained assuming a monomeric diffusion coefficient of 71$\mu m^2 s^{-1}$ (Figure 5-2). The experimental data (black circles) most closely resembles the data simulated assuming a dissociation constant of 0.36mM suggesting that the allosteric site is the critical site for MgATP induced stabilization of the tetramer.

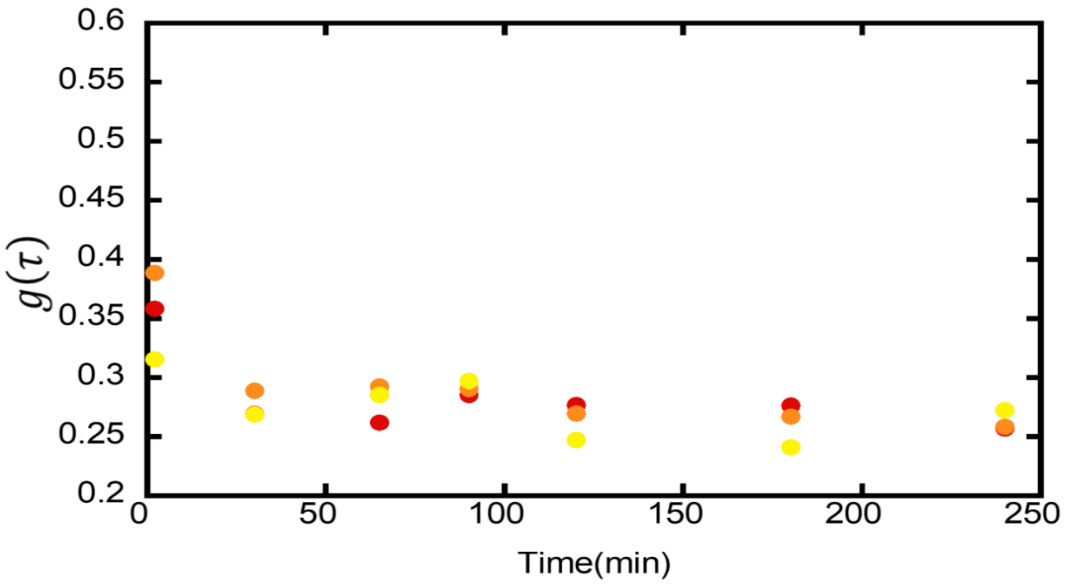

Figure 5-9: Dissociation of 15nM RLPFK as measured by decrease in the first $\boldsymbol{g(\tau)}$ value of the autocorrelation curve. Dissociation is measured for 4 hours after dilution to a concentration of 58nM in the presence of 3.2mM MgATP (red), 1.6mM MgATP (orange), and 0.8mM MgATP (yellow).

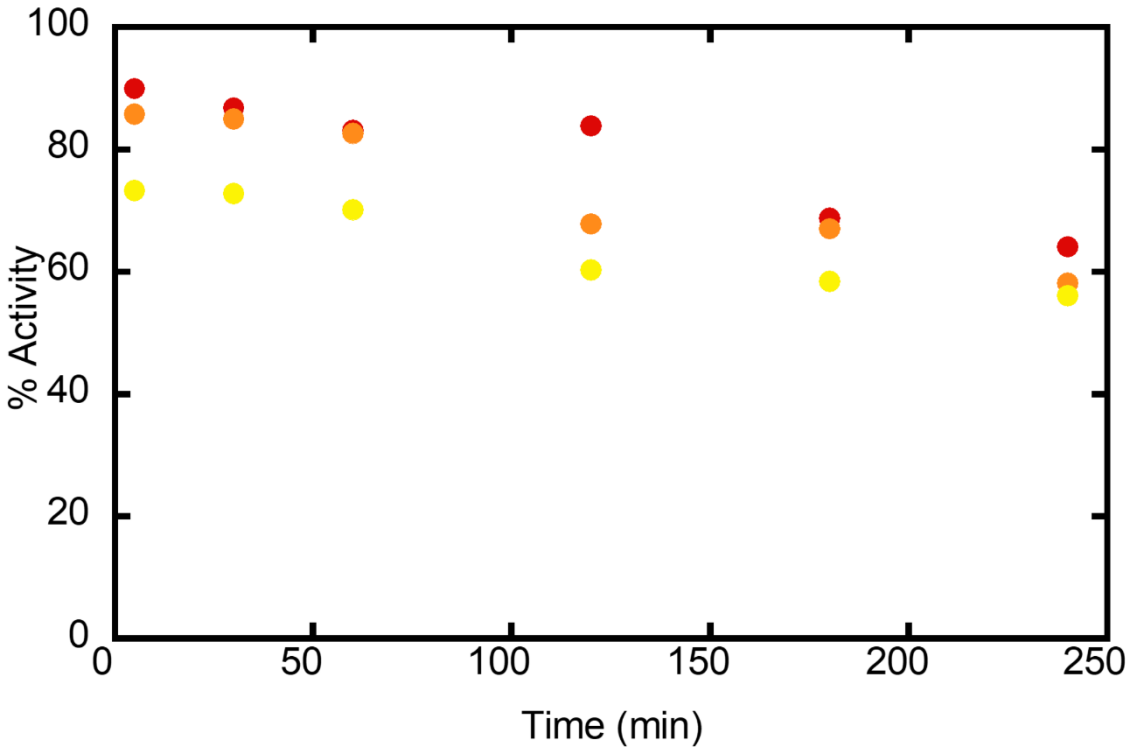

Figure 5-10: Stability of RLPFK after dilution to a concentration of 15nM in the presence of 3.2mM MgATP (red), 1.6mM MgATP (orange) and 0.8mM MgATP (yellow). Enzymatic activity is measured as described in material and methods and is normalized to the maximal activity.

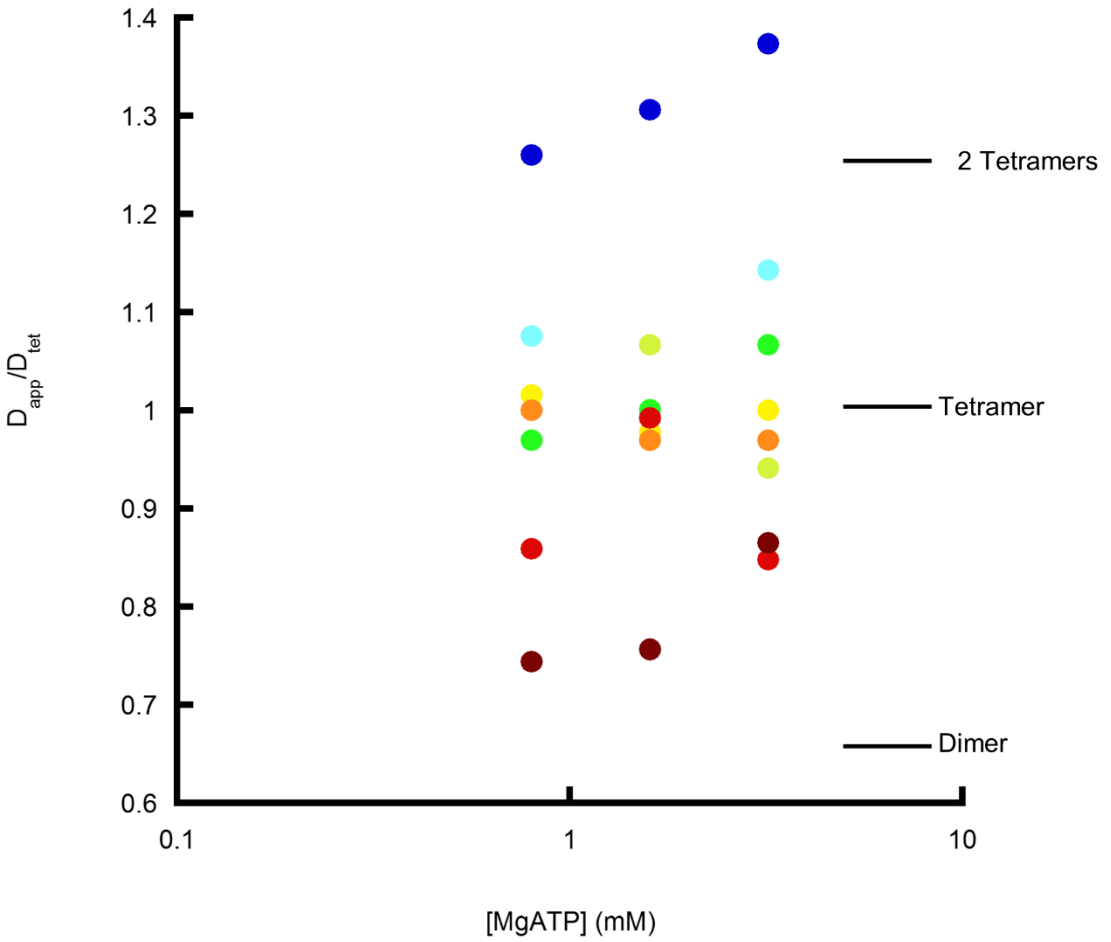

Figure 5-11: Effect of MgATP concentration on the apparent oligomeric size of 15nM RLPFK. Apparent oligomeric size is approximated by the diffusion coefficients measured by fitting autocorrelation curves as described in text. Insert lists the theoretical diffusion coefficients for the stated oligomeric size. The dependence of oligomeric size on MgATP was measured at the following time points after dilution: 2min (dark blue), 30 min (light blue), 60min (green), 80min (chartreuse), 100min (yellow), 120min (orange), and 180min (red) and 240 (dark red).

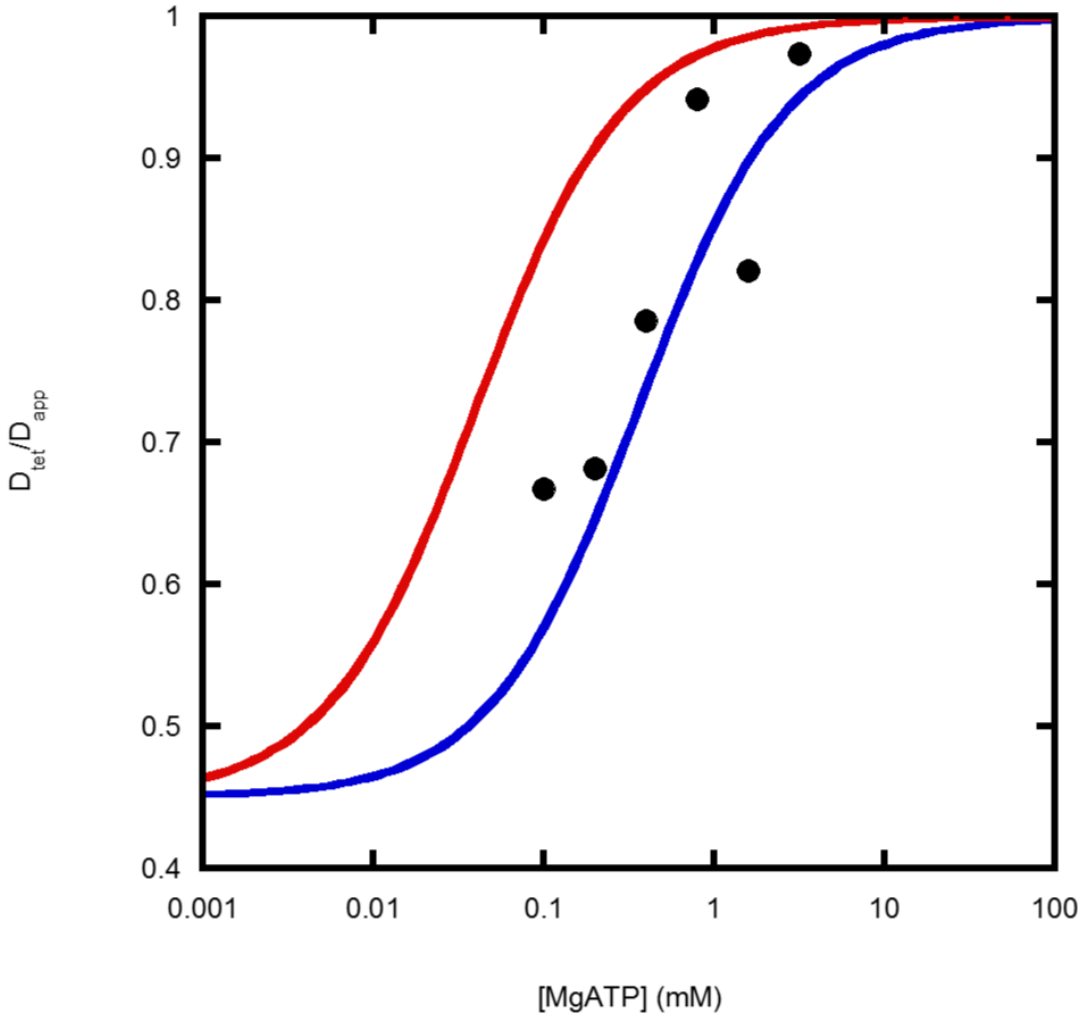

Figure 5-12: Approximation of critical MgATP for stabilization of tetramer. Normalized diffusion coefficients of 58nM RLPFK as a function of MgATP are plotted as black circles. Normalized diffusion coefficients range from 1 for tetramer to 0.45 for monomer. Solid curves represent simulated data of a ligand binding with a dissociation constant of 0.36mM (blue) or 0.04mM (red).

Discussion

Apparent diffusion coefficient of tetrameric RLPFK

In the previous chapter we presented a diffusion coefficient for the tetramer of 31μm^{2}sec^{-1}, corresponding to a Stokes radius of 71Å. We also demonstrated that a relatively wide range of values satisfactorily described the data. Ultracentrifugation studies performed on PFK from rabbit muscle measured a diffusion coefficient of 32μm^{2}s^{-1} corresponding to a stokes radius 67Å.[218] Using gel filtration, Pavelich and Hammes also reported 67Å as the Stokes radius of rabbit muscle PFK.[212] Rabbit muscle PFK has almost identical molecular weight as rat liver so one would expect the Stokes radius to be very similar. Indeed, Reinhart and Lardy found that a stokes radius of 67Å was consistent their polarization data.[50] We therefore use 32μm^{2}s^{-1} as the diffusion coefficient of the tetramer and express the apparent diffusion coefficients in terms of it. The normalized diffusion coefficients are clustered around 1 suggesting that FCS is able to detect the presence of the tetramer and that it predicts a diffusion coefficient consistent with literature.[218]

Presence of polymers

We approximated the dissociation of RLPFK polymers by measuring $g(\tau)$ at $\tau = 20\mu s$ as a function of time. This is taken to approximate $g(0)$, which is inversely proportional to number of particles. A $g(0)$ representative of the polymers immediately after dilution is approximated by measuring at an equivalent

concentration of RLPFK in the presence of Fru-6-P. We presume that this reflects the state of the enzyme prior to perturbation by MgATP, however, we see very little evidence of this state. It is true that in all conditions the $g(0)$ value at 2min after dilution is greater than later time points, but the magnitude of difference is much less than anticipated. We interpret this as a rate of dissociation to fast to detect intermediate values.

While the rapidity of the change in $g(0)$ suggest that all of polymer has been dispensed with after 30min, the normalized diffusion coefficient $\left(\frac{D_{tet}}{D_{app}}\right)$ at 116nM suggest a residual presence of species larger than a tetramer. The $\frac{D_{tet}}{D_{app}}$ of 116nM RLPFK in the presence of 3.2mM MgATP is larger than 1 suggesting that the average particle size is larger than a tetramer. At 58nM RLPFK the $\frac{D_{tet}}{D_{app}}$ is also greater than 1 after 30 minutes in the presence of 0.8mM, 1.6mM and 3.2mM MgATP. Reinhart and Lardy also observed species larger than a tetramer in the presence of 3mM MgATP.[50] They reported a clear dependence on enzyme concentration; data obtained with 58nM RLPFK was consistent with a tetramer whereas data obtained with 116nM RLPFK was nearly twice as large as a tetramer. Our diffusion data seems consistent with Reinhart and Lardy, and suggest that at high enzyme concentration some presence of larger polymers remain; that is, provided MgATP is present to stabilize RLPFK.

The apparently contradictory report on dissociation between $g(0)$ values and diffusion coefficient can be understood by recognizing the dependence of $g(0)$

sensitivity on the ratio of labeled tetramers. The value of $g(0)$ is inversely proportional to the number of fluorophores in the excitation volume, and can only detect a dissociation process if each dissociated species is labeled. If, for example, a polymer consisting of 5 tetramers has only a single fluorescence label, one particle will be detected regardless of whether the polymer is intact or fully dissociated. That is to say, the $g(0)$ value will not change upon dissociation. The RLPFK used for these experiments had less than 1 dye per tetramer. Therefore, dissociation of polymers does not result in a linear relationship between $g(0)$ and the number of tetramers in the polymer. In general, a greater degree of change and higher sensitivity to perturbations is seen in diffusion coefficient than in $g(0)$.

Dissociation to monomers and dimers

Experiments performed in the absence of ligand best demonstrate the impact of labeling ratio on the resolvability of sub-tetrameric species using $g(0)$ (see Figure 5-2). RLPFK completely dissociates to monomers within 30 minutes after dilution, evidence for this include a 90% loss of activity (Figure 5-1) and a diffusion coefficient consistent with a particle the size of a monomer (Figure 5-2). Despite a 4-fold increase in the number of particles, the concentration predicted by FCS only increases by 17%. A labeling ratio close to 1 dye per tetramer easily explains this result because a tetramer will rarely consist of multiple labeled monomers. Therefore, the change in $g(0)$ is insufficient for discerning species whose size range from a couple of tetramers to monomers and should only be used

to track dissociation of highly associated species to approximately tetrameric species.

To monitor dissociation beyond the tetramer we rely on the diffusion coefficient and activity. A diffusion coefficient greater than $32\mu m^2 s^{-1}$ $\left(\frac{D_{tet}}{D_{app}} < 1\right)$ indicates the presence of dimers or monomers and must be accompanied by a loss of activity. This is seen for RLPFK in several conditions but most consistently at MgATP concentrations lower than 0.8mM. Higher concentration of RLPFK seem to be able to stabilizer the tetramer, made evident by the observation of greater dissociation at 58nM than at 116nM (low MgATP) and by the evidence of tetramer dissociation at 15nM even in the presence of high MgATP. Unfortunately, only 3 concentrations of RLPFK were examined in this study, examination of more concentrations would strengthen conclusions on the impact of RLPFK concentration.

Perhaps surprisingly, a loss of activity is seen in a few conditions whose diffusion coefficient suggest an average size larger than a tetramer, namely 116nM RLPFK with 3.2 or 1.6mM MgATP. These conditions demonstrate a slow decrease in $g(0)$ after 30 minutes which suggest continued dissociation of RLPFK, possibly to species smaller than a tetramer. However even after 4 hours the diffusion coefficient is consistent with an average species size greater than a tetramer. Comparable observations were made by Reinhart and Lardy.[50] They reported a slow decrease in polarization following an initial dramatic decrease relative to that

measured with Fru-6-P and noted that this process was accompanied by a 40% loss of activity.[50] They also reported that at 10μg/ml (116nM) the rotational relaxation time was slightly larger than the theoretical value of a tetramer.[50] The simplest and most direct explanation for this apparent contradiction is that in the given condition RLPFK exist as a mixture of species which include tetramers, small polymers of tetramers and inactive monomers or dimers. There is no evidence that the maximal activity of RLPFK increases as it polymerizes so the activity would not average out the way physical properties reporting on the size would. Collectively, these observations suggest perhaps one of the most critical points of this study; there is no condition in which a single species of RLPFK is completely isolated.

An alternative explanation between the apparent contradictory stability data is a form of sequestering of dissociated monomers. We observed an increased presence of anomalous intensity spikes when RLPFK is diluted to 58nM RLPFK without ligand (data not shown) and suggested this could be evidence of aggregation of monomeric RLPFK into inactive aggregates. If the same process occurred on a lesser scale in the presence of MgATP contribution of monomers to the apparent diffusion coefficient may be systematically removed as a consequence of data analysis. The following is a list of evidence against this hypothesis. A progressive drift towards insoluble aggregates would never reach equilibrium and a complete loss of activity (and soluble protein) would occur in a relatively short time. It has been our observation that RLPFK is reasonably stable in the presence of MgATP for weeks at a time. Additionally, Reinhart and Lardy demonstrated that

addition of MgATP restored activity to highly dissociated RLPFK, demonstrating the propensity to stabilize the tetramer away from material loss. Finally, our experiments have demonstrated a few conditions with MgATP in which the predominant (or average) form is significantly smaller than the tetramer without an overwhelming presence of insoluble aggregates. At 0.1mM MgATP we lose 75% of activity but the apparent diffusion coefficient is consistent with the dimer, not monomer and no clear evidence of aggregates is seen. It seems most likely that RLPFK exist in an equilibrium of dimers, tetramers and dimer of tetramers. As the concentration of MgATP is decreased, the dimer form is enriched and thus maximum activity decreases.

As a final caveat, one should not immediately attribute loss of activity to tetramer dissociation. Several processes could lead to loss of enzyme activity including oxidation and loss of material. Oxidation is deleterious as evident by the constant addition of dithiothreitol necessary to maintain enzymatic activity. Procedures necessary to minimize protein surface adhesion during FCS measurements brings focus on the possibility of material loss as the culprit of decrease in activity. However, a loss in material would manifest itself as an increase in $g(0)$, not a decrease. It is possible that some of the loss of activity is a consequence of something completely independent of the oligomeric state and is thus inconsequential to FCS measurements.

A definitive statement on the oligomeric state of RLPFK and its consequential dependence on MgATP may unfortunately be beyond the scope of

this report. However, there is room yet for thinking on what we know. Previous publication have suggested that MgATP promotes the dissociation of rabbit muscle PFK to the dimer.[219] However, Reinhart and Lardy observed that MgATP was proficient at protecting the RLPFK from loss of activity and was even more facile than Fru-6-P at restoring tetrameric structure to dissociated RLPFK.[50] We observe diffusion coefficients characteristic of a tetramer at high concentrations of MgATP, those characteristic of a dimer at low concentrations of MgATP and a transition that appears to occur at a concentration consistent with the dissociation constant of MgATP at the allosteric site. Only the complete absence of MgATP generates a diffusion coefficient consistent with the monomer. The dissociation constant of MgATP from the allosteric site is much greater than that from the catalytic site. In fact, the dissociation constant of MgATP is only 0.04mM, half of the minimum concentration of MgATP used in these experiments (unpublished data from this lab). We hypothesize that binding of MgATP to the allosteric site stabilizes the tetramer form and binding to the catalytic site protects the dimer from further dissociation to monomers.

Assembly mechanism

As previously mentioned, no conditions explored in this report resulted in a homogenous species of RLPFK. In the previous chapter we presented electron microscopy data on reasonably homogeneous tetramers, however close inspection of this image (Figure 5-13) reveals the occasional polymer. Mostly, these polymers

appear to be octamers, but some are even larger. Similar results were found with pig liver PFK.[103] We hypothesize that RLPFK exists as a near continuous gradient of species who sizes range from very large polymers to monomers (Figure 5-14). Unligated monomers form inactive aggregates. MgATP binding to the active site protects the dimer from dissociation to monomers. The dimers form tetramers which are greatly stabilized by MgATP, presumably via the allosteric binding site. At an RLPFK concentration of 116nM, 3.2mM MgATP is sufficient to stabilize the tetramer such that it is the predominant species formed. In this condition, very little evidence of the dimer exist and RLPFK begins to sample octamers as a part of a continuum polymerization process.

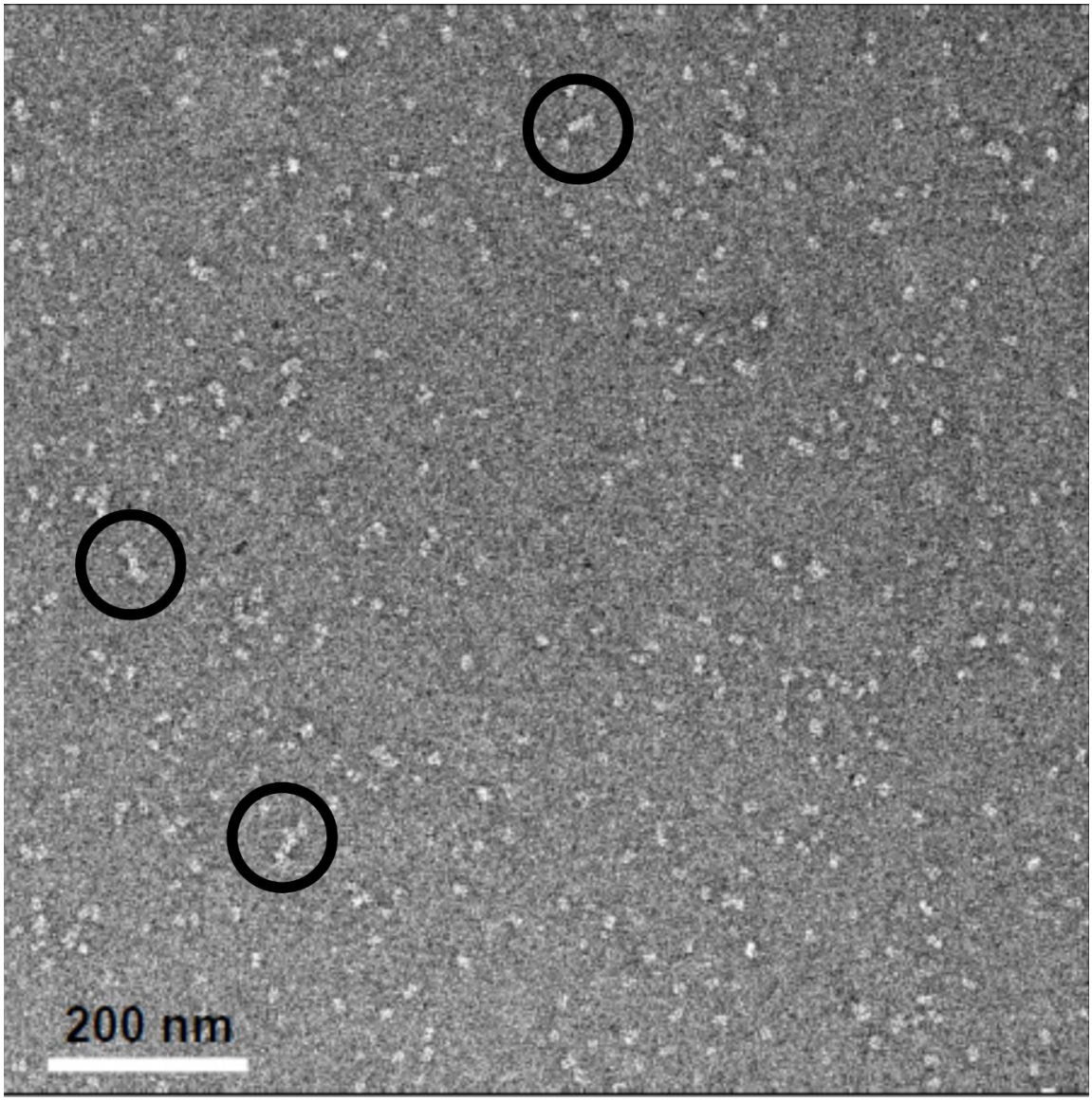

Figure 5-13: Annotated image of negative stained Electron Microscopy image of RLPFK in the presence of 3mM MgATP. Protein was diluted 200-fold from a stock concentration of 20μM and 4μl was applied to grids. PFK was negative stained with uranyl acetate. Scale bar included for size reference. Circle mark octamers.

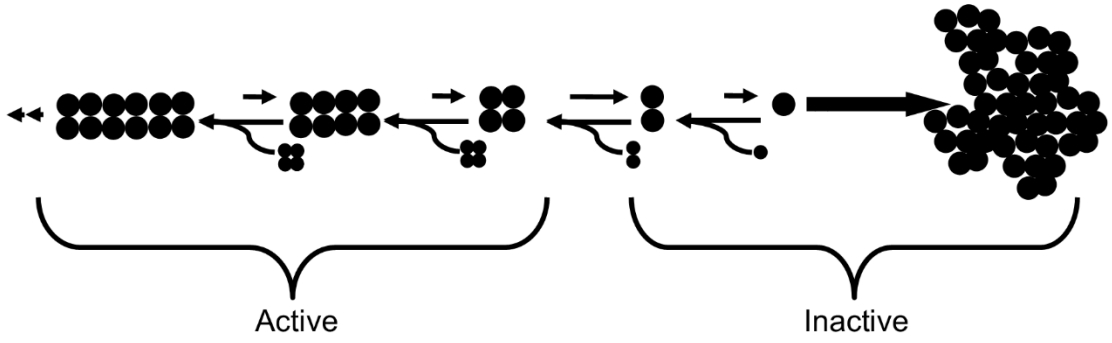

Figure 5-14: Possible assembly mechanism. See discussion for details.

Future directions

We hypothesize an assembly process which could be substantiated by FCS measurements. Support for this assembly mechanism will require measurements at a far greater number of enzyme concentrations than has been performed here. 5 decades of enzyme concentrations are recommended with at least 5 concentrations per decade. Naturally these experiments should be repeated at least 3 times. Expanding the number of protein concentrations this much while maintaining the full matrix of variables would be very time consuming. The effect of ligand concentration is more interesting than a time dependent change in state. A single time point after dilution, perhaps 3-4 hours, should be sufficient to describe the state of RLPFK. The data presented in this report suggest that the majority of change in oligomeric state has occurred within two minutes.

Conclusions

We have followed the oligomeric state of RLPFK at a concentration of 116nM, 58nM and 15nM RLPFK in the presence of 3.2, 1.6, 0.8, 0.4, 0.2 or 0.1mM MgATP. We find that the transition from large polymers to tetramers occurs very rapidly. We suggest evidence of the presence of species larger than a tetramer at 116nM RLPFK and high concentrations of MgATP. This supports the assertion that the polymer form is the most physiologically relevant form.[49-51] We observe dissociation of the tetramer at low enzyme concentrations and low MgATP concentrations. We present boundary conditions for which the tetrameric form is the predominant species.

CHAPTER VI

USE OF FLUORESCENCE CORRELATION SPECTROSCOPY TO INVESTIGATE THE OLIGOMERIC STATE OF RLPFK IN THE PRESENCE OF FRU-6-P

Introduction

In the previous chapter we investigated the dependence of the oligomeric state of phosphofructokinase from rat liver (RLPFK) on the enzyme and ligand concentration while in the presence of MgATP. We established that MgATP stabilizes the tetramer form of RLPFK but does not stabilize the polymer form. We see that the extent of tetramer stabilization is dependent on both the concentration of MgATP and RLPFK. Further, we have established that Fru-6-P stabilizes the polymer form of RLPFK. Reinhart and Lardy proposed that polymerized RLPFK is the primary form in cellular conditions and that the polymer exhibits a higher affinity for substrate Fru-6-P that the tetramer form.[49, 50, 104, 107]

The propensity of eukaryotic PFK, and RLPFK in particular, to form polymers much larger than a tetramer has been well established.[49-51, 75, 96, 103, 104, 107, 151] However, questions about the structural properties of these species remained unanswered. It remains to be determined whether highly associated RLPFK forms a uniform population of discrete, well defined polymers, and whether there is a limit

to the extent of polymerization. The broad elution peak observed for the polymerized RLPFK passed through size exclusion chromatography[50] and the heterogeneity seen in electron microscopy images of pig liver PFK[103] contradict, although do not discredit, the possibility of a discrete, well defined polymer. Fluorescence polarization measurements performed at incrementally higher concentrations of RLPFK suggest that the particle size continues to increase in the presence of Fru-6-P. However, the lifetime of pyrene imposes an upper limit to the size of particle resolvable by polarization measurements and the uncertainty of molar volume becomes quite large. Fluorescence correlation spectroscopy (FCS) has no upper limit to the size of particles it can resolve and can be used to distinguish between a solution of single and multiple species.

Invocation of polymerization induced activation of RLPFK[49] to explain the failure of kinetic assays to explain the activity of RLPFK measured in liver perfusion[51, 153, 154] assays relies on the observation that RLPFK is a tetramer at the subnanomolar concentrations used for kinetic assays.[50, 155] FCS is able to measure the particle size of RLPFK at concentrations ranging from the subnanomolar used in kinetic assays to the 300-600μM concentration of RLPFK in the cell. The ability to span such a large range of concentrations allow the observation of concentration dependent polymerization of RLPFK.

An understanding of the interplay between oligomeric state and substrate concentration requires a description of the limits of polymer stabilization. We report here time dependent fluorescence correlation spectroscopy (FCS)

measurements of either 116, 58 or 15nM RLPFK in the presence of various concentrations of Fru-6-P. We see that at high concentrations of Fru-6-P, RLPFK exist as a highly heterogeneous solution of polymers whose sizes do not increase as a function of RLPFK concentration. At Fru-6-P concentrations of 0.8mM and below, the particle size strongly depends on the concentration of RLPFK. Additionally, we see evidence that the tetramer form of RLPFK is unstable in the presence of Fru-6-P. Together, the data reported here illustrate the process of dissociation of Fru-6-P stabilized polymers.

Materials and Methods

Fluorescence correlation spectroscopy

FCS experiments and data analysis were performed as previously described. In short, fluorescence signal is collected from RLPFK fluorescein isothiocyanate (RLPFK-FITC) excited by a Tsunami Ti/Sapphire (Spectra Physics) pulsed-laser tuned to 900nm. Random spikes of high fluorescence intensity are curated from raw data as described previously. Temporal autocorrelation of fluorescence signal is analyzed by equation 6-1

$$g(\tau) = \frac{\langle \delta F(t) \delta F(t+\tau) \rangle}{\langle F \rangle^2} \qquad (6\text{-}1)$$

where F is the fluorescence signal, $\delta F(t)$ is the fluctuation in the fluorescent signal at time t $(F(t) - \langle F \rangle)$, and $\delta F(t+\tau)$ is the fluctuation in the fluorescent signal at

time $t + \tau$. The angular brackets denote a time average over the fluorescence signal. The value of $g(\tau)$ defines how long an average fluctuation persist after a period of time (τ) has passed. The excitation volume is described by a point spread function (PSF) of Gaussian shape in the x and y direction and Lorentzian in the axial direction. The dimensions of the Gaussian-Lorentzian excitation volume were calibrated daily using a solution of fluorescein in MOPS buffer pH=7.0.

Tracking dissociation

The autocorrelation curves contain two pieces of information which provide insight into a process of dissociation/association; the number of particles and the characteristic diffusion time[217]. The number of particles is inversely proportional to the value of g at $\tau = 0$ $\big(g(0)\big)$ according to the relationship:

$$\mathrm{g}(0) = \frac{\gamma}{\mathrm{N}} \qquad (6\text{-}2)$$

where the value of γ is dependent on the shape of the point spread function (PSF). Calculating an absolute concentration requires precise knowledge of the effective volume of excitation as well as model fitting to obtain a fitted $g(0)$ value. Dissociation of protein polymers will result in an increase in the number of particles manifesting itself as a decrease in the apparent $g(0)$ over time.

The characteristic diffusion time (τ_D) is the average time it takes for a fluorescent particle to diffuse through the excitation volume. The characteristic

diffusion time is obtained by fitting an autocorrelation curve to the following equation[164]

$$g(\tau) = \frac{g(0)}{1 + {}^{\tau}/_{\tau_D}} \tag{6-2}$$

where τ is the time of delay after an initial measurement, and $g(\tau)$ is the value of g at a particular value of τ. The characteristic diffusion time holds no physical meaning beyond a particular experimental setup because it depends on the excitation volume that is unique both to a particular instrument and an alignment that can vary from day to day. The diffusion coefficient can be calculated from the characteristic diffusion time provided the shape and dimensions of the excitation volume are known. A qualitative estimate of the characteristic diffusion time can be obtained by measuring the value of τ at which $g(\tau)$ is one half the value of $g(0)$. This value is referred to as the persistence time.[217] We use both the calculated diffusion coefficient and the persistence time to assess particle size.

Background autocorrelation signals

In addition to fluorescence signal from RLPFK-FITC, two background signals contributed to the autocorrelation curves. We refer to the three components as the fast correlating component, the protein diffusion component and the slow correlating component. The fast correlating component has a persistence time of 0.1ms or less. This signal was observed even in the absence of labeled protein and thus likely reflects buffer fluorescence and electronic noise. The relative

contribution of the fast correlating component was inversely depended on the concentration of labeled RLPFK. At high concentrations, the fluorescence intensity of RLPFK-FITC overpowered the intensity of fast diffusing contaminants and no fast correlating component could be detected. The slow correlating component had a characteristic diffusion time of approximately 50-100ms. The relative contribution of the slow correlating component varied between preparations of RLPFK-FITC. We suggest that the slow correlating component is due to insoluble particulates, most likely inactive protein aggregates. The protein diffusion component includes any signal with a characteristic diffusion time of 0.2ms-10ms and represents the range of oligomeric sizes expected.

The software used to fit autocorrelation curves could only fit with two components when using a Gaussian-Lorentzian model. One component had to be reserved for describing the diffusion properties of labeled RLPFK, so a decision had to be made to use the second component to describe the slow diffusing background component, fast diffusing background component or second oligomeric species of RLPFK-FITC. Every autocorrelation curve is fit using each of the three possible fits and the most appropriate fit is decided on based on minimization of χ^2, shape in the residuals and consideration of known properties of the system. For the sake of consistency, autocorrelation curves of a given experimental set are analyzed using the same model.

For the autocorrelation curves presented in this chapter, we found that most experiments demonstrated negligible contribution from the slow component (0.1%

fractional intensity) and no measurement demonstrated a contribution greater than 5%. Many experiments were well described with two diffusion components associated with RLPFK species (e.g. component 1 is a tetramer with a diffusion of 32μm^{2}s^{-1} and component 2 is a polymer with a diffusion coefficient of 12μm^{2}s^{-1}). However, these autocorrelation curves could be fit to a wide range of combinations of components with equivalent goodness of fits, none of which offered a demonstrable improvement over a single component fit. An undeniable presence of a fast diffusion component was seen in measurements taken of RLPFK-FITC at concentrations less than 5nM. Unless otherwise noted, the autocorrelation curves measured for this chapter were described using a two-diffuser model with one slow diffusion component and one protein diffusion component. When comparing measurements over a range of RLPFK-FITC concentrations, we included the fast component in all fits. When multiple oligomeric species of RLPFK-FITC is expected to exist, the protein diffusion component is taken to be the weighted average of each species of RLPFK-FITC.

Stability

Loss of activity in kinetic measurements indicate instability of the tetramer. Kinetic activity measurements were taken concurrently with FCS measurements to assess the stability of RLPFK. The PFK catalyzed conversion of Fru-6-P to Fru-1,6-BP was coupled to the oxidation of NADH, which resulted in a decrease in the absorbance at 340nm. The rate of decrease in A_{340} was monitored using a Beckman

Series 600 spectrophotometer. Assay conditions were chosen to promote maximum activity (pH=8.0, 50mM Tris-HCL, 100mM KCl, 20mM $(NH_4)_2SO_4$, 2mM DTT, 3mM $MgCl_2$, 1mM ATP, 1mM Fru-6-P). RLPFK was diluted into the cuvette so that the concentration during assays was 0.1µg/ml. Activity is reported as a percentage of the maximum activity measured independently of these experiments. The maximal activity of the RLPFK preparation used in this chapter was 80units/mg where 1 unit is equal to the production of 1 µmol of Fru-1,6- BP per min.

Oligomeric state

The Stokes-Einstein equation (equation 6-4) relates the diffusion coefficient (D) as a function of a particle's stokes radius.

$$D = \frac{kT}{6\pi\eta r} \qquad (6\text{-}3)$$

where k is the Boltzmann constant, T is the temperature in Kelvin and η is viscosity of the solvent. In the previous chapter we presented a diffusion coefficient of 32 $\mu m^2 sec^{-1}$ for the tetramer in water, corresponding to a Stokes radius of 70.9Å. We normalize the apparent size of experimental species to the size of the tetramer by dividing the diffusion coefficient of tetramer by the measured diffusion coefficient. This normalized diffusion coefficient $\left(\frac{D_{tet}}{D_{app}}\right)$ has a value greater than 1 when RLPFK is associated into species larger than a tetramer and smaller than 1 when species are dissociated to monomers or dimers.

A hypothetical $\frac{D_{tet}}{D_{app}}$ of 0.64 is calculated for a dimer using the stokes radius of 44Å reported by Pavelich and Hammes[212] and substantiated by Reinhart and Lardy[50]. A hypothetic $\frac{D_{tet}}{D_{app}}$ is proposed for a dimer of tetramers by invoking the cubed root dependence of the diffusion coefficient of a spherical particle on its molecular weight shown in equation 6-5.[220]

$$\frac{\mathrm{MW_a}}{\mathrm{MW_b}} = \left(\frac{\mathrm{D_a}}{\mathrm{D_b}}\right)^3 \qquad (6\text{-}4)$$

This likely overestimates the correct diffusion coefficient of a polymer because of the erroneous assumption that the polymer will be of spherical shape. However, the approximation should be close enough for the interest of this chapter. A value for "number of tetramers" is calculated by taking the cubed root of the normalized diffusion coefficient.

Results

Photo-bleaching complicates autocorrelation curves

In chapter 4 we presented data suggesting that 3.2mM Fru-6-P stabilizes polymers of RLPFK when the concentration of RLPFK is 116nM. Polymer stability was evident by a constant diffusion coefficient and concentration over 4 hours of measurements (Figure 4-8). We expand upon the previously reported data by including additional concentrations of RLPFK and Fru-6-P, however before discussing the new data we must address an apparent difference in the repeated

data. The diffusion coefficient of 116nM RLPFK in the presence of 3.2mM Fru-6-P is seen to decrease over time (Figure 6-1 top panel solid circles) instead of remaining constant as reported previously (Figure 4-8). A relatively small decrease in diffusion coefficient is seen in the presence of 3.2mM Fru-6-P but a substantial decrease is seen in the experiment with 1.6mM Fru-6-P (Figure 6-1 bottom panel solid circles). Should a decrease in diffusion coefficient be real, it would suggest some form of association was occurring. An association process is inconsistent with the increase in particle concentration observed (Figure 6-1 open squares). Dilution induced association of RLPFK is both illogical and contradicts most of the data.

To illustrate the implication of the time dependent decrease in diffusion coefficient, we interpret the diffusion coefficient in terms of number of tetramers per particle $\left(\frac{\#tet}{part}\right)$ according to equation 6-6

$$\frac{\#\text{tet}}{\text{part}} = \left(\frac{32}{\text{D}_{\text{app}}}\right)^3 \qquad (6\text{-}5)$$

where D_{app} is the measured diffusion coefficient and 32 is the diffusion coefficient of the tetramer. Even the minor decrease of diffusion coefficient measured for 116nM RLPFK in the presence of 3.2mM Fru-6-P suggests a 3-fold increase in the number of tetramers per particle (Figure 6-2). Instead of a decrease in particle concentration we see a slight increase in the total number of particles (Figure 6-2 insert). As stated previously, this is both illogical and inconsistent with other data.

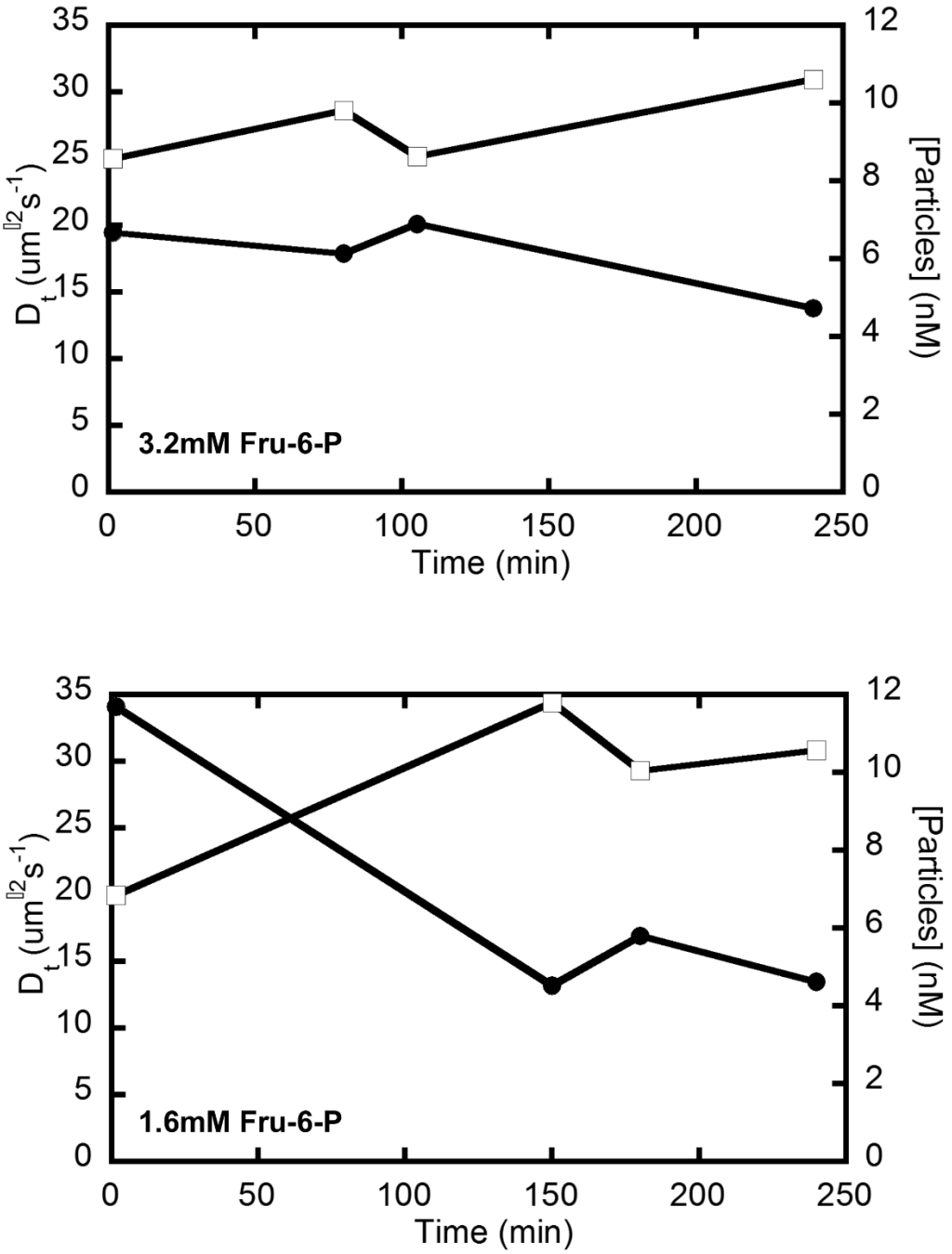

Figure 6-1: Change in diffusion coefficient (solid circles) and concentration (open squares) over time. 116nM RLPFK was diluted into buffer with either 3.2mM Fru-6-P (top panel) or 1.6mM Fru-6-P (bottom panel). FCS data was collected at several time points over a course of 4 hours. Values of diffusion coefficient and concentration are calculated from autocorrelation curves by fitting data to a single component model.

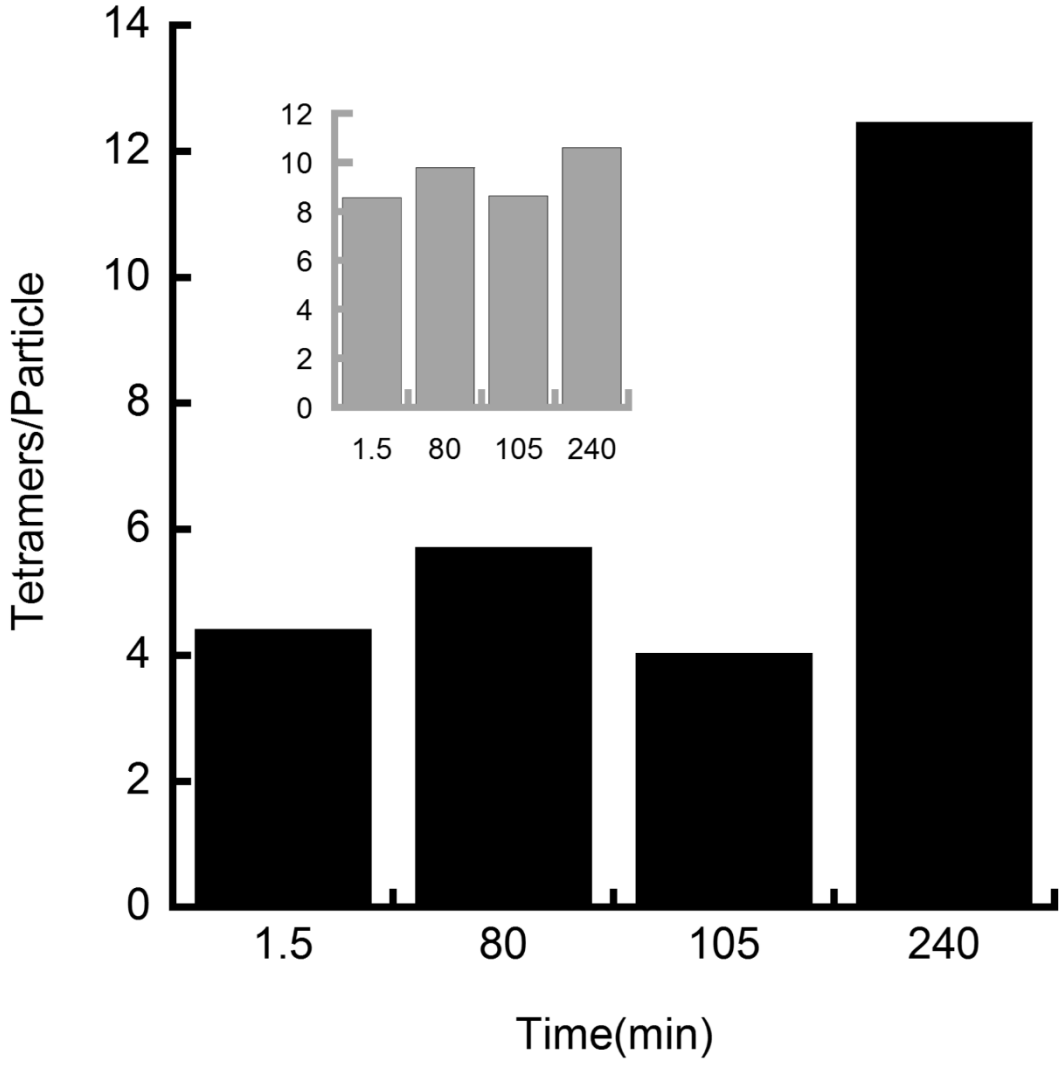

Figure 6-2: Number of RLPFK tetramers per polymer measured for 116nM RLPFK in the presence of 3.2mM Fru-6-P. The number of tetramers is calculated from the diffusion coefficient obtained from fitting FCS data. Insert displays the concentration of particles calculated from $\boldsymbol{g}(\mathbf{0})$. Data shows a time dependent increase in the apparent size of the particle but no time dependent decrease in particle concentration.

To understand the why the diffusion coefficient of 116nM RLPFK in the presence of 3.2mM Fru-6-P appears to decrease, we look at the shape of the autocorrelation curves and respective fits obtained at 1.5min (Figure 6-3 panel A) and 240min (Figure 6-3 Panel B) after dilution. The diffusion coefficient obtained from the fit is reported on the respective panel. The autocorrelation curve obtained after 1.5min fits "best" to a diffusion coefficient of 20$\mu m^2 s^{-1}$, however the fit clearly does not describe the data (Figure 6-3 Panel A). A significant improvement in the apparent fit is seen in the autocorrelation data obtained at 240min which fits best with a diffusion coefficient of 14 $\mu m^2 s^{-1}$. To determine which region of the autocorrelation curve changes from 1.5min to 240min, we normalized the data to their *g* value at τ=40μsec (Figure 6-3 Panel C). In Figure 6-3 panel C the first half of the two autocorrelation curves are nearly identical. The primary difference occurs at about 1msec where the 1.5min data goes to 0 much quicker than the 240min data. If the particles detected at 1.5min were diffusing faster than the particles detected at 240min, the difference in the autocorrelation curves should have been observed at the shorter τ values. Instead, the autocorrelation curve is retained at short τ values and then "kinks" at longer τ values.

The "kinking" that occurs at 1ms accounts for the poorer fit (relative to 240min data) as well as the surprisingly fast diffusion coefficient. As evident in Figure 6-3 panel D, the *g* values of τ ranging from 0.04-1msec is consistent with a diffusion coefficient of 10 $\mu m^2 s^{-1}$ and then decays much faster than would be

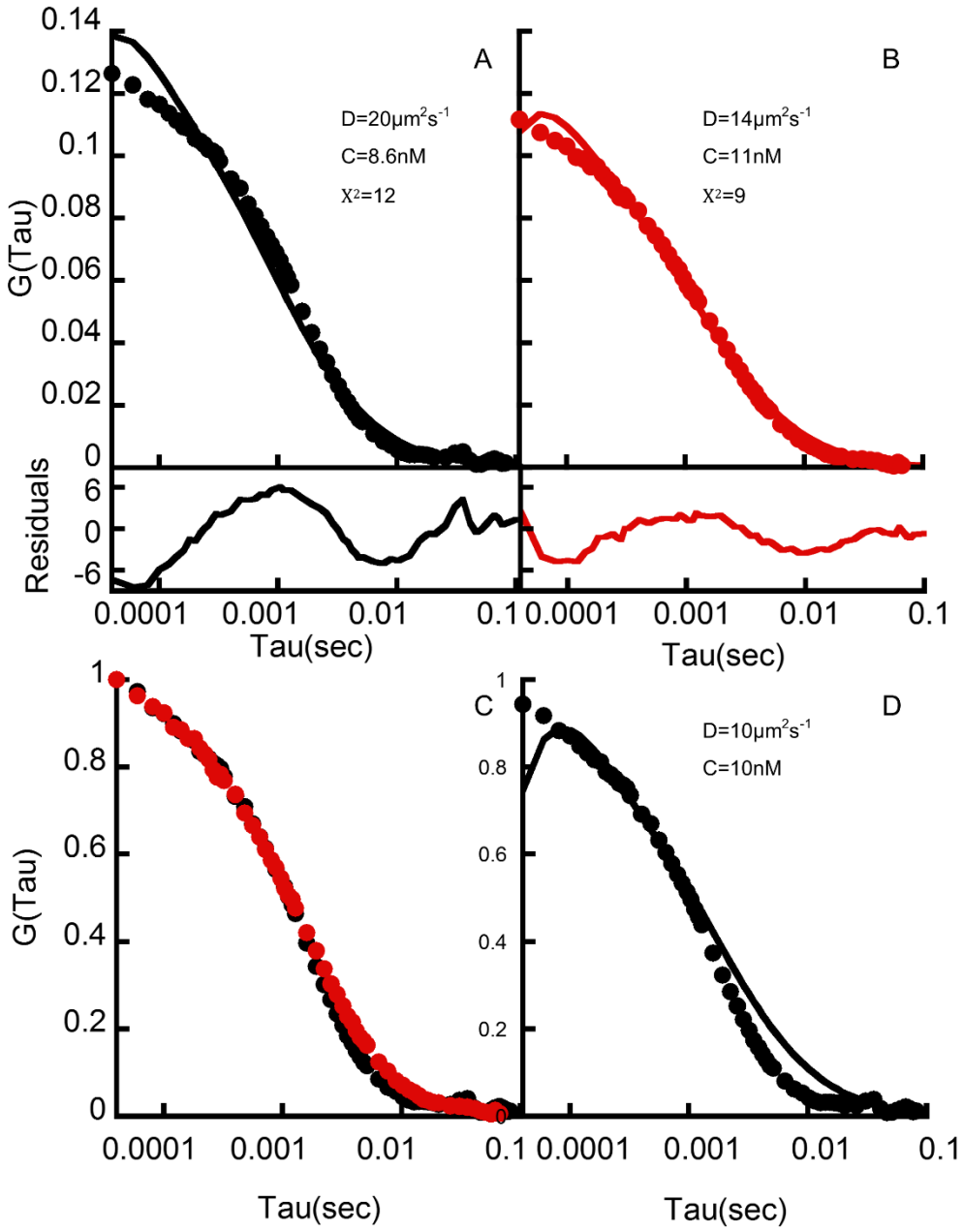

Figure 6-3: Autocorrelation curves obtained from 116nM RLPFK 1.5min (panel A), or 240min (panel B) after dilution into buffer containing 3.2mM Fru-6-P. The parameters obtained from the displayed fit are listed in the insert. In panel C the 1.5min (black) and 240min (red) autocorrelation curves are overlapped on top of each other. In panel D a simulated ACF representing a 10nM solution of particles with a diffusion coefficient of 10 $\mu m^2 s^{-1}$ is overlaid onto the 1.5min autocorrelation curve obtained from 116nM RLPFK in the presence of 3.2mM Fru-6-P.

expected. Attempts were made to fit the data with a two-component model in which one component diffused at 10 $\mu m^2 s^{-1}$ and the other was faster. Several different combinations of diffusion rates and contribution weights were used, however no combination of values sufficiently described the data (data not shown). Inclusion of a fast component could not describe the "kink" in the autocorrelation curve because a fast component would contribute to the autocorrelation curve at short τ values, not long τ values.[162]

Photobleaching could account for the "kink" in the autocorrelation curve. A particle photobleached while transiting the excitation volume would appear to diffuse normally until blinking out of existence, resulting in an otherwise normal autocorrelation curve that prematurely terminates. Modulating the intensity of the excitation laser would simultaneously prove the artifact to be from photobleaching and provide the method for eliminating it. Unfortunately, the possibility of photobleaching complicating the FCS measurements was not realized until after the experiments were performed. We propose that the slower diffusion seen at 240min is the result of less photobleaching. Photobleaching was most likely decreasing overtime because the particle is diffusing faster, and can escape the excitation volume before photobleaching occurs.

116nM RLPFK in the presence of Fru-6-P

In the previous chapter, we tracked MgATP induced dissociation of RLPFK polymers using the values of diffusion coefficient and concentration obtained by fitting FCS data to a two-component model. The intrinsic heterogeneity of the polymers stabilized by Fru-6-P, compounded by implication of photobleaching rendered diffusion models insufficient to describe the autocorrelation curve of RLPFK in many conditions in which Fru-6-P is present. In many cases the "best" fit clearly deviates from most of the data points (see Figure 6-3 for one example) leaving little doubt to the inaccuracy of the obtained parameters. In Figure 6-4 we plot the normalized diffusion coefficients from fitted FCS autocorrelation curves obtained from 116nM RLPFK diluted into buffer containing various concentrations of Fru-6-P. The diffusion coefficient is normalized to the tetramer by dividing the diffusion coefficient of the tetramer ($32\mu m^2s^{-1}$) by the measured diffusion coefficient. A value greater than 1 indicates species larger than a tetramer and a value smaller than 1 indicates species smaller. As a reference, side bars in Figure 6-4 indicate the expected diffusion coefficient of a monomer, dimer, tetramer and dimer of tetramers. In the presence of 3.2mM, 1.6mM, 0.8mM Fru-6-P, the size of the particles is seen to increase over time. We attribute the increase to a differential contribution of photobleaching. RLPFK in the presence of 0.4mM Fru-6-P is seen to maintain a diffusion coefficient approximately equal to that of the tetramer. After 110min, RLPFK in the presence of 0.2mM Fru-6-P was seen to dissociate from a polymer species to something slightly smaller than a tetramer.

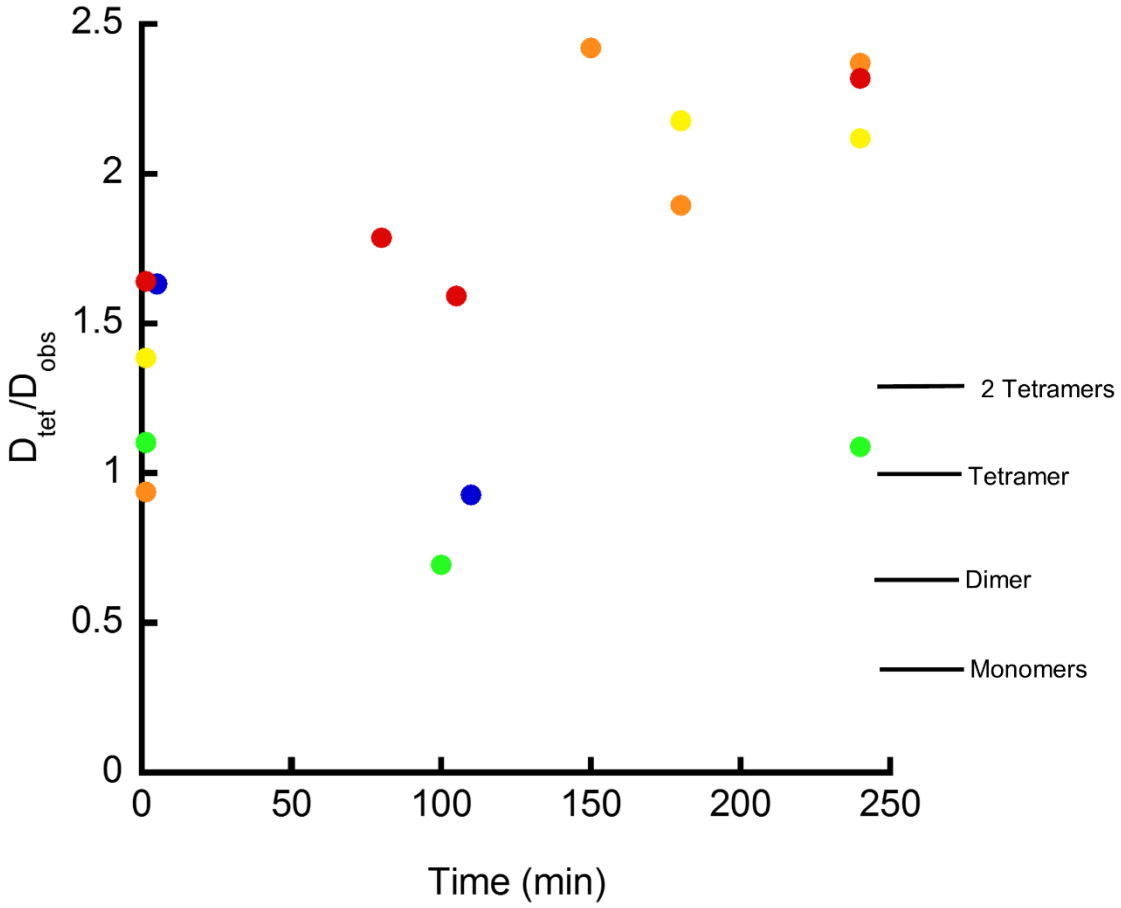

Figure 6-4: Normalized diffusion coefficients from fitted FCS autocorrelation curves obtained from 116nM RLPFK diluted into buffer containing either 3.2 (red), 1.6 (orange), 0.8 (yellow), 0.4 (green) or 0.2mM Fru-6-P (blue). Autocorrelation curves were fit using a two-component model with the second component fixed at 0.5 $\mu m^2 s^{-1}$.

Given the known inaccuracy of the fits used to describe these data, we attempt to use a qualitative description of the dilution induced change in particle size. In Figure 6-5 we present the autocorrelation curves obtained from 116nM RLPFK at various time points after dilution into buffer containing either 5mM, 3.2mM, 1.6mM, 0.8mM, 0.4mM, or 0.2mM Fru-6-P. For a given set of data, the concentration of Fru-6-P at which the experiments were performed is listed in the top right corner of the plot. The time after dilution is indicated by a shift in color of the data points. The color shifts from purple to red as time goes on. A change in value of g(0) is inversely proportional to a change in the number of particles.[164] Very little change in g(0) is seen in the presence of 5mM or 3.2mM Fru-6-P. At 1.6mM Fru-6-P and 0.8mM Fru-6-P a significant drop in g(0) is seen to occur, indicating an increase number of particles. An increase in the number of particles is indicative of a dissociation process. The extent of dissociation appears to increase at 0.4mM Fru-6-P and 0.2mM Fru-6-P.

At first glance, the decrease in g(0) seen in autocorrelation curves obtained in the presence of 1.6mM and 0.8mM Fru-6-P may imply that the polymers are less stable at these concentrations than at 3.2mM or 5mM Fru-6-P. However, it is interesting to note that the final g(0) values of the 1.6mM Fru-6-P and 0.8mM Fru-6-P plots are very similar to those of 5mM Fru-6-P and 3.2mM Fru-6-P. In fact, the autocorrelation curves of the 4-hour point in the presence of 5, 3.2, 1.6 and 0.8mM Fru-6-P are all very similar (Figure 6-6 top panel). The g(0) drops significantly at 0.4mM Fru-6-P and again at 0.2mM Fru-6-P. One can reasonably conclude from the

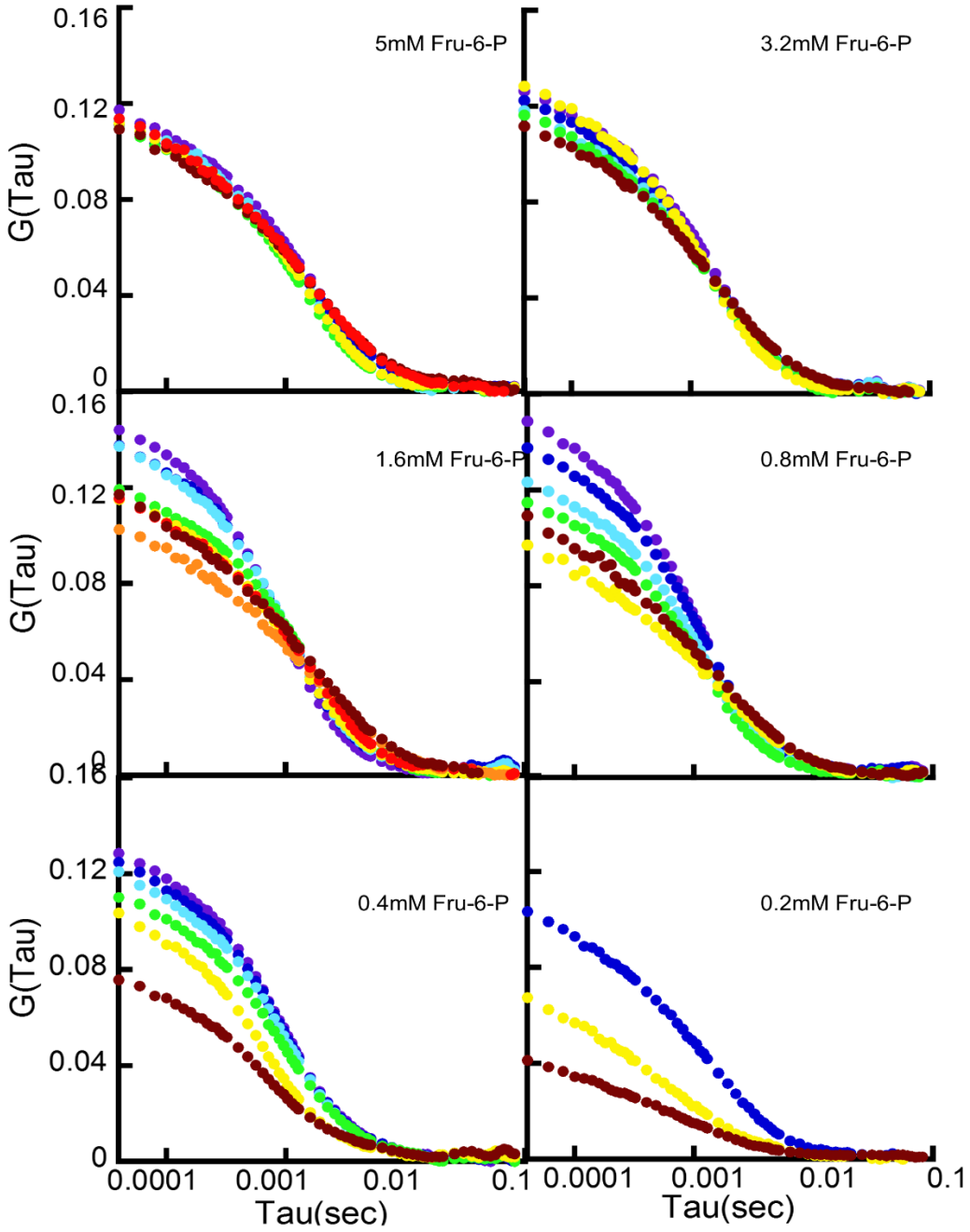

Figure 6-5: Autocorrelation curves of 116nM RLPFK measured at various time points after dilution into buffer with Fru-6-P. The concentration of Fru-6-P was either 5, 3.2, 1.6, 0.8, 0.4 or 0.2mM as indicated in the respective plot. The progress of time after dilution is indicated by a shift in color from purple to red. A time dependent decrease in the apparent value of g(0) indicates dissociation and a lateral shift in the autocorrelation curve indicates a change in the size of the particle.

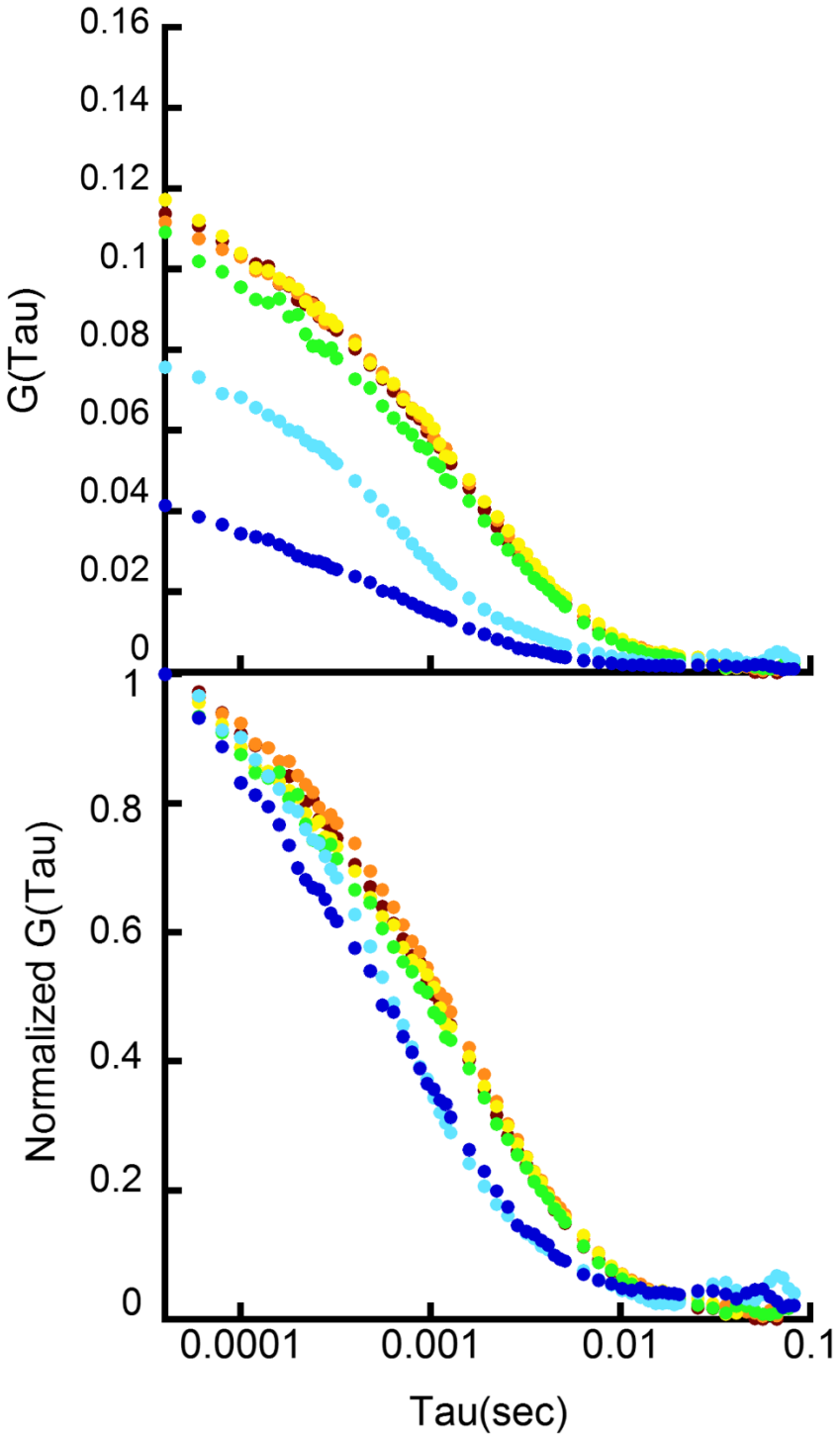

Figure 6-6: Four-hour time points of 116nM RLPFK diluted into buffer with various [Fru-6-P]. Top panel is not normalized, bottom panel is normalized to the g value at 0.04msec.

data that the RLPFK polymers are stable provided the Fru-6-P concentration is 0.8mM or above.

The prominent shift in g(0) of the autocorrelation curves presented in Figure 6-5 obfuscates any potential shift in the persistence time of the autocorrelation curves. The persistence time is the time it takes for the autocorrelation curve to decay to a value half the value of g(0) and is reflective of the characteristic diffusion time of the particle. Even without direct calculation, one can qualitative interpret a change in persistence time (and thus particle size) from an apparent lateral shift in the autocorrelation curve. To better visualize a potential lateral shift, we normalized the autocorrelation curves obtained from 116nM RLPFK in the presence of various concentration of Fru-6-P (Figure 6-7). As with Figure 6-5, the passage of time is represented by a shift in color from purple to red.

Autocorrelation curves obtained in the presence of Fru-6-P concentrations ranging from 0.8-5mM are characterized by an apparent increase in the persistence time (lateral shift to the right). The magnitude of the increase in persistence time was greatest for curves obtained in the presence of 1.6mM Fru-6-P. In each case, a decrease in "kinking" is observed along with the increase in the persistence time. We attribute the decreased "kicking" and consequential increase in the apparent persistence time to a decrease in photobleaching. A time dependent decrease in the persistence time (lateral shift to the left) was observed when the concentration of Fru-6-P was either 0.4mM or 0.2mM. A decrease in the persistence time could be interpreted as a reduction in particle size, likely due to dissociation.

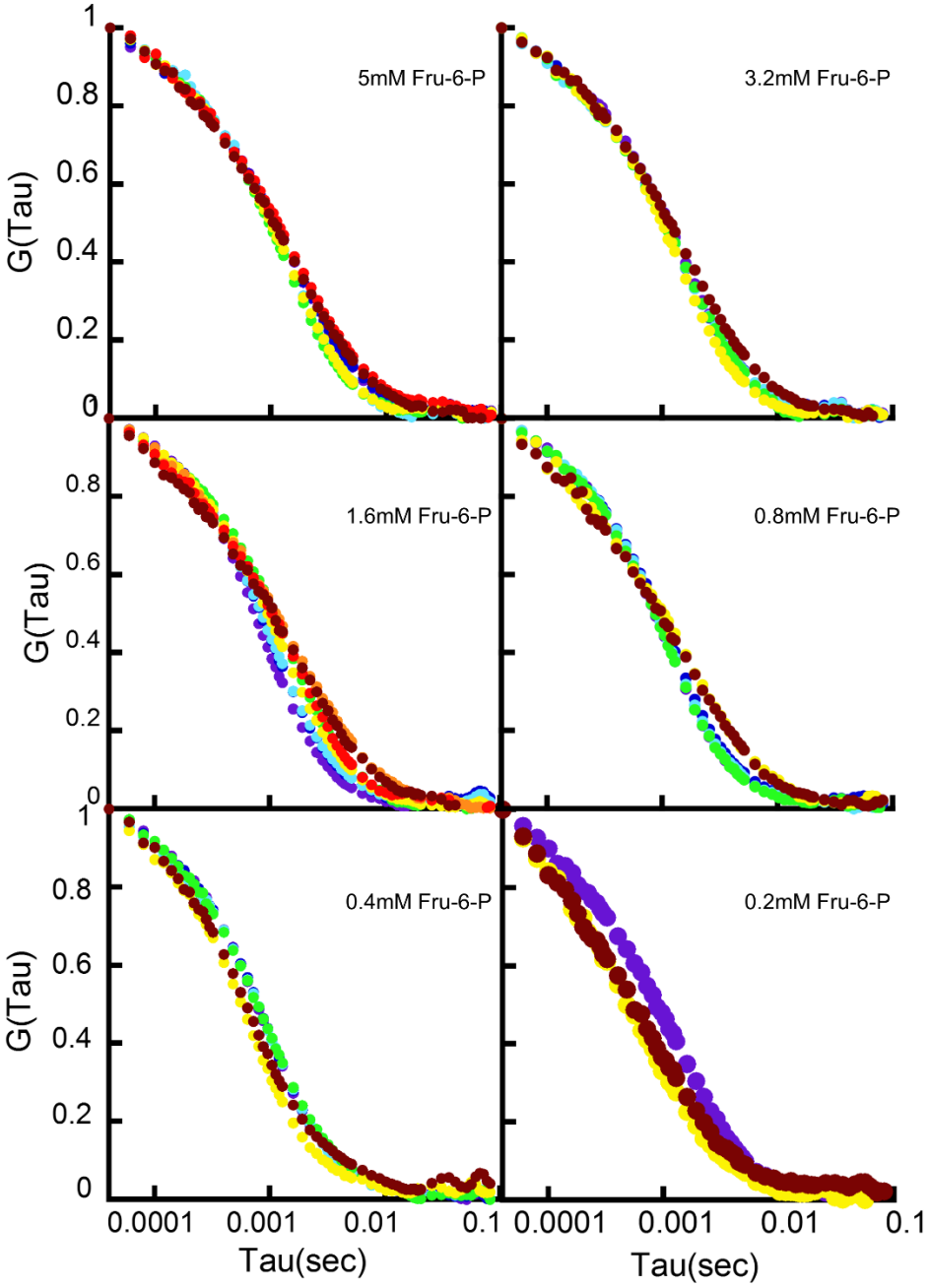

Figure 6-7: Normalized autocorrelation curves of 116nM RLPFK measured at various time points after dilution into buffer with Fru-6-P. The concentration of Fru-6-P was either 5, 3.2, 1.6, 0.8, 0.4 or 0.2mM as indicated in the respective plot. The progress of time after dilution is indicated by a shift in color from purple to red. Plots are normalized to the g value at 40µsec. A time dependent lateral shift in the autocorrelation curve indicates a change in the size of the particle.

The persistence time of the 240min autocorrelation curves decreases as a function of Fru-6-P. (Figure 6-6 bottom panel)

At a concentration of 116nM, RLPFK remained active for the entirety of the experiments provided the concentration of Fru-6-P was at least 0.4mM (Figure 6-8). If loss of activity occurred because of homogenous dissociation of the tetramer, the diffusion coefficient should decrease to a value below $32\mu m^2 s^{-1}$ (a normalized value less than one as presented in Figure 6-4). The normalized diffusion coefficient of 116nM RLPFK in the presence of both 0.4mM and 0.2mM Fru-6-P decrease to a value less than 1 at around 2 hours after dilution. However, the observed decrease in diffusion coefficient could be within the accuracy of the experiment considering 116nM RLPFK never lost activity in the presence of 0.4mM Fru-6-P and the normalized diffusion coefficient measured in these conditions increase back to 1 within 4 hours after dilution.

The data presented here is insufficient for rigorous conclusions. Our general impression is that at 116nM, RLPFK exist as stable polymers which do not change upon dilution provided the concentration of Fru-6-P is at least 0.8mM. At 0.4mM Fru-6-P and below the polymers begin to dissociate and the tetramers dissociate into dimers and monomers.

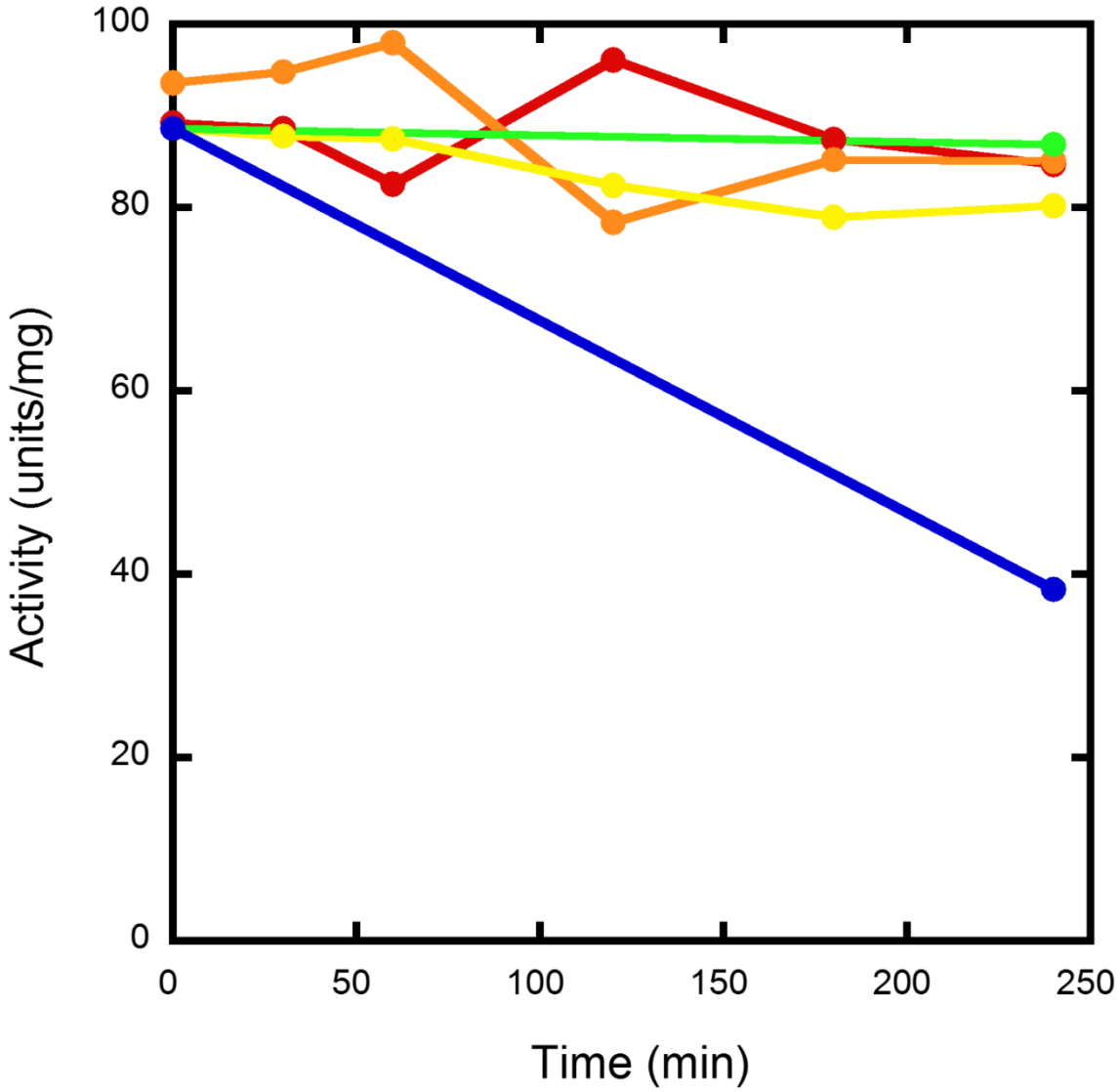

Figure 6-8: Stability of RLPFK after dilution to a concentration of 116nM in the presence of 3.2 (red), 1.6 (orange), 0.8 (yellow), 0.4 (green), and 0.2mM Fru-6-P (blue). Enzymatic activity is measured as described in material and methods.

58nM RLPFK in the presence of Fru-6-P

To determine the effect of RLPFK concentration on the stability of polymers we have performed the previously described experiment at several concentrations of RLPFK. Figure 6-9 displays the time dependent normalized diffusion coefficient of 58nM RLPFK in the presence of 3.2mM, 1.6mM, 0.8mM, 0.4mM, 0.2mM or 0.1mM Fru-6-P. It was not apparent from the autocorrelation curves if photobleaching was a problem in these data. Some autocorrelation curves seemed kinked (data not shown), but not in the dramatic fashion demonstrated for 116nM RLPFK.

Higher concentrations of Fru-6-P stabilized larger polymer species. Shortly after dilution, the normalized diffusion coefficient of 58nM RLPFK is 2, corresponding to a polymer of 8 tetramers, in the presence of all concentrations of Fru-6-P save 0.4mM Fru-6-P. In the presence of 3.2 or 1.6mM Fru-6-P, the polymer size of RLPFK was consistent for 4 hours. Variations during this time is thought to reflect the level of uncertainty in the measured diffusion coefficients. A decrease in the normalized diffusion coefficient was seen for 58nM RLPFK in the presence of 0.8-0.1mM Fru-6-P. The value obtained after 4 hours was very similar in all conditions. The rate of change appears to be very quick, except for 0.1mM Fru-6-P, the change seems to be complete within the first hour.

The stability of RLPFK is reported in Figure 6-10. Stability is reported as specific activity, measured as describe in the materials and methods. RLPFK was stable for 4 hours if the concentration of Fru-6-P was 0.8mM or higher. An increasing loss of activity was seen as the Fru-6-P concentration was decreased

from 0.4-0.1mM Fru-6-P. An observation of instability may seem to disagree with the observation that RLPFK had an average diffusion coefficient consistent with species larger than a tetramer at all concentrations of Fru-6-P (Figure 6-9). However, it is important to recognize that the diffusion coefficient and the activity report on the stability of different oligomeric forms of RLPFK. The diffusion coefficient measures the stability of the polymers, and the activity measures the stability of the tetramers. Collectively, Figure 6-9 and Figure 6-10 demonstrate that at a total RLPFK concentration of 58nM, the polymer form of RLPFK is stabilized by lower concentrations of Fru-6-P than the tetramer form.

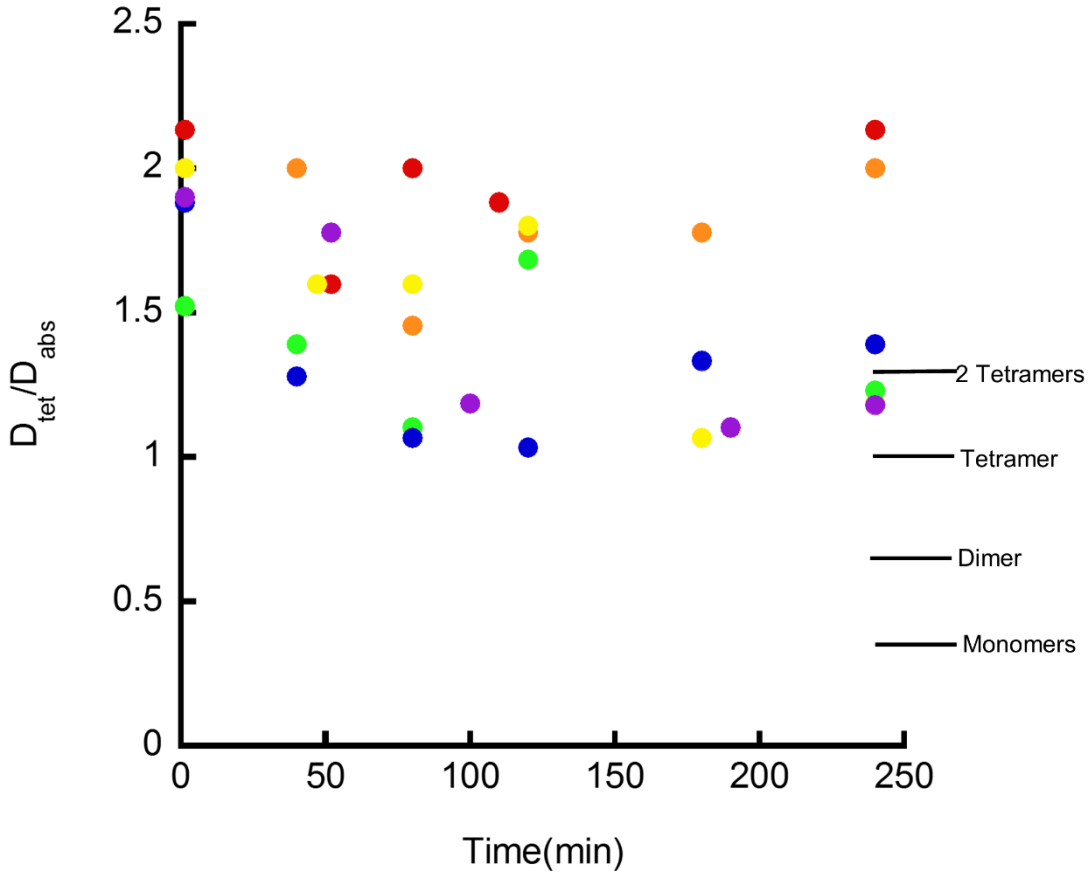

Figure 6-9: Normalized diffusion coefficients from fitted FCS autocorrelation curves obtained from 58nM RLPFK diluted into buffer containing either 3.2 (red), 1.6 (orange), 0.8 (green), 0.4 (yellow), 0.2mM (blue) or 0.1mM Fru-6-P (purple). Autocorrelation curves were fit using a two-component model with the second component fixed at 0.5 $\mu m^2 s^{-1}$.

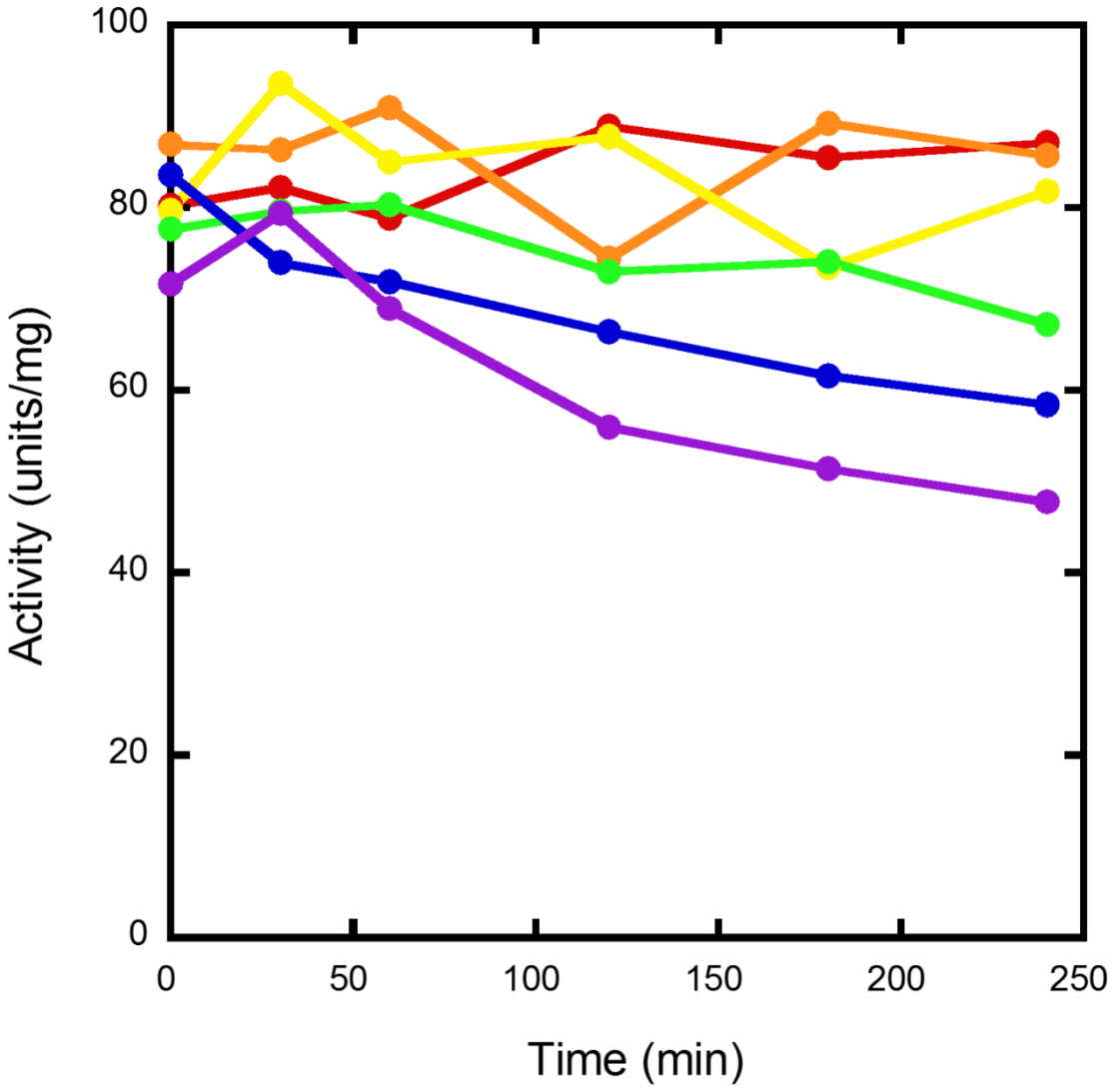

Figure 6-10: Stability of RLPFK after dilution to a concentration of 58nM in the presence of 3.2 (red), 1.6 (orange), 0.8 (yellow), 0.4 (green), 0.2 (blue) and 0.1mM Fru-6-P (purple). Enzymatic activity is measured as described in material and methods.

15nM RLPFK in the presence of Fru-6-P

The "kinked" feature observed in autocorrelation curves obtained from 116nM RLPFK was not observed in autocorrelation curves obtained from 15nM RLPFK (see Figure 6-11 for representative examples). The data obtained from 15nM RLPFK is described well using the two-component model system previously described (Figure 6-11). The primary error is from data obtained at very short τ values. A possible explanation for the discrepancy between the data and fit at short τ values is discussed below. Given the decent fit observed for these data we use the fitted diffusion coefficient as an indicator for change in particle size upon dilution of RLPFK to 15nM.

Figure 6-12 demonstrates the time dependent change in the normalized diffusion coefficient when RLPFK is diluted to 15nM in the presence of 3.2mM, 1.6mM, 0.8mM, 0.4mM, 0.2mM or 0.1mM Fru-6-P. In the presence of 3.2mM Fru-6-P or 1.6mM Fru-6-P the diffusion coefficient of 15nM RLPFK is not seen to change significantly over the course of the 4-hour experiment (note that the 1.6mM 4-hour data point in Figure 6-12 is equal to and hidden by the 3.2mM 4-hour data point). In the presence of 1.6mM or 3.2mM Fru-6-P the normalized diffusion coefficient was between a value of 1.75 and 2 correlating to a particle consisted of 5-8 tetramers. No significant change was observed over the course of the 4-hour experiment. Either no dissociation occurred relative to the particle size prior to dilution, or dissociation occurred to quickly to be detected.

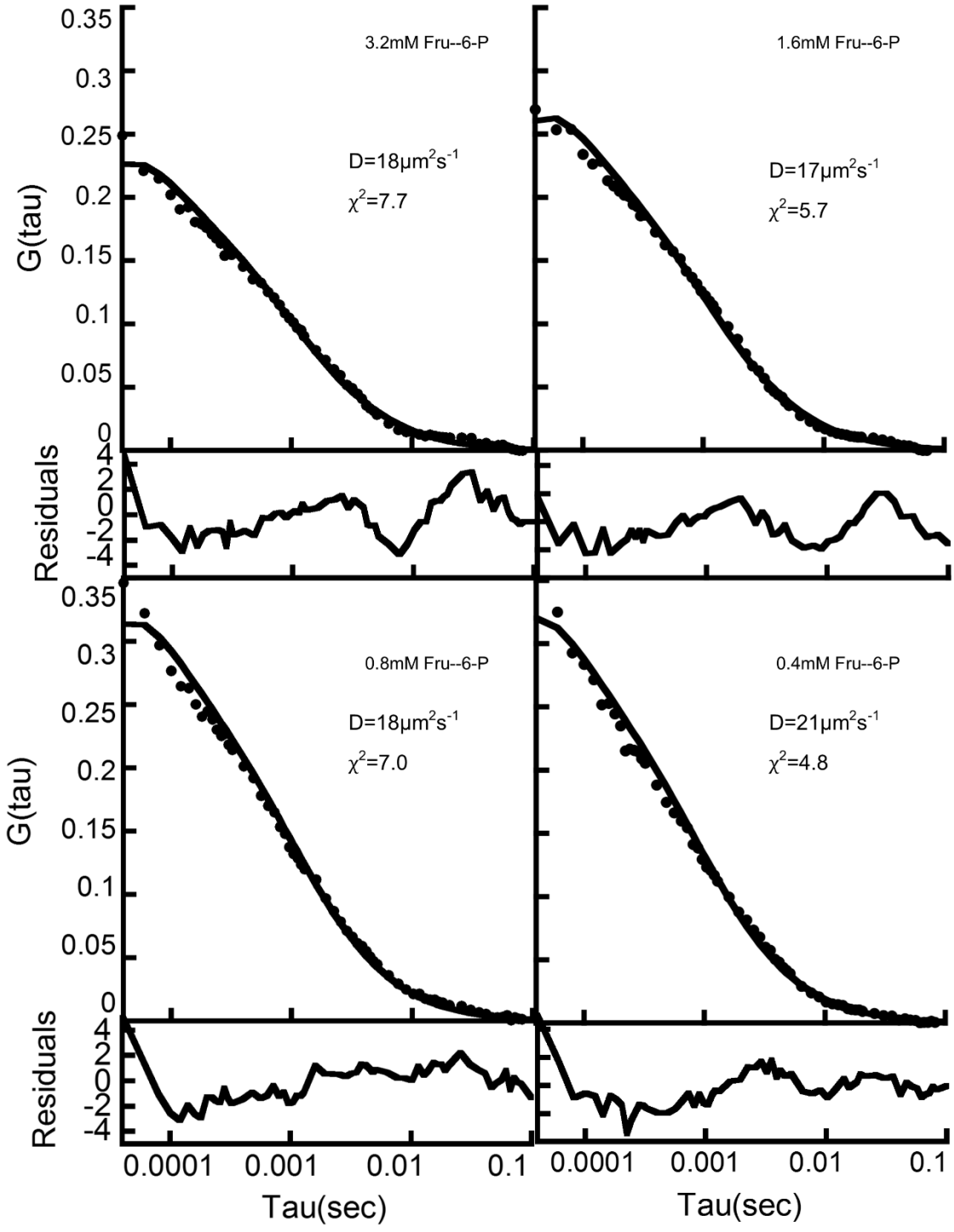

Figure 6-11: Autocorrelation curves generated from 15nM RLPFK 1.5min after dilution in the presence of various concentrations of Fru-6-P. Residuals presented below the respective plot was used to assess which parameter values provide the optimal description of the data.

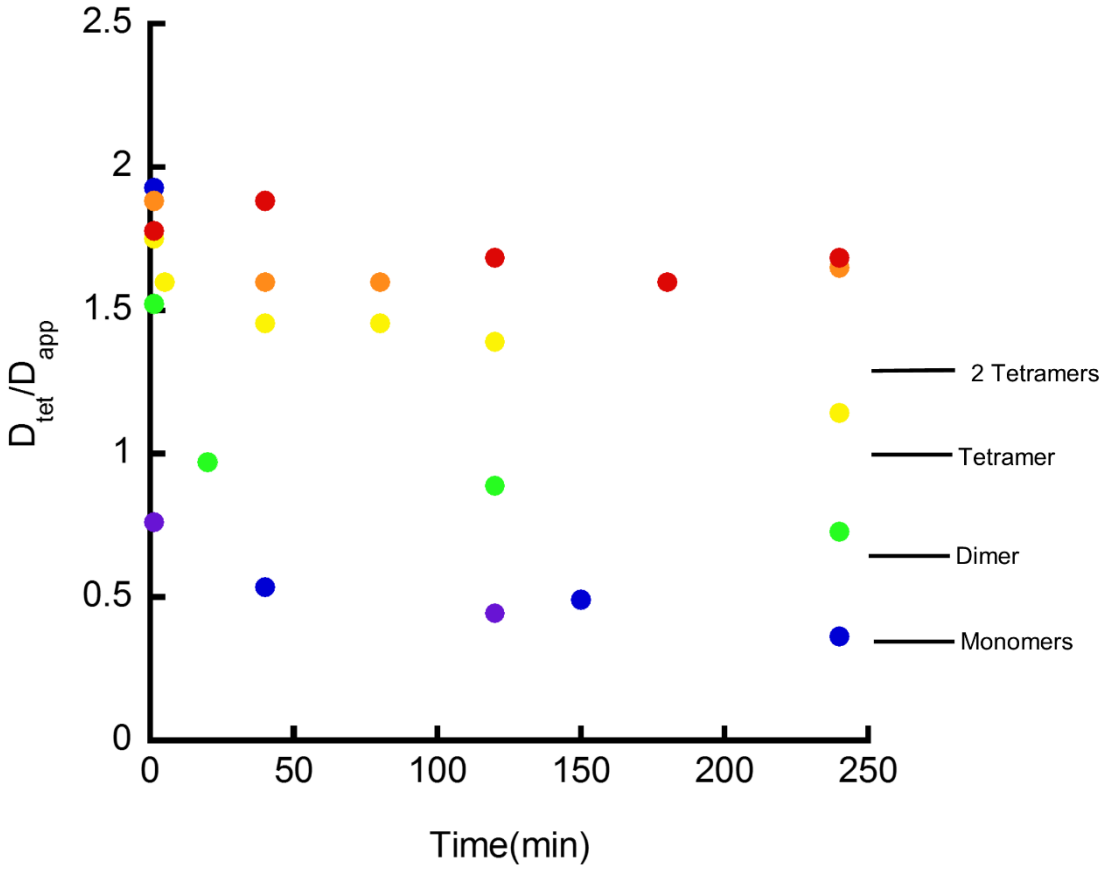

Figure 6-12: Normalized diffusion coefficients from fitted FCS autocorrelation curves obtained from 15nM RLPFK diluted into buffer containing either 3.2 (red), 1.6 (orange), 0.8 (green), 0.4 (yellow) 0.2 (blue) or 0.1mM Fru-6-P (purple). Autocorrelation curves were fit using a two-component model with the second component fixed at 0.5 $\mu m^2 s^{-1}$.

A systematic change in particle size was observed when 15nM RLPFK was in the presence of 0.8mM Fru-6-P. The initial value of the normalized diffusion coefficient ($1.5\mu m^2s^{-1}$) correlates to a trimer of tetramers ($1.5^3=3.4$)[220], approximately 2 times smaller than the size observed in the presence of 3.2mM or 1.6mM Fru-6-P. Over time, the normalized diffusion coefficient of 15nM RLPFK slowly decreased, ultimately correlating to an average particle size slightly larger than a tetramer. No plateau was observed in the change of diffusion coefficient of 15nM RLPFK in the presence of 0.8mM Fru-6-P. It is not certain, but it seems likely that a state of kinetic stability is not achieved after 4 hours and that the particles would likely continue to decrease to a smaller size.

An average particle size approximately equal to a dimer is achieved when 15nM RLPFK is in the presence of 0.4mM Fru-6-P. The initial size is only slightly smaller than that measured in the presence of 0.8mM. Within 40min RLPFK has dissociated to a particle size consistent with a tetramer. A steady process of dissociation is seen to continue for the remainder of the 4-hour experiment. At 4 hours, the average particle size of RLPFK in the presence of 0.4mM Fru-6-P is a monomer. A rapid dissociation to a particle size consistent with a monomer is observed when RLPFK is diluted to 15nM in the presence of 0.2mM or 0.1mM Fru-6-P. A glimpse of the polymer form is observed within 1.5min of dilution in the presence of 0.2mM Fru-6-P but not when only 0.1mM Fru-6-P is present. In either case, the resulting average particle size is approximately equal to a monomer.

Dissociation to a monomer in the presence of 0.2mM or 0.1mM Fru-6-P is supported by a concurrently observed loss of activity (Figure 6-13). Figure 6-13 demonstrates the stability of RLPFK is diluted to 15nM in the presence of 3.2mM, 1.6mM, 0.8mM, 0.4mM, 0.2mM or 0.1mM Fru-6-P. Stability is demonstrated by plotting the activity (reported as units/mg) as a function of time. The RLPFK used for experiments reported in this chapter had a maximal activity of 80units/mg in measurements preceding the FCS experiments. The activity of 15nM RLPFK remained around 80units/mg in the presence of 3.2mM or 1.6mM Fru-6-P. Progressive loss of activity was seen in the presence of 0.8mM Fru-6-P or 0.4mM Fru-6-P. Only 50% activity remained after 4 hours in the presence of 0.8mM Fru-6-P (Figure 6-13), slightly more activity remained in the presence of 0.8mM Fru-6-P than 0.4mM Fru-6-P.

It is surprising that 15nM RLPFK in the presence of 0.8mM Fru-6-P maintained a diffusion coefficient similar to the tetramer (Figure 6-12) as it lost almost 50% of its activity (Figure 6-13). Likewise, it is surprising that 15nM RLPFK in the presence of 0.4mM Fru-6-P only lost a little more than 50% of its activity despite having an average normalized diffusion coefficient well below that of a tetramer. If RLPFK existed as a homogenous solution of discrete species, the activity measurements should track exactly with the diffusion coefficient (i.e. when $D_\tau \geq 32\mu m^2 s^{-1}$ then activity=100%). However, we suggest that in the presence of Fru-6-P, RLPFK is not a homogenous solution of discrete species. In many conditions, RLPFK likely exist as mixture of active and inactive oligomeric

conformations. The diffusion coefficient reflects the abundance of large polymers and the activity reflects the abundance of inactive species. The data in Figure 6-12 and Figure 6-13 seems to suggest that 15nM RLPFK experience a similar rate of tetramer dissociation in the presence of 0.8mM or 0.4mM Fru-6-P, but the rate of polymer dissociation is faster in the presence of 0.4mM Fru-6-P.

The data presented above suggest that stability of polymers heavily depends on concentration of Fru-6-P when RLPFK is diluted to 15nM. Polymers are stable if Fru-6-P concentration is 1.6mM or 3.2mM but dissociate at 0.8mM and 0.4mM and disappear entirely at 0.2mM or 0.1mM. The tetramer is likely very unstable in these conditions as evident by the loss of activity observed when the apparent diffusion coefficient was close to a tetramer.

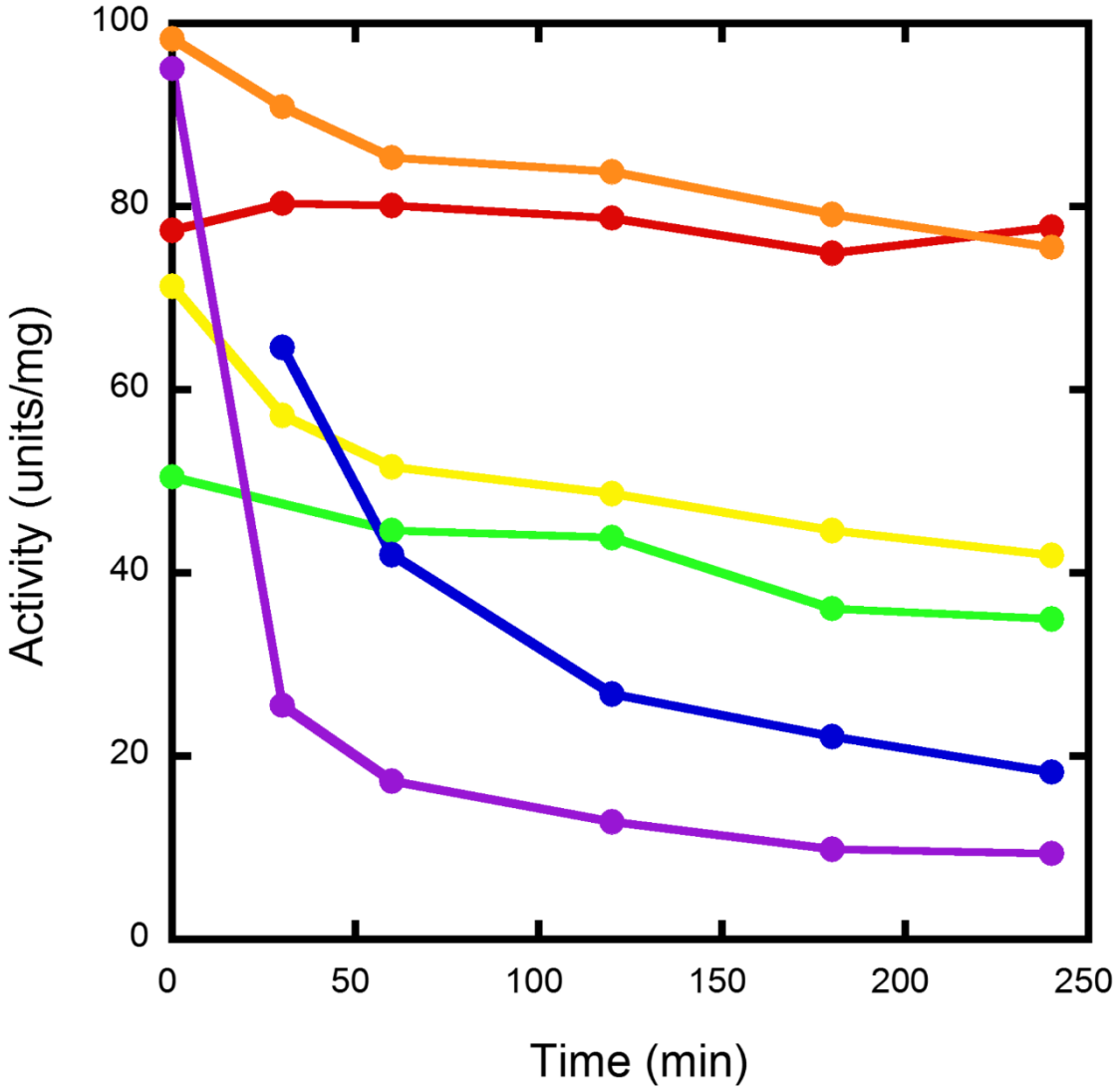

Figure 6-13: Stability of RLPFK after dilution to a concentration of 15nM in the presence of 3.2 (red), 1.6 (orange), 0.8 (yellow), 0.4 (green), 0.2 (blue) and 0.1mM Fru-6-P (purple). Enzymatic activity is measured as described in material and methods.

Experimental limit of RLPFK detection

One of the objectives of this study was to use FCS to measure the oligomeric state of RLPFK at concentrations ranging from 0.5nM to 100nM. Thus, spanning the concentrations used for kinetic assays and those relevant to physiological conditions. We have performed time dependent FCS of 5nM, 1.5nM and 0.5nM RLPFK in the presence of 0.1-3.2mM Fru-6-P. However, we feel that these data are compromised by buffer fluorescence.

Autocorrelation curves obtained from 116nM, 58nM, 15nM, 5nM, 1.5nM or 0.5nM RLPFK 1.5 minutes after dilution into the presence of 3.2mM Fru-6-P are plotted in Figure 6-14. These curves are normalized to the value of g at τ=0.04msec. The insert included with Figure 6-14 list the diffusion coefficients. Activity listed in the insert is the percent activity remaining after 4 hours in the given condition. As the concentration of RLPFK is decreased the autocorrelation curves shift to the left suggesting a decrease in the size of the particles. The fitted diffusion coefficient decreases from 45$\mu m^2 s^{-1}$ to 17$\mu m^2 s^{-1}$ as a function of RLPFK concentration, except for 116nM RLPFK whose diffusion coefficient is artificially raised because of photobleaching. A diffusion coefficient larger than 32$\mu m^2 s^{-1}$ would require dissociation of tetramer and should be correlated with a loss of activity. No activity loss is seen even after 4 hours (Figure 6-14 insert). An alternative explanation is necessary to explain the apparent rightward shift in the autocorrelation curves.

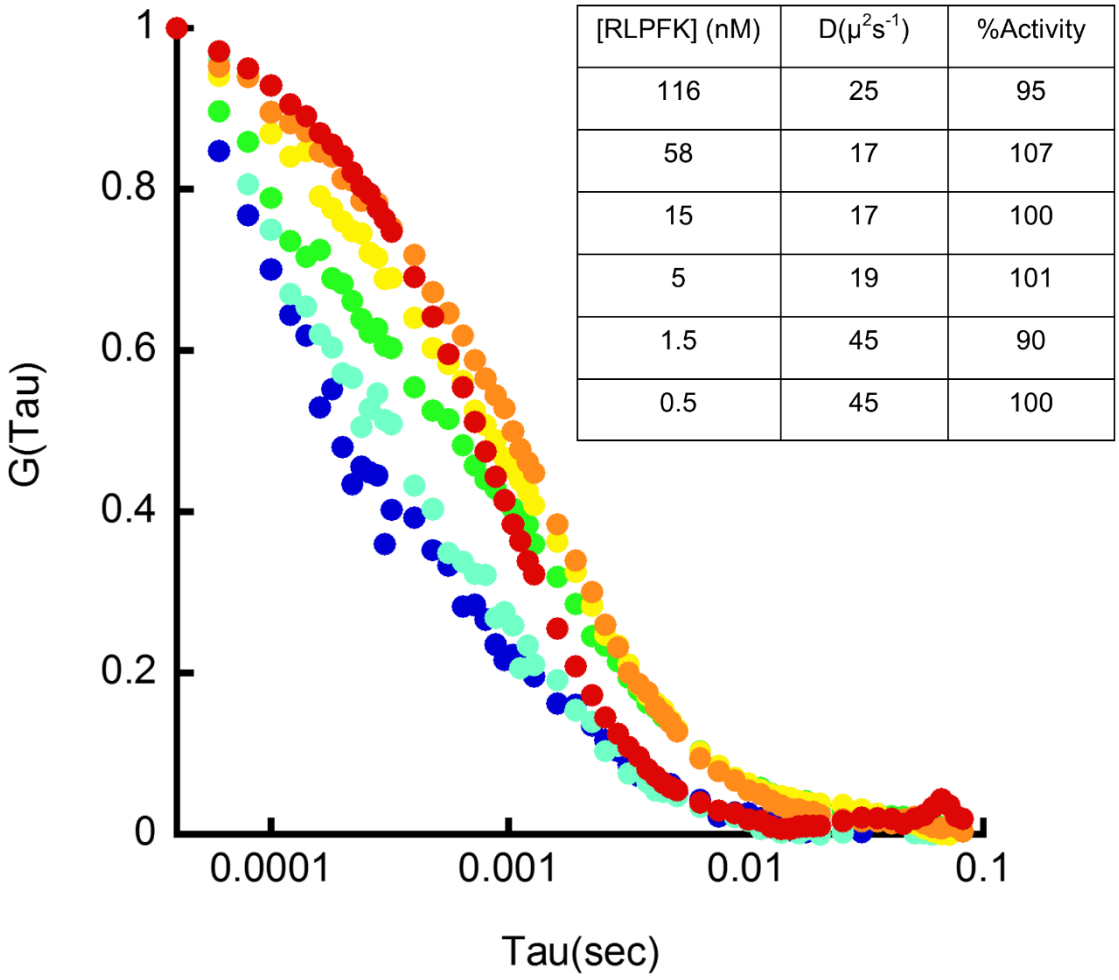

[RLPFK] (nM)	D($\mu^2 s^{-1}$)	%Activity
116	25	95
58	17	107
15	17	100
5	19	101
1.5	45	90
0.5	45	100

Figure 6-14: Autocorrelation curves normalized to the g value at τ=40μsec. RLPFK concentrations include 0.5nM (Blue), 1.5nM (turquoise), 5nM (green), 15nM (yellow), 58nM (orange) and 116nM (red). RLPFK is in the presence of 3.2mM Fru-6-P. Insert includes diffusion coefficients obtained by fitting the respective autocorrelation function as described in the text.

When the autocorrelation curves are normalized to the value 0.2msec instead of 0.04msec (Figure 6-15) it becomes visually apparent that the greatest difference between the curves is the region at short τ values which seems to flair as the concentration of RLPFK is decreased. A large change in the autocorrelation curve at short τ values implies that the primary change in the autocorrelation curves is not due to a change in the size of the polymers but from an increase contribution of the fast correlation component.

In the absence of fluorescent particles, the buffer used in these experiments is seen to have a correlated fluorescence signal (Figure 6-16). The autocorrelation curve obtained from buffer (50mM MOPS, 5mM $MgCl_2$, 0.1mM EDTA, 1.6mM Fru-6-P, 5mM DTT and 0.1mg/ml BSA) was best fit to a diffusion coefficient of 360$\mu m^2 s^{-1}$. The intensity of buffer fluorescence is relatively high, 1964cps compared to 2052cps and 2047cps for 0.5nM and 1.5nM RLPFK respectively. Given the high relative intensity of the buffer, it is reasonable to believe that it is greatly contributing to the autocorrelation curves when measured at low RLPFK concentration.

We have fit the autocorrelation curve obtained from 0.5nM RLPFK 1.5min in the presence of 3.2mM Fru-6-P with a two-component model in which one component is fixed at 360$\mu m^2 s^{-1}$ to account for background buffer fluorescence (Figure 6-17 Panel B). Fitting to a two-component model provides a significant improvement over fitting to a single component (Figure 6-17 Panel A) as judge by a reduction of χ^2 and by reduced shape in the residuals. The best fit was achieved

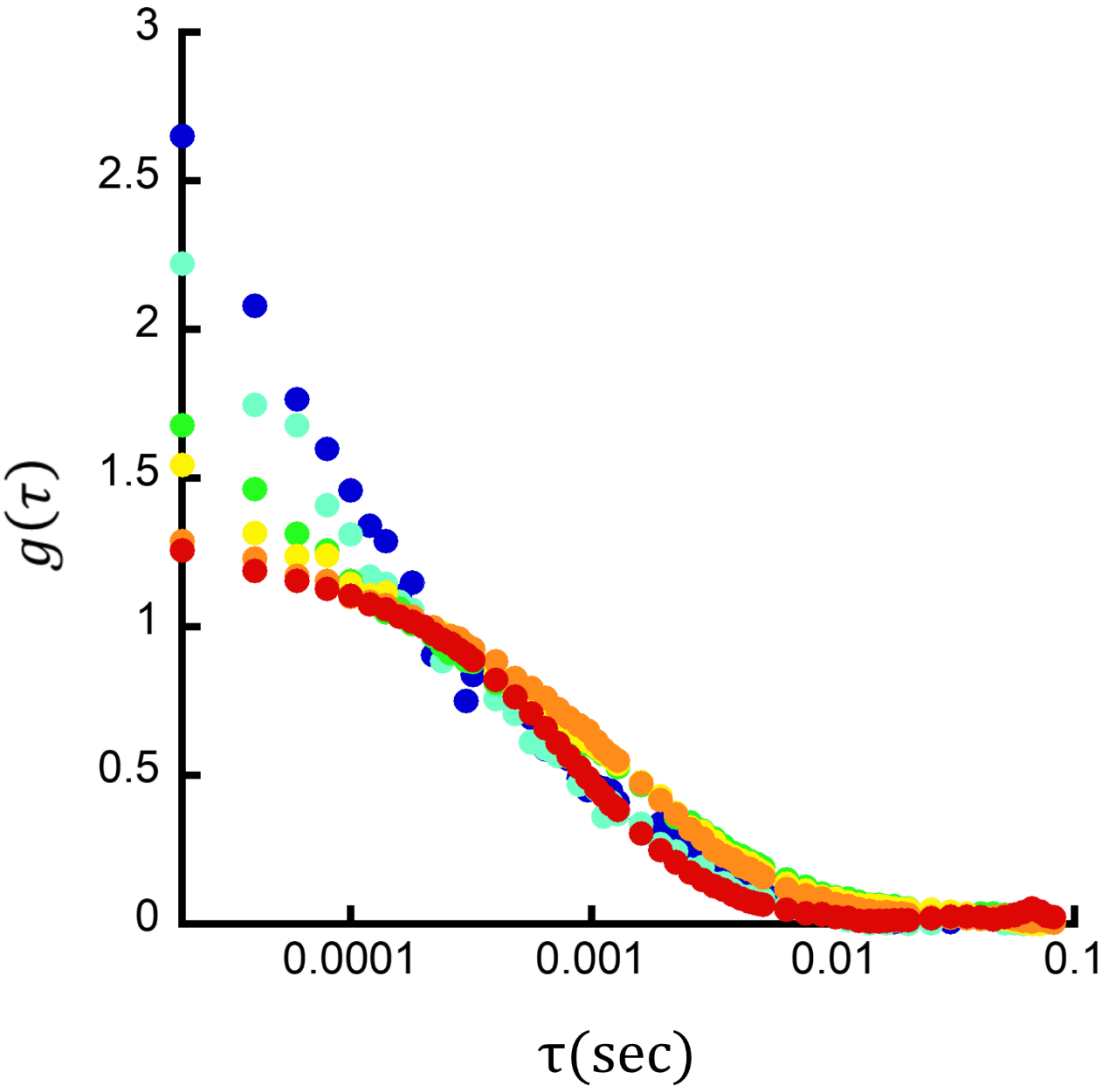

Figure 6-15: Autocorrelation curves normalized to the g value at τ=2msec. RLPFK concentrations include 0.5nM (Blue), 1.5nM (turquoise), 5nM (green), 15nM (yellow), 58nM (orange) and 116nM (red). RLPFK is in the presence of 3.2mM Fru-6-P.

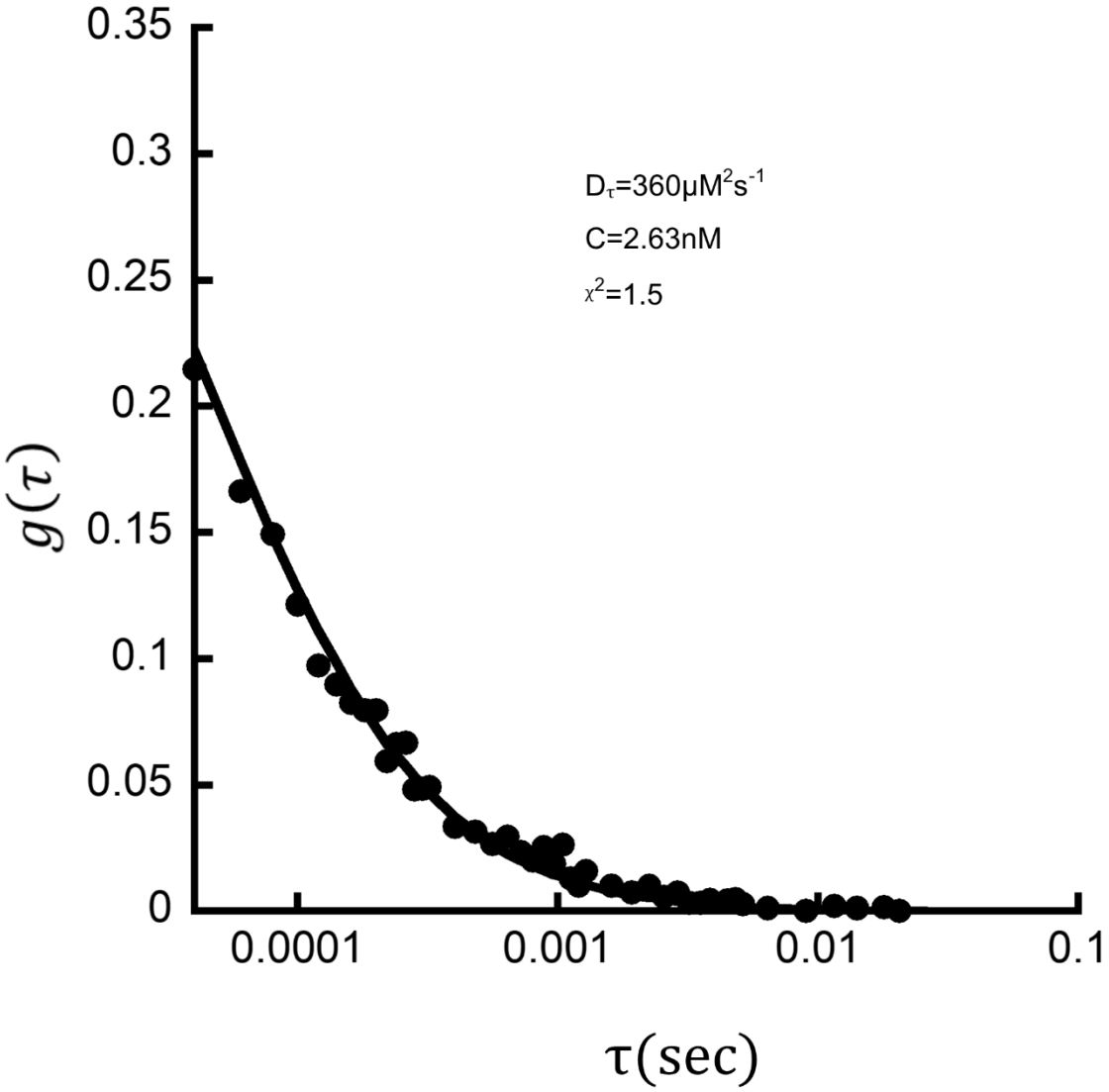

Figure 6-16: Autocorrelation curve of the buffer used in FCS experiments. Buffer contains 50mM MOPS, 5mM $MgCl_2$, 0.1mM EDTA, 1.6mM Fru-6-P, 5mM DTT and 0.1mg/ml BSA. Resulting autocorrelation curve fits well to a diffusion coefficient of 360$\mu m^2 s^{-1}$. Insert list fitted concentration, diffusion coefficient and χ^2 value.

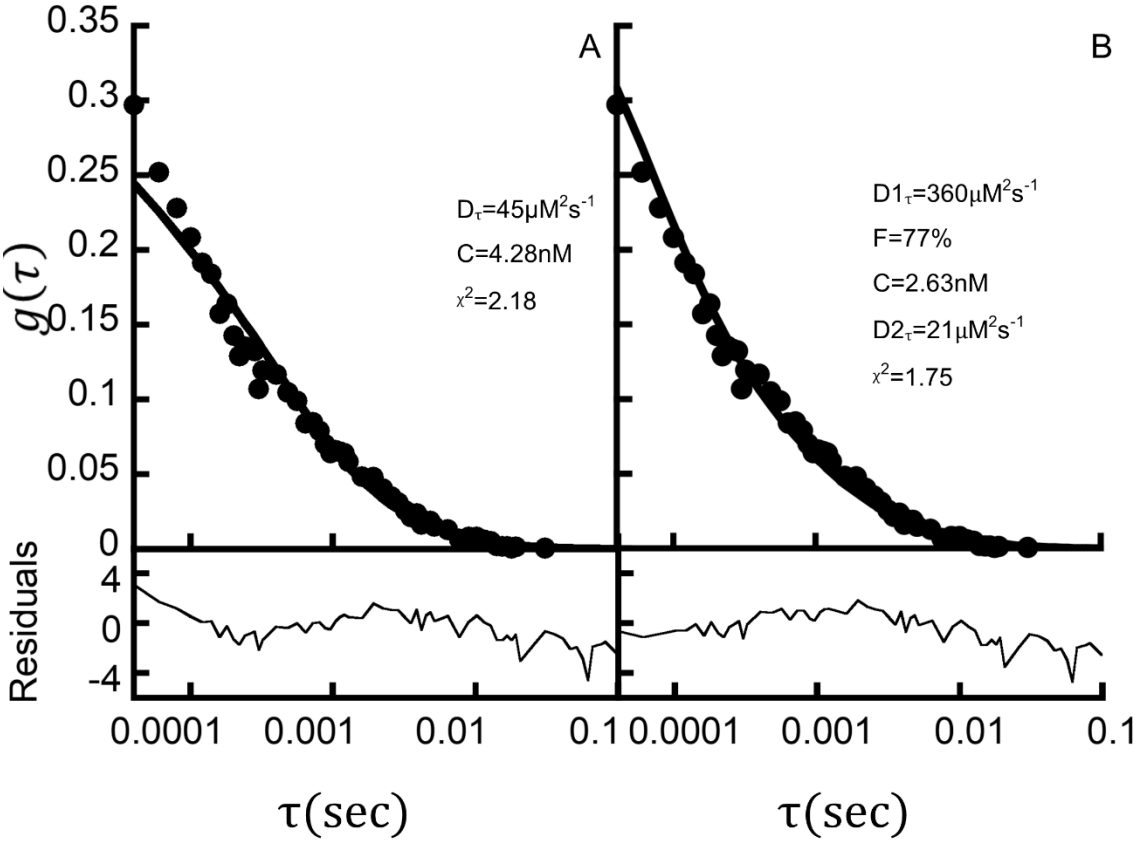

Figure 6-17: Autocorrelation curve resulting from FCS measurement of 0.5nM RLPFK in the presence of 3.2mM Fru-6-P. Autocorrelation curve was fit using a Gaussian-Lorentzian model (see text) assuming either a single component (A) or two components (B). The insert in each graph contains fitted parameters. The additional component (labeled $D1_\tau$) had a fixed diffusion coefficient of 360 $\mu m^2 s^{-1}$ and is taken to represent the contribution of buffer to the autocorrelation curve. Residuals are plotted below their respective plot.

when buffer component contributed 77% of the fluorescence signal and the diffusion coefficient of RLPFK was 21$\mu m^2 s^{-1}$.

We applied the 2-component fit to each the autocorrelation curves displayed in Figure 6-14 and reported the diffusion coefficients that provided the best fit in Figure 6-18. In Figure 6-18 the diffusion coefficient obtained by fitting to a single component model is represented by open circles and the diffusion coefficient obtained by fitting to a two-component model is represented by closed squares. (See Table 6-1 for fitted values) We see that both models provide the same diffusion coefficient at RLPFK concentrations of 116nM, 58nM or 15nM, and that a single component model yields a much larger diffusion coefficient when the concentration of RLPFK is 5nM or less. Additionally, we see that once the contribution of buffer is accounted for, the diffusion coefficient measured shortly after dilution changes very little as a function of RLPFK concentration.

While very little RLPFK concentration dependence is seen for the diffusion coefficient measured shortly after dilution, a large concentration dependence is seen 4 hours after dilution. Figure 6-19 reports the normalized diffusion coefficient of RLPFK at 1.5 and 240min after dilution in the presence of 3.2mM Fru-6-P. At a RLPFK concentration of 5nM or below, we measured a normalized diffusion coefficient of 1 indicating RLPFK has dissociated into a tetramer. Supporting the assertion that RLPFK is a tetramer at subnanomolar concentrations used for kinetic assays.

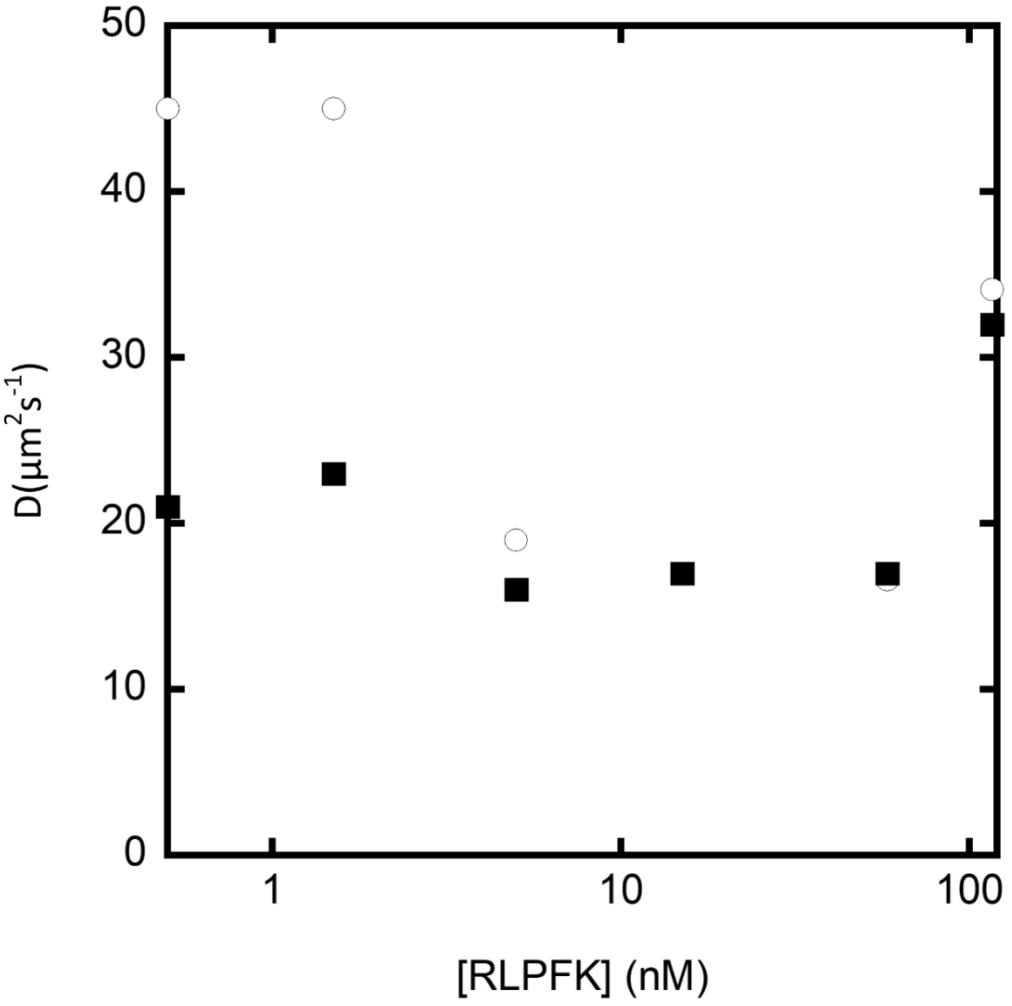

Figure 6-18: Diffusion coefficients obtain by fitting autocorrelation curves to a model that either ignores (open circle) or addresses (closed squares) contribution of buffer.

Table 6-1: Parameters obtain by fitting autocorrelation curves to a model in which a background component is addressed as either a fast correlating component, or a slow correlating component. The super column labeled "1st component slow" represents data obtained by a fit that is fit as described in the text. The super column labeled "1st component fast" represent data obtained by a fit that incorporates a fast correlation component, but not a slow correlation component. Data obtained from RLPFK 1.5minutes after dilution buffer with 3.2mM Fru-6-P. $D(\mu m^2 s^{-1})$ is the fitted diffusion coefficient for the protein component. $F_1(\%)$ is the fractional contribution of background component.

	1st Component Slow				1st Component Fast			
[RLPFK] (nM)	$F_1(\%)$	$D(\mu m^2 s^{-1})$	C(nM)	X^2	$F_1(\%)$	$D(\mu m^2 s^{-1})$	C(nM)	X^2
0.5	0	45	5.4	2	77	21	2.3	1.7
1.5	0	45	3.7	2.5	73	23	1.7	3.2
5	2.5	19	3.9	2.4	14	16	2.8	1.2
15	0	17	4.4	7.9	56	17	6.3	1
58	1	17	8.1	6.3	24	17	4.9	9.7
116	0	34	6.9	29	0.1	32	6.7	28

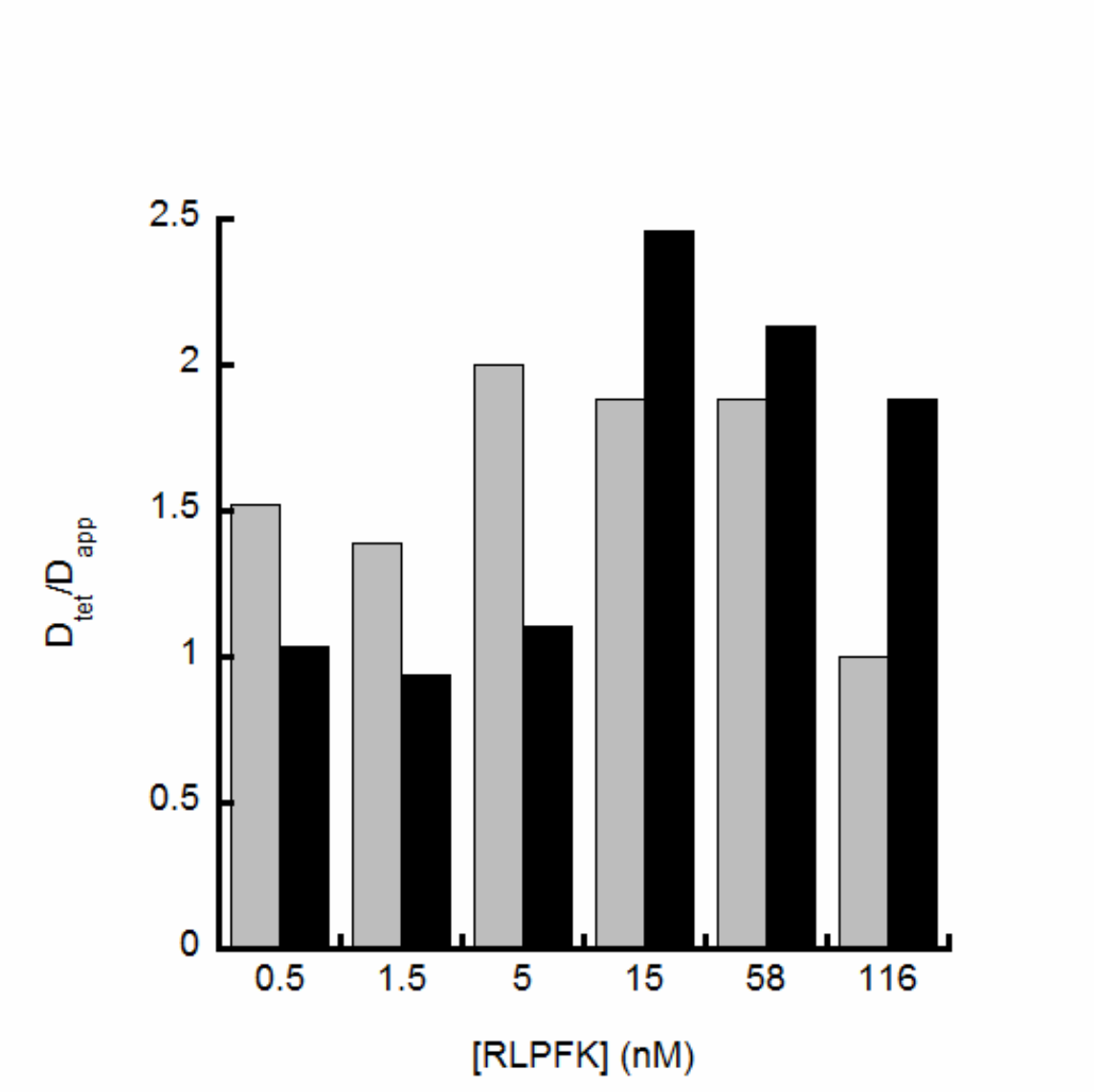

Figure 6-19: Normalized diffusion coefficient of RLPFK measured at 1.5min and 240min after dilution in the presence of 3.2mM Fru-6-P. Autocorrelation curves were fit to a two-component model with one component set to 360$\mu m^2 s^{-1}$.

Discussion

The autocorrelation curves were complicated by experimental artifacts such as, background buffer fluorescence (Figure 6-17), insoluble particulates and possibly photobleaching (Figure 6-3). We made no attempts to model in photobleaching but merely use it to explain anomalously high diffusion coefficients. Autocorrelation curves were fit with two components but only one component described the diffusion properties of RLPFK; the other component was used to account for either a fast correlation signal or a slow correlation signal. Software limitations prevented attempts to fit the data with more than two components. Selectively accounting for experimental artifacts on an individual basis threatens to complicate data interpretation by introducing bias. To avoid bias we attempted to fit our data as uniformly as possible. The slow correlation component, attributed to insoluble protein, appeared to be the most uniformly present across experimental conditions and therefore consideration was given to it in all experiments. The slow correlation component was uniformly present in that no systematic trend to its contribution was observed, however many experiments had no slow correlation component at all. In cases with negligible contribution from the slow correlation component, the two-component model essentially became a single component model as the fractional contribution from the slow component was zero.

In experiments performed at RLPFK concentrations above 15nM, signal from labeled protein overwhelms any background signal and the fast correlation

component could be justifiably ignored. When the concentration of RLPFK is 5-0.5nM the background component must be accounted for. For measurements with background fluorescence, a two-component model was used with one component accounting for the fast correlation signal. The fast correlation signal was given a diffusion coefficient determine by measuring an autocorrelation curve of buffer with no added fluorophores. For comparison of high and low RLPFK concentrations, diffusion coefficients were obtained using a component for the buffer.

The autocorrelation curve obtained for highly associated RLPFK (high concentration of RLPFK and/or Fru-6-P) was not well described by a single component indicating that polymerized RLPFK is not a discrete species. The assertion that PFK does not polymerize to a uniform population of discrete species was strongly supported by electron microscopy images obtained from this lab (chapter 4) as well as others[103]. We attempted to use a two-component model to describe the solution as a mixture of two species including a mixture of polymers and tetramers/dimers or monomers, and mixture of large polymers and smaller polymers. No attempted combination of diffusion coefficients improved the fit as assessed by the value of χ^2 and by the shape in the residuals. The degree of heterogeneity is too great to be improved by one additional component.

Our data does not demonstrate the formation of indefinitely large polymers. The apparent diffusion coefficient of RLPFK in the presence of 3.2mM Fru-6-P is approximately 16$\mu m^2 s^{-1}$ when the concentration of RLPFK is 15, 58 or 116nM

(Figure 6-4, Figure 6-9 and Figure 6-12). We do see a shift to larger species when comparing 15nM RLPFK (Figure 6-12) to 58nM RLPFK (Figure 6-9), consistent with RLPFK concentration dependent increase in particle size observed by Reinhart and Lardy[50]. The appearance of even larger species at 116nM RLPFK may be obscured by preferential photobleaching of the slowest diffusing species. Additionally, the error of fit increases (higher χ^2 and greater residual shape) with increasing RLPFK concentration, likely due to increased heterogeneity resulting from solution that has a few, very large polymers in a pool of moderately sized polymers. Our data is insufficient to assess the potential size RLPFK polymers can form.

When the concentration of RLPFK is reduced to 5nM or less the apparent diffusion coefficient is consistent with a tetramer, supporting the assertion that RLPFK is a tetramer in kinetic assays. Shortly after dilution in the presence of 3.2mM Fru-6-P, RLPFK maintains a polymerized state at all concentrations, but over time dissociates to a tetramer (Figure 6-19). The residual presence of the polymers could account for the hysteretic behavior of kinetic assays.[49-51] Shortly after addition of RLPFK, kinetic assays display a burst rate that dissipates into a slower rate over the course of several minutes. The time scale of dilution induced dissociation of polymers corresponds to the persistence time of the burst rate.

Loss of activity is seen in all conditions in which the diffusion coefficient suggest a predominance of tetramers (Figure 6-20) supporting the conclusion made by Reinhart and Lardy that Fru-6-P only poorly stabilizes the tetramer form of RLPFK[49, 50]. From kinetic assays, we reported the dissociation constant of Fru-6-P

to be approximately 2mM (chapter 2). If this dissociation constant uniformly applies to all oligomeric forms of RLPFK then we should see a loss of activity at any concentration less than 2mM. Indeed, we see loss of activity in the presence of 1.6mM Fru-6-P (Figure 6-20), but only at RLPFK concentrations low enough for the tetramer to be the predominant form. At 116nM RLPFK, full stability is seen with Fru-6-P concentrations as low as 0.4mM; 5-fold less than the dissociation constant.

Comparison of the normalized diffusion coefficient measured when the RLPFK concentration ranged from 15-116nM (Figure 6-4, Figure 6-9 and Figure 6-12) demonstrate that the concentration of Fru-6-P required to stabilize polymers of RLPFK depends on the concentration of RLPFK. Polymers were stabilized by 3.2 and 1.6mM Fru-6-P (red and orange respectively) at 15-116nM RLPFK. In the presence of 0.2 and 0.1mM Fru-6-P (blue and purple respectively) polymers were not stabilized at any concentration of RLPFK. At a concentration of 0.8mM Fru-6-P (yellow), RLPFK is highly polymerized at 116nM, a dimer of tetramers at 58nM and a tetramer at 15nM. When the concentration of Fru-6-P is 0.4mM (green), RLPFK is larger than a tetramer at 116nM and 58nM but a dimer at 15nM.

The paradigm we use to explain the described data is one in which polymerization increases the affinity of RLPFK for Fru-6-P, and Fru-6-P reciprocally promotes polymerization.[36, 49, 98]

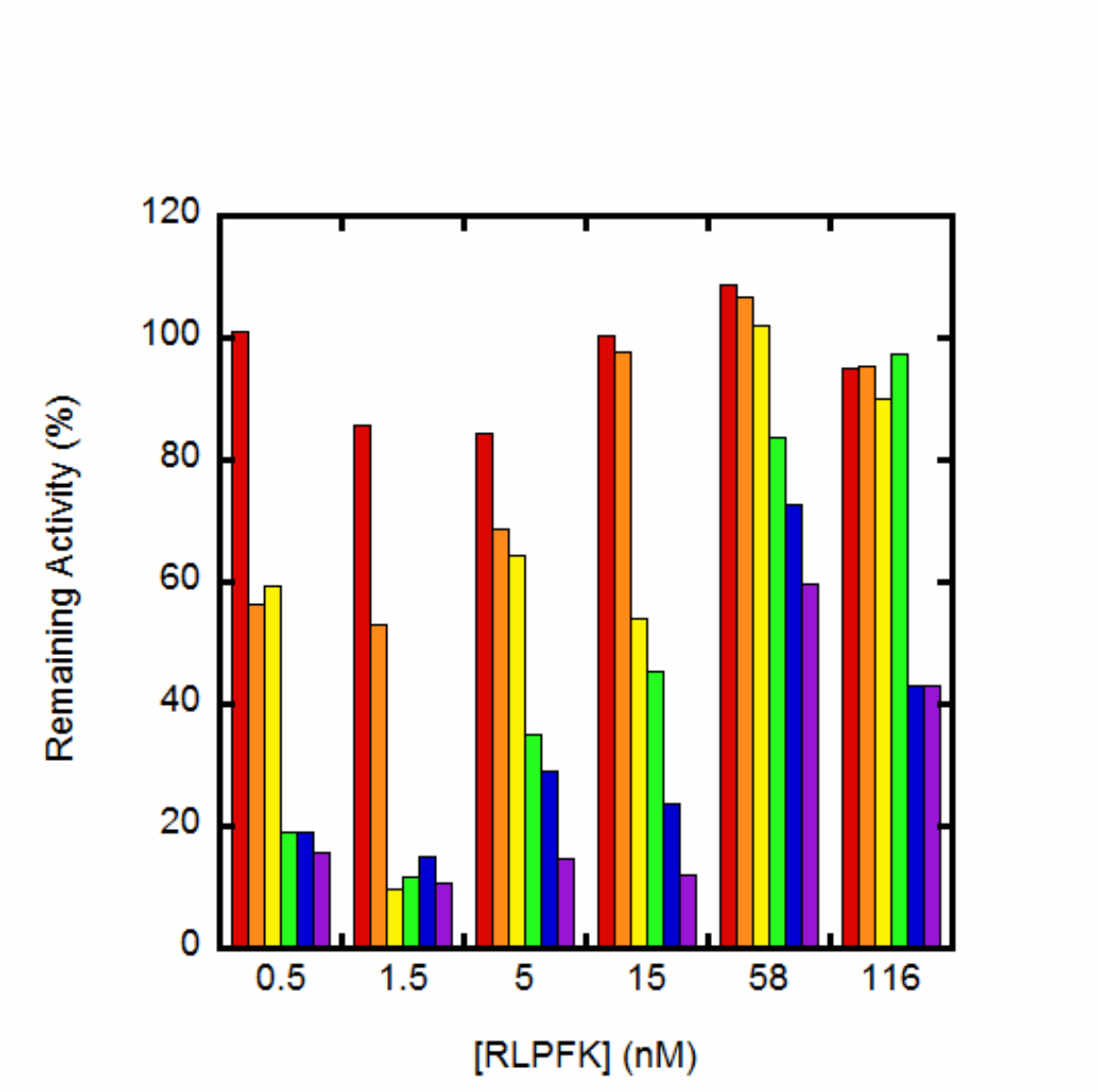

Figure 6-20: Stability of RLPFK in the presence of 3.2 (red), 1.6 (orange), 0.8 (yellow), 0.4 (green), 0.2 (blue) or 0.1mM (purple) Fru-6-P. Activity measurements were made as described in materials and methods and take concurrently to FCS measurements. Activity measured at the end of the experiment is reported as a percentage of the initial activity.

CHAPTER VII

CONTINUED EXPERIMENTAL DEVELOPMENT

Approximately two-thirds of human enzymes are oligomeric, bespeaking the importance of oligomerization in enzymatic function.[214] A fundamental understanding of the oligomeric state of an enzyme is necessary for a thorough understanding of an enzyme's biochemical and biophysical properties. For one to understand the state of oligomerization one must define both the stoichiometry and the thermodynamic stability of the oligomeric protein. Stoichiometry has been the primary parameter explored in the investigation into the oligomerization properties of rat liver phosphofructokinase (RLPFK). Notably, RLPFK has been defined by its differential stoichiometry in response to the concentration of ligands in solution. Specifically, in the presence of MgATP, RLPFK is stated to be a tetramer, and in the presence of Fru-6-P, RLPFK forms large polymers.[50] Further observations indicate that ligands that promote activation (e.g. AMP, Fru-1,6-BP, phosphate and ammonium sulfate) also promote polymerization, and ligands that inhibit RLPFK (e.g. Citrate and MgATP) promote the tetramer form of RLPFK.[49] To further the investigation of RLPFK oligomerization, it is desirable to measure the thermodynamic stability of RLPFK polymers, and measure the response of the thermodynamic stability to ligand conditions. The thermodynamic stability of an oligomer is characterized by the equilibrium dissociation constant (K_d).

Fluorescence correlation spectroscopy (FCS) provides a means to calculate the K_d, provided the appropriate experiment is performed.

Using the measured diffusion coefficient, we distinguished between populations of polymers, tetramers, dimers and monomers. We were not, however, able to measure the dissociation constant of RLPFK polymers $\left(K_d^{pol}\right)$. A quantitative measure of the polymer dissociation would allow us to more distinctly characterize the differential behavior of RLPFK in the presence of either MgATP or Fru-6-P and its functional dependence on the concentration of the respective ligand. Measurement of the K_d^{pol} would have required the use of a far greater number, and broader range of RLPFK concentrations than reported here. Additionally, our experiments were obfuscated by high background signal, photobleaching and low labeling efficiency. Unfortunately, we were unable to establish a rigorous quantitative description of the polymerization properties of RLPFK. In the following sections, we will discuss the experimental procedures necessary to ascertain a quantitative description of RLPFK polymerization and the reasons their implementation were not previously experimentally feasible. We propose avenues of troubleshooting, instrumental modification and sample preparation that will improve the experimental procedures. We will discuss the information that we could possible learn and the limitations of its interpretability. Finally, we will discuss high risk projects that, if successful, could provide powerful insight, but currently lack the necessary preliminary data to provide certainty of their feasibility.

The Ideal Experiment

To measure the equilibrium dissociation constant of a polymeric enzyme, a parameter is needed whose properties are dependent on the size of the polymer. The diffusion coefficient of an oligomeric particle is inversely proportional to the cubed root of the number of oligomers (assuming a spherical particle). Fluorescence correlation spectroscopy reports on a polymers size by measuring the diffusion coefficient and the number of particles. Measured as a function of RLPFK concentration, the diffusion coefficient and/or the particle number can be used to calculate an equilibrium constant for two oligomeric states of RLPFK.[210, 221, 222]

Measurement of $\left(K_d^{pol}\right)$ will likely require the use of RLPFK concentrations that span 4 orders of magnitude. Two orders of magnitude is the minimum range of enzyme concentrations necessary to reliably describe the equilibrium dissociation constant between two oligomeric states of a protein (one order of magnitude above and one below the value of K_d.[223] However, it is important to remember that RLPFK has not one, but three different equilibrium dissociation constants. These three include the equilibrium dissociation constant for monomer-dimer equilibrium $\left(K_d^{dim}\right)$, dimer-tetramer equilibrium (K_d^{tet}) and tetramer-polymer equilibrium $\left(K_d^{pol}\right)$. Increases in the diffusion coefficient resulting from the dissociation of RLPFK tetramers from polymers will be convoluted by increases in the diffusion coefficient resulting from the dissociation of dimers from tetramers. Deconvolution

can be achieved by measuring both the K_d^{tet} and the K_d^{pol}; assuming they differ from each other by at least 2 orders of magnitude.[222] Enzyme concentrations ranging an order of magnitude above and below two dissociation constants that differ from each other by at least 2 orders of magnitude result in a range of 4 orders of magnitude, or 4 decades of concentrations. Ideally at least 5 RLPFK concentrations will be measured within each decade.

Measuring the dissociation constants of RLPFK in the presence of saturating MgATP $\left(K_{d-ATP}^{pol}\right)$ and then again in the presence of saturating Fru-6-P $\left(K_{d-F6P}^{pol}\right)$ would provide a definitive description of the ligand dependent oligomeric state of RLPFK. By then varying the concentration of the respective ligand, and measuring the shift in the equilibrium constant, we can apply linkage analysis to quantitatively describe the modulation of oligomeric state as a function of ligand concentration. The reciprocal nature of two thermodynamically linked parameters means that we will simultaneously describe the modulation of ligand affinity as a function of oligomeric state. A thermodynamic description of the modulation of ligand affinity as a function of oligomeric state gives a glimpse into the extent that low RLPFK concentrations can skew the apparent affinity for substrate; and is therefore first, and most critical, step in bridging the gap between ligand affinities measured in kinetic assays and those that exist is cellular conditions.

The first question a researcher will have to decide is whether to vary the concentration of RLPFK using uniformly labeled RLPFK, or to mix labeled RLPFK with unlabeled RLPFK. One advantage of using uniformly labeled protein,

information on the oligomeric state can be obtained from both the persistence time and the change in g(0).[164] The same data used to calculate the autocorrelation function (ACF) could also be used to calculate the number and brightness[211, 224] and a photon counting histogram (PCH)[225]. Number and brightness analysis and PCH will inform on changes in the oligomeric state if RLPFK is uniformly labeled but not if it is mixed. Unfortunately, when using uniformly labeled RLPFK, data analysis is complicated by a signal to noise ratio that is dependent on RLPFK concentration. Additionally, an upper limit of RLPFK concentration exist at which one or both of the following can occur; correlation is loss due to insubstantial fluctuations of particles through the excitation volume[164], the average intensity of the fluorescent signal saturates the detectors[210].

The alternative is to maintain a constant concentration of labeled RLPFK and increase the total protein concentration by adding unlabeled RLPFK. A mixed protein solution will yield no change in g(0) as a function of RLPFK polymerization but it will benefit from a constant signal to noise ratio. Unfortunately, the signal to noise ratio will be relatively low, but any error resulting from the noise will be propagated evenly through the entire data set. Mixing a set concentration of labeled protein with unlabeled is commonly applied to such experiments[208, 226-229] but one must be sure that tetramers within a polymer exchange and that labeled RLPFK self assimilates the same as unlabeled RLPFK.

Efforts have been made to measure tetramer exchange between polymers of unlabeled RLPFK and labeled RLPFK, but the results have been inconclusive. We

mixed 15nM RLPFK-FITC with varying concentrations of unlabeled RLPFK and allowed to incubate at room temperature in the saturating presence of Fru-6-P. Figure 7-1 demonstrates that as the concentration of RLPFK increases the diffusion coefficient decreased and the particle concentration increased, consistent with process of polymerization. However, exchange was not seen in a separate experiment in which 116nM RLPFK-FITC was mixed with 116nM unlabeled RLPFK and allowed to incubate in the saturating presence of Fru-6-P for 3 hours. If exchange occurred, the concentration of observable particles would double. A process observable as a decrease in g(0). Figure 7-2 demonstrates the autocorrelation curve of unmixed 116nM RLPFK-FITC was indistinguishable from the 50:50 mixture suggesting no mixing had occurred.

The described attempts to mix labeled RLPFK with unlabeled involved tetramer exchange between polymers. Such a process is dependent on the rate of dissociation and association of tetramers. Many publications mix labeled and unlabeled species by mixing components in their smallest relevant size and then stimulating polymer formation.[210] In studying the polymerization of RLPFK, this would mean mixing labeled and unlabeled tetramers and then stimulating polymer formation. Such a procedure has not been explicitly demonstrated with RLPFK, methods to test this approach are discussed below.

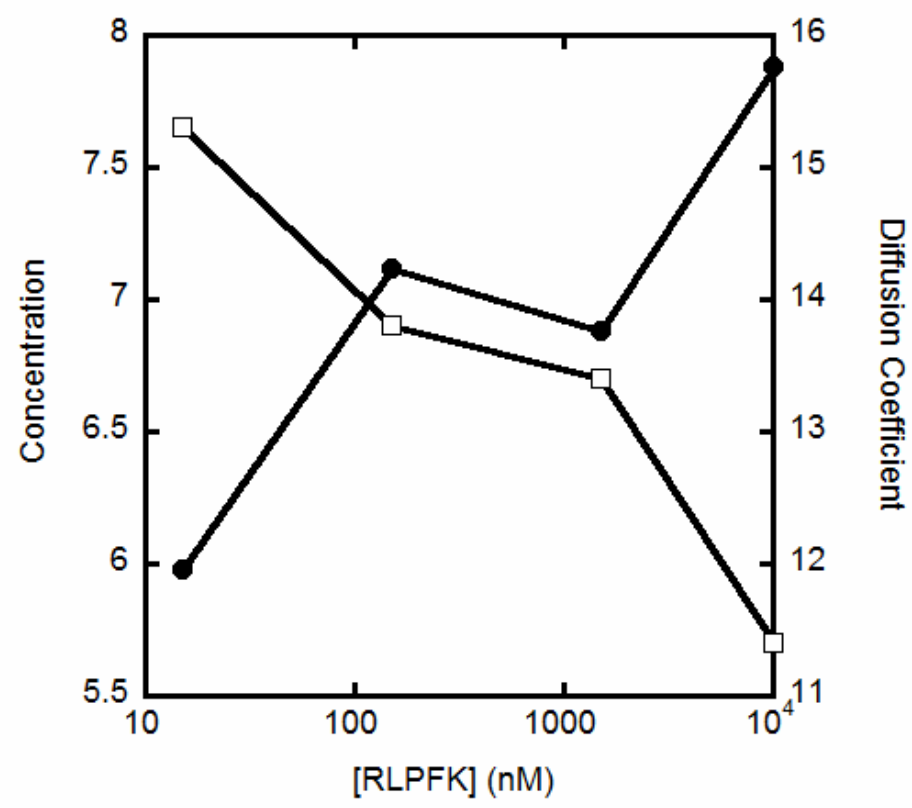

Figure 7-1: Concentration dependence of diffusion coefficient (open squares) and concentration (closed circles) of RLPFK. 15nM RLPFK-FITC was mixed with various concentrations of unlabeled RLPFK and allowed to incubate at room temperature for 4 hours. Buffer conditions are 50mM MOPS pH=7.0, 5mM $MgCl_2$, 0.1mM EDTA, 1mM DTT, 5mM Fru-6-P and 0.1µg/ml BSA

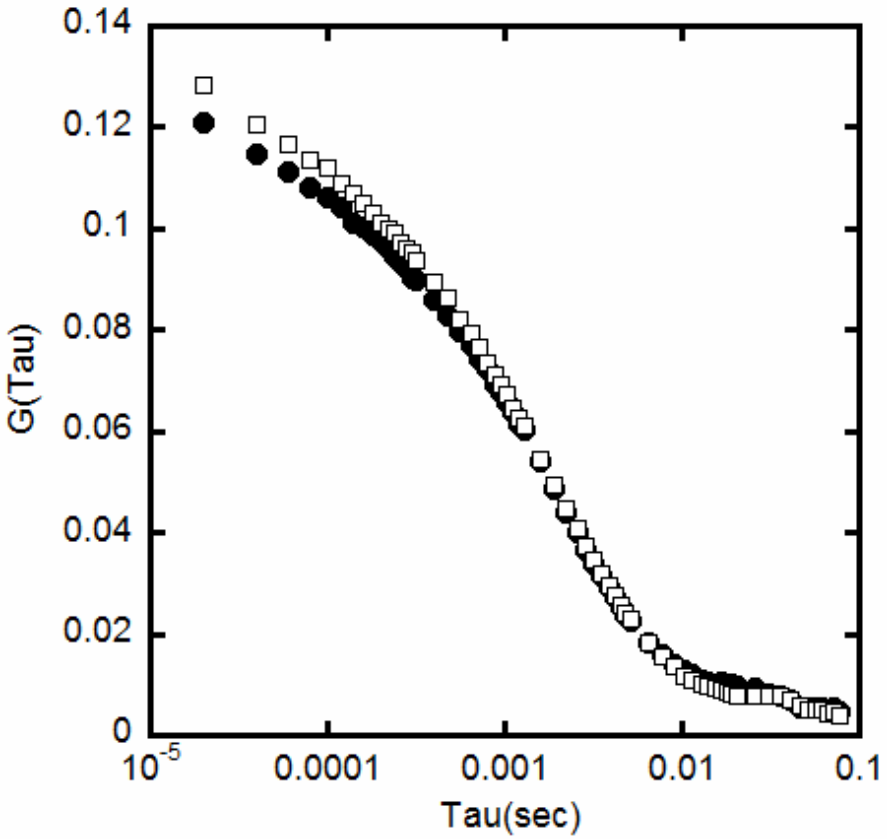

Figure 7-2: Autocorrelation curve of 116nM RLPFK-FITC in the absence (closed circles) or presence (open squares) of 116nM unlabeled RLPFK. In both conditions, RLPFK was incubated at room temperature for 3 hours in 50mM MOPS pH=7.0, 5mM $MgCl_2$, 0.1mM EDTA, 1mM DTT, 5mM Fru-6-P and 0.1µg/ml BSA.

Our shortcomings in establishing a procedure to interchange labeled and unlabeled tetramers as well as the inability to increase the low signal to noise ratio are the primary reason that the "ideal experiment" was not performed as desired. Additionally, it was previously uncertain how much time would be required to reach a state of oligomeric stability, so we were forced to take several measurements after dilution to determine when the oligomeric state stopped changing. The time dependent data presented in this dissertation suggest that 2 hours after dilution is enough time for the change in oligomeric state to occur. Future experiments can be measured after 2 hours and taken to be reflective of a state of relative stability. The RLPFK concentration dependent diffusion coefficients presented in chapter 5 and 6 of this dissertation informs on the concentration range of interest to future experiments. In the presence of Fru-6-P, RLPFK was a polymer at and above 15nM RLPFK, and a tetramer at 5nM RLPFK and below. One should take measurements at least 1 log unit above and below these values, so 150nM-0.5nM RLPFK would be a starting range of concentrations with most of the measurements between 15nM and 5nM RLPFK. However, in the presence of MgATP, very little evidence of polymer formation was seen at 116nM RLPFK. To potentially measure polymer formation in the presence of MgATP, the concentration of RLPFK will need to be increased by 1 or 2 orders of magnitude, potentially bringing the maximum concentration to 10μM RLPFK. We have discussed why measurements of RLPFK ranging in concentration from 0.5nM to

10μM was previously experimentally difficult. In the following sections, we discuss avenues of troubleshooting to improve the experimental procedures.

Troubleshooting

To move forward with FCS analysis of RLPFK, several issues must be resolved; the most pressing of which is the signal to noise ratio. A larger signal to noise ratio is essential to improving the ability to monitor diffusion at very low concentrations of labeled RLPFK. Improving the signal to noise requires one to address the background signal obtained during measurements, and to establish a better fluorescent probe. After improving the signal to noise ratio, we must explore options for mixing labeled and unlabeled RLPFK and establish a contingency plan if mixing fails to yield uniformly mixed species.

The background signal contaminating FCS measurements comes from fluorescence from buffer components and electronic noise such as afterpulsing[230]. Electronic noise can be greatly mitigated by using a 50:50 beam splitter and cross correlating the signal detected by two different detectors.[231, 232] An electronic artifact is unlikely to affect both APDs at the same time and thus will not be correlated. Cross-correlating will eliminate afterpulsing but will also reduce the signal intensity and thus increase the relative contribution from the background signal from buffer containments and scattered excitation. If the loss of signal is too great to justify, one could consider forgoing the use of a beam splitter and instead

remove afterpulsing detected by a single detector using a purely mathematical treatment as outlined by Zhao et.al.[233]

Once electronic noise is reduced, the potential of fluorescence from buffer components must be quantified. Fru-6-P and BSA are both known to contain fluorescent contaminates, however, these contaminants typically fluoresce when excited with ultra-violate light, not infrared as used in our experiments. It is worth dedicating time to determine which (if any) of the buffer components are fluorescing and whether the excitation is occurring by one-photon excitation (excited in the infrared) or two-photon excitation (excited by visible light). First, a typical FCS experiment should be performed on a buffer solution that contains no labeled protein. The concentration of each buffer component should be gradually increased, and the CPS detected by the APDs monitored. If an increase in correlated signal is seen as a function of component concentration, the mode locking of the laser should be removed to see If excitation still occurs by one-photon excitation[234]. Finally, fluorescence should be verified on a standard fluorometer. If one or more components are seen to be contaminated, a different supplier should be sought out. If no supplier provides sufficiently clean material, the contamination must be quantified and mitigated.

After minimizing the background signal as much as possible, the signal arising from labeled protein must be increased. In the experiments presented in this dissertation, we used fluorescein isothiocyanate (FITC) to label RLPFK and consequently had low brightness at pH 7.0[193], and had evidence of triplet state

excitation and photobleaching[193, 207]. Additionally, we found that the labeling procedure utilized here resulted in low labeling efficiency and lingering free dye contamination. As a first effort to improve the signal of labeled RLPFK we recommend the use of an amine specific Alexa fluorophore such as Alexa 488-NHS or Alexa 488-SDP.

Our first attempts to label RLPFK were made using Alexa 488-NHS and Alexa 488-SDP, these attempts resulted in low levels of conjugation and a large presence of free dye that was infuriatingly difficult to remove (data not shown). Upon transitioning to FITC, we immediately saw increased levels of conjugation and decreased residual free dye. Conjugation with FITC was further improved by a few small "tweaks". These "tweaks" were never retroactively applied to labeling with Alexa 488 to see if labeling with Alexa 488 could be improved in terms of degree of conjugation and presence of free dye. Labeling with Alexa 488 (NHS and/or SDP) should be re-attempted using the following lessons learned while labeling with FITC; 1. A freshly opened bottle should be used for each labeling procedure 2. 100mM ammonium sulfate should be included in the post-labeling dialysis buffer 3. Extensive dialysis requires at least 10 changes of 1:100 dialysis buffer and daily addition of DTT 4. Labeling should be performed at a pH of 9.2 and 5. Use 30-50-fold molar excess dye. The previously stated improvements should increase the labeling efficiency by Alexa 488 but may not fully resolve the biggest curiosity seen when labeling with Alexa 488. In our experience, Alexa 488 would associate very tightly with RLPFK when in the presence of Fru-6-P and then dissociate when in the

presence of MgATP (data not shown). We hypothesized that this occurred because of adhesion to hydrophobic pockets between tetramers in the polymer chain. MgATP liberated the free dye upon dissociation of the polymer chains. Free dye was efficiently eliminated by extensively dialyzing labeled RLPFK in the presence of MgATP, but this practice was abandoned because it had yet to be determined if RLPFK would re-polymerize to an equivalent species. Additional labeling strategies that could be utilized are fusion of EGFP to the N or C terminus [235], quantum dots[236], or site directed labeling [237-241].

Regardless of the label utilized, the laser system should be optimized to ensure the best signal possible. We suggested photobleaching and, possibly, triplet state excitation were affecting the ACF of polymerized RLPFK. To ensure this is not occurring in future experiments the laser intensity should be modulated.[220] Any change in the autocorrelation curve as a function of laser intensity is evidence of an undesirable artifact. Specifically, laser intensity dependent amplitude of a "shoulder" at short tau values is evidence of triplet state excitation[242] and a reduction in the characteristic diffusion time is evidence of photobleaching[243].

If possible, a way must be found to mix labeled and unlabeled RLPFK so that the concentration of labeled RLPFK can remain constant while the total protein concentration of RLPFK is increased. Previous efforts to exchange labeled and unlabeled tetramers between polymerized RLPFK yielded uncertain results, but seem to indicate that exchange does not readily occur. One final test could be performed to provide a definitive answer. The experiment would involve adding

125nM unlabeled RLPFK to a solution of 0.5nM labeled RLPFK and should be performed as follows. In the presence of saturating Fru-6-P, dilute labeled RLPFK to 0.5nM and monitor dissociation by changes in diffusion coefficient. Previous experiments suggest that within an hour 0.5nM RLPFK will be predominantly tetramer even in the presence of saturating Fru-6-P. When the diffusion coefficient is no longer changing, unlabeled RLPFK will be added so that the final concentration is 125nM RLPFK. A decrease in the diffusion coefficient could indicate that labeled RLPFK is being incorporated into the unlabeled polymers. Changes in the diffusion coefficient should be monitored for at least 24 hours because the rate of association may be very slow.

As a control, an aliquot of 0.5nM labeled RLPFK should be reserved and monitored for 24 hours without the addition of unlabeled RLPFK. Both enzymatic activity and diffusion coefficient should be measured for this control. The result most indicative of exchange is a diffusion coefficient that decreases in the experimental aliquot and remains constant in control aliquot. If instead, the diffusion coefficient decreases in both the experimental aliquot and the control aliquot then some form of aggregation is occurring that does not involve exchange with unlabeled tetramers. An increase in diffusion coefficient in the control would indicated that the tetramer is not stable for 24 hours, instability should be verified by a loss of enzymatic activity in the control. Tetramer instability may or may not manifest itself in the experimental aliquot depending on the relative rate of tetramer dissociation to polymer assembly. If the diffusion coefficient increases in

both the experimental aliquot and the control aliquot, the labeled tetramer dissociates faster than the tetramer associates into the polymer. An additional necessary control is to dilute labeled RLPFK to 125nM without unlabeled RLPFK and monitor its diffusion coefficient for 24 hours. 125nM labeled RLPFK should have a slow diffusion coefficient that doesn't change over the course of the experiment.

If mixing polymerized RLPFK does not result in exchange between labeled and unlabeled species, the next thing to try is stimulating polymerization in a solution of labeled and unlabeled tetramers. The two questions that must be answered are whether labeled and unlabeled RLPFK will be incorporated into polymers equally; and whether RLPFK will form equivalent polymers after dissociation.

To test the latter, an autocorrelation curve should be measured for two samples of labeled RLPFK, one in the presence of Fru-6-P (sample A) and the other in the presence of MgATP (sample B). The initial measurement is a control to verify that this sample behaves as expect, i.e. slow diffusion in the presence of Fru-6-P and fast diffusion in the presence of MgATP. Next, Fru-6-P would be added to sample B such that the concentration of Fru-6-P is at least 3mM higher than the concentration of MgATP. Upon addition of Fru-6-P, catalysis will occur leaving only Fru-6-P, Fructose-1,6-bisphosphate (Fru-1,6-P) and ADP; all of which stabilize the polymer form of RLPFK.[49, 50] After an appropriate period of time, the autocorrelation curves of sample A and sample B should be re-measured. Identical

autocorrelation curves indicate that RLPFK re-polymerized to its original state after being subjected to dissociation by MgATP. The process sample B is subjected to is referred to as "cycling" in reference to a period of dissociation followed by re-polymerization. Because the residual presence of Fru-1,6-P and ADP could affect the polymer formation, the experiment should be repeated with removal of MgATP performed by either desalting column or dialysis.

Equivalent polymerization properties between labeled and unlabeled RLPFK is critical for interpreting all performed and proposed experiments, and yet remains a lingering question. Varying the amount of dye used when labeling RLPFK such that the resulting products have different dye to protein ratios would be a valuable control to ensure that labeling does not affect polymerization properties. The challenge in performing such an experiment is getting a sufficient quantity of protein to perform multiple labeling reactions on a single pool of protein. Even after extensive optimization of the expression, growth and purification of RLPFK, a typical purification yields only 4-15mg of RLPFK. Often, an entire preparation of RLPFK is used in a single labeling procedure. While one could perform several purifications of RLPFK and use an entire preparation for each desired labeling ratio, it would be very difficult to minimize variations between preparations (e.g. purity, time after cell lysis, and RLPFK concentration during purification). Varying the ratio of label to protein using a single preparation is ideal for minimizing any complicating variables but requires a significant increase in the production of RLPFK or a significant decrease in the quantity of RLPFK used during labeling.

If proven to be successful, “cycling” could be used to answer whether labeled and unlabeled RLPFK incorporate into polymers equally without modifications to expression or labeling procedures. In this instance “cycling” would be performed by first dissociating a pool of labeled protein and a pool of unlabeled protein. The two pools would then be mixed, and polymerization induced by the addition of Fru-6-P. The resulting polymers will have a dye to protein ratio that depend on the proportion of unlabeled and labeled protein that were mixed. The following three experiments would use cycling to assess the effect of labeling ratio on polymer formation. The “expected” results described after each experiment are the results that would indicate that labeling exerts no influence on polymerization. 1. Measure FCS of multiple samples of 125nM RLPFK “cycled” to have ratios of labeled to unlabeled RLPFK ranging to 1:1 to 1:250. These samples should have identical diffusion coefficients, and the values of $1/g(0)$ should be linearly dependent on the mixing ratio. 2. Measure FCS of RLPFK samples that have been cycled so that each are comprised of 0.5nM labeled RLPFK and unlabeled RLPFK ranging from 0-124.5nM. Identical values of $g(0)$ should be seen for all samples, but the diffusion coefficients should decrease with increasing concentration of unlabeled RLPFK. 3. FCS should then be measured using fully labeled RLPFK at the same concentrations of total protein as was measured in the second experiment. The diffusion coefficients measured in the second experiment should be equal to that measured for uniformly labeled RLPFK of the same concentration. The values of $g(0)$

measured in the third experiment should decrease with increasing concentration of fully labeled RLPFK but will not be linearly dependent.

In the unfortunate case that no method of exchanging labeled, and unlabeled tetramers is fruitful, the polymer dissociation constant will have to be measured using fully labeled RLPFK. In this case a great deal of standards will be necessary to ensure that the values measured are meaningful.[162] A standard fluorophore will need to be chosen that best emulates the label ultimately decided upon for labeling RLPFK. Solutions of the standard fluorophore should be made with concentrations consistent with the range and increments intended for RLPFK. No change in particle brightness or diffusion coefficient should be observed, and the value of 1/g(0) and number of particles should be linearly dependent on the concentration of fluorophore. A monodispersed, labeled particle (protein or commercial nanosphere) with a size approximately the same as RLPFK should be measured at various concentrations to ensure no false report of association/dissociation. The monomer form of green fluorescent protein (EGFP), or one of its variants, makes for a convenient standard as it can be constructed as a monomer or a string of monomers, resembling the string of RLPFK tetramers.[244] EGFP is exceptionally well suited if RLPFK is labeled using a EGFP fusion, but could still be useful even if RLPFK is labeled with a small molecule fluorophore such as Alexa.

The most important improvements to be made are the fluorophore used to label RLPFK and decreasing the background signal, followed by establishing an efficient way to mix labeled and unlabeled RLPFK. If these avenues of improvement

prove unfruitful, then a comprehensive approach to calculating the K_d^{pol} of RLPFK will likely be unrealizable. That level of pessimism is unwarranted though. Some method of mixing labeled and unlabeled RLPFK is almost certainly going to work, and labeling RLPFK with fresh Alexa-488 NHS ester and cross-correlating the excitation signal between two detectors placed after a 50-50 beam splitter should greatly improve the signal. Once these improvements have been made and optimized, actualization of the ideal experiment for determining the K_d^{pol} should be straight forward. However, one should be aware that the ideal experiment will be quite time consuming and may still not deliver results that are interpretable in thermodynamically meaning ways.

Potential Difficulties in Determining a Thermodynamically Meaningful Values of K_d

In the previous section we have discussed how to perform the ideal experiment for determining the thermodynamic dissociation constant of RLPFK polymers, the current shortcomings to such an approach and the avenues of troubleshooting necessary to resolve the shortcomings. Even once the subtitles of experimental and procedural methods are perfected, the physical nature of RLPFK polymerization may make meaningful thermodynamic dissociation constants difficult to measure. These potential difficulties include the absence of an upper plateau to polymerization, ambient presence of insoluble protein aggregates,

convolution of dissociation constants and the potential of radically different aggregation in the presence of MgATP.

The data presented in this dissertation suggest that only a small change in the diffusion coefficient occurs as the concentration of RLPFK is increased from 15nM to 116nM in the presence of 3mM Fru-6-P. A small change in diffusion coefficient over almost and order of magnitude change of RLPFK concentrations suggest that at RLPFK is approaching an upper plateau in the presence of Fru-6-P. However, we discussed the possibility that photobleaching is artificially truncating the autocorrelation curve resulting in an underestimation of the particle size. Additionally, our data could be biased away from the largest of the functionally relevant RLPFK polymers by the procedure used for curating seemingly random intensity spikes. If these two biases have a more dramatic effect than initially assumed, future data may reveal a significant increase in polymerization at concentrations from 15-115nM and beyond. It is very unlikely that polymerization will occur in a linear fashion from a dimer of tetramers to a string of tetramers infinitely long and there is literature precedence for calculating an equilibrium dissociation constant between a species of distinct stoichiometry and a species described as "large" [226]. In the worst-case scenario, the propensity of polymerization may need to be describe by a parameter defining the concentration of RLPFK at which a polymer of a particular average size is obtained (e.g. the concentration of RLPFK at which the average polymer size is 5 tetramers).

Several intensity spikes were culled out of the raw data of FCS measurements. These spikes were rare (occurring at most once a minute) and the intensity did not seem to be correlated to any parameter (data not shown). They appeared in protein samples both in the presence of Fru-6-P and MgATP, and the frequency seemed proportional to protein concentrations. In the range of protein concentrations presented in this dissertation the spikes were never a huge problem. However, in unreported experiments that included micromolar concentrations of unlabeled RLPFK they became a far greater nuisance. At times, the spikes were so intrusive as to make samples unmeasurable. The occurrence of these spikes in samples predominantly consistent of unlabeled RLPFK (data not shown) is a compelling argument for insoluble aggregates as the causation. Unless these spikes can be prevented, the limit of total protein concentration may be 1μM. Centrifugation or filtering may be effective at removing aggregates, and one could try preparing protein samples in glass tubes instead of plastic, as this has been suggested to be beneficial for preventing aggregation in some proteins.[245]

It can be difficult to unequivocally determine two different dissociation constants using FCS if they differ from each other by less than 2 orders of magnitude[222]. Three equilibrium dissociation constants are necessary to fully describe RLPFK polymerization from monomers (dimers-monomers, tetramers-dimers, polymers-tetramers). The data presented in this dissertation suggest that, in many conditions, the K_d^{pol} and K_d^{tet} do not differ from each other by 2 orders of magnitude. In many conditions 3 different oligomeric forms of RLPFK are likely

present, complicating efforts to determine the K_d^{pol}. Two dissociation constants with very similar values can be resolved if they are sensitive to different measurable parameters.[222] Dissociation of RLPFK from a polymer to a tetramer involves species with invariant specific activity, but dissociation of tetramer into dimers (or monomers) always results in loss of enzymatic activity. Using enzymatic activity measurements, the K_d^{tet} could be determined and then used as a fix parameter when fitting concentration dependent diffusion coefficients.

The final issue that could complicate results, is the polymerization behavior of RLPFK in the presence of MgATP. In the experiments presented in this dissertation, RLPFK was never much larger than a tetramer in the presence of MgATP. Reinhart and Lardy[49, 50] showed evidence that at high enough concentrations, RLPFK could polymerize in the presence of MgATP. But it has never been demonstrated that RLPFK will polymerize in the same "end-on-end" fashion as it does in the presence of Fru-6-P. RLPFK may form globular aggregates in the presence of MgATP instead of the "spaghetti" like polymers it does in presence of Fru-6-P.

Additional Projects

Several experiments could be attempted that would provide valuable insight but currently lack the preliminary data necessary to ensure success. The first of these projects would be the construction of an RLPFK mutant that does not form

polymers but remains a stable tetramer. Faced with the challenge of polymerization and aggregation, Kloos et. at. constructed a truncation mutant of human platelet PFK in order to crystalize the tetramer.[142] The 22 residue C-terminal truncation prevented polymerization well enough for them to crystalize a fully active tetramer. If the same 22 residue C-terminal deletion completely prevents polymerization in RLPFK it would provide both a powerful negative control to the RLPFK concentration dependent polymerization experiments and an avenue for measuring the K_d^{tet} without convolution by the K_d^{pol}.

Even if the c-terminal truncation does not completely prevent polymerization, variations of c-terminal mutations could be very interesting for understanding the interdependence of RLPFK polymerization and activation. Kloos et.al. reports that the enzymatic activity of human platelet PFK increased as a result of the truncation.[142] Martínez-Costa et.al. identified highly conserved residues in the C-terminus of rabbit muscle and rabbit platelet PFK that were critical to the transmission of the allosteric signal of inhibition by MgATP.[167] It would be very interesting to determine the effect of isolated mutations and c-terminal truncation on the thermodynamic parameters describing MgATP inhibition of Fru-6-P binding (K_{ia}^0, K_{ix}^0, Q_{ax}) as well as their effect on the propensity of RLPFK to polymerize. A "dream scenario" would be a mutant that had diminished MgATP inhibition but retained the ability to polymerize, and a truncation that eliminated both MgATP inhibition and the ability to polymerize. This "dream scenario" would illustrate a mechanism in which polymerization activates RLPFK by impairing the ability of the

C-terminus to transmit the allosteric signal. If one could unequivocally determine the inter-tetramer interacting residues necessary for polymerization (using Förester resonance energy transfer (FRET) or some other technique) it could be determined whether polymerization sequesters the C-terminus and thereby prevents it from transmitting the allosteric signal of MgATP inhibition.

Another useful tool would be an MgATP analogue[49] that stabilizes the tetramer but does not turnover. Stabilizing the tetramer with an ATP analogue would prevent convolution of the K_d^{pol} by the K_d^{tet}. Increasing the concentration of Fru-6-P in the saturating presence of an ATP analogue would allow one to investigate which ligand influence dominates when both are present. Inducing polymerization of low concentrations of RLPFK with PEG could allow direct correlation to polymerization of RLPFK to an increase in Fru-6-P affinity[50, 107]. As a final experiment to consider, FCS-FRET could be used to identify a small population of short polymers (2-3 tetramers) among a sea of tetramers[245].

CHAPTER VIII

SUMMARY

The differential dependence of rat liver phosphofructokinase oligomer stoichiometry on bound ligand has been established utilizing fluorescent polarization, gel filtration and analytical ultra-centrifugation.[49, 50] The study reported here establishes that RLPFK retains the ability to polymerize when recombinantly expressed in E. coli cells. We pioneer the use of fluorescence correlation spectroscopy (FCS) to study the oligomeric form of RLPFK. Consistent with the observations made by Reinhart and Lardy[49, 50], our FCS measurements illustrate a paradigm in which Fru-6-P stabilizes polymers of RLPFK, and MgATP stabilizes the tetramer form of RLPFK. To investigate the polymerization process and its dependence on solution conditions, we performed a matrix of experiments in which RLPFK concentration, ligand concentration and time after RLPFK dilution were all variable. Although quantitative descriptions of the K_d of RLPFK polymerization $\left(K_d^{pol}\right)$ were not realized in this study, we report a qualitative description of the RLPFK polymer characteristics in the presence of either MgATP or Fru-6-P and discuss the limitations of the reported experiments.

In the presence of saturating concentrations of Fru-6-P, RLPFK remained polymerized after dilution to a concentration of 116nM, 58nM, or 15nM, but is seen to dissociate to a tetramer at a concentration of 5, 1.5 or 0.5nM RLPFK. Polymerized

RLPFK was highly heterogeneous. Formation of a discrete polymeric species was not observed. The polymer and the tetramer are both destabilized as the concentration of Fru-6-P is decreased. The concentration of Fru-6-P necessary to stabilize an active form of RLPFK (either a tetramer or a polymer) is consistent with the dissociation constant of Fru-6-P. However, the concentration of Fru-6-P necessary to stabilize active PFK seems to decrease to a value less than the dissociation constant as the concentration of RLPFK is increased. The interdependence of the minimum stabilizing concentration of Fru-6-P and the concentration of RLPFK supports the observation that the polymer form of RLPFK has a greater affinity for Fru-6-P than the tetramer. In the matrix of Fru-6-P conditions tested, RLPFK existed as a population predominately made of either active polymers or inactive monomers. An "island" of stable active tetramers exist when the concentration of Fru-6-P was 3.2mM and the concentration of RLPFK was 5nM, 1.5nM or 0.5nM. This "island" indicates that a Fru-6-P concentration greater than 1.6mM is necessary to stabilize the tetramer when the RLPFK concentration is too low for polymer stability. Generally, at concentrations of RLPFK above 5nM the polymer form was stabilized. A loss of activity was observed if the concentration of Fru-6-P was decreased enough so that the polymer was destabilized (≈0.2mM Fru-6-P), indicating that tetramer was not stabilized in these conditions.

When diluted in the presence of MgATP, RLPFK is seen to rapidly dissociate into tetramers. The species identified as tetramers had a diffusion coefficient of $32\mu m^2 s^{-1}$, consistent with the previous publications.[49, 50, 212, 218] At high

concentrations of MgATP and RLPFK, a minor presence of species larger than a tetramer was observed. In all conditions tested, RLPFK is believed to exist as a mixture of species. The population of components of the mixture is dependent on the concentration of both RLPFK and MgATP. Dissociation of the tetramer occurred much slower (1-2 hours) than the dissociation of the polymers (1-2 minutes). As expected, activity loss was observed in populations with a presence of sub-tetrameric species. A mixture primarily consisting of tetramers and dimers is seen at MgATP concentrations close to the dissociation constant of MgATP from the allosteric site. A mixture of dimers and monomers is observed at MgATP concentrations close to the dissociation constant of MgATP from the active site. We propose that binding of MgATP to the allosteric site stabilizes the tetramer.

Polymerization acts as form of allosteric regulation of RLPFK. Thermodynamic linkage analysis could quantitatively describe polymerization induced allosteric regulation of RLPFK if the appropriate equilibrium constants were determined. FCS provides an excellent method for determining polymerization equilibrium constants and how they respond to ligand concentrations. Although we were not able to determine the polymerization equilibrium constants in this study, the efforts of FCS development reported here provide the foundation for future efforts.

In addition to progressing efforts to describe the role of polymerization as a method of regulating RLPFK, we have furthered the thermodynamic understand of allosteric regulation of the tetramer form of the enzyme. We report here the

thermodynamic parameters describing the regulation of tetrameric RLPFK in the presence of two ligands; either MgATP and Citrate; or MgATP and AMP. We determined that activation by AMP and inhibition by citrate occur at concentrations of MgATP ranging from 0.1-25mM. However, we find that the magnitude of the regulatory affects diminishes with increasing concentrations of MgATP. Surprisingly, we find that the binding of the inhibitor MgATP is antagonistic to the binding of the inhibitor citrate. Additionally, we report that MgATP facilitates the binding of activator AMP. The unpredictability of these results illustrates the importance to empirically measure the thermodynamic parameters when explaining the mechanism allosteric regulation.

Complete characterization of the allosteric regulation of RLPFK will involve measuring the thermodynamic coupling parameters for each of the 5 primary allosteric regulators (MgATP, citrate, AMP, Fru-2,6-BP and pH) in concert with each other. Allosteric parameters can be defined for ten combinations of two-effector systems. Two combinations (MgATP-citrate and MgATP-AMP) have been described in this dissertation. Two others (MgATP-Fru-2,6-BP and MgATP-pH) have been previously described. The remaining 6 combinations have yet to be measured. After the 6 remaining pairwise combinations have been explored, a third allosteric regulator can be introduced to describe RLPFK regulation as a three-effector system. Determination of each of the unique thermodynamic coupling parameters would allow for precise modeling of RLPFK activity as it response to fluctuations in the concentration of substrate and the 5 primary allosteric regulators.

A greater understanding of the role of polymerization as a regulatory method will be obtained by determining the equilibrium constants describing RLPFK polymerization. Ultimately, the physiological role of RLPFK polymerization will best be understood by measuring polymerization in live cells. Advances in the field of microscopy, both in the field of fluorescence fluctuation spectroscopy and in super resolution microscopy, make such measurements feasible. The information learned from *in vitro* measurements will help inform the design and interpretation of *in vivo* measurements.

The data reported in this dissertation progress the understanding of the allosteric interactions that drive RLPFK regulation.

REFERENCES

[1] Bechtel, W., and Richardson, R. C. (1998) Vitalism, Taylor and Francis.

[2] Sumner, J. B. (1946) Nobel Lecture: The Chemical Nature of Enzymes, The Nobel Foundation, Amersterdam.

[3] Berg, J. M., Tymoczko JL, Stryer L. . (2002) Covalent Modification Is a Means of Regulating Enzyme Activity, In *Biochemistry* 5th ed., Freeman, W.H., New York.

[4] Weikum, E. R., Knuesel, M. T., Ortlund, E. A., and Yamamoto, K. R. (2017) Glucocorticoid receptor control of transcription: precision and plasticity via allostery, *Nat Rev Mol Cell Biol 18*, 159-174.

[5] Kon, T., Oyama, T., Shimo-Kon, R., Imamula, K., Shima, T., Sutoh, K., and Kurisu, G. (2012) The 2.8[thinsp]A crystal structure of the dynein motor domain, *Nature 484*, 345-350.

[6] Hynes, R. O. (2002) Integrins, *Cell 110*, 673-687.

[7] Hardie, D. G. (2015) AMPK: positive and negative regulation, and its role in whole-body energy homeostasis, *Current Opinion in Cell Biology 33*, 1-7.

[8] Matschinsky, F. M. (2009) Assessing the potential of glucokinase activators in diabetes therapy, *Nat Rev Drug Discov 8*, 399-416.

[9] Nussinov, R., and Tsai, C.-J. (2013) Allostery in Disease and in Drug Discovery, *Cell 153*, 293-305.

[10] Macpherson, J. A., and Anastasiou, D. (2017) Allosteric regulation of metabolism in cancer: endogenous mechanisms and considerations for drug design, *Current Opinion in Biotechnology 48*, 102-110.

[11] DeBerardinis, R. J., and Chandel, N. S. (2016) Fundamentals of cancer metabolism, *Science Advances 2*, e1600200.

[12] Li, X., Chen, Y., Lu, S., Huang, Z., Liu, X., Wang, Q., Shi, T., and Zhang, J. (2013) Toward an understanding of the sequence and structural basis of allosteric proteins, *Journal of Molecular Graphics and Modelling 40*, 30-39.

[13] Golinska, M., Troy, H., Chung, Y.-L., McSheehy, P. M., Mayr, M., Yin, X., Ly, L., Williams, K. J., Airley, R. E., Harris, A. L., Latigo, J., Perumal, M., Aboagye, E. O., Perrett, D., Stubbs, M., and Griffiths, J. R. (2011) Adaptation to HIF-1 deficiency by upregulation of the AMP/ATP ratio and phosphofructokinase activation in hepatomas, *BMC Cancer 11*, 198.

[14] Pauling, L. (1935) The Oxygen Equilibrium of Hemoglobin and Its Structural Interpretation, *Proceedings of the National Academy of Sciences of the United States of America 21*, 186-191.

[15] Monod, J., Jacob, F., Association, L. I. B., and Laboratory, B. (1961) *General Conclusions: Teleonomic Mechanisms in Cellular Metabolism, Growth, and Differentiation*, Biological Laboratory.

[16] Cui, Q., and Karplus, M. (2008) Allostery and cooperativity revisited, *Protein Science : A Publication of the Protein Society 17*, 1295-1307.

[17] Conway, A., and Koshland, D. E. (1968) Negative cooperativity in enzyme action. Binding of diphosphopyridine nucleotide to glyceraldehyde-3-phosphate dehydrogenase, *Biochemistry 7*, 4011-4023.

[18] Abeliovich, H. (2005) An Empirical Extremum Principle for the Hill Coefficient in Ligand-Protein Interactions Showing Negative Cooperativity, *Biophysical Journal 89*, 76-79.

[19] Hill, A. V. (1910) The possible effects of the aggregation of the molecules of haemoglobin on its dissociation curves, *The Journal of physiology 40*, 4-12.

[20] Monod, J., Wyman, J., and Changeux, J.-P. (1965) On the nature of allosteric transitions: A plausible model, *Journal of Molecular Biology 12*, 88-118.

[21] Koshland, D. E., Némethy, G., and Filmer, D. (1966) Comparison of Experimental Binding Data and Theoretical Models in Proteins Containing Subunits*, *Biochemistry 5*, 365-385.

[22] Koshland, D. E. (1959) Enzyme flexibility and enzyme action, *Journal of Cellular and Comparative Physiology 54*, 245-258.

[23] Changeux, J.-P. (2011) Allostery and the Mono-Wyman-Changeux Model After 50 Years, *Annual Review of Biophysics 41*, 103-133.

[24] Kister, J., Poyart, C., and Edelstein, S. J. (1987) An expanded two-state allosteric model for interactions of human hemoglobin A with nonsaturating

concentrations of 2,3-diphosphoglycerate, *Journal of Biological Chemistry 262*, 12085-12091.

[25] Forman, S. A., and Miller, K. W. (2011) Anesthetic sites and allosteric mechanisms of action on Cys-loop ligand-gated ion channels, *Canadian Journal of Anesthesia/Journal canadien d'anesthésie 58*, 191-205.

[26] Cuello, L. G., Jogini, V., Cortes, D. M., Pan, A. C., Gagnon, D. G., Dalmas, O., Cordero-Morales, J. F., Chakrapani, S., Roux, B., and Perozo, E. (2010) Structural basis for the coupling between activation and inactivation gates in K+ channels, *Nature 466*, 272-275.

[27] Cuello, L. G., Jogini, V., Cortes, D. M., and Perozo, E. (2010) Structural mechanism of C-type inactivation in K+ channels, *Nature 466*, 203-208.

[28] May, L. T., Leach, K., Sexton, P. M., and Christopoulos, A. (2007) Allosteric Modulation of G Protein–Coupled Receptors, *Annual Review of Pharmacology and Toxicology 47*, 1-51.

[29] Nussinov, R., and Tsai, C.-J. (2015) Allostery without a conformational change? Revisiting the paradigm, *Current Opinion in Structural Biology 30*, 17-24.

[30] Frauenfelder, H., Sligar, S., and Wolynes, P. (1991) The energy landscapes and motions of proteins, *Science 254*, 1598-1603.

[31] Levinthal, C. (1969) How to Fold Graciously, In *Mossbauer Spectroscopy in Biological Systems: Proceedings of a meeting held at Allerton House, Monticello, Illinois* (Debrunnder, J. T. P., and Munck, E., Eds.), pp 22-24, University of Illinois Press.

[32] Harrison, S. C., and Durbin, R. (1985) Is there a single pathway for the folding of a polypeptide chain?, *Proceedings of the National Academy of Sciences of the United States of America 82*, 4028-4030.

[33] Bryngelson, J. D., Onuchic, J. N., Socci, N. D., and Wolynes, P. G. (1995) Funnels, pathways, and the energy landscape of protein folding: A synthesis, *Proteins: Structure, Function, and Bioinformatics 21*, 167-195.

[34] Benkovic, S. J., Hammes, G. G., and Hammes-Schiffer, S. (2008) Free-Energy Landscape of Enzyme Catalysis, *Biochemistry 47*, 3317-3321.

[35] Goodey, N. M., and Benkovic, S. J. (2008) Allosteric regulation and catalysis emerge via a common route, *Nat Chem Biol 4*, 474-482.

[36] Weber, G. (1972) Ligand binding and internal equilibiums in proteins, *Biochemistry 11*, 864-878.

[37] Gunasekaran, K., Ma, B., and Nussinov, R. (2004) Is allostery an intrinsic property of all dynamic proteins?, *Proteins: Structure, Function, and Bioinformatics 57*, 433-443.

[38] Boehr, D. D., Nussinov, R., and Wright, P. E. (2009) The role of dynamic conformational ensembles in biomolecular recognition, *Nat Chem Biol 5*, 789-796.

[39] Cooper, A., and Dryden, D. T. F. (1984) Allostery without conformational change, *European Biophysics Journal 11*, 103-109.

[40] Tsai, C.-J., and Nussinov, R. (2014) A Unified View of "How Allostery Works", *PLoS Computational Biology 10*, e1003394.

[41] Motlagh, H. N., Wrabl, J. O., Li, J., and Hilser, V. J. (2014) The ensemble nature of allostery, *Nature 508*, 331-339.

[42] Hilser, V. J., Wrabl, J. O., and Motlagh, H. N. (2012) Structural and Energetic Basis of Allostery, *Annual review of biophysics 41*, 585-609.

[43] Jaffe, E. K. (2005) Morpheeins – a new structural paradigm for allosteric regulation, *Trends in Biochemical Sciences 30*, 490-497.

[44] Goodsell, D. S., and Olson, A. J. (2000) Structural symmetry and protein function, *Annual Review of Biophysics and Biomolecular Structure 29*, 105-153.

[45] Selwood, T., and Jaffe, E. K. (2012) Dynamic dissociating homo-oligomers and the control of protein function, *Archives of Biochemistry and Biophysics 519*, 131-143.

[46] Jaffe, E. K., and Lawrence, S. H. (2012) Allostery and the dynamic oligomerization of porphobilinogen synthase, *Archives of Biochemistry and Biophysics 519*, 144-153.

[47] Reinhart, G. D. (1980) Influence of polyethylene glycols on the kinetics of rat liver phosphofructokinase, *Journal of Biological Chemistry 255*, 10576-10578.

[48] Reinhart, G. D. (1980) Evaluation of first-order kinetic transients encountered during enzyme assay, *Analytical Biochemistry 104*, 99-105.

[49] Reinhart, G. D., and Lardy, H. A. (1980) Rat liver phosphofructokinase: Kinetic and physiological ramifications of the aggregation behavior, *Biochemistry 19*, 1491-1495.

[50] Reinhart, G. D., and Lardy, H. A. (1980) Rat liver phosphofructokinase: Use of fluorescence polarization to study aggregation at low protein concentration, *Biochemistry 19*, 1484-1490.

[51] Reinhart, G. D., and Lardy, H. A. (1980) Rat liver phosphofructokinase: Kinetic activity under near-physiological conditions, *Biochemistry 19*, 1477-1484.

[52] Reinhart, G. D. (1985) Influence of pH on the regulatory kinetics of rat liver phosphofructokinase: A thermodynamic linked-function analysis, *Biochemistry 24*, 7166-7172.

[53] Shen, Q.-J., Kassim, H., Huang, Y., Li, H., Zhang, J., Li, G., Wang, P.-Y., Yan, J., Ye, F., and Liu, J.-L. (2016) Filamentation of Metabolic Enzymes in Saccharomyces cerevisiae, *Journal of Genetics and Genomics 43*, 393-404.

[54] Noree, C., Sato, B. K., Broyer, R. M., and Wilhelm, J. E. (2010) Identification of novel filament-forming proteins in *Saccharomyces cerevisiae* and *Drosophila melanogaster*, *The Journal of Cell Biology 190*, 541-551.

[55] Aughey, G. N., and Liu, J.-L. (2016) Metabolic regulation via enzyme filamentation, *Critical Reviews in Biochemistry and Molecular Biology 51*, 282-293.

[56] Kim, C.-W., Moon, Y.-A., Park, S. W., Cheng, D., Kwon, H. J., and Horton, J. D. (2010) Induced polymerization of mammalian acetyl-CoA carboxylase by MIG12 provides a tertiary level of regulation of fatty acid synthesis, *Proceedings of the National Academy of Sciences 107*, 9626-9631.

[57] Li, H., Korennykh, A. V., Behrman, S. L., and Walter, P. (2010) Mammalian endoplasmic reticulum stress sensor IRE1 signals by dynamic clustering, *Proceedings of the National Academy of Sciences 107*, 16113-16118.

[58] Barry, R. M., Bitbol, A.-F., Lorestani, A., Charles, E. J., Habrian, C. H., Hansen, J. M., Li, H.-J., Baldwin, E. P., Wingreen, N. S., Kollman, J. M., and Gitai, Z. (2014) Large-scale filament formation inhibits the activity of CTP synthetase, *eLife 3*, e03638.

[59] Chang, C.-C., Lin, W.-C., Pai, L.-M., Lee, H.-S., Wu, S.-C., Ding, S.-T., Liu, J.-L., and Sung, L.-Y. (2015) Cytoophidium assembly reflects upregulation of IMPDH activity, *Journal of Cell Science 128*, 3550-3555.

[60] Kim, S.-Y., Kim, Y.-W., Hegerl, R., Cyrklaff, M., and Kim, I.-S. (2005) Novel type of enzyme multimerization enhances substrate affinity of oat β-glucosidase, *Journal of Structural Biology 150*, 1-10.

[61] Wyman, J. (1967) Allosteric Linkage, *Journal of the American Chemical Society 89*, 2202-2218.

[62] Weber, G. (1975) Energetics of Ligand Binding to Proteins, *Advances in Protein Chemistry 29*, 1-83.

[63] Frieden, C. (1967) Treatment of Enzyme Kinetic Data: II. THE MULTISITE CASE: COMPARISON OF ALLOSTERIC MODELS AND A POSSIBLE NEW MECHANISM, *Journal of Biological Chemistry 242*, 4045-4052.

[64] Cleland, W. W. (1963) The kinetics of enzyme-catalyzed reactions with two or more substrates or products, *Biochimica et Biophysica Acta (BBA) - Specialized Section on Enzymological Subjects 67*, 104-137.

[65] Reinhart, G. D. (1983) The determination of thermodynamic allosteric parameters of an enzyme undergoing steady-state turnover, *Archives of Biochemistry and Biophysics 224*, 389-401.

[66] Reinhart, G. D. (1988) Linked-function origins of cooperativity in a symmetrical dimer, *Biophysical Chemistry 30*, 159-172.

[67] Kemp, R. G., and Foe, L. G. (1983) Allosteric regulatory properties of muscle phosphofructokinase, *Molecular and Cellular Biochemistry 57*, 147-154.

[68] Fothergill-Gilmore, L. A., and Michels, P. A. M. (1993) Evolution of glycolysis, *Progress in biophysics and molecular biology 59*, 105-235.

[69] Mattaini, K. R., and Vander Heiden, M. G. (2012) Cancer. Glycosylation to adapt to stress, *Science (New York, N.Y.) 337*, 925-926.

[70] Rabinovitz, M. (1995) The phosphofructokinase-uncharged tRNA interaction in metabolic and cell cycle control: an interpretive review, *Nucleic acids symposium series (33)*, 182-189.

[71] Evans, P. R., and Hudson, P. J. (1979) Structure and control of phosphofructokinase from Bacillus stearothermophilus, *Nature 279*, 500-504.

[72] Schoneberg, T., Kloos, M., Bruser, A., Kirchberger, J., and Strater, N. (2013) Structure and allosteric regulation of eukaryotic 6-phosphofructokinases, *Biological chemistry 394*, 977-993.

[73] Dische, Z. (1935) Die Bedeutung der phosphorsäureester für den Ablauf und die Steuerung der Blutglykolyse, *Biochemische Zeitschrift 280*, 248-264.

[74] Ostern, P., Outhke, J.A., Terszakowee, J. (1936) Über die Bildung des Hexose-monophosphorsäure-esters und dessen Umwandlung in Fructose-diphosphorsäure-ester im Muskel, *Hoppe-Seyler's Zeitschrift fur Physiologische Chemie 243*, 9-37.

[75] Ling, K. H., Marcus, F., and Lardy, H. A. (1965) Purification and some Properties of Rabbit Skeletal Muscle Phosphofructokinase, *The Journal of biological chemistry 240*, 1893-1899.

[76] Uyeda, K. (1979) Phosphofructokinase, *Advances in Enzymology and Related Areas of Molecular Biology 48*, 193-244.

[77] Hue, L., and Rider, M. H. (1987) Role of fructose 2,6-bisphosphate in the control of glycolysis in mammalian tissues, *Biochemical Journal 245*, 313-324.

[78] Uyeda, K. (1970) Studies on the reaction mechanism of skeletal muscle phosphofructokinase, *The Journal of biological chemistry 245*, 2268-2275.

[79] Hanson, R. L., Rudolph, F. B., and Lardy, H. A. (1973) Rabbit muscle phosphofructokinase. The kinetic mechanism of action and the equilibrium constant, *The Journal of biological chemistry 248*, 7852-7859.

[80] Uyeda, K. (1972) Studies on the fructose 1-phosphate kinase activity of rabbit muscle phosphofructokinase, *The Journal of biological chemistry 247*, 1692-1698.

[81] Cook, P. F., and Cleland, W. W. (2007) *ENZYME KINETICS AND MECHANISM*, Vol. 1, Taylor & Francis Group, LLC, 270 Madison Avenue, New York, NY 10016.

[82] Bar-Tana, J., and Cleland, W. W. (1974) Rabbit muscle phosphofructokinase. I. Anomeric specificity; initial velocity kinetics, *The Journal of biological chemistry 249*, 1263-1270.

[83] Bar-Tana, J., and Cleland, W. W. (1974) Rabbit muscle phosphofructokinase. II. Product and dead end inhibition, *The Journal of biological chemistry 249*, 1271-1276.

[84] Taylor, C. B., and Bew, M. (1970) The distribution of two chromatographically distinguishable forms of phosphofructokinase in the tissues of the rat, *The Biochemical journal 119*, 797-799.

[85] Tarui, S., Giichi, O., Ikura, Y., Tanaka, T., Suda, M., and Nishikawa, M. (1965) Phosphofructokinase deficiency in skeletal muscle. A new type of glycogenosis, *Biochemical and biophysical research communications 19*, 517-523.

[86] Layzer, R. B., Rowland, L. P., and Bank, W. J. (1969) Physical and kinetic properties of human phosphofructokinase from skeletal muscle and erythrocytes, *The Journal of biological chemistry 244*, 3823-3831.

[87] Dunaway, G. A. (1983) A review of animal phosphofructokinase isozymes with an emphasis on their physiological role, *Molecular and cellular biochemistry 52*, 75-91.

[88] Kurata, N., Matsushima, T., and Sugimura, T. (1972) Multiple forms of phosphofructokinase in rat tissues and rat tumors, *Biochemical and biophysical research communications 48*, 473-479.

[89] Taketa, K. (1973) Electrophoretic multiplicity of phospho-fructokinase in rat liver and other tissues and effect of carbon tetrachloride intoxication, *Acta Medica Okayama 27*, 205-209.

[90] Tsai, M. Y., and Kemp, R. G. (1973) Isozymes of rabbit phosphofructokinase. Electrophoretic and immunochemical studies, *The Journal of biological chemistry 248*, 785-792.

[91] Kahn, A., Meienhofer, M. C., Cottreau, D., Lagrange, J. L., and Dreyfus, J. C. (1979) Phosphofructokinase (PFK) isozymes in man. I. Studies of adult human tissues, *Human genetics 48*, 93-108.

[92] Vora, S. (1981) Isozymes of human phosphofructokinase in blood cells and cultured cell lines: molecular and genetic evidence for a trigenic system, *Blood 57*, 724-732.

[93] Vora, S., and Francke, U. (1981) Assignment of the human gene for liver-type 6-phosphofructokinase isozyme (PFKL) to chromosome 21 by using somatic cell hybrids and monoclonal anti-L antibody, *Proceedings of the National Academy of Sciences of the United States of America 78*, 3738-3742.

[94] Vora, S., Durham, S., de Martinville, B., George, D. L., and Francke, U. (1982) Assignment of the human gene for muscle-type phosphofructokinase (PFKM) to chromosome 1 (region cen leads to q32) using somatic cell hybrids and monoclonal anti-M antibody, *Somatic cell genetics 8*, 95-104.

[95] Vora, S., Miranda, A. F., Hernandez, E., and Francke, U. (1983) Regional assignment of the human gene for platelet-type phosphofructokinase (PFKP) to chromosome 10p: novel use of polyspecific rodent antisera to localize human enzyme genes, *Human genetics 63*, 374-379.

[96] Kemp, R. G. (1971) Rabbit liver phosphofructokinase. Comparison of some properties with those of muscle phosphofructokinase, *The Journal of biological chemistry 246*, 245-252.

[97] Meienhofer Mc, C. D. D. J. C. K. A. (1980) Kinetic properties of human F4 phosphofructokinase: a poor regulatory enzyme, *FEBS Lett. 11*, 219-222.

[98] Dunaway, G. A., and Weber, G. (1974) Rat liver phosphofructokinase isozymes, *Archives of Biochemistry and Biophysics 162*, 620-628.

[99] Dunaway, G. A., and Kasten, T. P. (1987) Nature of the subunits of the 6-phosphofructo-1-kinase isoenzymes from rat tissues, *The Biochemical journal 242*, 667-671.

[100] Dunaway, G. A., Kasten, T. P., Sebo, T., and Trapp, R. (1988) Analysis of the phosphofructokinase subunits and isoenzymes in human tissues, *The Biochemical journal 251*, 677-683.

[101] Gonzalez, F., and Kemp, R. G. (1978) The A2B2 hybrid isozyme of phosphofructokinase, *The Journal of biological chemistry 253*, 1493-1497.

[102] Brand, I. A., and Soling, H. D. (1974) Rat liver phosphofructokinase. Purification and characterization of its reaction mechanism, *The Journal of biological chemistry 249*, 7824-7831.

[103] Foe, L. G., and Trujillo, J. L. (1980) Quaternary structure of pig liver phosphofructokinase, *Journal of Biological Chemistry 255*, 10537-10541.

[104] Reinhart, G. D. (1983) Influence of fructose 2,6-bisphosphate on the aggregation properties of rat liver phosphofructokinase, *Journal of Biological Chemistry 258*, 10827-10830.

[105] Reinhart, G. D. (1985) Characterization of fructose-2,6-bisphosphate activation of rat liver phosphofructokinase, *Federation Proceedings 44,* 2643-2647.

[106] Reinhart, G. D., and Hartleip, S. B. (1986) Relationship between fructose 2,6-bisphosphate activation and MgAT'P inhibition of rat liver phosphofructokinase at high pH. Kinetic evidence for individual binding sites linked by finite couplings, *Biochemistry 25*, 7308-7313.

[107] Reinhart, G. D., and Hartleip, S. B. (1987) Perturbation of the quaternary structure and allosteric behavior of rat liver phosphofructokinase by polyethylene glycol, *Archives of Biochemistry and Biophysics 258*, 65-76.

[108] Reinhart, G. D., and Hartleip, S. B. (1992) Influence of fructose 2,6-bisphosphate and MgATP on rat liver phosphofructokinase at pH 7: Evidence for a complex interdependence, *Archives of Biochemistry and Biophysics 296*, 224-230.

[109] Webb, B. A., Forouhar, F., Szu, F.-E., Seetharaman, J., Tong, L., and Barber, D. L. (2015) Structures of human phosphofructokinase-1 and atomic basis of cancer-associated mutations, *Nature 523*, 111-114.

[110] Sanchez-Martinez, C., Estevez, A. M., and Aragon, J. J. (2000) Phosphofructokinase C isozyme from ascites tumor cells: cloning, expression, and properties, *Biochemical and biophysical research communications 271*, 635-640.

[111] Tsai, M. Y., and Kemp, R. G. (1974) Rabbit Brain Phosphofructokinase: COMPARISON OF REGULATORY PROPERTIES WITH THOSE OF OTHER PHOSPHOFRUCTOKINASE ISOZYMES, *Journal of Biological Chemistry 249*, 6590-6596.

[112] Brand, I. A., and Söling, H. D. (1975) Activation and inactivation of rat liver phosphofructokinase by phosphorylation—dephosphorylation, *FEBS letters 57*, 163-168.

[113] Brand, I. A., Müller, M. K., Unger, C., and Söling, H. D. (1976) In vivo and in vitro interconversions of active and inactive forms of phosphofructokinase in rat liver, *FEBS letters 68*, 271-274.

[114] SÖLing, H.-D., and Brand, I. A. (1981) Covalent Modification of Phosphofructokinase by Phosphorylation—Dephosphorylation*, *Current topics in cellular regulation 20*, 107-138.

[115] Palm, D. C., Rohwer, J. M., and Hofmeyr, J. H. (2014) Incorporating covalent and allosteric effects into rate equations: the case of muscle glycogen synthase, *The Biochemical journal 462*, 525-537.

[116] Funato, Y., Hayashi, T., Irino, Y., Takenawa, T., and Miki, H. (2013) Nucleoredoxin regulates glucose metabolism via phosphofructokinase 1, *Biochemical and biophysical research communications 440*, 737-742.

[117] Kagimoto, T., and Uyeda, K. (1979) Hormone-stimulated phosphorylation of liver phosphofructokinase in vivo, *The Journal of biological chemistry 254*, 5584-5587.

[118] Kagimoto, T., and Uyeda, K. (1980) Regulation of rat liver phosphofructokinase by glucagon-induced phosphorylation, *Archives of Biochemistry and Biophysics 203*, 792-799.

[119] Claus, T. H., Schlumpf, J. R., el-Maghrabi, M. R., Pilkis, J., and Pilkis, S. J. (1980) Mechanism of action of glucagon on hepatocyte phosphofructokinase activity, *Proceedings of the National Academy of Sciences of the United States of America 77*, 6501-6505.

[120] Blair, J. B., Cook, D. E., and Lardy, H. A. (1973) Influence of glucagon on the metabolism of xylitol and dihydroxyacetone in the isolated perfused rat liver, *The Journal of biological chemistry 248*, 3601-3607.

[121] Pilkis, S. J., El-Maghrabi, M. R., McGrane, M., Pilkis, J., Fox, E., and Claus, T. H. (1982) Fructose 2,6-bisphosphate: A mediator of hormone action at the fructose 6-phosphate/fructose 1,6-bisphosphate substrate cycle, *Molecular and cellular endocrinology 25*, 245-266.

[122] Pilkis, S. J., El-Maghrabi, M. R., Pilkis, J., and Claus, T. H. (1982) Studies on the in vitro phosphorylation of 6-phosphofructo-1-kinase from rat liver, *Archives of Biochemistry and Biophysics 215*, 379-389.

[123] Uyeda, K., Furuya, E., and Luby, L. J. (1981) The effect of natural and synthetic D-fructose 2,6-bisphosphate on the regulatory kinetic properties of liver and muscle phosphofructokinases, *The Journal of biological chemistry 256*, 8394-8399.

[124] Furuya, E., and Uyeda, K. (1980) Regulation of phosphofructokinase by a new mechanism. An activation factor binding to phosphorylated enzyme, *The Journal of biological chemistry 255*, 11656-11659.

[125] Kitajima, S., Sakakibara, R., and Uyeda, K. (1983) Significance of phosphorylation of phosphofructokinase, *The Journal of biological chemistry 258*, 13292-13298.

[126] Sakakibara, R., and Uyeda, K. (1983) Differences in the allosteric properties of pure low and high phosphate forms of phosphofructokinase from rat liver, *The Journal of biological chemistry 258*, 8656-8662.

[127] Kemp, R. G., Foe, L. G., Latshaw, S. P., Poorman, R. A., and Heinrikson, R. L. (1981) Studies on the phosphorylation of muscle phosphofructokinase, *The Journal of biological chemistry 256*, 7282-7286.

[128] Hofer, H. W., and Fürst, M. (1976) Isolation of a phosphorylated form of phosphofructokinase from skeletal muscle, *FEBS letters 62*, 118-122.

[129] Riquelme, P. T., Fox, R. W., and Kemp, R. G. (1978) Mouse muscle phosphofructokinase is partially phosphorylated, *Biochemical and biophysical research communications 81*, 864-870.

[130] Hussey, C. R., Liddle, P. F., Ardron, D., and Kellett, G. L. (1977) The isolation and characterization of differentially phosphorylated fractions of phosphofructokinase from rabbit skeletal muscle, *European journal of biochemistry / FEBS 80*, 497-506.

[131] Uyeda, K., Miyatake, A., Luby, L. J., and Richards, E. G. (1978) Isolation and characterization of muscle phosphofructokinases with varying degrees of phosphorylation, *The Journal of biological chemistry 253*, 8319-8327.

[132] Foe, L. G., and Kemp, R. G. (1982) Properties of phospho and dephospho forms of muscle phosphofructokinase, *The Journal of biological chemistry 257*, 6368-6372.

[133] Luther, M. A., and Lee, J. C. (1986) The role of phosphorylation in the interaction of rabbit muscle phosphofructokinase with F-actin, *The Journal of biological chemistry 261*, 1753-1759.

[134] Liou, R. S., and Anderson, S. (1980) Activation of rabbit muscle phosphofructokinase by F-actin and reconstituted thin filaments, *Biochemistry 19*, 2684-2688.

[135] Da Silva, D., Zancan, P., Coelho, W. S., Gomez, L. S., and Sola-Penna, M. (2010) Metformin reverses hexokinase and 6-phosphofructo-1-kinase inhibition in skeletal muscle, liver and adipose tissues from streptozotocin-induced diabetic mouse, *Archives of Biochemistry and Biophysics 496*, 53-60.

[136] Jenkins, C. M., Yang, J., Sims, H. F., and Gross, R. W. (2011) Reversible high affinity inhibition of phosphofructokinase-1 by acyl-CoA: a mechanism integrating glycolytic flux with lipid metabolism, *The Journal of biological chemistry 286*, 11937-11950.

[137] Yi, W., Clark, P. M., Mason, D. E., Keenan, M. C., Hill, C., Goddard, W. A., 3rd, Peters, E. C., Driggers, E. M., and Hsieh-Wilson, L. C. (2012) Phosphofructokinase 1 glycosylation regulates cell growth and metabolism, *Science (New York, N.Y.) 337*, 975-980.

[138] Poorman, R. A., Randolph, A., Kemp, R. G., and Heinrikson, R. L. (1984) Evolution of phosphofructokinase—gene duplication and creation of new effector sites, *Nature 309*, 467-469.

[139] Heinisch, J., Ritzel, R. G., von Borstel, R. C., Aguilera, A., Rodicio, R., and Zimmermann, F. K. (1989) The phosphofructokinase genes of yeast evolved from two duplication events, *Gene 78*, 309-321.

[140] Banaszak, K., Mechin, I., Obmolova, G., Oldham, M., Chang, S. H., Ruiz, T., Radermacher, M., Kopperschlager, G., and Rypniewski, W. (2011) The crystal structures of eukaryotic phosphofructokinases from baker's yeast and rabbit skeletal muscle, *Journal of Molecular Biology 407*, 284-297.

[141] Kloos, M., Bruser, A., Kirchberger, J., Schoneberg, T., and Strater, N. (2014) Crystallization and preliminary crystallographic analysis of human muscle phosphofructokinase, the main regulator of glycolysis, *Acta crystallographica.Section F, Structural biology communications 70*, 578-582.

[142] Kloos, M., Bruser, A., Kirchberger, J., Schoneberg, T., and Strater, N. (2015) Crystal structure of human platelet phosphofructokinase-1 locked in an activated conformation, *The Biochemical journal 469*, 421-432.

[143] Kemp, R. G., and Gunasekera, D. (2002) Evolution of the allosteric ligand sites of mammalian phosphofructo-1-kinase, *Biochemistry 41*, 9426-9430.

[144] Li, Y., Rivera, D., Ru, W., Gunasekera, D., and Kemp, R. G. (1999) Identification of allosteric sites in rabbit phosphofructo-1-kinase, *Biochemistry 38*, 16407-16412.

[145] Van Schaftingen, E., Jett, M. F., Hue, L., and Hers, H. G. (1981) Control of liver 6-phosphofructokinase by fructose 2,6-bisphosphate and other effectors, *Proceedings of the National Academy of Sciences of the United States of America 78*, 3483-3486.

[146] Hers, H. G., and Van Schaftingen, E. (1982) Fructose 2,6-bisphosphate 2 years after its discovery, *The Biochemical journal 206*, 1-12.

[147] Chang, S. H., and Kemp, R. G. (2002) Role of Ser530, Arg292, and His662 in the allosteric behavior of rabbit muscle phosphofructokinase, *Biochemical and biophysical research communications 290*, 670-675.

[148] Strater, N., Marek, S., Kuettner, E. B., Kloos, M., Keim, A., Bruser, A., Kirchberger, J., and Schoneberg, T. (2011) Molecular architecture and structural basis of allosteric regulation of eukaryotic phosphofructokinases, *FASEB journal : official publication of the Federation of American Societies for Experimental Biology 25*, 89-98.

[149] Bruser, A., Kirchberger, J., and Schoneberg, T. (2012) Altered allosteric regulation of muscle 6-phosphofructokinase causes Tarui disease, *Biochemical and biophysical research communications 427*, 133-137.

[150] Akkerman, J. W., Gorter, G., Sixma, J. J., and Staal, G. E. (1974) Human platelet 6-phosphofructokinase. Purification, kinetic parameters and the influence of sulphate ions on enzyme activity, *Biochimica et biophysica acta 370*, 102-112.

[151] Trujillo, J. L., and Deal, W. C. (1977) Metabolic control and structure of glycolytic enzymes. 17. Pig liver phosphofructokinase: asymmetry properties, proof of rapid association-dissociation equilibriums, and effect of temperature and protein concentration on the equilibriums, *Biochemistry 16*, 3098-3104.

[152] Aragón, J. J., and Sols, A. (1991) Regulation of enzyme activity in the cell: effect of enzyme concentration, *The FASEB Journal 5*, 2945-2950.

[153] Soboll, S., Scholz, R., and Heldt, H. W. (1978) Subcellular metabolite concentrations. Dependence of mitochondrial and cytosolic ATP systems on the metabolic state of perfused rat liver, *European Journal Of Biochemistry / FEBS 87*, 377-390.

[154] Clark, M. G., Kneer, N. M., Bosch, A. L., and Lardy, H. A. (1974) The Fructose 1,6-Diphosphatase-Phosphofructokinase Substrate Cycle: A SITE OF REGULATION OF HEPATIC GLUCONEOGENESIS BY GLUCAGON, *Journal of Biological Chemistry 249*, 5695-5703.

[155] Lad, P. M., Hill, D. E., and Hammes, G. G. (1973) Influence of allosteric ligands on the activity and aggregation of rabbit muscle phosphofructokinase, *Biochemistry 12*, 4303-4309.

[156] Mok, Y. F., and Howlett, G. J. (2006) Sedimentation Velocity Analysis of Amyloid Oligomers and Fibrils, In *Methods in Enzymology*, pp 199-217, Academic Press.

[157] Folta-Stogniew, E. (2006) Oligomeric States of Proteins Determined by Size-Exclusion Chromatography Coupled With Light Scattering, Absorbance, and Refractive Index Detectors, In *New and Emerging Proteomic Techniques*, pp 97-112, Humana Press, Totowa, NJ.

[158] Gast, K., and Fiedler, C. (2012) Dynamic and Static Light Scattering of Intrinsically Disordered Proteins, In *Intrinsically Disordered Protein Analysis: Volume 2, Methods and Experimental Tools* (Uversky, V. N., and Dunker, A. K., Eds.), pp 137-161, Springer New York, New York, NY.

[159] Sung, J. J., Pardeshi, N. N., Mulder, A. M., Mulligan, S. K., Quispe, J., On, K., Carragher, B., Potter, C. S., Carpenter, J. F., and Schneemann, A. (2015) Transmission electron microscopy as an orthogonal method to characterize protein aggregates, *Journal of pharmaceutical sciences 104*, 750-759.

[160] Elson, E. L., and Magde, D. (1974) Fluorescence correlation spectroscopy. I. Conceptual basis and theory, *Biopolymers 13*, 1-27.

[161] Magde, D., Elson, E. L., and Webb, W. W. (1974) Fluorescence correlation spectroscopy. II. An experimental realization, *Biopolymers 13*, 29-61.

[162] Müller, J. D., Chen, Y., and Gratton, E. (2003) [4] Fluorescence correlation spectroscopy, In *Methods in Enzymology*, pp 69-92, Academic Press.

[163] Berland, K. M., So, P. T., and Gratton, E. (1995) Two-photon fluorescence correlation spectroscopy: method and application to the intracellular environment, *Biophysical Journal 68*, 694-701.

[164] Thompson, N. L. (1999) Fluorescence Correlation Spectroscopy, In *Topics in Fluorescence Spectroscopy: Techniques* (Lakowicz, J. R., Ed.), pp 337-378, Springer US, Boston, MA.

[165] Kensal E. van Holde, W. C. J., P. Shing Ho (2006) *Principles of Physical Biochemistry*, Vol. 1, Second ed., Pearson Education, Inc., Upper Saddle River, NJ.

[166] Li, J., Zhu, X., Byrnes, M., Nelson, J. W., and Chang, S. H. (1993) Site-directed mutagenesis of rabbit muscle phosphofructokinase cDNA. Mutations at glutamine 200 affect the allosteric properties of the enzyme, *The Journal of biological chemistry 268*, 24599-24606.

[167] Martinez-Costa, O. H., Hermida, C., Sanchez-Martinez, C., Santamaria, B., and Aragon, J. J. (2004) Identification of C-terminal motifs responsible for transmission of inhibition by ATP of mammalian phosphofructokinase, and their contribution to other allosteric effects, *The Biochemical journal 377*, 77-84.

[168] Gunasekera, D., and Kemp, R. G. (1999) Cloning, sequencing, expression, and purification of the C isozyme of mouse phosphofructokinase, *Protein expression and purification 16*, 448-453.

[169] Lovingshimer, M. R., Siegele, D., and Reinhart, G. D. (2006) Construction of an inducible, pfkA and pfkB deficient strain of Escherichia coli for the expression and purification of phosphofructokinase from bacterial sources, *Protein Expression and Purification 46*, 475-482.

[170] Whitaker, A. M., and Reinhart, G. D. (2016) The effect of introducing small cavities on the allosteric inhibition of phosphofructokinase from Bacillus stearothermophilus, *Archives of Biochemistry and Biophysics 607*, 1-6.

[171] Ausubel, F., Brent, R., Kingston, R., Moore, D., Seidman, J. G., Smith, J., and Struhl, K. (2003) *Current Protocols in Molecular Biology*, John Wiley & Sons, Inc.

[172] Reinhart, G. D. (2004) Quantitative Analysis and Interpretation of Allosteric Behavior, In *Methods in Enzymology*, pp 187-203.

[173] Bruser, A., Kirchberger, J., Kloos, M., Strater, N., and Schoneberg, T. (2012) Functional linkage of adenine nucleotide binding sites in mammalian muscle 6-phosphofructokinase, *The Journal of biological chemistry 287*, 17546-17553.

[174] Dunaway, G. A., and Weber, G. (1974) Effects of hormonal and nutritional changes on rates of synthesis and degradation of hepatic phosphofructokinase isozymes, *Archives of Biochemistry and Biophysics 162*, 629-637.

[175] Dunaway, G. A., Leung, G. L., Thrasher, J. R., and Cooper, M. D. (1978) Turnover of hepatic phosphofructokinase in normal and diabetic rats. Role of insulin and peptide stabilizing factor, *Journal of Biological Chemistry 253*, 7460-7463.

[176] Hotta, K., Nakajima, H., Yamasaki, T., Hamaguchi, T., Kuwajima, M., Noguchi, T., Tanaka, T., Kono, N., and Tarui, S. (1991) Rat-liver-type phosphofructokinase mRNA, *European Journal of Biochemistry 202*, 293-298.

[177] Pilkis, S. J., Claus, T. H., Kountz, P. D., and El-Maghrabi, M. R. (1987) Enzymes of the Fructuse 6-Phosphate-Fructosee 1,6-Bisphosphate Substrate Cycle, In *The Enzymes* (Kaguni, L. S., and Tulio Oliveira, M., Eds.), pp 3-46, Academic Press, Inc., New York.

[178] Neely, P., El-Maghrabi, M. R., Pilkis, S. J., and Claus, T. H. (1981) Effect of diabetes, insulin, starvation, and refeeding on the level of rat hepatic fructose 2,6-bisphosphate, *Diabetes 30*, 1062-1064.

[179] Hue, L. (1982) Role of fructose 2,6-bisphosphate in the stimulation of glycolysis by anoxia in isolated hepatocytes, *Biochemical Journal 206*, 359-365.

[180] Vander Heiden, M. G., Cantley, L. C., and Thompson, C. B. (2009) Understanding the Warburg Effect: The Metabolic Requirements of Cell Proliferation, *Science 324*, 1029-1033.

[181] Koppenol, W. H., Bounds, P. L., and Dang, C. V. (2011) Otto Warburg's contributions to current concepts of cancer metabolism, *Nat Rev Cancer 11*, 325-337.

[182] WEINHOUSE, S., WARBURG, O., BURK, D., and SCHADE, A. L. (1956) On Respiratory Impairment in Cancer Cells, *Science 124*, 267-272.

[183] Brown, J. M., and Giaccia, A. J. (1998) The Unique Physiology of Solid Tumors: Opportunities (and Problems) for Cancer Therapy, *Cancer Research 58*, 1408-1416.

[184] Lin, C.-C., Cheng, T.-L., Tsai, W.-H., Tsai, H.-J., Hu, K.-H., Chang, H.-C., Yeh, C.-W., Chen, Y.-C., Liao, C.-C., and Chang, W.-T. (2012) Loss of the respiratory enzyme citrate synthase directly links the Warburg effect to tumor malignancy, *Scientific Reports 2*, 785.

[185] Pacini, N., and Borziani, F. (2014) Cancer Stem Cell Theory and the Warburg Effect, Two Sides of the Same Coin?, *International Journal of Molecular Sciences 15*, 8893-8930.

[186] Uyeda, K., Furuya, E., and Luby, L. J. (1981) The effect of natural and synthetic D-fructose 2,6-bisphosphate on the regulatory kinetic properties of liver and muscle phosphofructokinases, *Journal of Biological Chemistry 256*, 8394-8399.

[187] Spelsberg, T. C., Reinhart, G. D., and Barham, S. (1984) The isolation of large quantities of undamaged cellular organelles and cytosolic enzymes using a low-shear continuous tissue homogenizer, *Analytical Biochemistry 143*, 237-248.

[188] del Sol, A., Tsai, C.-J., Ma, B., and Nussinov, R. (2009) The Origin of Allosteric Functional Modulation: Multiple Pre-existing Pathways, *Structure 17*, 1042-1050.

[189] Passonneau, J. V., and Lowry, O. H. (1963) P-Fructokinase and the control of the citric acid cycle, *Biochemical and Biophysical Research Communications 13*, 372-379.

[190] Colombo, G., Tate, P. W., Girotti, A. W., and Kemp, R. G. (1975) Interaction of inhibitors with muscle phosphofructokinase, *Journal of Biological Chemistry 250*, 9404-9412.

[191] Mediavilla, D., Metón, I., and Baanante, I. V. (2008) Purification and Kinetic Characterization of 6-Phosphofructo-1-kinase from the Liver of Gilthead Sea Bream (Sparus Aurata), *The Journal of Biochemistry 144*, 235-244.

[192] David, P. B., and Henry, A. L. (1973) Phosphofructokinase, In *The Enzymes* (Boyer, P. D., Ed.), pp 239-278, Academic, New York.

[193] Sjöback, R., Nygren, J., and Kubista, M. (1995) Absorption and fluorescence properties of fluorescein, *Spectrochimica Acta Part A: Molecular and Biomolecular Spectroscopy 51*, L7-L21.

[194] Jameson, D. M., and Ross, J. A. (2010) Fluorescence Polarization/Anisotropy in Diagnostics and Imaging, *Chemical reviews 110*, 2685-2708.

[195] Unruh, J. R., Price, E. S., Molla, R. G., Hui, R., and Johnson, C. K. (2006) Evaluation of a femtosecond fiber laser for two-photon fluorescence correlation spectroscopy, *Microscopy Research and Technique 69*, 891-893.

[196] Marrocco, M. (2008) Two-Photon Excitation Fluorescence Correlation Spectroscopy of Diffusion for Gaussian−Lorentzian Volumes, *The Journal of Physical Chemistry A 112*, 3831-3836.

[197] Petrášek, Z., and Schwille, P. (2008) Precise measurement of diffusion coefficients using scanning fluorescence correlation spectroscopy, *Biophysical Journal 94*, 1437-1448.

[198] Brinkley, M. (1992) A brief survey of methods for preparing protein conjugates with dyes, haptens and crosslinking reagents, *Bioconjugate Chemistry 3*, 2-13.

[199] Houseman, B. T., Gawalt, E. S., and Mrksich, M. (2003) Maleimide-Functionalized Self-Assembled Monolayers for the Preparation of Peptide and Carbohydrate Biochips, *Langmuir 19*, 1522-1531.

[200] Kemp, R. G., and Forest, P. B. (1968) Reactivity of the sulfhydryl groups of muscle phosphofructokinase, *Biochemistry 7*, 2596-2603.

[201] Simpson, I. A., Hollaway, M. R., and Beard, J. (1977) The subunit structure of rabbit skeletal-muscle phosphofructokinase and the amino acid sequence of the tryptic peptide containing the highly reactive thiol group, *Biochemical Journal 163*, 309-316.

[202] Latshaw, S. P., Bazaes, S., Randolph, A., Poorman, R. A., Heinrikson, R. L., and Kemp, R. G. (1987) Identification of highly reactive cysteinyl and methionyl residues of rabbit muscle phosphofructokinase, *Journal of Biological Chemistry 262*, 10672-10677.

[203] Banas, T., Gontero, B., Drews, V. L., Johnson, S. L., Marcus, F., and Kemp, R. G. (1988) Reactivity of the thiol groups of Escherichia coli phosphofructo-1-kinase, *Biochimica et Biophysica Acta (BBA) - Protein Structure and Molecular Enzymology 957*, 178-184.

[204] Rauch, J. N., and Gestwicki, J. E. (2014) Binding of Human Nucleotide Exchange Factors to Heat Shock Protein 70 (Hsp70) Generates Functionally Distinct Complexes in Vitro, *The Journal of Biological Chemistry 289*, 1402-1414.

[205] Banks, P. R., and Paquette, D. M. (1995) Comparison of Three Common Amine Reactive Fluorescent Probes Used for Conjugation to Biomolecules by Capillary Zone Electrophoresis, *Bioconjugate Chemistry 6*, 447-458.

[206] Johansson, L. B. A. (1990) Limiting fluorescence anisotropies of perylene and xanthene derivatives, *Journal of the Chemical Society, Faraday Transactions 86*, 2103-2107.

[207] Hungerford, G., Benesch, J., Mano, J. F., and Reis, R. L. (2007) Effect of the labelling ratio on the photophysics of fluorescein isothiocyanate (FITC) conjugated to bovine serum albumin, *Photochemical & Photobiological Sciences 6*, 152-158.

[208] Rajagopalan, S., Huang, F., and Fersht, A. R. (2010) Single-Molecule characterization of oligomerization kinetics and equilibria of the tumor suppressor p53, *Nucleic Acids Research 39*, 2294-2303.

[209] Turner, D. K., Wayman, A. E., Rolando, C. N., Dande, P., Carter, P. W., and Remsen, E. E. (2013) Reduction of Artifacts in Fluorescence Correlation Spectroscopy Due to Sample Adsorption on Optical Glass Surfaces, *Applied Spectroscopy 67*, 692-698.

[210] Sahoo, B., Drombosky, K. W., and Wetzel, R. (2016) Fluorescence Correlation Spectroscopy: A Tool to Study Protein Oligomerization and Aggregation In Vitro and In Vivo, *Methods in molecular biology (Clifton, N.J.) 1345*, 67-87.

[211] Qian, H., and Elson, E. L. (1990) Distribution of molecular aggregation by analysis of fluctuation moments, *Proceedings of the National Academy of Sciences of the United States of America 87*, 5479-5483.

[212] Pavelich, M. J., and Hammes, G. G. (1973) Aggregation of rabbit muscle phosphofructokinase, *Biochemistry 12*, 1408-1414.

[213] Meseth, U., Wohland, T., Rigler, R., and Vogel, H. (1999) Resolution of fluorescence correlation measurements, *Biophysical journal 76*, 1619-1631.

[214] Ali, M. H., and Imperiali, B. (2005) Protein oligomerization: How and why, *Bioorganic & Medicinal Chemistry 13*, 5013-5020.

[215] Kosuke, H., Hafumi, N., Stephen, B., and Anna, R. P. (2011) Caught in self-interaction: evolutionary and functional mechanisms of protein homooligomerization, *Physical Biology 8*, 035007.

[216] Hesterberg, L. K., and Lee, J. C. (1980) Sedimentation study of a catalytically active form of rabbit muscle phosphofructokinase at pH 8.55, *Biochemistry 19*, 2030-2039.

[217] Jameson, D. M., Ross, J. A., and Albanesi, J. P. (2009) Fluorescence fluctuation spectroscopy: ushering in a new age of enlightenment for cellular dynamics, *Biophysical Reviews 1*, 105.

[218] Leonard, K. R., and Walker, I. O. (1972) The self-association of rabbit-muscle phosphofructokinase, *European Journal Of Biochemistry / FEBS 26*, 442-448.

[219] Zancan, P., Marinho-Carvalho, M. M., Faber-Barata, J., Dellias, J. M. M., and Sola-Penna, M. (2008) ATP and fructose-2,6-bisphosphate regulate skeletal muscle 6-phosphofructo-1-kinase by altering its quaternary structure, *IUBMB Life 60*, 526-533.

[220] Bacia, K., Haustein, E., and Schwille, P. (2014) Fluorescence correlation spectroscopy: principles and applications, *Cold Spring Harbor protocols 2014*, 709-725.

[221] Engelborghs, Y. (2012) An Elegant Way to Quantitatively Analyze Oligomer Formation in Solution, *Biophysical Journal 103*, 1811-1812.

[222] Kanno, D. M., and Levitus, M. (2014) Protein Oligomerization Equilibria and Kinetics Investigated by Fluorescence Correlation Spectroscopy: A Mathematical Treatment, *The Journal of Physical Chemistry B 118*, 12404-12415.

[223] weber, g. (1986) Phenomenological description of the association of protein subunits subjected to conformational drift. Effects of dilution and of hydrostatic pressure., *Biochemistry 25*, 3626-3631.

[224] Digman, M. A., Dalal, R., Horwitz, A. F., and Gratton, E. (2008) Mapping the Number of Molecules and Brightness in the Laser Scanning Microscope, *Biophysical journal 94*, 2320-2332.

[225] Chen, Y., Müller, J. D., So, P. T. C., and Gratton, E. (1999) The Photon Counting Histogram in Fluorescence Fluctuation Spectroscopy, *Biophysical Journal 77*, 553-567.

[226] Chakraborty, M., Kuriata, A. M., Nathan Henderson, J., Salvucci, M. E., Wachter, R. M., and Levitus, M. (2012) Protein Oligomerization Monitored by Fluorescence Fluctuation Spectroscopy: Self-Assembly of Rubisco Activase, *Biophysical journal 103*, 949-958.

[227] Krouglova, T., Vercammen, J., and Engelborghs, Y. (2004) Correct Diffusion Coefficients of Proteins in Fluorescence Correlation Spectroscopy. Application to Tubulin Oligomers Induced by Mg(2+) and Paclitaxel, *Biophysical Journal 87*, 2635-2646.

[228] Garai, K., and Frieden, C. (2010) The Association−Dissociation Behavior of the ApoE Proteins: Kinetic and Equilibrium Studies, *Biochemistry 49*, 9533-9541.

[229] Binder, J. K., Douma, L. G., Ranjit, S., Kanno, D. M., Chakraborty, M., Bloom, L. B., and Levitus, M. (2014) Intrinsic stability and oligomerization dynamics of DNA processivity clamps, *Nucleic Acids Research 42*, 6476-6486.

[230] Overbeck, E., Sinn, C., Flammer, I., and Rička, J. (1998) Silicon avalanche photodiodes as detectors for photon correlation experiments, *Review of Scientific Instruments 69*, 3515-3523.

[231] Burstyn, H. C., and Sengers, J. V. (1983) Time dependence of critical concentration fluctuations in a binary liquid, *Physical Review A 27*, 1071-1085.

[232] Zhu, J. X., Durian, D. J., Müller, J., Weitz, D. A., and Pine, D. J. (1992) Scaling of transient hydrodynamic interactions in concentrated suspensions, *Physical Review Letters 68*, 2559-2562.

[233] Zhao, M., Jin, L., Chen, B., Ding, Y., Ma, H., and Chen, D. (2003) Afterpulsing and its correction in fluorescence correlation spectroscopy experiments, *Appl. Opt. 42*, 4031-4036.

[234] Mark B. Cannell, A. M., and Christian Soeller. (2006) Practical Tips for Two-Photon Microscopy, In *Handbook of Biological Confocal Microscopy* (Pawley,

J. B., Ed.) Third ed., pp 900-905, Springer Science+Business Media, New York.

[235] Rizzuto, R., Brini, M., Pizzo, P., Murgia, M., and Pozzan, T. (1995) Chimeric green fluorescent protein as a tool for visualizing subcellular organelles in living cells, *Current Biology 5*, 635-642.

[236] He, X., Gao, L., and Ma, N. (2013) One-Step Instant Synthesis of Protein-Conjugated Quantum Dots at Room Temperature, *3*, 2825.

[237] Keppler, A., Pick, H., Arrivoli, C., Vogel, H., and Johnsson, K. (2004) Labeling of fusion proteins with synthetic fluorophores in live cells, *Proceedings of the National Academy of Sciences of the United States of America 101*, 9955-9959.

[238] Gautier, A., Juillerat, A., Heinis, C., Corrêa, I. R., Kindermann, M., Beaufils, F., and Johnsson, K. (2008) An Engineered Protein Tag for Multiprotein Labeling in Living Cells, *Chemistry & Biology 15*, 128-136.

[239] Jing, C., and Cornish, V. W. (2013) A Fluorogenic TMP-tag for High Signal-to-Background Intracellular Live Cell Imaging, *ACS chemical biology 8*, 1704-1712.

[240] Los, G. V., Encell, L. P., McDougall, M. G., Hartzell, D. D., Karassina, N., Zimprich, C., Wood, M. G., Learish, R., Ohana, R. F., Urh, M., Simpson, D., Mendez, J., Zimmerman, K., Otto, P., Vidugiris, G., Zhu, J., Darzins, A., Klaubert, D. H., Bulleit, R. F., and Wood, K. V. (2008) HaloTag: A Novel Protein Labeling Technology for Cell Imaging and Protein Analysis, *ACS Chemical Biology 3*, 373-382.

[241] Lotze, J., Reinhardt, U., Seitz, O., and Beck-Sickinger, A. G. (2016) Peptide-tags for site-specific protein labelling in vitro and in vivo, *Molecular BioSystems 12*, 1731-1745.

[242] Widengren, J., Rigler, R., and Mets, Ü. (1994) Triplet-state monitoring by fluorescence correlation spectroscopy, *Journal of Fluorescence 4*, 255-258.

[243] Widengren, J., and Rigler, R. (1996) Mechanisms of photobleaching investigated by fluorescence correlation spectroscopy, *Bioimaging 4*, 149-157.

[244] Nguyen, T. A., Sarkar, P., Veetil, J. V., Koushik, S. V., and Vogel, S. S. (2012) Fluorescence Polarization and Fluctuation Analysis Monitors Subunit Proximity, Stoichiometry, and Protein Complex Hydrodynamics, *PLOS ONE 7*, e38209.

[245] Wennmalm, S., Chmyrov, V., Widengren, J., and Tjernberg, L. (2015) Highly Sensitive FRET-FCS Detects Amyloid β-Peptide Oligomers in Solution at Physiological Concentrations, *Analytical Chemistry 87*, 11700-11705.